



**HAL**  
open science

# Direct synthesis of long-chain hydrocarbons by plasma-catalysis from syngas and CH<sub>4</sub>-CO<sub>2</sub> mixtures

Di Li

► **To cite this version:**

Di Li. Direct synthesis of long-chain hydrocarbons by plasma-catalysis from syngas and CH<sub>4</sub>-CO<sub>2</sub> mixtures. Chemical and Process Engineering. Université Paris sciences et lettres, 2019. English. NNT : 2019PSLEM059 . tel-02899601

**HAL Id: tel-02899601**

**<https://pastel.hal.science/tel-02899601>**

Submitted on 15 Jul 2020

**HAL** is a multi-disciplinary open access archive for the deposit and dissemination of scientific research documents, whether they are published or not. The documents may come from teaching and research institutions in France or abroad, or from public or private research centers.

L'archive ouverte pluridisciplinaire **HAL**, est destinée au dépôt et à la diffusion de documents scientifiques de niveau recherche, publiés ou non, émanant des établissements d'enseignement et de recherche français ou étrangers, des laboratoires publics ou privés.



**THÈSE DE DOCTORAT**  
**DE L'UNIVERSITÉ PSL**

Préparée à MINES ParisTech

**Direct synthesis of long-chain hydrocarbons by  
plasma-catalysis from syngas and CH<sub>4</sub>-CO<sub>2</sub> mixtures**

**Synthèse directe d'hydrocarbures supérieurs par  
plasma-catalyse à partir de gaz de synthèse et de  
mélanges CH<sub>4</sub>-CO<sub>2</sub>**

Soutenue par

**Di Li**

Le 28/11/2019

Ecole doctorale ISMME n° 621 :

**Ingénierie des Systèmes,  
Matériaux, Mécanique et  
Energétique**

Spécialité

**Energétique et génie des  
procédés**

Composition du jury:

Elena Galvez Parruca Maitre de conf. HDR UPMC	<i>Rapporteur</i>
Xin Tu Reader, University of Liverpool	<i>Rapporteur</i>
Catherine Batiot Dupeyrat Prof. Université de Poitiers	<i>Examineur</i>
Patrick Da Costa Prof. Sorbonne Université	<i>Président de jury</i>
Vandad-Julien Rohani Maitre-assistant, MINES ParisTech	<i>Examineur</i>
Laurent Fucheri Directeur de Recherche, MINES ParisTech	<i>Directeur de thèse</i>



# Contents

<b>NOMENCLATURE .....</b>	<b>5</b>
ABBREVIATIONS .....	5
SYMBOLS .....	7
<b>RESUME EN FRANÇAIS .....</b>	<b>8</b>
<b>CHAPTER I. INTRODUCTION .....</b>	<b>15</b>
1.1. BACKGROUND .....	15
1.2. A BRIEF INTRODUCTION TO PLASMA .....	19
1.3. A REVIEW ON FTS .....	21
1.3.1 Main reactions and mechanism of FTS .....	24
1.3.2 Catalysts for FTS .....	30
1.4. A REVIEW ON REFORMING CO <sub>2</sub> WITH CH <sub>4</sub> .....	35
1.4.1 Reactions and thermodynamics .....	36
1.4.2 Catalysts for reforming .....	39
1.4.3 New approach: directly synthesizing value-added liquid products from CO <sub>2</sub> and CH <sub>4</sub> .....	42
1.5. WHY PLASMA-ASSISTED REFORMING AND FTS MAKES A DIFFERENCE .....	45
1.5.1 Plasma assisted FTS .....	46
1.5.2 Plasma assisted converting CO <sub>2</sub> with CH <sub>4</sub> .....	47
1.6. OUTLINE OF THIS THESIS .....	50
<b>CHAPTER II. EXPERIMENTAL, METHOD CHARACTERIZATIONS AND SYSTEM DIAGNOSTICS .....</b>	<b>53</b>
RESUME DU CHAPITRE .....	53
ABSTRACT .....	54
2.1. DESCRIPTION OF EXPERIMENTAL BENCH .....	55
2.1.1 DBD reactor .....	56
2.1.2 Power supply system .....	56

2.1.3 Power measurement and diagnostics .....	57
2.1.4 Measurement and products analysis .....	59
2.2. PREPARATION AND CHARACTERIZATION OF CATALYSTS .....	61
2.2.1 Preparation of catalysts .....	61
2.2.2 Characterization of catalysts .....	63
2.3. CHARACTERIZATION RESULTS OF CATALYSTS .....	65
2.3.1 Textural properties of Co/SiO <sub>2</sub> aerogel catalysts .....	65
2.3.2 Structural properties of cobalt species.....	67
2.3.3 Electron microscope.....	71
2.4. SYSTEM DIAGNOSTICS .....	75
SUMMARY .....	79
<b>CHAPTER III. PLASMA-CATALYTIC CONVERSION OF CO AND H<sub>2</sub>.....</b>	<b>81</b>
RESUME DU CHAPITRE .....	81
ABSTRACT .....	82
3.1. INTRODUCTION.....	83
3.2. PLASMA TESTS WITHOUT CATALYST.....	84
3.2.1 H <sub>2</sub> /CO ratio.....	86
3.2.2 Total flow rate.....	88
3.2.3 Frequency.....	90
3.3. PLASMA TESTS WITH CATALYSTS .....	92
CONCLUSION.....	99
<b>CHAPTER IV. PLASMA-CATALYTIC CONVERSION OF CO<sub>2</sub> AND CH<sub>4</sub>...</b>	<b>101</b>
RESUME DU CHAPITRE .....	101
ABSTRACT .....	102
4.1. INTRODUCTION.....	102
4.2. EXPERIMENTAL .....	105
4.2.1 Preparation of Fe/SiO <sub>2</sub> aerogel catalysts.....	105

4.2.2 <i>Experimental analysis</i> .....	107
4.3. RESULTS AND DISCUSSION .....	109
4.3.1 <i>Characterization of catalysts</i> .....	109
4.3.2 <i>Thermodynamic equilibrium calculation</i> .....	116
4.3.3 <i>Plasma experiments without catalysts</i> .....	118
4.3.4 <i>Plasma experiments with catalysts</i> .....	124
4.4. SUMMARY .....	131
<b>CHAPTER V. DIRECT SYNTHESIS OF LIQUID CHEMICALS AND FUELS FOR CO<sub>2</sub> AND CH<sub>4</sub>.....</b>	<b>133</b>
RESUME DU CHAPITRE .....	133
ABSTRACT .....	134
5.1. INTRODUCTION.....	135
5.2. EXPERIMENTAL AND MATERIALS .....	137
5.2.1 <i>HZSM-5 and Co or Fe doped zeolite catalysts</i> .....	137
5.2.2 <i>Experimental configuration</i> .....	138
5.3. CHARACTERIZATION OF ZEOLITE CATALYSTS.....	141
5.3.1 <i>N<sub>2</sub> adsorption/desorption</i> .....	141
5.3.2 <i>X-ray diffraction</i> .....	142
5.3.3 <i>X-ray photoelectron spectroscopy</i> .....	144
5.3.4 <i>SEM and TEM</i> .....	147
5.3.4 <i>TG analysis</i> .....	150
5.4. PLASMA EXPERIMENTS .....	152
5.4.1 <i>Effects of packing zeolite</i> .....	152
5.4.2 <i>Composite catalysts and packing method</i> .....	155
5.4.3 <i>Effects of CO<sub>2</sub>/CH<sub>4</sub> ratio on the performance of composite catalysts</i> .....	164
5.5. SUMMARY .....	172
<b>CHAPTER VI. CONCLUSION AND FUTURE PERSPECTIVES .....</b>	<b>174</b>

CONCLUSIONS ET PERSPECTIVES D'AVENIR .....	174
6.1. COMPARISON WITH LITERATURE.....	176
6.1.1 Plasma-catalytic conversion of CO with H <sub>2</sub> .....	177
6.1.2 Plasma-catalytic conversion of CO <sub>2</sub> with CH <sub>4</sub> .....	178
6.2. CONCLUSIONS .....	181
6.2.1 Plasma-catalytic FTS.....	181
6.2.2 Plasma-catalytic conversion of CO <sub>2</sub> with CH <sub>4</sub> .....	183
6.3. FUTURE PERSPECTIVES AND RECOMMENDATION .....	186
<b>REFERENCES.....</b>	<b>188</b>
RELATED PUBLICATIONS: .....	204

# Nomenclature

## Abbreviations

FTS, Fischer-Tropsch Synthesis;

BTL, Biomass To Liquids;

GTL, Gas To Liquids;

WGS, Water Gas Shift Reaction;

RWGS, Reverse Water Gas Shift Reaction;

NTP, Non-thermal Plasma;

DBD, Dielectric Barrier Discharge;

DMR, Dry Methane Reforming;

SSITKA, Steady State Isotopic Transient Kinetic Analysis;

HV, High Voltage;

BET, Brunauer-Emmett-Teller;

BIH, Barrett-Joyner-Halenda;

IUPAC, International Union of Pure and Applied Chemistry;

XRD, X-Ray Diffraction;

NIST, National Institute of Standards and Technology;

PDF, Powder Diffraction File;

FWHM, Full Width at Half Maximum;

XPS, X-Ray Photoelectron Spectroscopy;

SEM, Scanning Electron Microscope;

TEM, Transmission Electron Microscope;

STEM, Scanning Transmission Electron Microscopy;

HRTEM, High-resolution Transmission Electron Microscopy;

EDS, Energy-dispersive X-Ray Spectroscopy;

EDX, Energy-dispersive X-ray;

GIF, Gatan Imaging Filter;

HAADF, High-angle Annular Dark-field Imaging;

FCC, Face-centered Cubic;

CCD, Charge-coupled Device;

DRIFTS, Diffuse Reflectance Infrared Fourier Transform Spectroscopy;

NMR, Nuclear Magnetic Resonance Spectroscopy;

TGA, Thermogravimetric Analysis;

FT-IR, Fourier-transform Infrared Spectroscopy;

GC, Gas Chromatography;

MS, Mass Spectrometry;

GC-MS, Gas Chromatography-Mass Spectrometry;

Rt-Molsieve, fused silica PLOT column;

Rt-Q-Bond, fused silica PLOT column;

TCD, Thermal Conductivity Detector;

P75W20, polyethoxydisiloxane;

APTES, (3-Aminopropyl) triethoxysilane;

HMDZ, hexamethyldisilazane;

BE, Binding Energy;

SIE, Specific Input Energy;

EE, Energy Efficiency;

C<sub>x</sub>, hydrocarbon molecular including x carbon atoms;

MTHC, Methanol to Hydrocarbons;

HHV, High Heating Value;

LHV, Low Heating Value;

CB, Carbon Balance;

EC, Energy Cost;

## Symbols

$i$ , current;

$Q$  and  $q$ , charge;

$U$  and  $V$ , voltage;

$V_{pp}$ , peak-to-peak voltage;

$R$ , resistance;

$C$ , capacitance;

$L$ , inductance;

$E_a$ , activation energy;

$P$ , power;

$W$ , energy;

$x_n$ , conversion rate of reactant  $n$ ;

$x_{total}$ , total conversion rate of reactants;

$S_n$ , selectivity to product  $n$ ;

$S_{CH_4/CO}$ , selectivity of  $CH_4$  to  $CO$ ;

$E_n$ , energy efficiency of reactant  $n$ ;

$Y_n$ , yield of product  $n$ ;

$R$ , ratio of unsaturated hydrocarbons/saturated hydrocarbons;

$Err$ , experimental uncertainties;

$E_{total}$ , total energy efficiency;

# Résumé en Français

Le réchauffement planétaire lié à l'accumulation continue de gaz à effet de serre dans l'atmosphère au cours des derniers siècles, constitue l'un des problèmes les plus critiques des sociétés modernes. La surexploitation de combustibles fossiles tels que le charbon et le pétrole a conduit à l'émissions d'énormes quantités de CO<sub>2</sub> dans l'atmosphère et a intensifié de manière considérable l'effet de serre atmosphérique naturel, provoquant un important réchauffement planétaire et un dérèglement climatique dont les conséquences pourraient s'avérer dramatiques pour l'avenir même de l'humanité.

D'un autre côté, la demande mondiale en combustibles fossiles, en particulier de pétrole, ne cesse d'augmenter chaque année. Dans ce contexte, la production d'hydrocarbures synthétiques liquides (et d'oxydes d'hydrocarbures) à partir de matière renouvelable (biomasse, déchets) ; de CO<sub>2</sub> ; de méthane (gaz naturel ou biogaz) via les procédés BTL (*Biomass To Liquids*) ou GTL (*Gas To Liquids*), pouvant éventuellement être associés à des installations de captage du CO<sub>2</sub>, suscitent un intérêt croissant dans la plupart des pays industrialisés.

En parallèle, de nombreuses recherches sont en cours pour la capture du CO<sub>2</sub> sur des sites industriels centralisés (centrales thermiques, pétrochimie, cimenteries, sidérurgie,...). Dans ce contexte, la rétro-conversion du dioxyde de carbone et la synthèse Fischer-Tropsch (FTS) pourraient, dans l'avenir, jouer un rôle majeur pour la production de carburants liquides « faiblement carbonés ».

Le méthane, est un gaz à effet de serre qui existe dans la nature (gaz naturel, biogaz). De grandes quantités de CH<sub>4</sub> (notamment dans les champs de gaz associé au pétrole) restent inexploitées et sont gaspillées, souvent directement brûlées (torchées) en raison des difficultés de stockage et des coûts de transport.

Au cours du siècle dernier, de nombreux efforts ont été consacrés à l'étude de la conversion de Méthane en produits liquides à plus forte valeur ajoutée et ainsi de

surmonter les inconvénients liés au stockage et au transport.

Dans ce contexte, en « consommant » de deux gaz à effet de serre, le reformage catalytique à haute température, du  $\text{CH}_4$  au  $\text{CO}_2$  qui permet de produire du gaz de synthèse (mélange  $\text{CO}/\text{H}_2$ ) connaît un regain d'intérêt par rapport à d'autres méthodes de reformage telles que le reformage à la vapeur (*steam reforming*). De plus, la synthèse Fischer Tropsch (FTS), permet de transformer le gaz de synthèse en hydrocarbures liquides, et autres composés oxygénés organiques à forte valeur ajoutée. La combinaison de ces deux techniques pourrait constituer une solution réaliste au recyclage du  $\text{CO}_2$  anthropique et à la diversité énergétique pendant la période de transition actuelle.

La molécule de  $\text{CO}_2$  est bien connue sur le plan thermodynamique et son activation nécessite l'apport d'une importante quantité d'énergie. Ainsi, le reformage du  $\text{CO}_2$  et du  $\text{CH}_4$  (couramment appelé reformage à sec) nécessite un important apport d'énergie ; des températures élevées (supérieure à  $600\text{ °C}$ ), et l'ajout de catalyseurs spécifiques.

Le plasma, en tant que milieu fluide chimiquement actif, est maintenant largement utilisé dans de nombreux domaines industriels tels que : revêtements, gravure, traitement de surfaces, synthèse de matériaux, destruction de déchets, traitement des gaz, synthèse chimique, soudage, découpage... Il offre un moyen unique et attrayant pour activer et déclencher certaines réactions chimiques et apporter de l'énergie à un processus endothermique. Les plasmas peuvent facilement être générés par apport d'énergie électrique (en appliquant une tension par exemple) ce qui apparaît particulièrement intéressant pour le futur dans la perspective d'un large déploiement des ENR (solaire, éolien, biomasse) pour la production d'énergie électrique faiblement carbonée. En conséquence, l'utilisation de plasma offre de nouvelles perspectives pour (i) de remplacement des procédés thermiques basés sur la combustion et (ii) le stockage d'énergie électrique renouvelable, qui par nature est intermittente, sous forme de produits chimiques (*Power To X*).

Ainsi, le procédé FTS plasmocatalytique et la conversion directe du CO<sub>2</sub> et du CH<sub>4</sub> en produits liquides de forte valeur ajoutée apparaissent comme des voies prometteuses pour l'utilisation du CO<sub>2</sub> permettant de surmonter certains inconvénients des voies thermochimiques traditionnelles telles que la pression et la température élevées. L'objectif de cette thèse concerne l'étude de la conversion directe du CO<sub>2</sub> et du CH<sub>4</sub> en produits liquides de forte valeur ajoutée par un procédé plasma-catalyse.

Après un premier chapitre introductif, le Chapitre II est consacré à la description et au diagnostic électrique du banc d'expérimentation. Tout d'abord, nous avons mis en place un réacteur plasma à barrière diélectrique (DBD) tubulaire avec ses appareils d'analyse physiques et chimiques. Le réacteur DBD comprend deux électrodes en configuration coaxiale, un tube en céramique diélectrique et deux bouchons ajustables aux extrémités. Un catalyseur solide se présentant sous la forme de granules catalyseur/support vient remplir l'espace inter-électrode entre l'électrode interne et le tube diélectrique. La puissance électrique est fournie par un générateur à courant variable. La puissance injectée dans le plasma DBD est calculée via la méthode de Lissajous en plaçant une capacité en série avec le réacteur. Les produits gazeux sont analysés en ligne par Chromatographie en phase Gazeuse (GC). Les liquides sont séparés des gaz par un piège à eau glacée, puis ils sont analysés hors ligne via un Chromatographe en phase Gazeuse couplé à un spectromètre de masse (GC-MS). Il est important de noter que des sondes de température et de pression, situées à l'entrée et à la sortie du réacteur, enregistrent température et pression avant et pendant décharge, afin de calibrer les résultats de conversion et sélectivité. Pour cerner les caractéristiques électriques du réacteur, des décharges ont d'abord été générées sous une atmosphère gazeuse inerte pour la caractérisation. L'aérogel de silice utilisé comme support de catalyseur avec la zone spécifique élevée a été préparé via un procédé de séchage à l'air ambiant après traitement de surface par HMDZ afin d'obtenir des surfaces spécifiques importantes et une hydrophobicité. Le catalyseur

Co a été synthétisé par deux procédés différents pour étude comparative : un procédé d'imprégnation et un procédé sol-gel via précurseur. Les différentes qualités de catalyseur Co obtenues ont été caractérisées par diverses méthodes.

Le chapitre III est consacré à l'étude expérimentale de la synthèse d'hydrocarbures à partir de gaz de synthèse par plasma non-thermique associé à de la catalyse hétérogène. Remplacer une synthèse thermo-catalytique à haute pression de type Fischer-Tropsch par une synthèse plasmocatalytique à pression atmosphérique pourrait conduire à un gain d'énergie pour la production d'hydrocarbures et d'oxydes organiques synthétiques. La première partie de ce chapitre est consacrée à la conduite d'essais de synthèse à partir de gaz de synthèse par plasma seul (sans catalyseur), à pression atmosphérique. Ces essais ont été réalisés à différents débits de gaz de synthèse, de rapports H<sub>2</sub>/CO et de fréquence d'excitation du plasma, afin d'évaluer l'efficacité du plasma seul. Puis, la deuxième partie du chapitre présente les essais avec l'ajout de cobalt comme catalyseur sur support d'aérogel de silice, dans une configuration de réacteur rempli. Les résultats indiquent que des quantités considérables d'hydrocarbures C1-C5 ont été synthétisées dans des conditions ambiantes avec des énergies d'entrée spécifiques relativement basses (inférieures à 18 kJ/l). De plus, le catalyseur Co sur support d'aérogel de silice semble favoriser non seulement la synthèse d'hydrocarbures C2-C5, mais aussi la formation d'oxydes organiques liquides. Les catalyseurs cobalt obtenus par procédé d'imprégnation avec un précurseur de nitrate (présenté en chapitre 2) ont montré une excellente performance catalytique dans cette configuration de réacteur. Sur la base des connaissances existantes sur le sujet, des voies de réaction possibles sont alors proposées. Les résultats obtenus dans ce chapitre démontrent au final qu'une nouvelle approche de synthèse organique à partir de syngaz est possible, en alternative à la synthèse Fischer-Tropsch traditionnelle.

Le chapitre IV aborde l'étude de la conversion plasmocatalytique directe à pression et température ambiantes de CO<sub>2</sub> et CH<sub>4</sub> en produits liquides (hydrocarbures,

alcools, cétones, etc.) et gaz de synthèse. Pour cela le même réacteur rempli a été utilisé, testé avec différents catalyseurs sur support d'aérogel de silice (Co et Fe) et pour différents rapports  $\text{CO}_2/\text{CH}_4$ . Là encore la même démarche que le chapitre précédent a été suivie, à savoir une série d'essais en plasma seul, puis une avec introduction du catalyseur sur son support d'aérogel. La performance des catalyseurs en couplage plasmocatalytique a ainsi été évaluée. Selon les conditions opératoires, la sélectivité globale en CO et  $\text{H}_2$  peut atteindre respectivement 75% et 50%, les taux de conversion du  $\text{CO}_2$  et du  $\text{CH}_4$  environ 30% et 43%. Il est constaté que le rapport  $\text{CO}_2/\text{CH}_4$  affectait de manière significative les taux de conversion et la distribution des produits finis. Peu de liquides sont produits sans catalyseur, le catalyseur favorise clairement la synthèse de produits liquides. De plus, le support d'aérogel augmente les taux de conversion des réactifs et améliore légèrement la sélectivité vis-à-vis des produits liquides. La sélectivité en produits liquides peut atteindre jusqu'à 40% avec catalyseur sur support d'aérogel. Les principaux produits liquides étant le méthanol et l'acide acétique. En faisant varier les taux de  $\text{CH}_4$  et de  $\text{CO}_2$  en couplage plasmocatalytique nous produisons un petit nombre d'hydrocarbures à longue chaîne (hexane, heptane) mais aussi d'alcools (hexanol). La synergie positive de la catalyse et du plasma pour la conversion du  $\text{CH}_4$  et  $\text{CO}_2$  semble ainsi démontrée. Cela représente de façon évidente un potentiel pour la synthèse directe de produits chimiques liquides à valeur industrielle et de carburants à partir de  $\text{CO}_2$  et de  $\text{CH}_4$ .

Le chapitre V est dédié à l'étude de la synthèse directe de produits liquides à partir de  $\text{CO}_2$  et  $\text{CH}_4$  à l'aide du réacteur plasmocatalytique du chapitre précédent dans lequel il a été introduit non pas un catalyseur mais deux en même temps. Des combinaisons simples ou mixtes sont ainsi effectuées et testées parmi les matériaux suivants : Co, Fe,  $\text{SiO}_2$  et HZSM-5. Les catalyseurs sont disposés dans le réacteur sous forme de granules mixtes (préparés par dopage/imprégnation) ou simples, mélangés ou séparés (configuration double lits). Les résultats semblent montrer que l'association sous forme de granules mixtes Co/HZSM-5 est particulièrement

favorable à la conversion directe de CO<sub>2</sub> et CH<sub>4</sub> en produits liquides à longue chaîne. L'association sous forme de granules mixtes Fe/HZSM-5 permet de son côté d'obtenir lorsque la proportion de CO<sub>2</sub> est élevée une sélectivité importante vis-à-vis du méthanol. L'association en configuration double lits de granules Fe / aérogel de silice et de granules de HZSM-5 permet quant à elle, lorsque la proportion de CH<sub>4</sub> est élevée, d'atteindre une importante sélectivité vis-à-vis de l'acétique acétique. La synergie positive entre la combinaison de deux catalyseurs et du plasma pour la production de produits liquides à partir de CO<sub>2</sub> et CH<sub>4</sub> est ainsi démontrée.

Pour résumer, cette thèse a initié une première étude complète sur : (i) d'une part, la synthèse Fischer-Tropsch et (ii) d'autre part, la conversion directe du CO<sub>2</sub>/CH<sub>4</sub>, par la voie plasmocatalytique en conditions de pression et température ambiantes. Tandis que la synthèse Fischer-Tropsch plasmocatalytique ne permet pour l'heure de produire de chaînes carbonées supérieures à C<sub>4</sub>, la conversion plasmocatalytique du CO<sub>2</sub>/CH<sub>4</sub> montre elle un remarquable potentiel pour la production de composés liquides : alcools, acides carboxyliques et hydrocarbures à longue chaîne C<sub>5</sub>+. Dans ce dernier cas, le passage à l'emploi simultané de deux catalyseurs à la place d'un seul permet de manipuler la distribution des produits liquides tout en améliorant la sélectivité vis-à-vis des hydrocarbures à longue chaîne et le taux de conversion global du CO<sub>2</sub>/CH<sub>4</sub>. Les travaux de cette thèse démontrent ainsi la faisabilité d'une conversion plasmocatalytique efficace d'un mélange CO<sub>2</sub>/CH<sub>4</sub> en carburants de synthèse ou molécules nobles. Sur la base de nos travaux et en perspective des travaux futurs, quelques recommandations peuvent être finalement émises dont la nécessité de :

1. Optimiser la source de plasma afin de mieux contrôler l'énergie spécifique injectée et l'élévation de la température électronique. Cela passe en grande partie par l'évolution de l'alimentation électrique et davantage d'accord avec la décharge.

2. Améliorer les catalyseurs : lien plus fort entre le catalyseur et son support, meilleurs aérogels et meilleurs couches catalytiques en termes de porosité et

structuration, nouvelles combinaisons catalytiques, étendre la gamme métallique des catalyseurs, l'emploi simultanée de plusieurs catalyseurs, introduction de promoteurs tels que des métaux alcalins...

3. Compléter l'étude de l'influence de la stœchiométrie du gaz réactif sur la conversion et les produits.

4. Etudier l'effet d'une dilution du gaz réactif dans un gaz plasmagène inerte.

5. Enfin, tenter de modéliser la chimie en phase plasma puis la conversion plasmocatalytique dans son ensemble en cherchant à savoir s'il y a une interaction directe entre le plasma et le catalyseur.

# Chapter I. Introduction

## 1.1. Background

In recent centuries, global warming due to the continuous accumulation of greenhouse gases in the atmosphere has been one of the most critical issues. The overuse of fossil fuels such as coal and oil, have contributed to the excessive emission of CO<sub>2</sub> and mightily intensified the atmospheric greenhouse effect and climate change, causing global warming according to the statistical data from International Energy Agency (IEA) (Figure 1-1) [1]. However, the demands of fossil fuels, especially oil production, continue increasing with each passing year, as shown in Figure 1-2 [2]. Under this context, the synthetic hydrocarbons and hydrocarbon oxides produced from biomass, CO<sub>2</sub>, natural gas, biogases and wastes through BTL (Biomass To Liquids) or GTL (Gas To Liquids) process integrated with CO<sub>2</sub> capture have drawn significant interests for researchers in recent years.

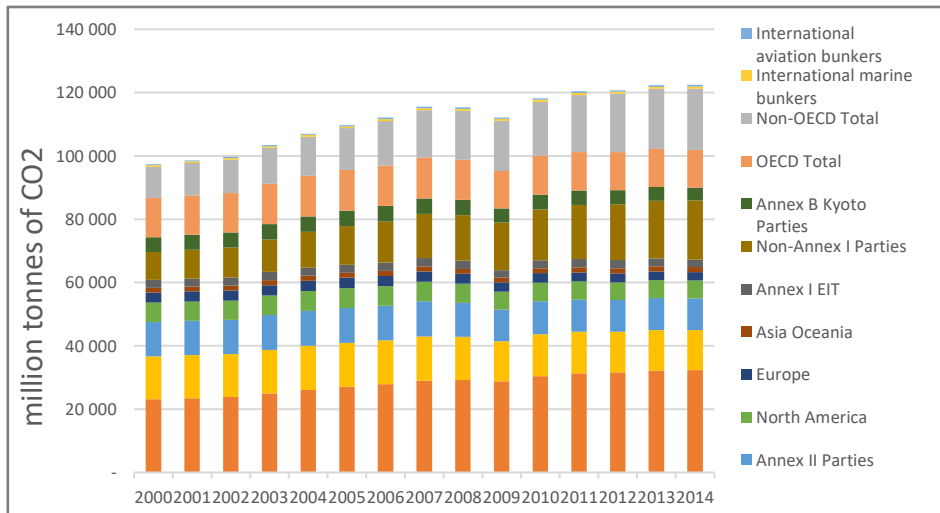


Figure 1-1. CO<sub>2</sub> emission by the combustion of fossil fuel from 2000 to 2014 [1].

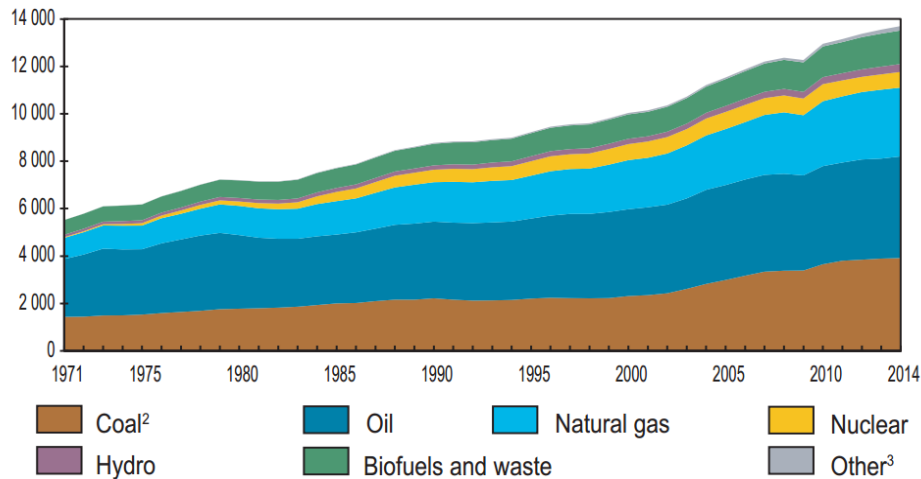


Figure 1-2. World total primary energy supply (TPES) from 1971 to 2014 by fuel (Mtoe) [2].

Carbon capture and storage (CCS) is the process of capturing waste CO<sub>2</sub> usually from the use of fossil fuels in electricity generation and industrial processes, such as cement factories, oil refinery plants or biomass power plants, transporting it to a storage site, and then depositing it usually under an underground geological formation. Until now, abundant efforts have been made in the technique of CCS and other the related fields and techniques of BTL or GTL during recent decades. Since time has mellowed them, the installation of CO<sub>2</sub> capture devices has been more and more frequent in the industrial field especially in thermal power plants and natural gas processing as the statistics data shown in Figure 1-3 [3]. However, the subsequent storage of CO<sub>2</sub> after capture has significant drawbacks regarding the high investment, transportation, and uncertainty of long-term storage [4]. Thus, Carbon Dioxide Reforming and Fischer–Tropsch synthesis (FTS) can play a crucial role to sustain liquid fuel consumption and achieve a low carbon economy while avoiding the drawbacks of storage in industries.

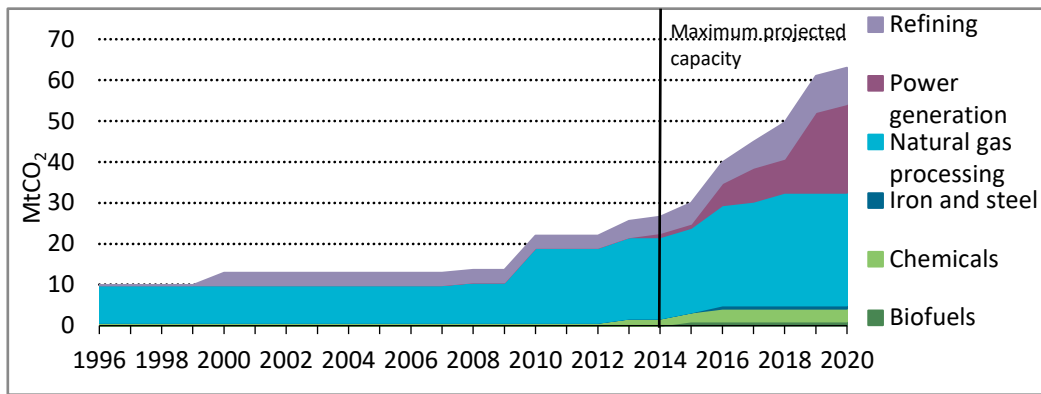


Figure 1-3. Large-scale CO<sub>2</sub> capture projects from 1996 [3].

Methane, as one of the greenhouse gases, is widely existed in nature (such as shale gas, biogas, and oil fields). A large amount of CH<sub>4</sub> is directly combusted due to difficulties of storage in many industries such petroleum industry, oil refinery, and coal industry. Great efforts have been devoted to the study of Methane to Liquid during the past century to produce value-added liquid products and overcome the drawbacks of storage and transportation. Benefitting from the consumption of two greenhouse gases, CO<sub>2</sub> reforming with CH<sub>4</sub>, which is a method to produce syngas products with a catalyst at a high temperature, has become more attractive than other reforming methods such as steam reforming. Moreover, FTS, as a relatively advanced and promising technique, is a process to transform syngas into liquid paraffin, olefins, and another value-added organic oxygenates. The combination of these two techniques could be a feasible solution to anthropogenic CO<sub>2</sub> recycling and energy diversity during the transitional period from the current fossil fuel-based stage to the final sustainable age.

Indeed, the FTS process is typically achieved in two steps by integrating with petroleum industry processes or coal industry processes, where CH<sub>4</sub> and CO<sub>2</sub> can be easily available to satisfy the demand of feedstocks in many plants. The direct utilization and reformation of CH<sub>4</sub> byproducts with CO<sub>2</sub>, who is captured from the exhausted gases or even the atmosphere, is regarded as a feasible and environmentally friendly approach to solve the storage issue meanwhile supplying FTS, achieving the anthropogenic carbon recycling. However, the limitations are evident, including

essential integration with petroleum or coal plants, additional energy consumption, and necessary pretreatments. The CO<sub>2</sub> molecule is well-known thermodynamically stable, and the activation of CO<sub>2</sub> generally requires significant energy consumption. Thus, the reforming of CO<sub>2</sub> and CH<sub>4</sub> generally requires high temperature (more than 600 °C) even with catalysts for a reasonable conversion rate and production. Moreover, external heating (around 150 to 300 °C) and high pressure (around 3MPa in the industrial process) are essential for the chain propagation reactions to produce C5-11 hydrocarbons in FTS process. As a result, the capital invests for the related component, the energy efficiency and consumption are not favorable. Optimization is essential for the whole processes regarding practical, economic, and environmental perspectives.

Plasma, as a group of chemically active media, is now widely applied in the fields of surface coatings, waste destruction, gas treatments, chemical synthesis, machining and etching due to its wide temperature range and high chemical activity. Generally, it offers an attractively unique way to activate and initiate chemical reactions due to its unique features [5]: (1) temperatures of some components in plasmas and energy density can remarkably exceed those in conventional chemical technologies, (2) the concentrations of energetic and chemically active species in plasmas, including electrons, ions, atoms and radicals, excited states, can be extremely high to promote chemical reactions and (3) plasmas are not necessarily generated under thermodynamic equilibrium conditions, thus providing high concentrations of energetic and chemically active species in a very low bulk temperature. Hence, it provides an approach to carry out the CO<sub>2</sub> reforming with CH<sub>4</sub> and FTS under atmospheric pressure without external heating, meanwhile promoting the conversions and energy efficiency. Moreover, plasma can be easily generated by applying electric energy (voltage), where clean and renewable energy resources such as solar, wind, and biomass are sharing more and more in power generation. Due to the 2014 annual energy report of IEA [6], renewables contributed 22.3% to the world

electricity production, and since 1990 the growth rate of renewable electricity generation was on average 3.6% per annum which is a little bit higher than the growth rate of total electricity generation (2.9%). Consequently, applying plasma to reforming following FTS, or even integrating into a process, expands the application of renewable energy and provides a new perspective to store renewable energy in an environmentally friendly way.

## **1.2. A brief introduction to plasma**

Plasma was first introduced by chemist Irving Langmuir in the 1920s [7]. As one of the four fundamental states of matter, plasma is a group of ionized or partially ionized, but electrically neutral gases. The term “ionized” implies that partial electrons are not bound to atoms or molecules, inducing the atoms or molecules into positively charged ions. Instead of association with heating, plasma can be easily generated from gas by applying electric fields, microwave or adiabatic gas compression. This increasing energy of gas molecules leads to a complicated mixture of unbound positive and negative particles and neutral gas components, which are freely moving. The movement of these charged particles generates an electric current within a magnetic field. Subsequently, any movement of a charged particle affects the general electromagnetic field, and in turn, being affected by the electromagnetic field. As a consequence, in a macroscopic view, the equal density of electrons and positive ions make the plasma quasi-neutral; however, in a microcosmic view, the small scale of gaseous groups can be positive or negative which make plasma electrically conductive and internally interactive [5], which distinguishes plasma from regular gas as an insulator. Although under normal surface conditions plasma is almost inexistent, plasma is the most abundant form of ordinary matter throughout the universe and consists of nearly 99% of the observable cosmos including corona and nebula [8]. Plasma occurs naturally, such as lightning storms and aurora, but also can be effectively generated in a laboratory or industry. It has already been widely applied to

multitudinous areas in practice such as thermonuclear synthesis, lasers, fluorescent lamps, surface modification, thin film deposition, plasma coating, pollutant treatment, biochemical technique, chemical synthesis and deposition [9].

The components of plasma include electrons, excited molecules, and atoms, ions, radicals, neutral gas species, and photons. Since ionization is necessary for the existence of a plasma, the term "electron density", as the number of free electrons per unit volume, is a vital parameter. The ionization degree of a plasma is the proportion of atoms or molecules that are positive or negative due to losing or gaining electrons to the neutral gas. Even though a group of partially ionized gas in which as little as 1% of the particles are ionized can behave the remarkable characteristics of a plasma. Based on the degree of ionization, plasma can be classified as entirely ionized plasma and weakly ionized plasma. Like normal gas, the temperature of a plasma depends on the average energies of all the plasma particles and their relevant degrees of freedom (translational, rotational, vibrational, and those related to electronic excitation). Thus, as multi-component systems, plasma exhibit multiple temperatures. According to the temperature difference of plasma components, plasma can be categorized as thermal plasma (or high-temperature plasma, equilibrium plasma) and non-thermal plasma (or low-temperature plasma, non-equilibrium plasma). In a thermal plasma, sufficient applied energy and time for equilibration lead to a plasma discharge that can be specified by a single temperature, as the gas temperature, ion temperature, rotational temperature (rotational degrees of freedom of molecules), vibrational temperature (temperature of vibrational excitation of molecules) and electron temperature are almost uniform and thermal equilibrium, typically exceeding  $10^4$  K. Unlike a thermal plasma, a non-thermal plasma is carried out far from equilibrium conditions, which means different relating plasma species characterize its multiple temperatures. As a result, the electron temperature can be as high as a thermal plasma, while the temperatures of other species such as excited species, ions, and neutral molecules are much lower. Moreover, the temperature of the bulk gas even exhibits as low as room

temperature. The energy level of a non-thermal plasma usually depends on the high energy electrons [10].

The engineering application areas of thermal and non-thermal plasma are very different due to their unique properties. Non-thermal plasmas which are usually generated at low pressures or lower power levels, or in different kinds of pulsed discharge system are more selective while thermal plasmas, which are mainly produced by atmospheric arcs, plasma torches, sparks, and flames, are usually more powerful and exhibit high temperature [11]. Regarding FTS and reforming, the high temperature is theoretically favorable to unexpected coking reactions. Besides, the energy consumption of generating thermal plasma is much higher than that of generating non-thermal plasma. Generally, non-thermal plasma, which is mainly produced by corona discharge, dielectric barrier discharge (DBD), and nanosecond pulsed discharge [11] are more applicative for chemical synthesis.

### **1.3. A review on FTS**

The Fisher-Tropsch process was first introduced and published by two Germany chemists Franz Fischer and Hans Tropsch in 1925 [12]. The technology of FTS has been developed for around ninety years as one of the research focuses. According to Bartholomew's work [13], the first experiments on the catalytic hydrogenation of CO with H<sub>2</sub> were conducted at the beginning of the 20<sup>th</sup> century. In 1902, Sabatier and Senderens [14] firstly succeeded in the synthesis of methane from CO with H<sub>2</sub> and the process was performed through cobalt (Co), iron (Fe) or nickel (Ni) catalysts at temperatures of 473 K and ambient pressure. Shortly in 1913, an improvement of which liquid products were discovered was carried out over cobalt catalysts by BASF SE under very particular conditions. Shortly after that, Hans Fischer and Franz Tropsch reported the Synthol process in 1922, in which oxygenated hydrocarbons were produced by catalytic hydrogenation reaction of CO with H<sub>2</sub> through alkali catalysts at high temperature (near 673 K) and extremely high pressure (more than

100bar). Right after, significant progress was made, they found that when the Synthol process was conducted at around 7 bars, the production of heavy hydrocarbons were detected [15]. In 1925 they successfully improved the process and produced hydrocarbon liquid and solid wax as the main products over Fe/ZnO and Co/Cr<sub>2</sub>O<sub>3</sub> catalysts at much milder reaction conditions. Finally, in 1926, Fisher and Tropsch [12, 15] published the reports about this process of hydrocarbon synthesis, which is lately named as Fisher-Tropsch synthesis. According to their reports, some important conclusions were published:

- 1) FTS typically needs to operate at temperatures of 150-300 °C and pressures of one to several tens of atmospheres to achieve the formation of liquid hydrocarbons.
- 2) Nickel catalysts are more favorable to the production of methane; iron catalysts are generally more active to WGS reaction; cobalt catalysts are more favorable to long-chain hydrocarbons production.

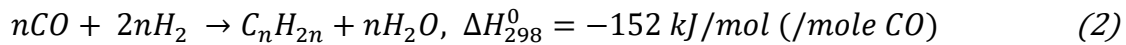
After 1927, researchers found that Co catalyst was more effective than Fe and Ni considering the yield of long-chain hydrocarbons. Then some commercial fixed bed reactors and commercial circulating bed reactors were brought out based on Co catalyst during the 1930s and 1940s, in which coal was used as feedstock to produce syngas were developed [16]. These earliest commercial applications and developments of FTS had provided demonstrations for the future industrial processes. The first large scale industrial FTS plant was established and operated in Germany in 1936. After World War II, the UK and the USA began to show interests in the technique of FTS. Moreover, later in the 1950s, the world-widely perceived shortage of oil had induced many countries to invest in the research and development of FTS. During this period, ARGE (Arbeitsgemeinschaft Ruhrchemie und Lurgi) developed a large-scale fixed bed reactor for FTS. Meanwhile, Kellogg proposed a circulating catalyst bed reactor. Furthermore, in 1955, both the fixed bed and circulating catalyst bed processes were brought out by Sasol in South Africa, which was established as

Sasol One plant. The first oil crisis later in 1973, continued to attract the world's interests on FTS due to the deep anxieties about fuel depletion. From that on, many researchers had devoted to the research of FTS, particularly on the catalysts for FTS and some progress had made on research of the active sites of catalysts structure. These works had provided relevant references for subsequent research in design and preparation of highly active sites density, high surface area and additional metal-doped catalysts, which could improve the higher hydrocarbons selectivity, active period and efficiency. Since the 1980s, the rising concerns of environmental issues and the requirements for energy diversification have propelled vast amounts of investments and progresses on the establishment of FTS programs in many famous petroleum companies such as Shell and Sasol. Generally, the liquid fuels productions obtained from these FTS programs advantageously contained much lower contents of aromatic components and sulfur compared with gasoline and diesel refined from crude oil. However, the distribution of hydrocarbons components and the formation of oxygenates and carbon deposits were still problems. Even though, FTS has been widely considered as a promising Gas To Liquids (GTL) technology whose products are more valuable than refining distillates. Until now, many fuel plants based on FTS technique have been established [17, 18]. In 1993, one of the largest implementations of FTS technology was built up and operated by Shell in Bintulu, Malaysia. The plant converts natural gas into low-sulfur Diesel fuels and food-grade wax through Co catalysts with a scale of 12,000 barrels per day. In 2006, a cooperative program between Qatar Petroleum and Sasol was commissioned with a capacity of 34,000 barrels per day in Ras Laffan, in which a Sasol slurry phase distillate process was utilized through Co catalysts. In 2011, PetroSA brought out semi-commercially demonstrated GTL complexes with a capacity of 36,000 barrels per day in Mossel Bay of South Africa. Moreover, this plant consumes multiple feedstocks, including natural gas, biomass, or coal, to produce synthetic fuels. In 2012, Sasol announced another plan to build an FTS plant of 96,000 barrels daily output in Westlake of

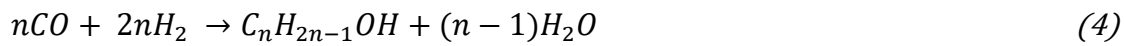
Louisiana, using natural gas obtained from local tight shale formations as feedstock. Recently, another cooperative GTL plant of Shell and Exxon based on FTS technique, whose daily output is estimated as 150,000 barrels, was signed in Qatar. Overall, the technology of FTS has already been mature on an industrial scale and achieved worldwide commercialization after decades of research and development.

### 1.3.1 Main reactions and mechanism of FTS

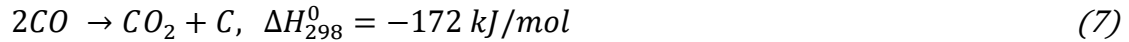
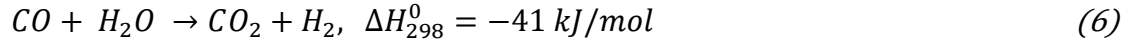
Generally, the FTS process contains two main reactions and several side reactions. The synthesis of long-chain paraffin and olefins with water from syngas are the two main reactions [19-22]:



When H<sub>2</sub>:CO ratio is high or strong hydrogenation catalysts such as cobalt and nickel are used, reaction (1) is dominant. In contrast; on the other hand, when H<sub>2</sub>:CO ratio is low or weak hydrogenation catalysts such as iron are used, reaction (2) is dominant. Except for the two main reactions, the methanation reaction (3), formation of oxygenated hydrocarbons reaction (4) and CO<sub>2</sub> generation reaction (5) could occur depending on the operating conditions and the nature of catalysts:



When using Ni catalysts for FTS, the methanation reaction is more preferential compared with iron or cobalt catalyst, while the iron catalysts are confirmed to be more active to the formation of oxygenated hydrocarbons. Besides, the Water Gas Shift (WGS) Reaction (6) and Boudouard reaction (or CO disproportionation reaction) (7), where CO molecules disproportionate to form CO<sub>2</sub> and surface carbon, are also important side reactions in FTS:



The CO disproportionation reaction is the causation of catalysts deactivation mainly due to the deposition of carbon black on the surface of catalysts, which results in the occlusion of active sites and pore structure. Besides, the unexpected carbon deposition on the reactor mainly obstructs the heat exchange and damages the reactor. Obviously, the possible main reactions in the FTS process are exothermic, and volume reduction, which implies the conversions of the reactants in this process are more affected by pressures than temperatures. It has been reported that the selectivity of C5+ higher hydrocarbons increases with the pressure increasing up to 3 MPa. Moreover, even in a particular range, increasing pressure cannot increase the conversion rates of the reactants, the production rates, and the selectivity towards different products could be improved [23]. Thus, the production distribution of FTS is more sensitive to pressure than temperature, and high pressure is essential to obtain a high selectivity of C5+ liquid hydrocarbons for a conventional FTS process.

As the study on FTS developed in depth, more and more researchers have dedicated to the mechanical aspect and reaction pathway of FTS, while the mechanism of FTS is still regarded as complicated and debated. It has been widely accepted that FTS reactions at least involve a specific procedure including dissociative chemisorption of CO and H<sub>2</sub> in the active sites of catalysts, chain initiation, chain growth, and chain termination. Based on these comprehensions, three widely recognized mechanisms for the activation of reactants and chain initiation are proposed as figures shown [24]: carbene mechanism (Figure 1-4), hydroxyl-carbene mechanism (Figure 1-5) and carbonyl insertion or carbon insertion mechanism (Figure 1-6), where the carbene mechanism is most widely accepted.

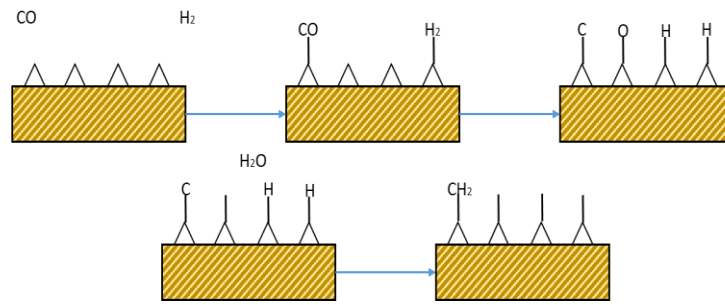


Figure 1-4. Scheme of carbene mechanism [24].

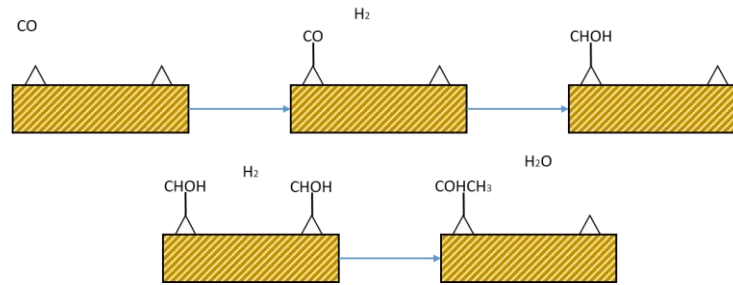


Figure 1-5. Scheme of hydroxyl-carbene mechanism [24].

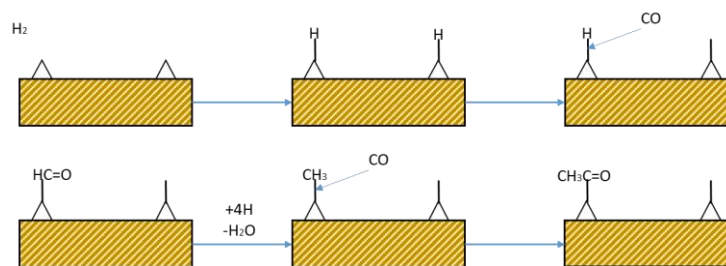


Figure 1-6. Scheme of carbonyl insertion or carbon insertion mechanism [24].

The carbene mechanism initiates when the active sites of catalysts chemisorb  $H_2$  and  $CO$  and disperse on the active sites. After activation, the molecules of  $CO$  and  $H_2$  dissociate to form metal carbide, metal oxide and metal hydride on the surface. Then the metal oxide may react and combine with another molecule of activated  $H_2$  to produce hydroxyl group, which could be hydrogenated into water molecule then desorbed by catalysts. Meanwhile, the metal carbide can react with the vicinal activated hydrogen to produce the methylene groups, which is called the chain initiation process as the methylene groups are responsible for the propagation of long-chain hydrocarbons.  $CO_2$  desorbed by catalyst could be produced initially from the reaction of metal oxide and activated  $CO$ . For the hydroxyl-carbene mechanism, the

processes initiate with the chemisorption of CO molecules. H<sub>2</sub> molecules in the atmosphere react with these sorbed CO molecular to form the carbinol groups. Then two vicinal carbinol groups can react with additional H<sub>2</sub> molecules in the atmosphere to form long-chain oxygenates with desorbed water. The carbonyl or carbon insertion mechanism begins with the chemisorption and dissociation of H<sub>2</sub> molecules at first. Then CO molecule could insert into the metal hydride to form formyl groups. After that, these formyl groups react with the H<sub>2</sub> molecules in the atmosphere, meanwhile losing water molecules to form a methyl group, which is the chain initiation. Then the insertion reaction continues to result in chain growth.

Figure 1-7 and Figure 1-8 illustrate the chain growth process and chain termination process of FTS [19]. The formation of a methylene group is regarded as the chain initiation process, and it is widely accepted that the methylene group mainly takes responsibilities for chain growth. According to this mechanism, many researchers and publications defined the groups, which contribute most to chain propagation as -CH<sub>x</sub> pool or -CH<sub>2</sub> pool. As shown in Figure 1-7, methylene groups combine with vicinal methylene groups, growing from the end to propagate the chain. Figure 1-8 describes the three main steps of the chain termination process. A hydrocarbon chain can be directly hydrogenated with H<sub>2</sub> then desorbed. Besides, two vicinal chains can react and combine. Two possible reaction routes are proposed, one is an interaction between two chains to produce one H<sub>2</sub> molecular and two olefins molecular, the other one is an interaction between one chain and the other (or methyl) to produce one olefin and one paraffin (or methane).

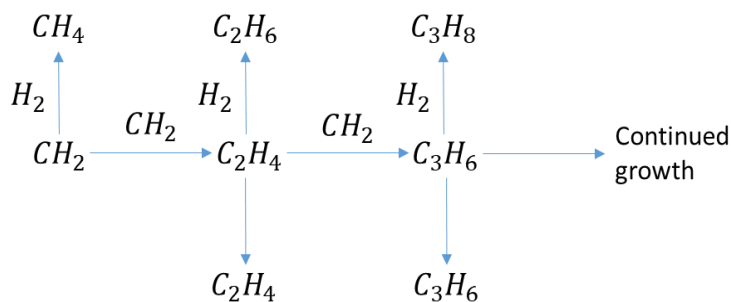


Figure 1-7. The chain growth process of F-T synthesis [19].

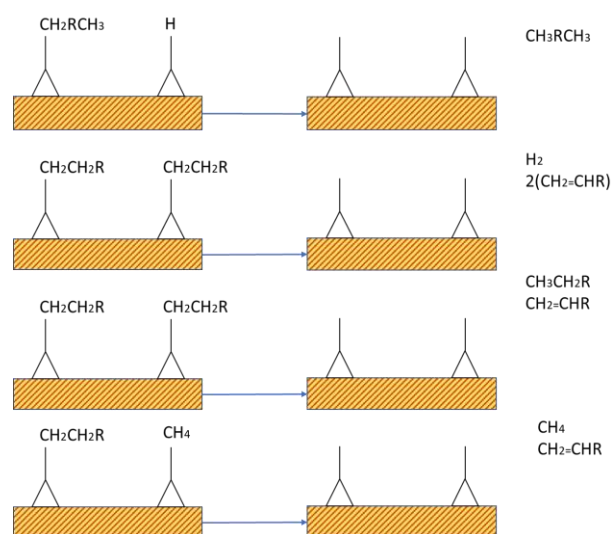


Figure 1-8. Chain termination process of F-T synthesis.

Although these mechanisms are very illustrative, there are still some debates and confusions about the in-depth mechanism of F-T reaction. During recent decades, steady state isotopic transient kinetic analysis (SSITKA) and quantum chemistry simulation have helped researchers to get better comprehensions on the detailed mechanism of FTS. Charles et al. [25] have done some SSITKA study on the chain growth process of FTS. They found direct evidence supported for a rapid chain growth, which was even much faster than the activation of CO on the surface of catalysts during FTS. This process appeared to require a rapid formation of monomers within diffusion distances of growing chains [25]. This conclusion was different from previous ideas that chain growth is a relatively slow process in FTS. Later, Frøseth's research [26] and Yang's works [27] showed good coincidence with the conclusion. Furthermore, it has been reported that a remarkable high energy barrier ( $\sim 250$  kJ/mol) was observed for the direct dissociation of C-O band on catalysts due to some publications of density functional theory simulation on FTS [28-32]. Theoretically, directly cleaving the C-O band was very difficult and unfavorable on the view of energy threshold during chemisorption. Therefore, the practical process of CO activation and dissociation is considered more complicated than previous ideas. Later a new pathway for the cleavage of C-O, which is called H-assisted route was

proposed. More and more evidence derived from experimental data and theoretical simulations showed that this pathway was more favorable during FTS process. Figure 1-9 derived from Manuel Ojeda's work [29] demonstrated the individual energy barriers for every elementary step of CO dissociation and combination with other radicals on the surface of Co catalysts with 0.5 ML CO coverage. Apparently, the energy penalty of H-assisted pathway was lower than that of CO direct dissociation. These works implied that there should be two primary pools for the chain initiation:  $\text{CH}_x$  pool and  $\text{CH}_2\text{O}$  pool, all of which took the responsibilities for the following chain growth.

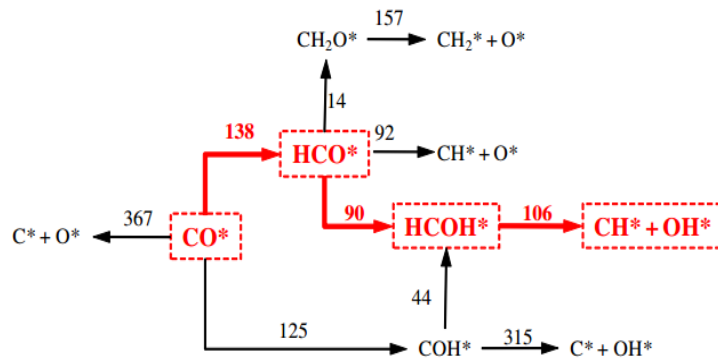


Figure 1-9. Individual energy barriers for elementary steps of CO the scission in the surface of Cobalt catalyst with 0.5 ML CO coverage by Manuel Ojeda [29].

According to these conclusions, one possible reaction pathway for H-assisted dissociation of CO is put forward:



In these reactions, \* indicates an active site of catalysts. Clearly, in H-assisted

dissociation pathway, the CH group can react with H to form CH<sub>2</sub> group, which is the critical group for chain growth. So according to these works on the aspect of FTS mechanism, some important conclusions can be summarized:

- 1) Two common pools of monomer units (-CH<sub>2</sub> and -CH<sub>2</sub>O) on the surface of catalysts that are responsible for the synthesis of hydrocarbons during FTS process.
- 2) Nature of catalysts, process conditions, and gas feed compositions that suppress hydrogen coverage favor the generation of long hydrocarbon chains.
- 3) FTS reactions are susceptible to the nature of catalysts due to the promotion to different pathways with different energy barriers for CO dissociation.
- 4) Catalysts also significantly affect the final distribution of product compositions.

### **1.3.2 Catalysts for FTS**

As catalyst played a vital role in FTS due to its significant influences on the final product distribution, the later study on FTS was mainly focused on developing new and potent catalyst with its support. The general properties and principles which should consider are affordability, high activity, high selectivity to high hydrocarbons, and stable performance. Thus, the most critical variables of FTS catalysts are the selection of the metal precursor quantity of metal loading, selection of supports, and preparation with pretreatment methods. It has been widely reported that all metals of group VIII and some other alkali metals such as copper, zinc, and rhenium have noticeably catalytic activity for FTS reactions [33]. Initially, Fisher and Tropsch had studied the performance of a Fe-Cu catalyst. Later more and more noble and non-noble catalysts were used and studied for FTS, among which ruthenium, iron, nickel, and cobalt were considered the most effective catalysts for the hydrogenation of carbon monoxide considering the performance and economic perspective. Currently, researchers mainly focused on the developments of Co and Fe-based catalysts due to their high activity, high stability and good selectivity rather than Ni, which is

considered extremely active to methanation or Ru, which is too expensive and not economical to industrial scale. Regardless of price, Co is found almost three times more active in the view of site basis than Fe due to some chemisorption analysis [34]. Moreover, Fe is highly active to WGS Reaction, which is undesirable during FTS and leads to the formation of the oxygenated hydrocarbons [35-37]. On the other hand, even cobalt catalysts do not exhibit significant WGS activity [37], water seems to have some positive effects on FTS process and the activity of cobalt catalysts depending on catalyst composition, nature of the support, catalyst preparation method and pretreatment [38]. Table 1-1 [39] shows a brief comparison between Co and Fe catalysts. Besides, both Co and Fe catalysts are extremely sensitive to sulfur, leading to contamination and deactivation. It has been reported that the sulfur components in the feed gas should be less than 0.1 ppm. Although Co catalysts are more active to methanation reaction at high temperatures than Fe catalysts, the selectivity towards C5+ hydrocarbons is remarkably 20%-30% more when using Co catalysts at relatively low temperatures. In total, because of the high hydrocarbon productivity, high stability, high conversion rate, cobalt catalysts are currently one of the most optimal and practical catalysts for the synthesis of C5+ hydrocarbons in FTS process and will continue to concentrate researchers' focuses in the future.

Table 1-1. A brief comparison between Co and Fe catalysts [39].

parameter	cobalt	iron
cost and lifetime	expensive but excellent resistance to deactivation	Cheap but short lifetime, easy to deactivation (coking, etc.)
activity	higher activity and selectivity to F-T synthesis	lower activity and selectivity to F-T synthesis
WGS activity	not significant	high activity to WGS reaction
methanation activity	high activity to methanation reaction under high temperature	low activity to methanation reaction especially under 350 °C

flexibility

more sensitive to reaction  
condition, fewer flexibilities

less sensitive to reaction  
condition, more flexibilities

---

Despite the catalysts, some researchers focused on the development of supports for catalysts. Active metallic catalysts deposited on higher surface area supports usually have higher contact area with the reactants, thus leading to more active sites for FTS reactions. It has also been widely reported that the structure of support affects the catalytic performance of catalysts due to its direct or indirect influences on the crystallite size, distribution, reduction, crystal structure of metal catalysts. Also, the diffusion behavior of the important reactive species in FTS process such as H is altered when introducing supports depending on their transport length, pore size, which could lead to a higher diffusion rate and contribute to the promotion of main reactions. Therefore, the design of supports is an essential part of the design of catalysts. Silica, alumina, and titania are the most common supports for Co catalysts.

Silica-supported cobalt catalysts, particularly silica aerogel supported cobalt catalysts, in general, exhibit high catalytic activity and liquid hydrocarbon selectivity in FTS process. Some notably physical and chemical properties of silica aerogel have been studied and confirmed to favor the main reactions of FTS such as: (i) high surface area which makes moderately high Co dispersion at relatively high loadings of Co [40-42], (ii) controllably wide range of pore size which ensures an excellent diffusion of gas components, and (iii) adjustable surface chemistry property which enables a high reducibility of metal [43]. Li et al. [44, 45] have researched the catalytic effects of Co loaded MCM-41, SBA-15, and SiO<sub>2</sub> with different pore size. Their works showed that the mesoporous structure of SiO<sub>2</sub> support could contribute to a moderate cobalt particle size and the highest dispersion of cobalt, which led to a high hydrogenation activity of CO. These results were in a good coincidence with Saib's research [46]. Iglesia [47] has shown that water molecules, whether indigenous or additionally added to feeding reactants, increased the reaction rates of the reactants on Co/SiO<sub>2</sub> catalysts. Furthermore, Li and Iglesia [48] again investigated the positive

effects of water on the CO conversion, olefin, and C5+ selectivity for silica-supported Co catalysts. The results complied with Das and his co-workers' researches [49], in which they suggested that the addition of water in FTS process over a 12.4% Co/SiO<sub>2</sub> (wt.%) catalyst led to a significant increase in CO conversion. Recently, Gunasooriya et al. [50] have investigated the possible elementary reactions based on Co catalysts in FTS process by DFT simulation. Their works revealed that surface hydroxyl groups on Co catalysts are found to be potent hydrogenating species for the conversion of CO during FTS process, which is accordant with the H-assisted dissociation mechanism mentioned above. Dunn et al. [51-55] have reported a series of researches on silica aerogel and xerogel supported nanocrystal Co catalysts for FTS process. They found all their mesoporous Co loaded silica aerogel catalysts were very active to the main reactions of FTS with good selectivity towards the C10+ hydrocarbons. Danilo et al. [56] found that silica aerogel supported bimetallic Fe and Co nanocrystal catalysts have significantly high dispersion of metals and high thermal stability, which led to a remarkably high CO conversion (as high as 87%) at 200 °C. Besides, some researchers [46, 57-60] have revealed that the surface hydroxyl groups on the surface of silica formed during the preparation process could react with cobalt oxide to form cobalt hydroxide, which is extremely hard to be reduced. This negative interaction was also found common among the other catalysts with supports. However, for silica aerogel, it is possible to modify the hydrophobic surface property by introducing a hydrophobic group during preparation [61, 62].

Alumina and titania are also typical supports for FTS catalysts due to their high surface area, pore structure, and high dispersion of metals. Commonly,  $\alpha$ -alumina and titania exhibit lower acidity than  $\gamma$ -alumina, which is assumed to be the reason for higher wax selectivity [63]. It was also widely accepted that the Brønsted acid sites should be more active than Lewis sites not only to FTS process, but also many other catalytic processes. However, to determine the kind of acid sites was not easy during preparation. Unlike SiO<sub>2</sub> supports, hydrophobic modification of alumina and titania,

which results in the formation of difficultly reductive metal oxides. Moreover, it was found that in most cases a hydroxyl group in alumina supported catalysts played a negative role [64, 65] and water weakly affected the rate and selectivity of titania supported catalysts at high water concentrations [38, 48, 66]. Above all, Co loaded hydrophobic silica aerogel could be a very promising catalyst for FTS.

As FTS process has been successfully industrialized, Table 1-2 listed some of the applied industrial FTS processes since the 1930s with their applied technologies, reactors and catalysts [67]. The applied conditions of these processes varied from normal pressure (1 atm) and low temperature (< 250 °C) to high temperature (> 320 °C) and high pressure (up to 100 bar). With the in-depth of research, the later study and appliance are focused on the low-temperature or medium-temperature (~ 270 °C) but high-pressure processes to reach a considerable selectivity towards liquid paraffin and olefins. Variety types of FT reactor have been successfully carried out to industrial FTS process, including fixed bed, fixed or circulating fluidized bed, slurry bubble column, and so on. In industrial scale, Co and Fe are the most widely applied catalysts for not only hydrocarbon synthesis, but also the production of synthol.

Table 1-2. Industrial FTS processes since 1930s [67].

FT technology	FT type	FT reactor	FT catalysts	Built year
Normal-pressure synthesis	Low temperature	Fixed bed (tube cooled)	Co	1936
Medium-pressure synthesis	Low temperature	Fixed bed (tube in tube)	Co	1937
Hydrocol	High temperature	Fluidized bed (fixed)	Fe	1951
Kellogg Synthol	High temperature	Circulating fluidized bed	Fe	1955
Arge	Low temperature	Fixed bed (multitubular)	Fe	1955
Sasol Synthol	High temperature	Circulating fluidized bed	Fe	1980
Shell middle distillate synthesis (SMDS)	Low temperature	Fixed bed (multitubular)	Co	1993
Sasol Advanced Synthol (SAS)	High temperature	Fluidized bed (fixed)	Fe	1993

Sasol slurry bed process (SSBP)	Low temperature	Slurry bubble column	Fe	1995
Statoil slurry bubble column process	Low temperature	Slurry bubble column	Co	2005
Sasol slurry bed process (SSBP)	Low temperature	Slurry bubble column	Co	2007
High-temperature slurry FT process (HTSFTP)	Medium temperature	Slurry bubble column	Fe	2008

## 1.4. A review on reforming CO<sub>2</sub> with CH<sub>4</sub>

By coincidence, the dry reforming methane with carbon dioxide (DMR) was also first explored by Franz Fischer and Hans Tropsch in 1928 over Co and Ni catalysts [68]. According to their reports, a severe deactivation problem occurred due to the formation of carbon on the catalysts. Later in 1949, Lewis et al. [69] and Reitmeier et al. [70] reported different approaches to suppress the carbon deposition via the control of reactant composition, operating conditions and the stoichiometric amount of metal oxide supports respectively. Their study has helped to identify the conditions for reforming to suppress the deactivation issue. In 1964 and 1965, Rostrup-Nielsen first extensively explored and reported catalysts and their preparation process for the reforming of CH<sub>4</sub> and higher vaporizable hydrocarbons [71, 72]. A co-precipitation process of a fine intimate mixture containing magnesium oxide, aluminum hydroxide, and nickel hydroxide was proposed. Up to a calcining temperature of 1100 °C, the conversion of alumina and part of the magnesia into spinel framework activated CO<sub>2</sub> and promoted the oxidation of carbon on the catalysts. The concept that the introduction of basic metal oxide suppressed the deactivation then has been applied by the later researchers; however, the mechanism was not proposed. Subsequently, the research on reforming was more focused on the developments of catalysts with their supports and the catalytic mechanisms. Sodesawa et al. reported the reforming of CO<sub>2</sub> with CH<sub>4</sub> over a stable Ni/SiO<sub>2</sub>, where the carbon decomposition was remarkably

limited in 1979 [73]. Gadalla et al. studied detailedly on different Ni/Al<sub>2</sub>O<sub>3</sub> catalysts and the effects of supports. They reported an optimum temperature range occurred for a different ratio of reactant component. In 1991, Ashcroft et al. tested a variety of noble-metal catalysts, including Pd, Ru, Rh, and Ir, and a high yield of syngas production was achieved [74]. Later various catalysts based on the noble and non-noble metals were tested, and their effects were studied [75-84]. Generally, noble metals such as Ir, Rh, Ru, Pt, and Pd, were found to exhibit high resistance to the unexpected carbon formation, despite the economic perspective, while non-noble alkali metals such as Ni, Fe, and Co were widely used for CO<sub>2</sub> reforming with CH<sub>4</sub>. Thus, a small number of noble metals as promoters can be loaded along with the non-noble alkali metals, enhancing the dispersion, providing additional active sites, and improving the resistance to carbon formation. The influence of support, the promoters and the methods of preparation and activation were also investigated by many researchers [85-93], and several important points to improve the catalytic performance were proposed including the porosity, the dispersion, nature of promoters, the interaction between metals and supports and the active sites.

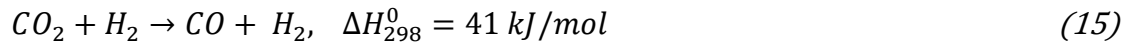
#### 1.4.1 Reactions and thermodynamics

The primary reaction for CO<sub>2</sub> reforming CH<sub>4</sub> is extremely endothermic, requiring a large amount of energy for the products [94]:



As well-known, the molecules of CH<sub>4</sub> and CO<sub>2</sub> are stable, whose dissociation energy is 435 kJ/mol (for CH<sub>3</sub>-H) and 526 kJ/mol (for CO-O) respectively. It requires high temperatures to achieve reasonable equilibrium conversions to syngas products. Moreover, as the main reaction is extremely endothermic, a continuous heating supplement is essential. Similar to FTS, the equilibrium conversions of the production in CO<sub>2</sub> reforming CH<sub>4</sub> are also affected by the simultaneous occurrence of reverse water gas shift (RWGS) reaction, which generally leads to a higher conversion of CO<sub>2</sub>

than CH<sub>4</sub>:



Besides, some other additional reactions can occur continuously depending on the conditions, including operating temperatures, the ratio of reactants, and the nature of catalysts. Among those, the decomposition reaction of CH<sub>4</sub> and the Boudouard reaction attribute to the formation of carbon deposition on the surface of catalysts, which leads to the deactivation of catalysts [95]:

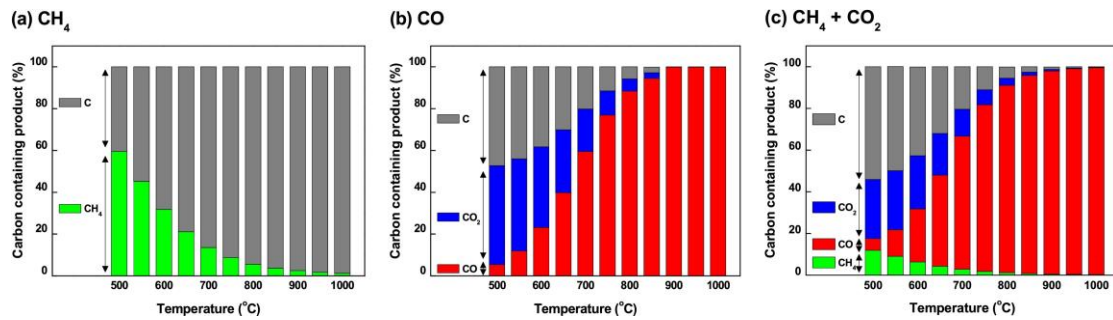


Figure 1-10. Carbon containing product for the catalytic reactions: (a) CH<sub>4</sub> decomposition (CH<sub>4</sub> only), (b) the Boudouard reaction (CO only), (c) CO<sub>2</sub> reforming with CH<sub>4</sub> (1:1). Adapted from [95], copyright Elsevier.

The thermal equilibrium of these side reactions can be analyzed and determined by standard free energy at different temperatures. Wang et al. proposed that the equilibrium of the primary reaction proceeds in the forward direction when the temperature is above 640 °C [96]. Moreover, they also found that the decomposition of CH<sub>4</sub> and the Boudouard reaction occur above 557 °C and below 700 °C, respectively, and the RWGS reaction only occurs up to 820 °C. Thus, they suggested an optimum temperature range of 870 to 1040 °C at a CO<sub>2</sub>/CH<sub>4</sub> ratio of 1:1, reconciling the conversion and carbon formation [96]. Nikko et al. have conducted the thermodynamic equilibrium analysis on the multi-reaction system for carbon

dioxide reforming of methane and the effects of operating temperature (300-1200 °C), a CO<sub>2</sub>/CH<sub>4</sub> ratio (0.5-3) and operating pressure (1-25 atm) on equilibrium conversions and products composition were studied [97]. They reported that high operating temperatures (above 850 °C) and low operating pressures are necessary to achieve high conversions of reactants and low yield of carbon formation, which is essential for stable operation. Papadopoulou et al. [98] proposed a detailed reaction mechanism of reforming CO<sub>2</sub> with CH<sub>4</sub>, as shown in Figure 1-11. Generally, the mechanism can be summarized in four steps: (i) the primary elementary step is the adsorption and dissociation of CH<sub>4</sub> on active sites on the metallic surface and CO<sub>2</sub> on the surface of the support, forming hydrogen with methyl-like adsorbed species and CO with adsorbed oxygen species, respectively. (ii) Surface reactions occur, and most of the reaction steps quickly arrive at the equilibrium, leading to the fast desorption of CO and H<sub>2</sub>. (iii) Hydrogen species spillover from the surface of metal catalyst to the support where the hydrogen species react with oxygen species, forming surface hydroxyl groups and leading to the WGS reaction. (iv) Oxygen species migrating on the surface of metal catalyst react with hydrogen-depleted -CH<sub>x</sub> species, forming -CH<sub>x</sub>O species which could finally either decompose into CO and H<sub>2</sub> or lead to the formation of oxygenated hydrocarbons [99-102].

However, it is not always suitable to generalize the thermal equilibrium conversions, the carbon formation, and the composition of the product only by thermodynamic calculation as the process is strongly depended on the nature and type of the catalysts and their supports. At these high temperatures, supported metallic catalysts are liable to deactivate due to the sintering and the unexpected interaction of the metal with supports. On the other hand, catalysts can be significantly active to the reforming reaction and resistant to carbon formation as well as RWGS reaction. Therefore, the study of reforming CO<sub>2</sub> with CH<sub>4</sub> is more focused on the aspects of catalysts.

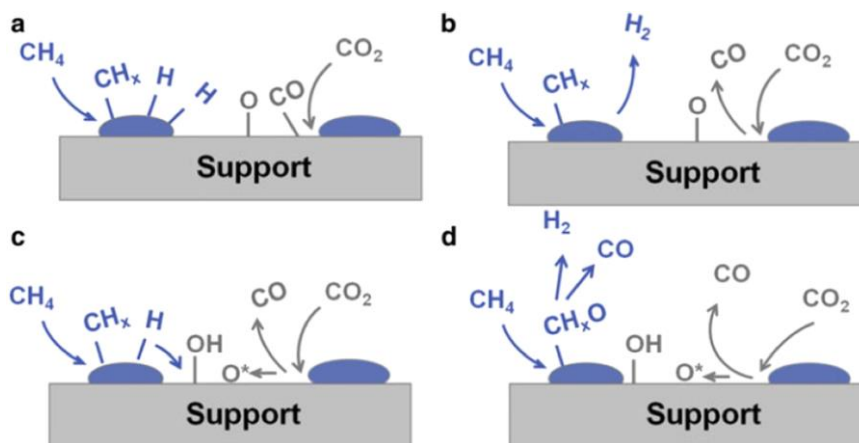


Figure 1-11. Reaction steps for CO<sub>2</sub> reforming with CH<sub>4</sub>: (a) Adsorption and dissociation of CO<sub>2</sub> and CH<sub>4</sub>. (b) Desorption of CO and H<sub>2</sub>. (c) Formation of surface hydroxyls and oxygen spillover. (d) Surface hydroxyls and oxygen species oxidize hydrogen depleted -CH<sub>x</sub> species and formation of CO and H<sub>2</sub>. Adapted from [98], Copyright Springer.

### 1.4.2 Catalysts for reforming

To achieve the successful large-scale industrialization of CO<sub>2</sub> reforming with CH<sub>4</sub>, the development of highly stable, active, and economic catalysts with excellent resistance to deactivation is indispensable. Apart from the nature of active metals, supports, additional promoters, morphology, preparation methods, and activation methods also directly affect the activity and stability of these heterogeneous catalysts, the conversion rates of reactants, selectivity to syngas and the resulting H<sub>2</sub>/CO molar ratio when designing the catalysts. Many researchers have dedicated to study CO<sub>2</sub> reforming with CH<sub>4</sub> over metal catalysts based on noble (mainly Pd, Ru, Rh, and Ir) and transition (mainly Ni, Fe, Cu, and Co) metals.

Due to low price, availability, and high catalytic activity, the transition metal (Ni, Co et al.) catalysts were widely investigated and applied in reforming CO<sub>2</sub> with CH<sub>4</sub> [103-107]. However, except the apparent feasibility for large-scale industrialization, the apparent coke deposition which leads to the deactivation of catalysts is a main drawback for the practical operation. On the other hand, though the noble metal catalysts were confirmed to be highly resistant to coke deposition, remarkably stable and active to the reactions [108-111], the steep cost and the poor availability has

severely limited the practical application of noble metal catalysts to an industrial scale [112]. Therefore, reconciling the economic feasibility and availability, one approach to overcome the deactivation issue is to develop an alloy catalyst, where a minor noble metal is introduced to a primary major transition metal. It has been reported that this approach showed great potential to overcome excessive coke deposition, meanwhile increased the dispersion of the metal and retained good economic feasibility, catalytic activity, and stability [112-115]. Menegazzo et al. [116] compared the catalytic performance of bimetallic Pd or Pt-Ni based catalysts with Al<sub>2</sub>O<sub>3</sub> or ZrO<sub>2</sub> supports. They found the introduction of Pt or Pd, preferably by co-impregnation, clearly prevented coke formation and prolonged the life span compared to the monometallic Ni/Al<sub>2</sub>O<sub>3</sub> or Ni/ZrO<sub>2</sub>. Nagaoka et al. [117, 118] have investigated the effects of additional Pt and Ru on the catalytic performance over Co/TiO<sub>2</sub> catalysts. They found that the oxidation of metallic Co by CO<sub>2</sub> can lead to the deactivation of catalysts, which was consistent with the conclusions of Lucrédio et al. [119]. The two groups all confirmed that the doped Pt or Ru could retain the Co species in a metallic form, thus increasing activity and stability of the catalyst. Faroldi et al. [120] compared the catalytic performance of Ru doped La<sub>2</sub>O<sub>3</sub>/SiO<sub>2</sub> pretreated and reduced at different temperatures, and the results clearly showed that the samples reduced at relatively low temperatures exhibited higher activity than those pretreated at higher temperatures in the premise of sufficient reduction. A similar result was also reported by Ghelamallah and his co-workers [121], where they investigated the catalytic performance of Ba and La doped Pt and Rh/ $\alpha$ -Al<sub>2</sub>O<sub>3</sub> catalysts. They suggested that different temperatures of pretreatment and reduction could affect the particle size and dispersion of the metal on the supports, leading to the differences in catalytic behavior. Arandiyan et al. [122] have prepared a series of perovskite-type catalysts based on La<sub>0.4</sub>M<sub>0.6</sub>Al<sub>0.2</sub> Ni<sub>0.8</sub>O<sub>3</sub> (M=doped noble metal) with different noble metals doped ( Ir, Pd, Pt, Rh, and Ru), the activity performance of these catalysts prepared by a sol-gel method was excellent. El Hassan et al. [123] investigated the effect of metal

sintering, and coke deposition on the performance of SBA-15 or SiO<sub>2</sub> supported Rh and Co catalysts. They proposed that the doped noble metal can reduce metal sintering and alter the type of coke deposition, thus providing a better catalytic activity and stability.

Nominally, the role of support (e.g., SiO<sub>2</sub> and Al<sub>2</sub>O<sub>3</sub>) is to provide high surface area for the dispersion of the active metals. Furthermore, researches have revealed that the interaction between the metals and supports could have positive or negative effects on the catalytic performance due to the high temperature of pretreatment or operation. Besides, some textural and physicochemical properties of the support such porosity, basicity oxygen capacity, also have implications to deactivation. Therefore, the performance of a catalyst is not only a function of the active metals and promoters, but the intrinsic behavior of the supports in catalytic reactions should be considered [124]. Wang et al. [125] have investigated the effects and performance of various supports including reducible (CeO<sub>2</sub>, Nb<sub>2</sub>O<sub>5</sub>, Ta<sub>2</sub>O<sub>5</sub>, ZrO<sub>2</sub>, and TiO<sub>2</sub>) and irreducible ( $\gamma$ -Al<sub>2</sub>O<sub>3</sub>, La<sub>2</sub>O<sub>3</sub>, MgO, SiO<sub>2</sub>, and Y<sub>2</sub>O<sub>3</sub>) oxides based on Rh catalysts. They found the catalytic performance significantly varied with different supports under the same conditions, and the catalyst samples supported on the irreducible supports exhibited higher activity. However, the sintering of metals led to deactivation after a certain period of operation over some of the supports. Wu et al. [126] have reported that the weak interaction between metals and supports exhibits positive effects over acidic/basic supports and

improves the metal-metal interaction of bimetallic catalysts by comparing the boron nitride support with  $\gamma$ -Al<sub>2</sub>O<sub>3</sub> based on Rh–Ni catalysts. Zhang et al. [127] studied the catalytic performance of Ni catalysts supported on SiO<sub>2</sub>, TiO<sub>2</sub>, Al<sub>2</sub>O<sub>3</sub>, MgO modified Al<sub>2</sub>O<sub>3</sub>, ZrO<sub>2</sub>, and MgO supports. According to the research, the large surface area of SiO<sub>2</sub> support attributed to the high dispersion of metal while the strong interaction between NiO and Al<sub>2</sub>O<sub>3</sub> caused the formation of NiAl<sub>2</sub>O<sub>4</sub>, which was difficult to be reduced. Moreover, the low surface area of TiO<sub>2</sub>, ZrO<sub>2</sub>, and MgO supports also led to

a low dispersion of metal. Steinhauer et al. [128] investigated the catalytic activity and stability of various supports, including  $\text{La}_2\text{O}_3$ ,  $\text{ZrO}_2$ ,  $\text{La}_2\text{O}_3$ ,  $\text{ZrO}_2$ ,  $\text{SiO}_2$ ,  $\text{Al}_2\text{O}_3$ , and  $\text{TiO}_2$  based on Pd-Ni bimetallic catalysts. They proposed that the difference in metal dispersion and metal-support interaction mainly attributed to the difference in catalytical behavior at high temperatures due to the intrinsic nature of materials. However, the difference was not significant at low operating temperatures.

In a word, the performance of catalysts for  $\text{CO}_2$  reforming with  $\text{CH}_4$  is strongly affected by the intrinsic nature of metals and supports. Particularly, the different physicochemical properties of metals with supports showed a significant difference in the interaction between components, metal dispersion, particle size, basicity, oxygen storage capacity, reducibility, porosity and surface area, which are considered to be important in the catalytic performance. The general idea for the preparation of catalysts is to develop a high surface area and porosity support with weak metal-support interaction (e.g.,  $\text{SiO}_2$ ) based on efficient non-noble metal (e.g., Co) perhaps with an additional noble metal doped.

### **1.4.3 New approach: directly synthesizing value-added liquid products from $\text{CO}_2$ and $\text{CH}_4$**

Instead of the stepwise approach, which is supposed to convert  $\text{CO}_2$  and  $\text{CH}_4$  into syngas then produce value-added liquid hydrocarbons and oxygenates via FTS process, a direct approach to directly synthesize the value-added liquid products from  $\text{CO}_2/\text{CH}_4$  mixture has been proposed recently. Comparing to the indirect approach, the direct synthesis of high-value chemicals from  $\text{CO}_2$  and  $\text{CH}_4$  under soft conditions is confirmed to be more efficient; however, more challenging regarding the process design and catalysts design.

Early in 1997, Raskó et al. [129, 130] observed the rapid formation of  $\text{CH}_2\text{O}$  and  $\text{CH}_3\text{O}$  species from adsorbed  $\text{CH}_3$  species and  $\text{CO}_2$  at low temperatures over Rh/ $\text{SiO}_2$  and  $\text{TiO}_2$  catalysts. This phenomenon indicated the possibility of directly synthesizing liquid oxygenated hydrocarbons such as alcohols and organic acids from  $\text{CO}_2$  and

CH<sub>4</sub>. At about the same time, Fujiwara et al. [131] reported a high yield production of acetic acid process, where the acetic acid was synthesized in the presence of a homogeneous Pd(OAc)<sub>2</sub>/Cu(OAc)<sub>2</sub>/K<sub>2</sub>S<sub>2</sub>O<sub>8</sub>/TFA catalyst at 80 °C. This work demonstrated a new way of synthesizing acetic acid from CO<sub>2</sub> and CH<sub>4</sub>; however, extremely high pressures were essential for this process to liquify the reactants. In 2001, Huang et al. [132] explored the possibility of directly converting CO<sub>2</sub> and CH<sub>4</sub> to high-value products at soft conditions over a Cu/Co catalyst. By varying the operating condition, they successfully produced C1-C4 alcohols, formic acid, acetic acid, formaldehyde, and some other liquid oxygenates within a temperature range from 100 to 400 °C. They suggested that the final products of this process were highly depended on the operating conditions, especially temperatures. Wilcox et al. [133] operated diffuse reflectance infrared Fourier transform spectroscopy (DRIFTS) experiments to explore the direct formation of acetic acid from CO<sub>2</sub> and CH<sub>4</sub> on Pd/carbon and Pt/alumina catalysts. Their results clearly showed the formation of absorbed acetates on both catalysts at 400 °C. Zerella et al. [134] reported a process of directly synthesizing acetic acid from CO<sub>2</sub> and CH<sub>4</sub> over a Pd/Cu complexes catalyst in K<sub>2</sub>S<sub>2</sub>O<sub>8</sub> (15 mol%)/CF<sub>3</sub>COOH solvent. However, they explained later that CO<sub>2</sub> scarcely participated in the reaction. Ding et al. [135] investigated the theoretical and experimental feasibility of direct conversion of CH<sub>4</sub> and CO<sub>2</sub> to acetic acid by an isothermal step-wise route within a temperature range from 170 to 400 °C over Pd/SiO<sub>2</sub> and Rh/SiO<sub>2</sub> catalysts; however, the formation rate and the selectivity were limited. In 2010, Huang et al. [136] designed a continuous step-wise reactor and achieved an efficient production of both acetic acid and ethanol with overall optimal yields obtained at the highest temperature of 423 K, the pressure of 2.0 MPa over a Co-Pd/TiO<sub>2</sub> catalyst. Rabie et al. [137] reported the direct formation of acetic acid by the concurrent feed of CO<sub>2</sub> and CH<sub>4</sub> under the continuous flow micro-reactor system by the concurrent feed of methane and carbon dioxide over series of Cu loaded M<sup>+</sup>-ZSM-5 (M = Li<sup>+</sup>, Na<sup>+</sup>, K<sup>+</sup>, and Ca<sup>2+</sup>) catalysts. They observed the formation of acetic

acid in a temperature range of 425-525 °C with a considerable formation rate.

Apart from the experimental exploration, some researchers dedicated to the theoretical and mechanistic study on the formation of liquid chemicals from CO<sub>2</sub> and CH<sub>4</sub>. As early as in 1990, Nishiyama and Aika have investigated the mechanism of the CO<sub>2</sub> assisted oxidation of CH<sub>4</sub> over a PbO/MgO catalyst at very high temperatures [138]. Shortly later, the same group again reported a process of converting CO<sub>2</sub> and CH<sub>4</sub> into C<sub>2</sub> hydrocarbons over seventeen metal oxides with the highest selectivity of 30% at 850 °C [139]. In 2002, Labinger et al. [140] has summarized the understanding and exploiting C-H bond activation and concluded the C-H bond activation mechanisms. In 2003, Hristov et al. [141] studied the reactions pathway of the direct conversion of methane to acetic acid and methanol by a homogeneous RhCl<sub>3</sub> catalyst based on density functional theory. Meanwhile, Chempath et al. [142] reported a similar work based on Pd<sup>2+</sup> in sulfuric acid. Even though these studies were based on CH<sub>4</sub> reacting with CO or O<sub>2</sub>, the oxidation steps for CH<sub>4</sub> have been illustrated. Wannakao et al. [143] demonstrated the utilization of Au-exchanged zeolites for methane activation using a density functional theory study. They investigated the effect of pore sizes by comparing different catalysts (including Au-ferrierite, Au-ZSM-5, and Au-MCM-22 zeolites) which represent different structures with small, medium, and large pores, respectively. According to their research, the zeolite with the largest pores, Au-MCM-22 exhibits the highest activity due to better stabilization of its transition state structure. Later, Panjan et al. [144] used the same method to study the catalytic activity of the Au(I)-ZSM-5 zeolite on the conversion of CO<sub>2</sub> and CH<sub>4</sub> to acetic acid and revealed the reactions pathway and mechanism on Au-ZSM-5 catalyst. Wu et al. [145] investigated the mechanism on the direct formation of acetic acid from the conversion of CH<sub>4</sub> and CO<sub>2</sub> over a Zn modified H-ZSM-5 zeolite catalyst. By solid-state <sup>13</sup>C and <sup>1</sup>H MAS NMR investigation, they found the Zn sites can efficiently activate CH<sub>4</sub> to form Zn-CH<sub>3</sub> species, and the Zn-C bond is the further subject to the CO<sub>2</sub> insertion to produce Zn-OOCCH<sub>3</sub> species. This

research demonstrated the possible formation of surface acetate species on transition metal catalyst. Zhang et al. [146] systematically investigated the interaction mechanism of CO<sub>2</sub> with CH<sub>3</sub> and H on the Cu surface by the first-principle DFT–GGA calculations. They proposed four possible reaction pathways for the formation of acetic acid and compared the detailed mechanism and kinetics. Moreover, it was found that the pathway of Cu-OOCCH<sub>3</sub> exhibited the lowest value of the activation barrier, which is suggested the most advantageous in dynamics. The result was in good accordance with Wu’s research. Recently, Shavi et al. [147] has applied multiple techniques including quick solid-state NMR, TGA, and FT-IR, with Langmuir-Hinshelwood model to investigate mechanistic steps with the related kinetics for the carbonylation of CH<sub>4</sub> with CO<sub>2</sub> over single and dual component catalysts with different combinations of ZnO-, CeO<sub>2</sub>-, and MnO<sub>2</sub>- supported montmorillonite. Moreover, they also theoretically confirmed the experimental results by DFT calculations. The consistent experimental and theoretical results elucidated the detailed mechanism on the formation of acetic acid over catalysts.

Thus far, some efforts have been devoted to the mechanistic and theoretical study on the activation of CH<sub>4</sub> and CO<sub>2</sub> and the reactions pathway mainly towards acetic acid. Meanwhile, some experimental study has been conducted for the direct conversion of CO<sub>2</sub> with CH<sub>4</sub> into liquid chemicals, mainly acetic acid. However, the poor selectivity and unfavorable operating conditions of this approach still need to be improved, and few studies were carried out on direct synthesis of value-added liquid hydrocarbons or alcohols (such as methanol) from CO<sub>2</sub> with CH<sub>4</sub>. This approach is still regarded as promising but challenging.

## **1.5. Why plasma-assisted reforming and FTS makes a difference**

As mentioned in the preceding that plasma process can provide a unique pathway to chemical reactions, applying plasma instead of the thermochemical process may

offer a new perspective of reversal conversion of CO<sub>2</sub> into value-added liquid chemicals with CH<sub>4</sub> directly or indirectly. Indeed, considerable efforts have been devoted to explore and develop the thermal or non-thermal plasma assisted reforming CO<sub>2</sub> with CH<sub>4</sub>, especially for the syngas products, and remarkable achievements have been obtained in laboratory scale. Nevertheless, limited efforts have been bent either on plasma-assisted FTS or plasma-assisted directly synthesizing high-value liquid chemicals.

### 1.5.1 Plasma assisted FTS

Although the conventional FTS has been successfully achieved an industrial scale, plasma is plausible to be applied on FTS and offer a new pathway to overcome some obstacles that existed in FTS process. However, the plasma approach is practically very challenging to realize even in laboratory scale. On the one hand, a high pressure (usually ~2-3MP) is essential for FTS to ensure reasonable conversion rate of CO and the considerable yield of high hydrocarbons. On the other hand, generating plasma in such high pressure is very difficult. Thus far, little research is related to plasma-catalytic route for FTS either on the theoretical aspect or the experimental aspect. Our group [148, 149] have conducted some experimental studies on arc discharge assisted FTS without catalysts. In the study, very high-pressure plasma was successfully generated for FTS. However, the results showed that even at very high temperatures (~2 MP) with high specific input energy (varies from 1000-10000 kJ/mol), light hydrocarbons were dominant products. The absence of catalysts may be the reason for the low selectivity to C<sub>5</sub>+ paraffin and olefins. Al-Harrasi et al. [150] studied plasma promoted FTS at low temperatures and ambient pressure with a total 35% (w/w) Cu/Co=1 (weight ratio) alloy loaded aluminosilicate (Al<sub>2</sub>SiO<sub>5</sub>) ceramic foam monolith. The results demonstrated the existence and formation of C<sub>5</sub>+ high hydrocarbons at a low H<sub>2</sub>/CO ratio (~0.5) and ambient pressure, but with very high specific input energy (2500 kJ/mol). Compared to Rohani and Samuel's researches, which applied an arc discharge with much higher pressure and energy

input, the catalysts could play a vital role in plasma-assisted FTS process. Thus, it could be to bring out FTS process through a plasma-catalytic route at low temperature and ambient pressure by optimizing the catalyst properties and reaction parameters.

### **1.5.2 Plasma assisted converting CO<sub>2</sub> with CH<sub>4</sub>**

Compared with plasma-assisted FTS process, plasma-assisted conversion of CO<sub>2</sub> with CH<sub>4</sub> has been researched and developed for decades along with the conventional thermochemical approach of utilizing CO<sub>2</sub> and CH<sub>4</sub>. Generally, the same as the thermochemical approach, two technical routes of converting CO<sub>2</sub> with CH<sub>4</sub> under plasma-catalytic conditions are proposed: converting CO<sub>2</sub> with CH<sub>4</sub> for syngas products or direct formation of value-added liquid hydrocarbons and oxygenates. Until now, researches are mainly focused on the plasma-assisted dry reforming of CO<sub>2</sub> and CH<sub>4</sub> into syngas production and some notable progress have been achieved in laboratory scale while only limited efforts were devoted to the more challenging direct formation of value-added liquid products.

Early in 1998, Gesser et al. [151] have studied the dry reforming CO<sub>2</sub> with CH<sub>4</sub> in a silent discharge reactor. In the same year, Zhou and Eliasson [152] investigated the effects of gas components, pressure, and temperature on plasma-catalysis assisted dry reforming via a DBD reactor. They proposed that high temperatures led to the formation of wax and carbon deposition in methane-enriched feeding gas while low gas pressures favored syngas production. Later, Eliasson et al. [153-155] have published a series of researches on plasma-assisted reforming of CO<sub>2</sub> with CH<sub>4</sub> for syngas products through a DBD reactor with or without catalysts. Their reactor has achieved a considerable selectivity towards syngas products with relatively high input energy. Besides, C<sub>2</sub>-4 hydrocarbons and few oxygenates were also detected in the products. It was also found that temperature is less important on the conversion rate and selectivity compared to other parameters such as specific input energy and catalysts. Bin et al. [156] used pulse corona plasma to reform CO<sub>2</sub> with CH<sub>4</sub> without catalysts, and the main products were syngas, which was similar to Yao's research

[157]. Huang et al. [158] conducted the dry reforming experiments in atmospheric pressure ac discharge plasmas without catalysts, while they observed visible coke deposits during the discharge. These early researches of plasma techniques on reforming CO<sub>2</sub> with CH<sub>4</sub> have exemplified the applications of plasma-assisted dry reforming for the future study.

Qi et al. [159] developed a new atmospheric pressure abnormal glow discharge reactor to investigate synthesis gas production from reforming CO<sub>2</sub> and CH<sub>4</sub>. The experiments showed that high conversion rate of CH<sub>4</sub> and CO<sub>2</sub> (91.9% and 83.2%) was achieved with high selectivity of CO and H<sub>2</sub> (80% and 90%). Li et al. [160] designed a specific plasma reactor of atmospheric pressure glow discharge for CO<sub>2</sub> reforming of CH<sub>4</sub> to syngas. The conversion rates of CH<sub>4</sub> and CO<sub>2</sub> achieved 60.97% and 49.91% with the selectivity of H<sub>2</sub> and CO, up to 89.30% and 72.58%, respectively. Krawczyk et al. [161, 162] researched plasma-catalysis promoted CH<sub>4</sub> conversion with CO<sub>2</sub> with various catalysts including Fe/Al<sub>2</sub>O<sub>3</sub>, NaY, Na-ZSM-5, Ag/Al<sub>2</sub>O<sub>3</sub> and Pd/Al<sub>2</sub>O<sub>3</sub> under variable temperatures (from 130 to 340 °C) and moderate pressure (1.2 bar). They reported that a considerable yield of syngas and C<sub>2</sub>-4 hydrocarbons were synthesized, and alcoholic products can be synthesized at low temperatures over Fe/Al<sub>2</sub>O<sub>3</sub>, Ag/Al<sub>2</sub>O<sub>3</sub>, and Pd/Al<sub>2</sub>O<sub>3</sub> catalysts. Tu et al. [163-167] have investigated the effects of packing materials, packing method, catalyst material, and some other variables. Their researches were mostly in agreement with the simulation work of Bogaerts [168-170]. Zhang et al. [171] also conducted similar experimental studies on CO<sub>2</sub> and CH<sub>4</sub> conversion to synthesis gas and C<sub>2</sub>-C<sub>4</sub> hydrocarbons by DBD over BaTiO<sub>3</sub>, Ni-Fe/SiO<sub>2</sub>, and Ni/SiO<sub>2</sub> catalysts. They found that BaTiO<sub>3</sub> catalysts significantly promoted the conversion of CO<sub>2</sub> and CH<sub>4</sub>, while Ni/SiO<sub>2</sub> catalysts favored the conversion of CH<sub>4</sub> to CO. These works revealed that only a part of CH<sub>4</sub> contributes to the higher hydrocarbons while one part of CH<sub>4</sub> finally transformed into CO, resulting in a higher conversion of CH<sub>4</sub> than CO<sub>2</sub>, which is contrary to thermochemical dry reforming. Meanwhile, oxygen or hydroxyl groups

in the process are essential for higher hydrocarbons. Wang's DFT simulation works [172, 173] and Pistonesi's simulation [174] also supported the conclusions. Besides, many experimental studies on syngas generation from CO<sub>2</sub> and CH<sub>4</sub> have been carried out with various catalysts, plasma sources, power supplies as concluded in Table 1-3 [159, 162, 166, 175-190].

Table 1-3. Comparison of syngas generation based on non-thermal plasmas by reforming of CO<sub>2</sub>.

Reactor type	Power supply	Input Power (W)	Total flow rate (ml/min)	CH <sub>4</sub> /CO <sub>2</sub> ratio	Conversion rate (%)		Selectivity (%)	
					CH <sub>4</sub>	CO <sub>2</sub>	H <sub>2</sub>	CO
DBD	AC	50	90	0.35	48.7	11.5	44.0	75.0
	AC	6.3	40	1.0	24.0	18.9	35.8	42.4
	AC	38.4	30	1.0	22.0	12.0	90.0	92.0
	AC	21.4	40	1.0	64.6	51.0	59.1	54.0
	AC	2500	500	4.0	64.0	54.0	52.8	23.3
	AC	18	16.7	0.5	58.0	33.0	32.8	39.6
corona discharge	AC	46.3	43	1.0	62.4	47.8	70.0	66.8
	DC	63	63	0.5	94.1	77.9	69.4	97.1
	AC	45	60	0.5	75.0	60.0	70.6	96.0
	DC	10	100	0.5	66.0	44.0	66.0	80.0
	DC	21	180	1.0	33.0	23.0	68.0	65.0
glow discharge	AC	495	500	0.67	67.4	54.3	79.8	84.6
	AC	23	120	1.0	60.8	49.8	77.5	63.2
	AC	66.7	4000	0.67	14.7	9.7	96.8	52.1
plasma jet	AC	770	8300	0.67	45.7	34.0	78.1	85.4
	AC	68.95	1000	0.67	93.3	85.0	79.2	83.5
gliding arc	AC	200	1000	1.0	40.0	31.8	42.4	53.6
	AC	520.7	12700	0.5	41.7	37.1	38.4	55.0
	AC	95	5000	0.43	9.9	6.8	35.1	57.8

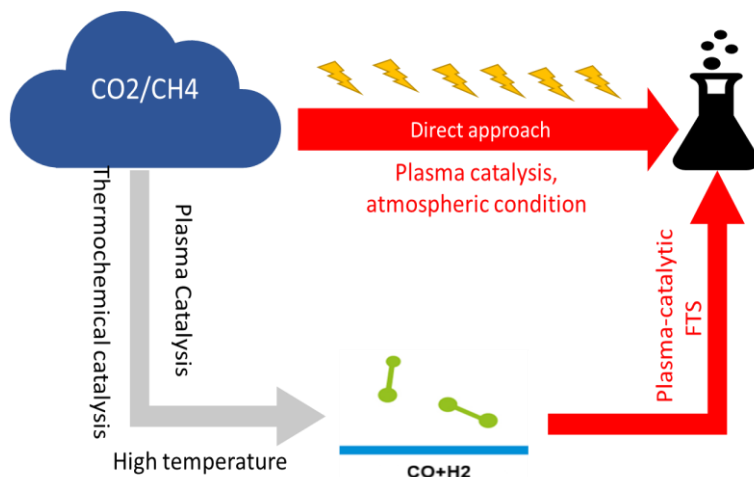
Except for the syngas products, few efforts were focused on the more challenging direct plasma-catalytic synthesis of high-value liquid chemicals and fuels. Eliasson's group firstly [154, 191-193] explored the direct formation of alcohols and acetic acid via DBD plasma with the presence of catalysts both on experimental and theoretic aspects. It was reported that the direct formation of acetic acid was accessible theoretically; however, the selectivity and yield of liquid products were poor. Scapinello et al. [194, 195] reported the direct synthesis of C1-5 alcohols and acid from CO<sub>2</sub> and CH<sub>4</sub> through a DBD reactor. Meanwhile, they also computed a DFT calculation to investigate the reactions for the formation of acids. However, the conversion rate of reactants was limited. Scarduelli et al. [196] reported the formation

of a liquid (20% in weight) during the dry reforming of methane in a DBD plasma reactor at atmospheric pressure with very high specific input energy (64 kJ/L), and liquid hydrocarbons were detected among the liquid products. Nevertheless, the overall selectivity towards aiming products was negligible.

Therefore, the plasma-catalysis associated conversion of CO<sub>2</sub> and CH<sub>4</sub> into syngas products with high conversions of reactants and substantial yield of syngas production has been successfully achieved in a laboratory scale. The following research will be focused on the improvements of energy efficiency, the development of catalysts and supports, and the understanding of complicated synergistic effects and interactions between plasma and catalysts. Nevertheless, the plasma-catalysis associated direct synthesis of value-added liquid chemicals even hydrocarbon fuels are still very challenging. Achieving the process successfully and practically will be remarkable progress in CO<sub>2</sub> utilization and offer a new pathway to convert the two main greenhouse gases into useful products.

## **1.6. Outline of this thesis**

As described in the previous sections, the plasma-catalytical FTS and direct conversion CO<sub>2</sub> and CH<sub>4</sub> into high-value liquid products are promising pathways for the CO<sub>2</sub> utilization to overcome some drawbacks in conventional thermochemical pathway such as high pressure and temperature. The work of this thesis focuses on achieving FTS and direct conversion CO<sub>2</sub> and CH<sub>4</sub> into high-value liquid products by a non-thermal plasma process associated with catalysts. The scheme of the processes is shown in Scheme 1-1.



Scheme 1-1. The scheme of the thesis.

In chapter II, a coaxial vertical DBD reactor with its analytical and diagnostic apparatuses was designed and described, and the plasma experiments were carried out under ambient conditions. Moreover, one pressure probe and two temperature probes were applied right in the inlet and outlet to measure the change of temperature and pressure; the volumetric change was measured by a soap film flowmeter. Considering these variables, the results of the gas chromatography was calibrated. Co catalysts and SiO<sub>2</sub> aerogel supports for plasma-catalytic FTS were also described and characterized in this chapter. The SiO<sub>2</sub> aerogel supports were synthesized by ambient drying method after surface modification. The Co catalysts were prepared by different methods and precursors.

The experimental study of plasma-catalytic FTS was demonstrated in chapter III. The variable study experiments were first conducted without placing catalysts at ambient conditions, including total flow rate, H<sub>2</sub>/CO ratio, and frequency. Then the performance of the catalysts was evaluated by introducing silica aerogel support and different Co/SiO<sub>2</sub> aerogel catalysts. Chapter IV and V are focused on the direct plasma-catalytic conversion of CO<sub>2</sub> and CH<sub>4</sub> into value-added liquid products and syngas. In chapter IV, except Co/SiO<sub>2</sub> aerogel catalysts described in the previous chapter, a series of Fe/SiO<sub>2</sub> aerogel supports was synthesized, characterized and applied into the plasma experiments to explore the direct synthesis of liquid chemicals

from CO<sub>2</sub> and CH<sub>4</sub>. In chapter V, HZSM-5 catalyst (also as support) was introduced with Fe and Co silica aerogel catalysts. Different composite catalysts were prepared, characterized, and introduced to directly synthesize high-value liquid chemicals (alcohols and acids) and C<sub>5</sub>+ fuels. In chapter VI, the results were compared with existed work for energy efficiency and productivity. Some possible reaction pathway was also illustrated. Finally, recommendations on the future improvement of plasma-catalytic FTS and direct conversion of CO<sub>2</sub> and CH<sub>4</sub> into liquid chemicals were outlined.

# Chapter II. Experimental, method characterizations and system diagnostics

## Résumé du chapitre

Ce chapitre est consacré à la description et au diagnostic électrique du banc d'expérimentation. Tout d'abord, nous avons mis en place un réacteur DBD tubulaire avec ses appareils d'analyse physiques et chimiques. Le réacteur DBD comprend deux électrodes en configuration coaxiale, un tube en céramique diélectrique et deux bouchons ajustables aux extrémités. Un catalyseur solide se présentant sous la forme de granules catalyseur/support vient remplir l'espace inter-électrode entre l'électrode interne et le tube diélectrique. La puissance électrique est fournie par un générateur à courant variable. La puissance injectée dans le plasma DBD est calculée via la méthode de Lissajous en plaçant une capacité en série avec le réacteur. Les produits gazeux sont analysés en ligne par Chromatographie en phase Gazeuse (GC). Les liquides sont séparés des gaz par un piège à eau glacée, puis ils sont analysés hors ligne via un Chromatographe en phase Gazeuse couplé à un spectromètre de masse (GC-MS). Il est important de noter que des sondes de température et de pression, situées à l'entrée et à la sortie du réacteur, enregistrent température et pression avant et pendant décharge, afin de calibrer les résultats de conversion et sélectivité. Pour cerner les caractéristiques électriques du réacteur, des décharges ont d'abord été générées sous une atmosphère gazeuse inerte pour la caractérisation. L'aérogel de silice utilisé comme support de catalyseur avec la zone spécifique élevée a été préparé via un procédé de séchage à l'air ambiant après traitement de surface par HMDZ afin d'obtenir des surfaces spécifiques importantes et une hydrophobicité. Le catalyseur Co a été synthétisé par deux procédés différents pour étude comparative : un procédé d'imprégnation et un procédé sol-gel via précurseur. Les différentes qualités de catalyseur Co obtenues ont été caractérisées par diverses méthodes.

## Abstract

This chapter focuses on the description and electrical diagnostics of the experimental bench. First, we established a DBD reactor with its analytical apparatuses for the plasma-catalysis associated FTS and CO<sub>2</sub> reforming with CH<sub>4</sub> directly into value-added liquid products. The DBD reactor mainly included two coaxially installed electrodes, a dielectric ceramic tube, and two adjustable caps with solid catalysts packing inside the volume between the inner electrode and dielectric tube. The power into DBD plasma was calculated via the Lissajous method by connecting a capacitance in series with the DBD reactor. The gas products are analyzed by an on-line GC. The gas products and liquid products are separated by an icy water trap, and then the liquid products are analyzed offline through a GC-MS. Importantly, two temperature probes and a pressure probe right in the inlet and outlet of the reactor to record the temperature difference of the gas flow and the pressure before and during discharge, which is used to calibrate the results of conversions and selectivity. To understand the electrical performance of the bench, discharges were first generated under the inert gaseous atmosphere for electrical diagnostics. Meanwhile, the SiO<sub>2</sub> aerogel support with the high specific area was prepared via ambient drying method after surface modified by HMDZ for hydrophobicity. Different Co catalysts were synthesized by an impregnation method, and a sol-gel method with a different precursor for plasma promoted FTS. The Co catalysts were characterized by various methods.

## 2.1. Description of experimental bench

The schematic diagram of the bench established for plasma-catalysis assisted FTS, and direct synthesis of liquid products from  $\text{CO}_2$  and  $\text{CH}_4$  is shown in Figure 2-1 and photo of the bench is shown in Figure 2-2. It was comprised of a power supply, a DBD reactor, a product collector, and an analysis system.

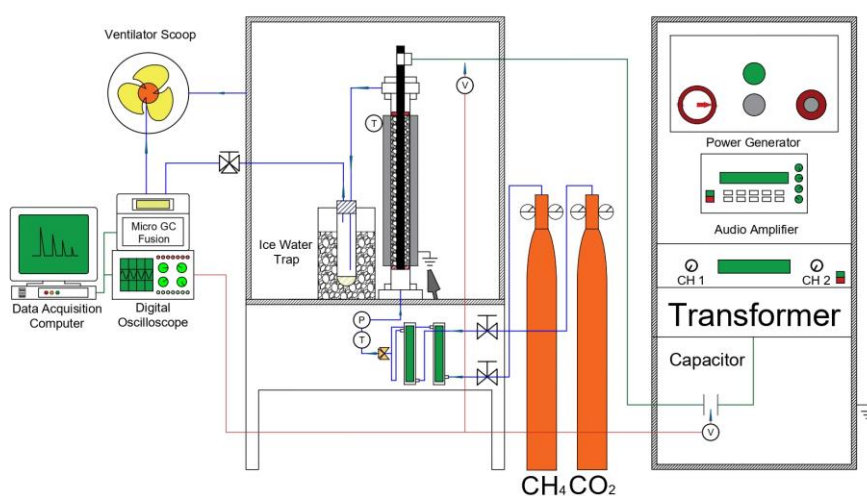


Figure 2-1. Experimental setup of the experimental bench.



Figure 2-2. Photo of the experimental bench.

### 2.1.1 DBD reactor

The schematic diagram of the DBD reactor is presented in Figure 2-3. The DBD reactor mainly included two coaxial electrodes, a dielectric ceramic tube, and two adjustable caps. The inner high voltage electrode is an aluminum rod with a diameter of 6mm coaxially installed in the dielectric ceramic tube (10 mm i.d. × 12 mm o.d.); two adjustable Teflon caps with inner diameter and outer diameter of 6 mm × 10 mm were coupled with the aluminum rod to ensure the concentricity of the electrode in the ceramic tube and to fix the full-packed catalysts. Moreover, 12 pores (semi-circle) with a diameter of 1 mm evenly distributed around the caps, which can guarantee the uniformity of gas inlet. The outer grounded electrode was a 200 mm-long stainless-steel coil wrapped around the dielectric tube. Thus the length of the plasma zone in the reactor is 200 mm. According to the distance between the inner surface of the dielectric tube and the inner electrode, the discharge volume is calculated as 10.1 cm<sup>3</sup>, where the catalysts were placed. A compressed air gun was installed facing the reactor to avoid possible overheating.

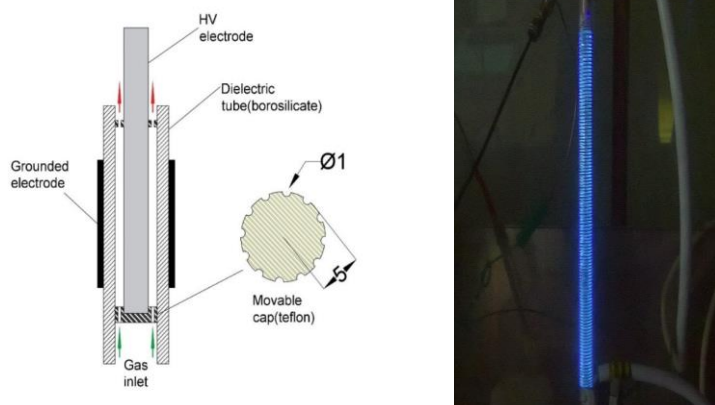


Figure 2-3. Schematic diagram of DBD reactor.

### 2.1.2 Power supply system

The power supply system applied to the reactor is composed of a signal function generator (HP 33120A), an audio amplifier (IMG Stageline STA-1400) and a

transformer. Five standard waveforms with variable applying frequency (from 1 to 10 kHz) can be generated including sinusoidal, square pulsed, and triangle pulsed signal. The amplifying output level of the audio amplifier varies from “-80 dB” to “0 dB” with three different operation modes (stereo mode, parallel mode, and bridge mode) to adjust the peak-to-peak voltage of output signal. The transformer is coupled with the audio amplifier for high enough peak-to-peak voltages to breakdown the gas and generates discharges in the reactor. Instead of accurately recording the microdischarge current spikes, which needs a high sensibility of apparatus and not easy to process the data, one capacitor (3.9 nF) was connected in series after the transformer. The current through the reactor is accumulated in the capacitor and thus can be determined by measuring the voltage on the capacitor.

### 2.1.3 Power measurement and diagnostics

The DBD reactor and the related elements can be represented by an equivalent electrical circuit before and during plasma ignition, as shown in Figure 2-4. The frame A represents the transformer that supplies electrical power to the circuit, which is its secondary circuit. It consists of a voltage source  $U$ , a resistor  $R_t$  and an inductor  $L_t$ . The frame B represents the simplified construction of the DBD reactor. It includes two equivalent capacitors (or three if there are two dielectric barriers) in a serial connection:  $C_g$  for the gap with gas and  $C_d$  for the dielectric barrier(s). By applying an electric field with enough strength, a local field breakdown in the gap can be initiated. In the equivalent circuit, this is symbolized by closing a switch and forcing some of the current through the microdischarge channels, whose resistance  $R_m$  rapidly changes with time. The total charge  $Q$  transferred in microdischarges depends on the gas properties and can be influenced by the gap spacing and by the properties of the dielectric. By measuring the voltage on the DBD reactor ( $V_D$ ) and the voltage on the capacitor ( $V_C$ ), the power of the DBD plasma can be integrated and calculated due to the following equation:

The charge ( $q(t)$ ) and the current  $i(t)$  of the capacitor can be calculated as:

$$q(t) = C_s * V_c(t) \quad (1)$$

$$i(t) = \frac{dq}{dt} = C_s * \frac{dV_c}{dt} \quad (2)$$

The energy per cycle  $W$  with a period  $T$  can be expressed as:

$$W = \int_{t-T/2}^{t+T/2} V_D(t) * i(t) dt \quad (3)$$

By integration of these equations, the energy per cycle becomes:

$$W = \int_{q_{min}}^{q_{max}} V_D * dq \quad (4)$$

By recording  $V_D(t)$  and  $V_c(t)$  as a series of points over one period the energy can be approximated by integration based on equation 1-4, using trapezoidal integration, as:

$$W \approx \sum_{k=1}^n \left( \frac{V_{k+1} + V_k}{2} \right) (q_{k+1} - q_k) \quad (5)$$

Then according to (1), the energy per period can be transformed as:

$$W = C_s * \sum_{k=1}^n \left( \frac{V_D(k+1) + V_D(k)}{2} \right) * (V_c(k+1) - V_c(k)) \quad (6)$$

Then the power in the DBD plasma reactor can be determined by:

$$P = W * f = f * C_s * \sum_{k=1}^n \left( \frac{V_D(k+1) + V_D(k)}{2} \right) * (V_c(k+1) - V_c(k)) \quad (7)$$

Since the voltage on DBD  $V_D$  and voltage on capacitor  $V_c$  are measured by the voltage probes, capacitor  $C_s$  is already known, and frequency is set by a power supply, the energy and power can be calculated. This method is called Lissajous method, which is firstly introduced by Manley in 1943[197].

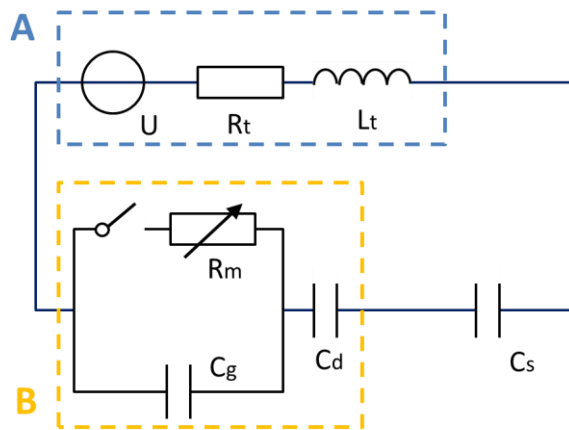


Figure 2-4. Equivalent circuit of DBD reactor.

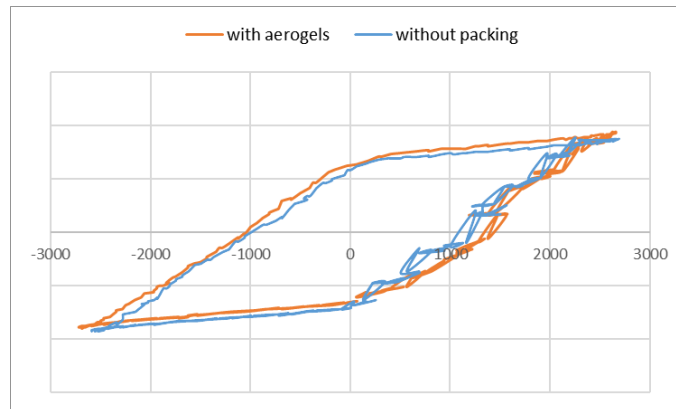


Figure 2-5. A typical Lissajous figure of oscilloscope during the experiments.

#### 2.1.4 Measurement and products analysis

Before the reactor, the flow rate of the inlet gas is controlled by two flowmeters (The Brooks Sho-Rate Models 1355G, calibrated by massive flowmeter) respectively, where the flow rate of each gas can be adjusted from 0 to 40 ml/min. Then both the two gases are inserted into the discharge area via the pores in the bottom cap. After the discharge area, the gas travels through the pores of the top cap (the same configuration as inlet) to the final outlet. Two high-voltage probes were applied to measure the voltage of the plasma reactor and the capacitor; two temperature probes were installed inside the reactor's gas inlet and outlet respectively to measure the temperature of the inlet and outlet gas; one pressure probe was installed before the gas

inlet to monitor the pressure of inlet gas.

The characterization of production and experimental diagnostics system consists of online and offline portions. All the products of the reactor passed through the ice water trap at first for the condensation of the liquid. Then all the rest gaseous species are analyzed by micro gas chromatography (Micro GC Fusion) equipped with two channels (an Rt-Molsieve 5 Å, R 0.25 mm, L 10 m column and an Rt-Q-Bond, R 0.25 mm, L12 m column) and two thermal conductivity detectors (TCD). Meanwhile, all the liquid products condensed are analyzed offline using a gas chromatography-mass spectrometer (GC-MS-QP2010, Shimadzu) equipped with a SUPEL-Q PLOT (R 0.32mm, L 30 m) column. Before the Micro GC, a three-way valve is installed to measure the difference in gas volume before and after the discharge at the outlet by a soap-film flowmeter. The results of Micro GC are acquired and analyzed by the GC Fusion software; the results of GC-MS are acquired by Shimadzu GC-MS real-time software and analyzed by Shimadzu GC-MS offline software equipped NIST Library 2017.

The real-time temperature and pressure data are monitored and recorded simultaneously on a computer via a Keysight 34970A Data Acquisition unit, the datafile of temperature and pressure were directly monitored and recorded simultaneously on the data acquisition computer. The temperature of the resistance in the transformer is also monitored on this computer in case of overheating of the transformer. The electrical data were monitored in real-time via a digital oscilloscope (HP Hewlett Packard 54615B). A soft programmed by Keysight VEE Pro 9.33 is applied to record the electrical data in the same data acquisition computer. The software can record 1,000 points one time of 2 channels (one for the reactor and the other one for capacitor). By adjusting the recording time (from nanosecond to the millisecond), one period of discharge behavior can be recorded.

## 2.2. Preparation and characterization of catalysts

As illustrated in Chapter I, silica aerogel supported catalysts could be ideal catalysts for conventional catalytic reactions due to the notably physical and chemical properties of silica aerogel, including high specific surface area, controllably wide range of pore size, strong adsorption ability, and adjustable surface chemistry property. However, few publications have reported to introducing silica aerogel supported catalysts for the plasma-catalytic process. Due to the preparation method of aerogels, the metallic precursors can be doped on the aerogel support before gelation or by typical impregnation after aerogels are formed. Moreover, the possibility of surface modification on silica aerogel can bring out a hydrophobic surface, which is possible to avoid the formation of irreducible metal hydroxides. Herein, we designed a hydrophobic silica aerogel with catalysts loading by different methods. Importantly, the silica aerogel (or with catalysts) was modified by HMDZ while synthesizing for a hydrophobic surface. Taking advantage of surface modification, the silica aerogel (or with catalysts) can be easily dried under ambient condition.

### 2.2.1 Preparation of catalysts

A series of Co/SiO<sub>2</sub> aerogel catalysts with a various targeted mass ratio of Co to SiO<sub>2</sub> aerogel were firstly prepared via a sol-gel method as illustrated in Figure 2-6. The aiming amount of CoCl<sub>2</sub>·6H<sub>2</sub>O and Co(NO<sub>3</sub>)<sub>2</sub>·6H<sub>2</sub>O (Acros Organics, ≥ 99%) was dissolved in 15.0 g of ethanol (Fisher Scientific, Absolute) in a polyethylene vial while stirring. Simultaneously, 10.0 g of polyethoxydisiloxane (P75W20, PCAS, <30%) was added to the ethanolic solution and stirred for 5 min. After that, 2625 μL of distilled water was added to the mixed solution, and 2955 μL (3-Aminopropyl) triethoxysilane (APTES, Thermo Fisher, 98%) solution (APTES: Ethanol = 1:50) was added to adjust the pH value for gelation. The final mixture solution was covered and allowed to gel and age at 60 °C for 48 h. Nevertheless, we found that the sample synthesized by the nitrate precursor cannot form homogeneous gels. Following the

aging, 35 ml of hexamethyldisilazane (HMDZ, Acros Organics, 98%) was added to the gels synthesized by the chloride precursor and remained covered for three nights at ambient conditions to remove the hydroxyl groups. Following hydrophobizing, the hydrophobic silica gels were washed in ethanol for five times (in 2 days) to remove excessive HMDZ. The gels were transferred into an oven and dried for 2 h at 140 °C. The final gels were first calcined in air at 400 °C for 5 h with a heating rate of 10 °C/min to obtain Cobalt-silica aerogels. These series of catalysts were named as 10 or 20Cl-S (the number refers to the percentage of loading amount).

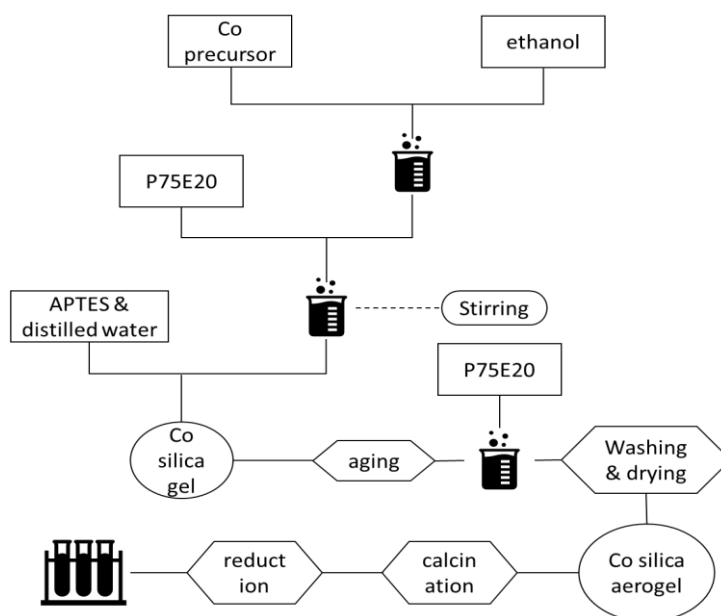


Figure 2-6. Schematic diagram of catalysts synthesis

Another series of Co/SiO<sub>2</sub> aerogel catalysts with the same targeted mass ratio as which were prepared via the sol-gel method were prepared by the wetness impregnation method. The targeted ethanolic solution of CoCl<sub>2</sub>·6H<sub>2</sub>O and Co(NO<sub>3</sub>)<sub>2</sub>·6H<sub>2</sub>O (Acros Organics, ≥99%) were introduced into the same volume of 0 wt% SiO<sub>2</sub> aerogels prepared by the sol-gel method and impregnated for one night. Following the impregnation procedure, the samples were dried, calcined, and reduced as the same procedures as those prepared by the sol-gel method. These series of catalysts were named as 20Cl-I or 20NO-I (Cl and NO refer to the different precursors). Before the experiments, the catalysts samples were reduced in a

continuous H<sub>2</sub>/N<sub>2</sub> (5%/95%) flow under a flow rate of 40 ml/min at 600 °C for 10 h with a heating rate of 10 °C/min.

All raw materials and instruments used in this study are shown in Table 2-1 and Table 2-2.

Table 2-1. Experimental material for the preparation of catalysts

Raw materials and reagents	Molecular formula or abbreviation	Specification or purity
Cobalt chloride hexahydrate	CoCl <sub>2</sub> ·6H <sub>2</sub> O	100g, ≥99.99%
Ethanol	C <sub>2</sub> H <sub>6</sub> O	2.5L, 99%
Polydimethylsiloxane	PEDS(P75E20)	--
Distilled water	H <sub>2</sub> O	--
(3-Aminopropyl) triethoxysilane	APTES H <sub>2</sub> N(CH <sub>2</sub> ) <sub>3</sub> Si(OCH <sub>2</sub> CH <sub>3</sub> ) <sub>3</sub>	100g, 98%
Hexamethyl-disilazane	HMDZ	500ml, 98%
Cobalt nitrate hexahydrate	Co(NO <sub>3</sub> ) <sub>2</sub> ·6H <sub>2</sub> O	100g, ≥99.99%

Table 2-2. Devices used in the preparation of catalysts

Instrument Name	Model
Electric thermostat blast drying oven	Carbolite ELF11/6
Electronic balance	Sartorius
Muffle furnace	STIK
Drying oven	Binder
pH meter	Mettler Toledo

### 2.2.2 Characterization of catalysts

The XRD patterns of the samples were recorded with an X-ray powder diffractometer (Cu K $\alpha$  = 1.5405 Å, X'Pert pro, Philips diffractometer PW1830). The diffractometer was operated at 45 kV and 30 mA. The samples were ground into fine powders for the measurements and recorded for 2 $\theta$  from 10° and 90° with a 0.08° step size for 14 min. The grain sizes of the cobalt oxides were determined with the Scherrer equation. The XRD patterns were processed via HIGHSCORE PLUS V3.05 and compared with PDF standard data base.

The specific surface areas, pore volumes, and average pore sizes were obtained from the N<sub>2</sub> adsorption/desorption analyses conducted at 77 K (ASAP2020, Micromeritics Instrument Corporation). The BET specific surface areas were

calculated from the adsorption isotherms at the relative pressure range of 0.1-1.0, and the BJH pore volumes were determined from the desorption isotherms. The micropore volume and micropore surface area were determined with the t-plot method. The pore sizes and pore size distributions were obtained through both DFT (density functional theory) simulations and BJH method.

The X-ray photoelectron spectroscopy (XPS) experiments were performed on a Thermo Scientific K-Alpha spectrometer with an Al K $\alpha$  monochromator X-ray source running at 3 kV, a hemispherical electron energy analyzer, and a multichannel detector. The test chamber pressure was maintained below  $2 \times 10^{-9}$  Torr during spectral acquisition. A low-energy electron gun was used to neutralize the possible surface charge. The XPS binding energy (BE) was internally referenced to the C 1s peak (BE=284.6 eV). Survey scans were made with a pass energy of 200 eV - step 1 eV; dwell time 50 ms; 8 scans. High-resolution scans were made with pass energy 40 eV - step 0.1 eV; dwell time 50 ms; 8 scans (Voltage 12 V; I=6 mA) The ellipsoid spot size is about 400  $\mu\text{m}$  x 800  $\mu\text{m}$ . The data are acquired and processed by "AVANTAGE 5.98".

SEM observations were carried out on a 30 kV SUPRA 40 (Carl Zeiss AG) electronic microscope based on the 3rd generation GEMINI $\text{\textcircled{R}}$  column. Before observation, the samples were deposited on an adhesive conducting carbon tape and coated with a platinum layer with a thickness of 7 nm via Quorum (Q150 TES). The SEM images were acquired at 3 kV, and 6-10 mbar on a CCD camera with 7.5 $\mu\text{m}$  diaphragm and 4mm working distance, high-efficiency in-lens detector (in the chamber) or Everhart-Thornley secondary electron detector (in the column) was applied for high magnification.

TEM observations and analysis were carried out on a 200 kV FEI Tecnai F20-ST field emission gun microscope equipped with energy dispersive X-ray (EDX) device, scanning transmission electron microscopy (STEM) system, high angle annular dark-field (HAADF) detector and Gatan Imaging Filter (GIF). Powder samples were first

crushed then dispersed in absolute Ethanol suspension, and a few drops were deposited on a copper grid covered with a very thin holey carbon film. Conventional TEM images and diffraction patterns were acquired at 200 kV on a high-angle CCD camera using bright-field imaging mode. High-resolution TEM (HRTEM) images were acquired using a CCD slow-scan camera. Local area fast Fourier transform (FFT) diffractograms, equivalent to electron diffraction patterns, were exploited to determine structural and crystallographic characteristics of observed samples. EDX microanalysis was combined with STEM-HAADF images (Z-contrast images) to perform chemical analyses on studied samples.

## **2.3. Characterization results of catalysts**

### **2.3.1 Textural properties of Co/SiO<sub>2</sub> aerogel catalysts**

Figure 2-7 shows the N<sub>2</sub> adsorption/desorption isotherms of the as-prepared Co/SiO<sub>2</sub> aerogel catalyst samples prepared by different methods and precursors and calcinated with different loading amount. All these isotherms are confirmed to type IV curve (IUPAC classification), indicating that Co/SiO<sub>2</sub> aerogel samples are typical mesoporous materials with ink-bottle shaped and cylindrical-like pore structure[198-201]. The existence of a hysteresis loop is because when the relative pressure is low (usually less than 0.3), the gas in the pore structure of the aerogel is adsorbed by the monolayer. After the adsorption is saturated, the adsorption of the multi-molecular layer begins to occur in the aerogel, which results in an increment of adsorption capacity. When the relative pressure increases (usually at 0.5-0.6), capillary condensation happens, leading to a sharp rise of adsorption curve. While during desorption, the capillary force hinders this process, causing the inconsistency [202]. As the hysteresis loops of all catalysts are type H2 with mesopore which means the presence of interconnected pore system and a random distribution of pores, the BJH results derived from adsorption isotherm are more reliable [203].

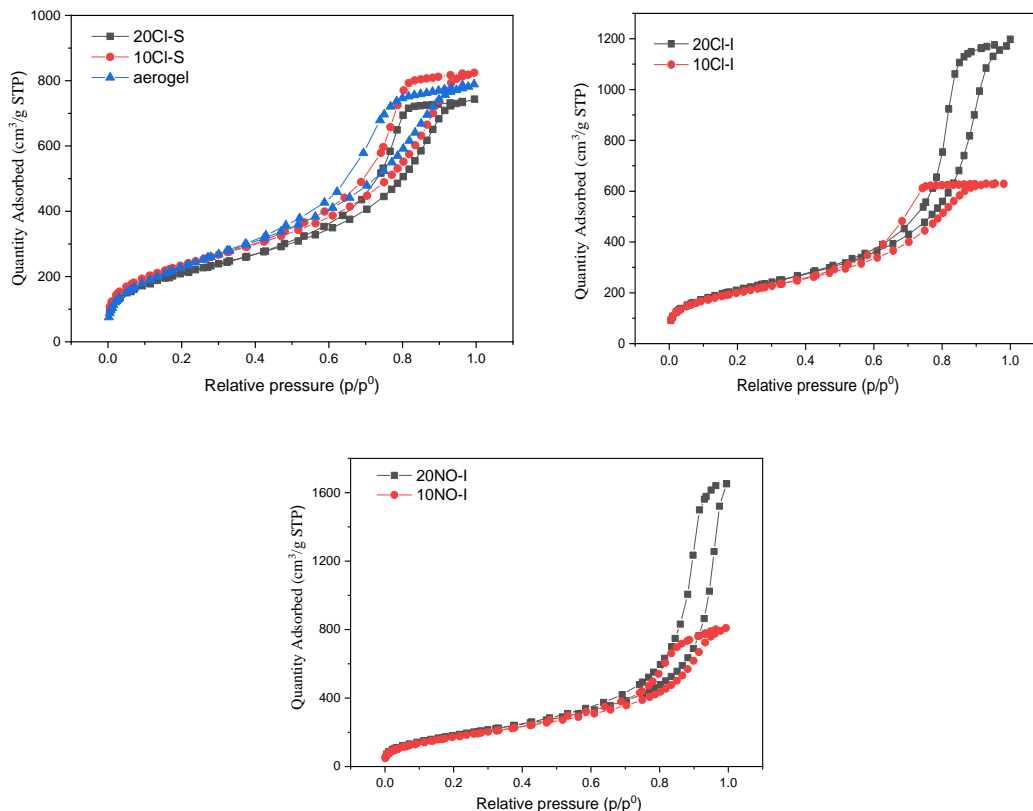


Figure 2-7 N<sub>2</sub> adsorption/desorption isotherms of the as-prepared Co/SiO<sub>2</sub> aerogel catalyst samples prepared by different methods and precursors and calcinated with different loading amount.

Table 2-3 illustrates the specific surface area, pore volume, and average pore size of these catalyst samples. The results revealed that all the samples were a mesoporous structure with negligible or inexistence of micropores. Compared to the blank sample, the surface area and pore volume of Co/SiO<sub>2</sub> aerogel was lower since the cobalt compounds could block the smaller nanopore structure, which results in the decrease in pore volume and surface area. It was found that even 20% of Cobalt loading amount did not obviously decrease the surface area and pore volume, indicating no apparent pore blocking or collapse occurred in the sample. Increasing the loading amount of metal, the surface area naturally decreased. Compared with the samples prepared by the sol-gel method, the surface area of the samples prepared by the impregnation method is lower. The reason is that as widely known, the dispersion of metal catalyst in the sample prepared by incipient wetness impregnation method is not uniform as the solution is drawn into pores by capillary action [204]. When calcining, the samples prepared by impregnation are more accessible to aggregate and block the smaller pores [205].

Table 2-3 Surface area and porous properties of the as-prepared Co/SiO<sub>2</sub> aerogel samples

Catalysts	surface area <sup>a</sup> (m <sup>2</sup> /g)	pore volume <sup>b</sup> (cm <sup>3</sup> /g)	t-plot micropore area <sup>c</sup> (m <sup>2</sup> /g)
aerogel	736	1.57	20.79
10Cl-S	719	1.31	26.87
20Cl-S	708	1.27	28.96
10NO-I	721	1.29	/
20NO-I	624	1.18	/
10Cl-I	713	1.27	/
20Cl-I	655	1.22	/

a Brunauer-Emmett-Teller method.

b Barrett-Joyner-Halenda method determination via N<sub>2</sub> adsorption data.

c t-plot method via Harkins-Jura equation.

### 2.3.2 Structural properties of cobalt species

#### *X-ray diffraction*

The XRD patterns of these as-prepared catalyst samples are presented in Figure 2-8. The prominent broad diffuse diffraction peaks exist among all the XRD patterns of the catalysts between 15° and 30°, where is a characteristic diffraction pattern of an amorphous material, attributing to amorphous silica. However, the peaks of crystalline cobalt phases were barely observed in the figure. The absence of diffraction peaks of cobalt species can be due to the high dispersion of cobalt species, which is attributed to nanosized clusters of cobalt species inside the mesopores or on the surface, leading to evade the detection by XRD [206-208]. Moreover, the formation of nanocrystallized cobalt phase induced by a strong cobalt-support interaction can also result in the inapparent peaks, which are beyond the detection of apparatus [209]. The position of SiO<sub>2</sub> peak shifts toward lower 2θ values slightly with the loading of cobalt due to the collapse of the structure.

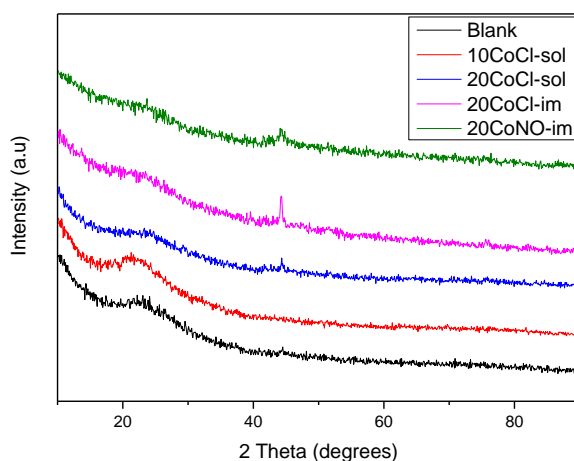


Figure 2-8 The XRD patterns of the as-prepared Co/SiO<sub>2</sub> catalyst samples prepared by different methods and precursors and calcinated with different loading amount.

However, it is clear that the peaks of cobalt species are better forming with higher loading amount of Co even the species of Co are still difficult to define. The Co peaks of the samples prepared by the impregnation method with chloride precursor are more obvious than those prepared by the sol-gel method and nitrate precursor. The reason could be that the Co species can interact with silica supports, resulting in the loss of Co peaks when gelling [210]. As the catalysts prepared from the cobalt nitrate precursors are easier to decompose than cobalt chloride, this facilitates a better dispersion of Co species, leading to a less obvious crystalline peak. The crystallite sizes of cobalt calculated using Scherrer equation are presented in Table 2-4. The crystallite size of the samples prepared by the sol-gel method is smaller than that prepared by the impregnation method, which contributes to the differences in pore size and surface area.

Table 2-4. The crystallite sizes of Co species in the as-prepared

Catalysts	Calcining temperature (°C)	Crystallite size <sup>a</sup> (nm)
20Cl-S	400	6.5
20Cl-I	400	20.3
20NO-I	400	14.3

a Scherrer equation.

### *X-ray photoelectron spectroscopy*

The original XPS spectra of 20% loading Co/SiO<sub>2</sub> aerogel prepared the sol-gel method are shown in Figure 2-9. Clearly, the 2p peak of chloride is trace, the main elements of Co/SiO<sub>2</sub> aerogels are Co, O, and Si indicating the cobalt chloride in the catalyst samples has been successfully transformed to oxides or other species with silicon. As the half-peak width of Co2p<sub>3</sub> is more than 3 eV, implying the existence of superposition of several peaks, different cobalt species exist in the supports. The comparison of Co 2p XPS spectra of different loading amount on silica aerogel is shown in Figure 2-10. Obviously, the more loading on the silica aerogel, the better the Co 2p peaks are defined.

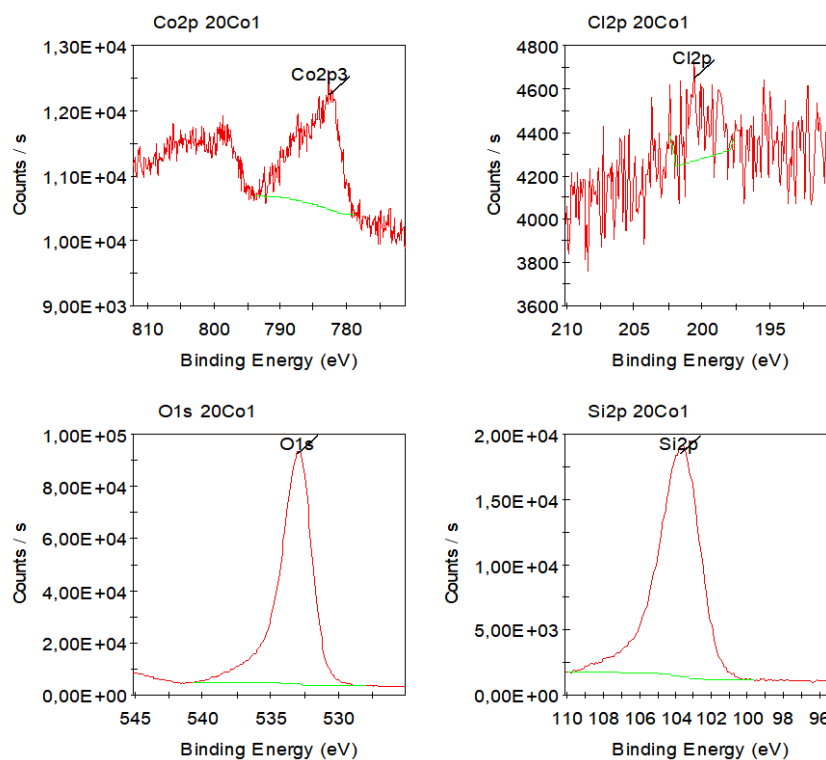


Figure 2-9. The XPS spectra of the as-prepared 20Cl-S sample.

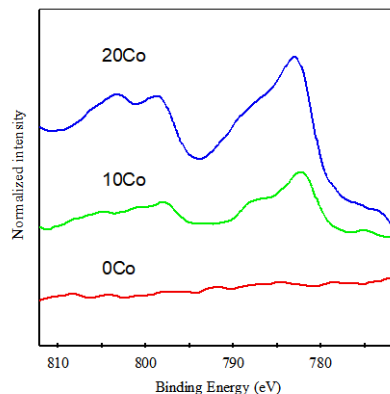


Figure 2-10. The Co 2p XPS spectra of the aerogel and the Cl-S samples.

The further fitted peaking results of Co2p peaks are shown in Figure 2-11. The peaking method is referred to Pin-Juyu's work [211]. Three Co species are known to exist in the 777–815 eV region:  $\text{Co}^0$ ,  $\text{Co}^{2+}$ , and  $\text{Co}^{3+}$ , which attribute to  $\text{CoO}$ ,  $\text{Co}_2\text{O}_3$ , and  $\text{Co}_3\text{O}_4$ . The BE of  $\text{Co}^0$  2p<sub>3/2</sub> is about 778.6 eV, and the splitting between the 2p<sub>3/2</sub> and 2p<sub>1/2</sub> is almost 15 eV. The BE values of  $\text{Co}^{2+}$  and  $\text{Co}^{3+}$  2p<sub>3/2</sub> have been reported by many authors yet, but unfortunately, the exact BE shifts up to 0.6 eV from one to the other [212-215]. Considering that the binding energy of  $\text{Co}^{3+}$  is uncharacteristically lower than that of  $\text{Co}^{2+}$  attributed to the final state (relaxation) effect, and some researchers reported that the Co2p lines of  $\text{Co}^{2+}$  when Co is deposited onto other oxides such as Si, Mo and Ti followed by oxidation, shift to higher BE up to 781.7 eV [216]. The main oxidized peak was considered as  $\text{Co}^{2+}$ , and the other oxidized Co peak with lower binding energy was referred to  $\text{Co}_3\text{O}_4$ . However, another oxidized Co peak is detected, which could be assumed as  $\text{CoO}$  and  $\text{CoO}_2\text{-Si}$ , according to Matsuzaki's and Jiménez's research [214, 217]. Further study was essential to identify the oxidized cobalt peaks of high binding energy. Despite the difference in the peak intensity, the peaking results of the samples prepared by the impregnation method are similar to the samples prepared via the sol-gel method with less prominent the oxidized cobalt peaks of high binding energy.

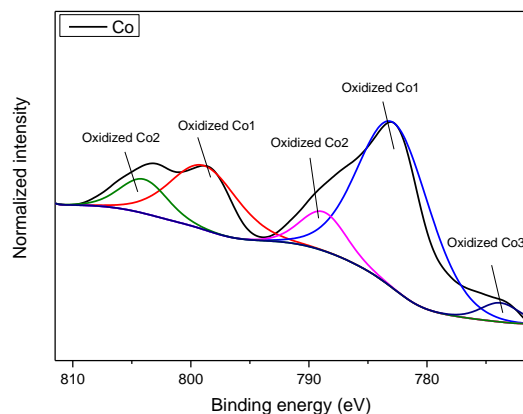


Figure 2-11. XPS peaking of the Co 2p region of the 20Cl-S sample.

To confirm the assumption above, the comparison of Si 2p and O 1s peaks of different cobalt loading catalysts prepared by the sol-gel method is shown in Figure 2-12. As the loading amount increasing, the O1s and Si2p peaks become broader fitted to the same intensity, which means the existence of overlaps. The overlaps related to the loading amount of cobalt imply the existence of a phase, which consists of Co, Si, and O, thus supporting the assumption above.

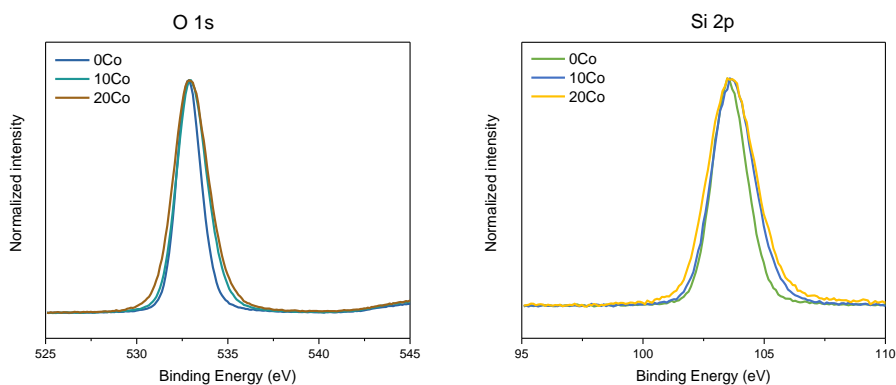


Figure 2-12. The comparison of Si2p and O1s peaks of different cobalt loading catalysts prepared by the sol-gel method.

### 2.3.3 Electron microscope

#### *Scanning electron microscope*

The scanning electron microscope (SEM) was applied to study the surface

morphology of Co/SiO<sub>2</sub> aerogel catalysts. Figure 2-13 illustrates the micrographs of the as-prepared catalyst samples. The matrix of silica aerogel is easily observed, which is made up of many visible clusters of spherical particles. In figure (a), a uniform three-dimensional skeleton structure with a loose framework, which results in the porous structure, is clearly observed. Considering that the catalyst samples with low loading amounts well maintained the skeleton structure consisted by spherical clusters, the fact that the pores of these catalysts are mainly ink-bottle shaped, which is consistent with the results of N<sub>2</sub> adsorption/desorption. Meanwhile, a small number of cobalt particles and species with different structures are found comparing figure (b), (c), (d), (2), (3) and (4), which reveals that the not only cobalt oxides but also other cobalt species. Particularly, in figure (2) a fibrous or filamentous structure is found as a different phase from spherical clusters, thus providing circumstantial evidence for the assumption above on the formation of CoO<sub>2</sub>-Si. As shown in Figure 2-14, it has been reported that one part of the cobalt phase in aerogels can connect with -O- during the hydrolytic and polycondensation and form -O-Co-O- bridge and the chain structure. This interaction between cobalt catalysts with the support finally leads to an inactivate species due to the difficulties of reduction [218]. The SEM micrographs of the samples prepared by the different method with different loading amount are also illustrated in these figures. The cobalt particles are observed in the samples prepared by different methods. Besides, the different fibrous structure is much less existent in the sample prepared by the impregnation method. Instead, an aggregation structure of cobalt species is observed, which confirmed the results of XRD and N<sub>2</sub> ad/desorption, leading to the partial block of porous structure and the decrease of specific surface area.

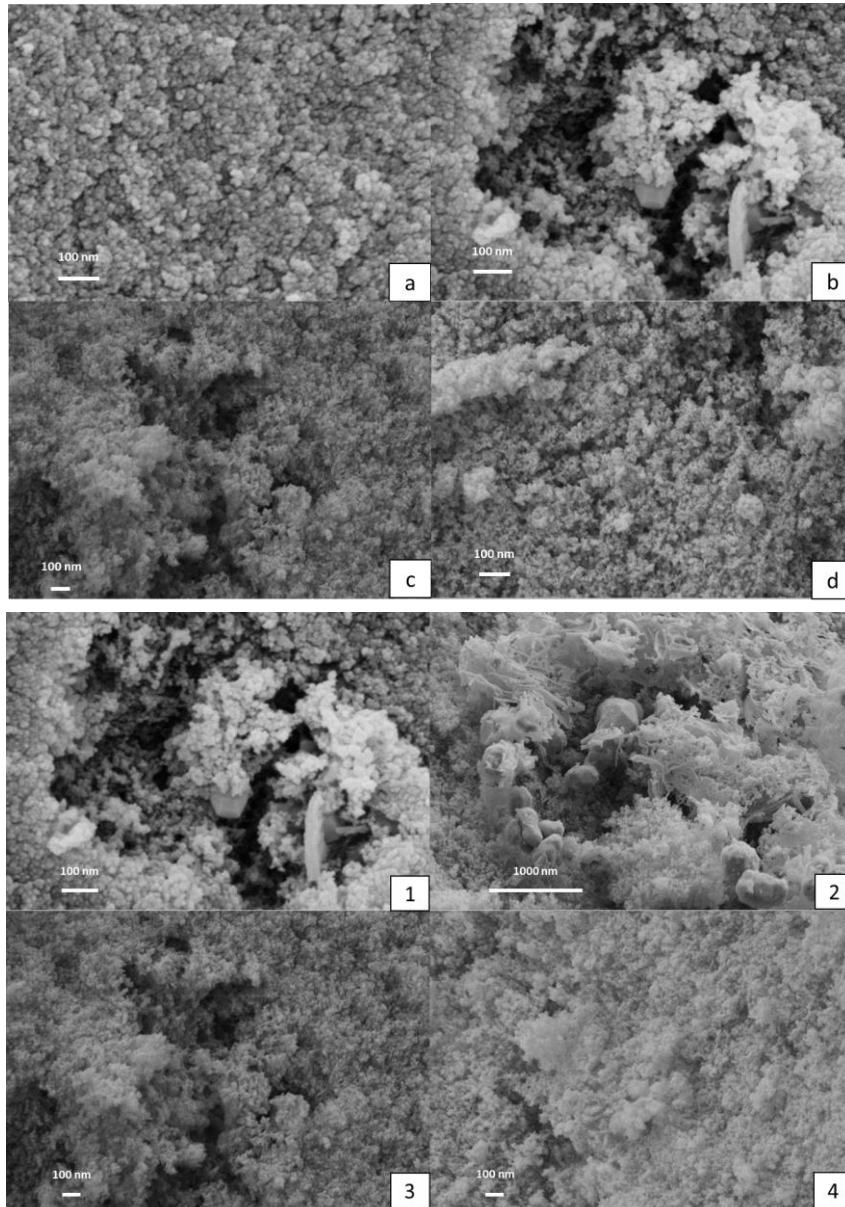


Figure 2-13. The SEM micrographs of: (a) aerogel, (b) 10Cl-S, (c) 10Cl-I, (d) 10NO-I, (1) 10Cl-S, (2) 20Cl-S, (3) 20Cl-I, (4) 20NO-I.

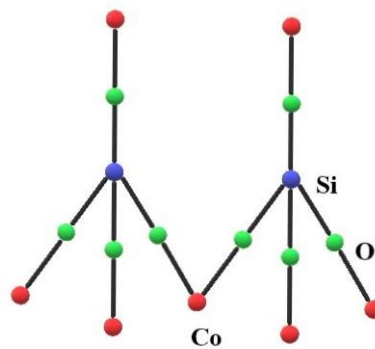


Figure 2-14. The unit of the fibrous structure of Co/SiO<sub>2</sub>.

*Transmission electron microscope and Energy-dispersive X-ray spectroscopy*

TEM bright-field images corresponding to different samples are shown in Figure 2-15. The typical porosity of amorphous silica matrix with a loose framework consisting of spherical units is clearly shown in the figures. As estimated from TEM images, the pore size is among several nanometers range. The TEM observations of these samples also indicate an excellent dispersion of cobalt phase with a particle size of several nanometers. However, the aggregation of the cobalt phase can be observed, which is consistent with previous characterization results.

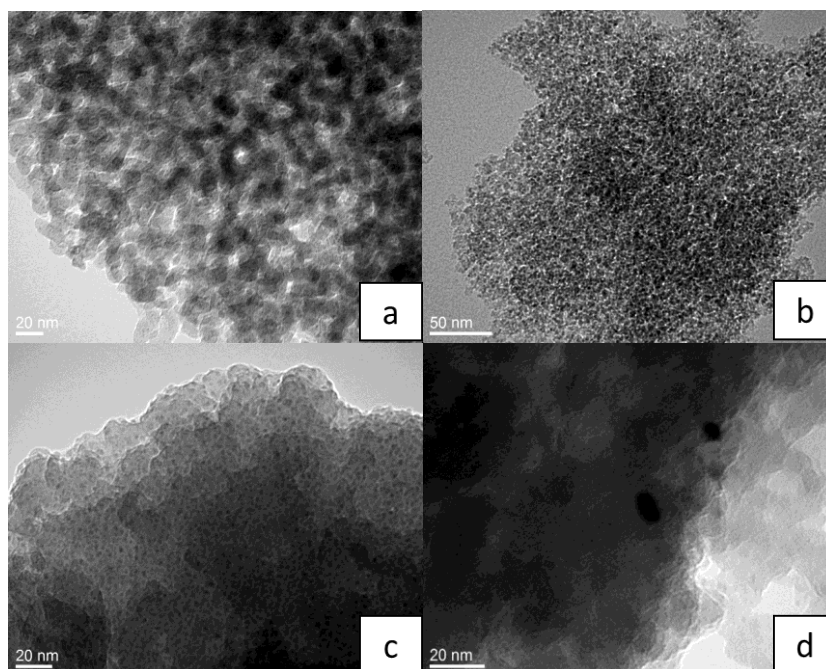


Figure 2-15. TEM bright-field images of (a) 10Cl-S, (b) 20Cl-S, (c) 20Cl-I and (d) 20NO-I.

Later the HRTEM bright-field images and selected area diffraction applied to explore the species and crystalline structure of cobalt particles as shown in Figure 2-16 and Figure 2-17, respectively. The results show the selected cobalt species in Figure 2-16 is a hexagonal cobalt oxide crystallite in space group P-3m1 with a lattice parameter of  $a=2.82 \text{ \AA}$ ,  $b=2.82 \text{ \AA}$ ,  $c= 4.24 \text{ \AA}$ , which is confirmed to be  $\text{CoO}_2$  structure [219]. As calcining cobalt precursors in the air could hardly form the unstable  $\text{CoO}_2$ , the speculation of the existence of  $\text{CoO}_2\text{-Si}$  structure is reasonable. On the contrary to

CoO<sub>2</sub>, which is highly reducible, the CoO<sub>2</sub>-Si structure exhibits low reducibility and low catalytic activity according to the mentioned publications. Based on the results, the Co species in the SiO<sub>2</sub> aerogel support is confirmed to be catalytically active CoO and Co<sub>3</sub>O<sub>4</sub> catalytically inactive CoO<sub>2</sub>-Si formed by the strong interaction between catalyst and support due to the difficulties on reduction.

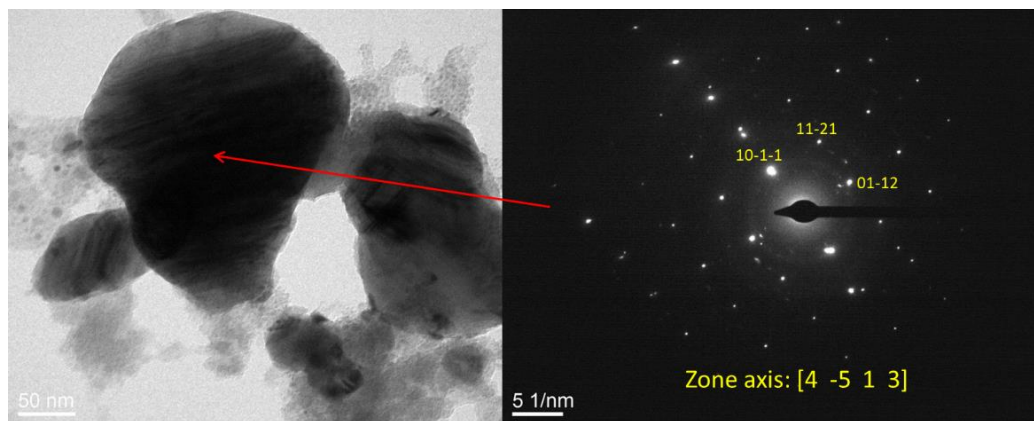


Figure 2-16 The HRTEM bright-field images and selected area diffraction of 20Cl-S sample.

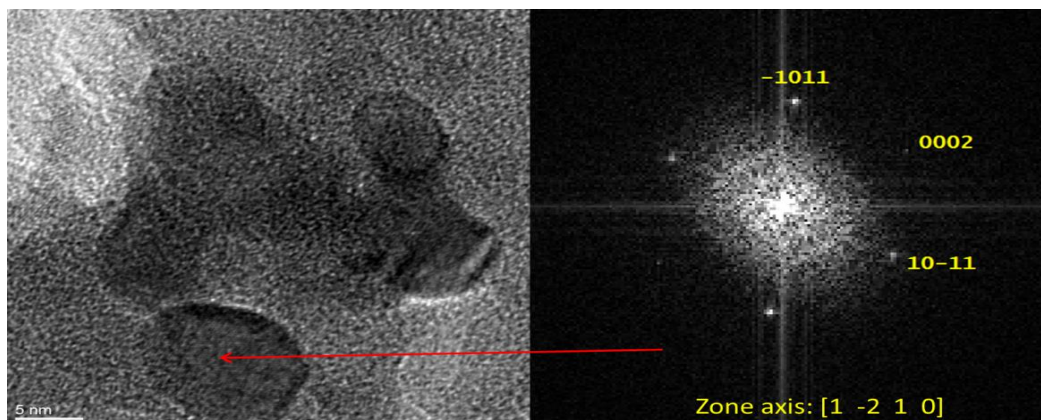


Figure 2-17 The HRTEM bright-field images and selected area diffraction of 20NO-I sample.

## 2.4. System diagnostics

It is of great importance to fully understand the electrical characteristic of CO and H<sub>2</sub> at different voltage and frequency in a DBD plasma generating circuit before igniting CO and H<sub>2</sub> plasma in the reactor. For the consideration of safety, inert gas is

normally used in the testing experiment. The experimental circuit with the configuration of the transformer is shown in Figure 2-18.

In the first testing experiments with nitrogen, by varying the peak-to-peak voltage and the frequency of the signal, a proper range of the variables can be found for a reasonable discharge power with enough voltage to break down the gas.

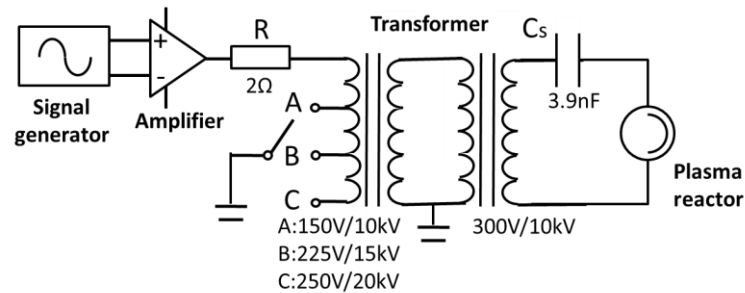


Figure 2-20. The experimental circuit with the configuration of the transformer.

Figure 2-21 and Figure 2-22 present the peak-to-peak voltage of the DBD reactor and the capacitor varying by the frequency of the input signal. With a certain input signal from the power supply, the increase of frequency lead to the increase of peak-to-peak voltage of DBD reactor and capacitor at first, then the peak-to-peak voltages decrease dramatically with the increase of frequency. This phenomenon is because when the frequency of the circuit reaches the resonance frequency, the peak-to-peak voltage can reach the peak value. The same tendency can also be observed in the power of DBD plasma. The energy consumption of DBD in an electric cycle firstly increases with the increase of frequency followed by a decline after peaking around resonance frequency at 3000 Hz. In contrast, the peak of power consumption of DBD reactor versus frequency delays slightly at around 3000 Hz to 9.8 W.

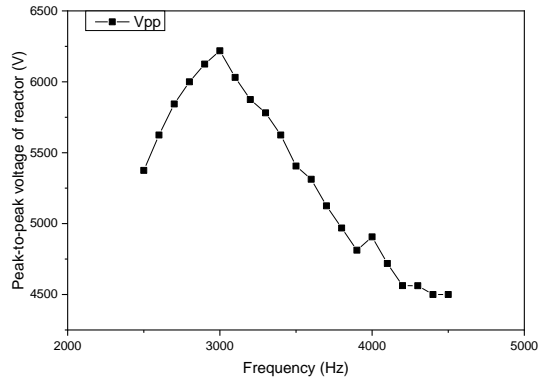


Figure 2-21. Peak-to-peak voltage of N<sub>2</sub> DBD reactor versus frequency (Signal generated: 0.45 V; N<sub>2</sub> flow rate: 20 ml/min; Amplification: -4 dB).

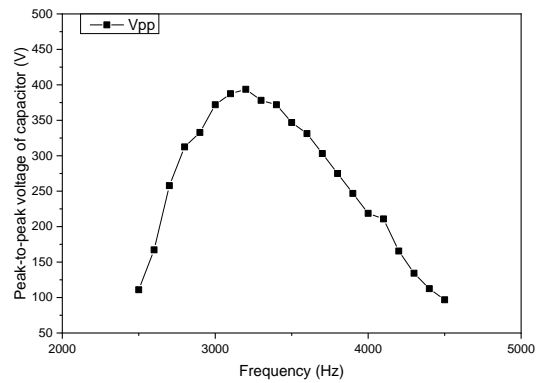


Figure 2-22. Peak-to-peak voltage of capacitor C<sub>s</sub> versus frequency (Signal generated: 0.45 V; N<sub>2</sub> flow rate: 20 ml/min; Amplification: -4 dB).

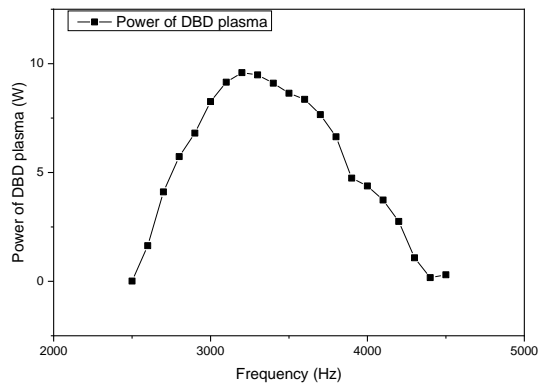


Figure 2-23. Power consumption of N<sub>2</sub> DBD reactor versus frequency (Signal generated: 0.45 V; N<sub>2</sub> flow rate: 20 ml/min; Amplification: -4 dB).

Figure 2-24 shows the increasing tendency of power consumption of DBD with

the increase of frequency from 2500 to 4000 Hz. In this case, the peak-to-peak voltage on the DBD reactor is fixed at 5500 V, while the total power input to the circuit is varying. Normally, with the increase of the frequency, the power input increase as well resulting in the growth of the power consumption of DBD. It is reported that the power consumption of surface DBD shows linear revolution with varying frequency [220]. However, the thermal instability issue is more dramatic with the increase of frequency after resonance.

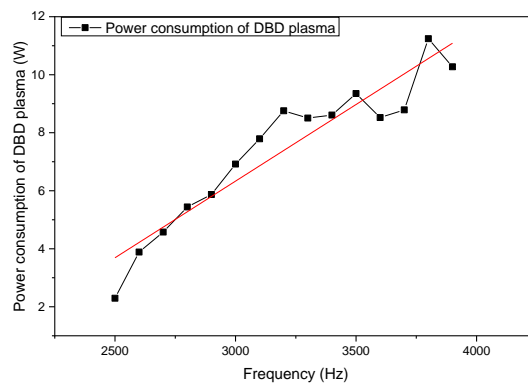


Figure 2-24. Power consumption of N<sub>2</sub> DBD versus frequency (Signal generated: 0.45 V; N<sub>2</sub> flow rate: 20 ml/min; Peak-to-peak voltage of DBD: 5500 V).

Figure 2-25 shows the increasing tendency of power consumption with the increase of the peak-to-peak voltage of the sine signal supplied to the circuit of the DBD reactor. In this experimental group, the frequency of the signal was fixed at 3300Hz. The energy consumption of DBD in a cycle increases with the increase of V<sub>pp</sub> on DBD, which conforms to others reports [220-222].

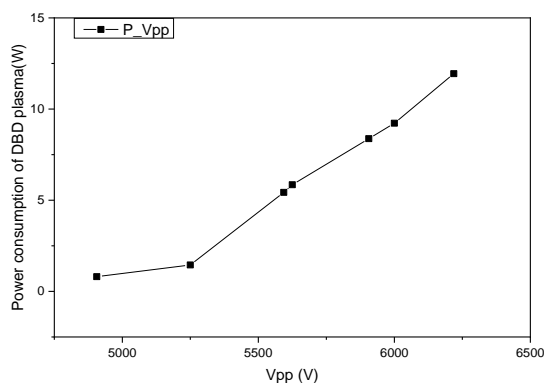


Figure 2-25. Power consumption of N<sub>2</sub> DBD in an electric cycle versus voltage on DBD (Frequency: 3300 Hz; N<sub>2</sub> flow rate: 20 ml/min; Amplification: -4 dB).

## Summary

In this chapter, the experimental bench was first designed and established and analytical and diagnostic apparatuses are illustrated. By connecting a capacitance in series with the DBD reactor, the power into DBD plasma can be calculated via the Lissajous method instead of using a mathematical method to process the spikes in current data. A pressure probe and two temperature probes are applied to calibrate the reaction condition in the DBD reactor. Moreover, a soap film flowmeter is applied to calibrate the volume change of the inlet gas during the discharge to lessen the experimental deviation. Later, different Co loaded silica aerogel catalysts were designed, prepared by different methods and characterized for plasma promoted FTS in DBD reactor. According to the characterization results, the SiO<sub>2</sub> aerogel prepared by ambient drying after surface modification exhibits a mesoporous structure with very high specific surface area and high adsorption capacity. It is found that whatever method the samples are prepared by, even the difference in specific surface area and porous structure exist, the alteration on the specific surface area after doping Co on the support is not significant within a range less than 20 wt% (metal to silica), implying the porous structure is well maintained, which is also observed by SEM and TEM. The results of XRD spectra illustrate Co species are well dispersed on the

supports. However, different oxidized Co species with different morphological characteristics on the supports are detected in the as-prepared samples after later characterization. Except for CoO and Co<sub>3</sub>O<sub>4</sub>, a fibrous structure different from SiO<sub>2</sub> bone cluster is observed on the sample prepared by the impregnation method. Combining the results of XPS and TEM with some published work, the Co species are assumed to be CoO<sub>2</sub>-Si structure. Due to the difficulties of reduction, it is considered catalytically inactive. At last, the system diagnostic tests were conducted by N<sub>2</sub>. It is found that when fixing the N<sub>2</sub> flow rate and the peak-to-peak voltage of DBD, the power in the discharge increases with the frequency, and the thermal instability issue becomes more dramatic after resonance.

# Chapter III. Plasma-catalytic conversion of CO and H<sub>2</sub>

## Résumé du chapitre

Ce chapitre est consacré à l'étude expérimentale de la synthèse d'hydrocarbures à partir de gaz de synthèse par plasma non-thermique associé à de la catalyse hétérogène. Remplacer une synthèse thermo-catalytique à haute pression de type Fischer-Tropsch par une synthèse plasmocatalytique à pression atmosphérique pourrait conduire à un gain d'énergie pour la production d'hydrocarbures et d'oxydes organiques synthétiques. La première partie de ce chapitre est consacrée à la conduite d'essais de synthèse à partir de syngaz en plasma seul à pression atmosphérique. Ces essais ont été réalisés à différents débits de syngaz, de rapports H<sub>2</sub>/CO et de fréquence d'excitation du plasma, afin d'évaluer l'efficacité du plasma seul. Puis, la deuxième partie du chapitre présente les essais avec l'ajout de cobalt comme catalyseur sur support d'aérogel de silice, dans une configuration de réacteur rempli. Les résultats indiquent que des quantités considérables d'hydrocarbures C1-C5 ont été synthétisées dans des conditions ambiantes avec des énergies d'entrée spécifiques relativement basses (inférieures à 18 kJ/l). De plus, le catalyseur Co sur support d'aérogel de silice semble favoriser non seulement la synthèse d'hydrocarbures C2-C5, mais aussi la formation d'oxydes organiques liquides. Les catalyseurs cobalt obtenus par procédé d'imprégnation avec un précurseur de nitrate (présenté en chapitre 2) ont montré une excellente performance catalytique dans cette configuration de réacteur. Sur la base des connaissances existantes sur le sujet, des voies de réaction possibles sont alors proposées. Les résultats obtenus dans ce chapitre démontrent au final qu'une nouvelle approche de synthèse organique à partir de syngaz est possible, en alternative à la synthèse Fischer-Tropsch traditionnelle.

## Abstract

This chapter is dedicated to the experimental study of hydrocarbon synthesis from syngas via a non-thermal plasma pathway associated with heterogeneous catalysis in a packed bed reactor configuration. An ambient plasma-catalytic process instead of a conventional thermo-catalytic process at high pressure could lead to a new FTS pathway for synthesizing hydrocarbons and organic oxides with lower energy consumption. The first part of this chapter is devoted to conducting the plasma FTS tests from syngas without catalysts at atmospheric pressure; the plasma experiment was first conducted without placing catalysts at ambient conditions. These tests were carried out by different experimental variables, including total flow rate, H<sub>2</sub>/CO ratio, and frequency to evaluate the effects of the variables under plasma discharge. Then the second part of the chapter presents the performance of the catalysts by introducing silica aerogel support and different Co/SiO<sub>2</sub> aerogel catalysts. The results indicate that a considerable concentration of C1 to C5 hydrocarbons were synthesized at ambient conditions with relatively low specific input energies (below 18 kJ/l). Moreover, the Co/SiO<sub>2</sub> aerogel catalysts can promote not only the formation of C2-C5 hydrocarbons rather than CH<sub>4</sub> and CO<sub>2</sub> but also the formation of liquid organic oxides. The cobalt catalysts obtained by the impregnation method with nitrate precursor (presented in Chapter II) exhibited excellent catalytic performance. Based on the knowledge of existing work, the possible reaction pathways of the non-thermal plasma promoted FTS associated with catalysis are proposed. The results demonstrate a new approach of plasma-catalytic promoted FTS at ambient conditions and broadens the field of further improvement on FTS.

### 3.1. Introduction

As mentioned in Chapter I, non-thermal plasmas, which are far from thermodynamic equilibrium, can be generated at ambient temperature and pressure with a low power requirement. The combination of plasma and catalysts described as plasma-catalysis, which has been widely considered as a promising method for organic synthesis, is a complicated and vague process in a one-stage system, where the catalyst is introduced in the discharge zone directly. The synergistic effects between plasma and catalysts can modify both the chemical and physical properties of each other [223-225]. On the one hand, plasma might restructure the catalysts and the surface of supports to promote chemical adsorption and reaction and the catalysts with supports, in turn, might enhance the plasma phenomenon [163, 226, 227]. On the other hand, the dramatic reduction of discharge volume could alter, even impair the discharge behavior, therefore decreasing the power of plasma [163, 228]. Until now, only a few research is done on plasma promoted hydrocarbon synthesis via FTS. Our group [148, 149] has conducted some experiments on FTS via very high-pressure plasma without catalysts; the results indicated that even at very high pressure (~2 MP) with high specific input energy (varying from 1000 to 10000 kJ/mol), light hydrocarbons are dominant among all the products. The absence of catalysts may be the reason for the low selectivity to C<sub>5+</sub> paraffin and olefins. Meanwhile, Al-Harrasi et al. [150] have studied plasma promoted FTS with external heating and operating pressure and w35% (w/w)Cu/Co=1 (weight ratio) alloy loaded aluminosilicate (Al<sub>2</sub>SiO<sub>5</sub>) ceramic foam monolith. The results have shown the existence of C<sub>5+</sub> at a low H<sub>2</sub>/Co ratio (~0.5) with specific input energy of 2500 kJ/mol. Until now, no research on non-thermal plasma promoted FTS at ambient conditions is found.

Herein, this chapter aims to explore the possibility of hydrocarbons synthesis from syngas via plasma-catalytic promoted FTS at ambient conditions. The plasma experiments were firstly conducted in a tubular dielectric barrier discharge reactor at

ambient pressure and temperature, and the influence of different variables like total flow rate and a different ratio of H<sub>2</sub> and CO were investigated. The hydrophobic SiO<sub>2</sub> aerogel was synthesized as the support for Co catalyst due to its hydrophobicity and high porosity, which could avoid the extreme reduction of discharge volume. The Co loaded hydrophobic SiO<sub>2</sub> aerogel catalysts (Co/SiO<sub>2</sub>) were designed, synthesized by different methods and Co precursors, and then dried at ambient conditions. Finally, the catalysts were calcined, placed into the reactor, and the catalytic performance of the catalysts was investigated and presented. This study offers a new perspective of hydrocarbon synthesis at ambient pressure and temperature via plasma promoted FTS associated with catalysis.

### **3.2. Plasma tests without catalyst**

The experimental conditions of tests without catalyst are presented in Table 3- 5. The liquid product was collected for 90 min and then washed out by 3 ml of pure acetone for the analysis via GC-MS. Among all tests without catalysts, liquid products were barely collected, only the results of gas products were listed. For the quantitative study of the concentration of gas products and electrical parameters, the measurements were repeated three times (at 30 min, 60 min, and 90 min) after the discharge was stable. The plasma experiments were repeated three times. The experimental uncertainties (Err) of ±10% for GC and 12% for GC-MS were mainly contributed by the calibration (Err<sub>calibration</sub>) and sample measurements (Err<sub>repeatability</sub>).

$$\text{Err} = \text{Err}_{\text{calibration}} + \text{Err}_{\text{repeatability}} \approx 10\% \text{ (for GC)}, 12\% \text{ (for GC-MS)}$$

Table 3-1. Experimental variables of plasma tests without catalysts.

Total flow rate (ml/min)	H <sub>2</sub> /CO ratio	Frequency (Hz)
40	1	3000
30	1	3000
20	1	3000
30	2	2600 to 3400
30	0.5	3000

According to the measurements of GC before and during each experiment, the conversion rate ( $x$ ) of H<sub>2</sub> and CO is calculated as:

$$x_{H_2} = \frac{\text{moles of } H_2 \text{ consumed}}{\text{moles of } H_2 \text{ inlet}} \% \quad (1)$$

$$x_{CO} = \frac{\text{moles of } CO \text{ consumed}}{\text{moles of } CO \text{ inlet}} \% \quad (2)$$

The selectivity of gaseous products can be calculated as:

$$S_{CO_2} = \frac{\text{moles of } CO_2 \text{ produced}}{\text{moles of } CO \text{ consumed}} \times 100 \% \quad (3)$$

$$S_{C_xH_y} = \frac{x \times \text{moles of } C_xH_y \text{ produced}}{\text{moles of } CO \text{ consumed}} \times 100 \% \quad (4)$$

Then the total selectivity of liquid products can be calculated by subtracting the selectivity to CO<sub>2</sub> and gaseous hydrocarbons:

$$S_{liquid} = 100\% - S_{CO_2} - S_{C_xH_y} \quad (5)$$

The specific input energy (SIE) is defined as the formula following:

$$SIE = \frac{\text{Plasma power (kW)}}{\text{Flow rate}(\frac{l}{min})} * 60(\frac{s}{min}) \quad (6)$$

The energy efficiency of the reactor based on the gas conversion is defined as the gas converted per unit of discharge power:

$$E_{CO} = \frac{x_{CO}}{\text{power of discharge}} \times 100 (\%/W) \quad (7)$$

$$E_{H_2} = \frac{x_{H_2}}{\text{power of discharge}} \times 100 (\%/W) \quad (8)$$

The carbon balance (CB) is calculated as:

$$CB = \frac{CO_{out} + CO_{2\ out} + \sum C_x H_y\ out}{CO_{in}} \quad (9)$$

### 3.2.1 H<sub>2</sub>/CO ratio

The first series of plasma experiments without placing catalysts were aimed at exploring the influence of H<sub>2</sub>/CO ratio. The liquid products were collected for 90 min and then dissolved by 3 ml of pure acetone. Due to the negligible liquid produced via these tests, only the results of the gas products were listed. The measurements were repeated three times (at 30 min, 60 min, and 90 min) after the discharge behavior was stable. Figure 3-1 illustrates the SIE and conversion rate as a function of different H<sub>2</sub>/CO ratio. The results listed in Table 3-2 demonstrate the gaseous products analysis, the energy efficiency of the reactants, and carbon balance. Table 3-3 demonstrates the concentration of C<sub>2</sub>-C<sub>5</sub> hydrocarbon species in the product gas.

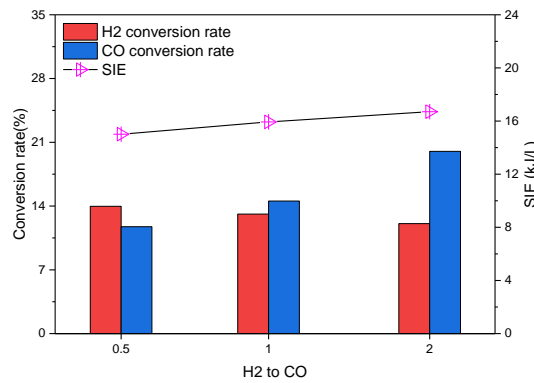


Figure 3-1. The SIE and conversion rate as a function of different H<sub>2</sub>/CO ratio (total flow rate: 30 ml/min, frequency: 3000 Hz, peak-to-peak voltage: 6 kV)<sup>1</sup>.

Table 3-2. Gaseous products analysis of the experiments varying by different H<sub>2</sub>/CO ratio (total flow rate: 30 ml/min, frequency: 3000 Hz, peak-to-peak voltage: 6 kV)<sup>1</sup>.

H <sub>2</sub> /CO ratio	Selectivity			Energy efficiency (%/W)		Carbon balance
	CO <sub>2</sub>	CH <sub>4</sub>	C <sub>2</sub> -C <sub>5</sub>	H <sub>2</sub>	CO	
0.5	0.59	0.29	0.10	1.86	1.56	0.969

1	0.57	0.31	0.11	1.65	1.83	0.985
2	0.48	0.36	0.13	1.45	2.41	0.989

Table 3-3. Concentration distribution of C2-C5 hydrocarbons in the product gas varying by different H<sub>2</sub>/CO ratio<sup>1</sup>.

H <sub>2</sub> /CO ratio	C <sub>2</sub> H <sub>6</sub> (ppm)	C <sub>2</sub> H <sub>2</sub> +C <sub>2</sub> H <sub>4</sub> (ppm)	C <sub>3</sub> H <sub>8</sub> (ppm)	C <sub>3</sub> <sup>2</sup> (ppm)	C <sub>4</sub> H <sub>10</sub> (ppm)	C <sub>4</sub> <sup>2</sup> (ppm)	C <sub>5</sub> <sup>2</sup> (ppm)
0.5	2270	106	490	350	72	195	82
1	2583	64	550	420	68	175	49
2	2425	46	496	347	61	148	37

<sup>1</sup> The overall error of the result is within ± 10%

<sup>2</sup> Referring to C<sub>n</sub> species excluding n-paraffin

It is quite interesting that C2-C5 hydrocarbon species, which were barely detected in the previous work of our group via high-pressure plasma [148, 149], were found among the yield of the products with a relatively low SIE. The CO disproportioning reaction has been well comprehended that the vibrational excitation could significantly accelerate it under non-thermal plasma [229]:



The activation energy of the disproportioning reaction is much less than the energy of direct CO bond dissociation (11.2 eV). This explains the high concentration of CO<sub>2</sub> among the gaseous products. The increase of the CO portion in the feeding gases increased the selectivity to CO<sub>2</sub> as the CO disproportioning reaction was promoted. As a result, the carbon balance was lower, and more carbon deposits were formed. Similar to the initial reactions of FTS, methane, and acetylene can be synthesized from syngas in non-thermal plasma conditions [230]:



Thus, the ratio of H<sub>2</sub>/CO significantly affected the conversions, selectivity, and distribution of different gaseous species. A high portion of H<sub>2</sub> benefited the conversion of CO to CH<sub>4</sub> instead of CO<sub>2</sub> and the discharge power at a certain peak-to-peak voltage as the dissociation energy (4.52 eV), and relative breakdown voltage of H<sub>2</sub> are lower than those of CO. Besides, the CO<sub>2</sub> produced via the disproportioning reaction could be excited (~5.5 eV) again to generate highly active O species. It should also be noticed that the conversion rate of H<sub>2</sub> decreased with the increase of H<sub>2</sub> in the feed gases due to its extremely fast deexcitation. More saturated hydrocarbons were found rather than unsaturated species in the gaseous products logically with a large portion of H<sub>2</sub>. This is also because the discharge atmosphere was more enriched with excited H due to its low dissociation energy, leading to the formation of saturated hydrocarbons even with a high portion of CO. Considering the FTS mechanism and the overall high carbon balance, we assumed that a part of carbon from CO disproportioning reaction could participate in chain initiation and growth reactions in the reactor:



Where \* refers to an excited state.

### 3.2.2 Total flow rate

The SIE, conversion rates of CO and H<sub>2</sub> varying by total flow rate are shown in Figure 3-2. Table 3-4 and Table 3-5 represent the analysis of gaseous products analysis, the energy efficiency of the reactants, and carbon balance and the concentration of C2-C5 hydrocarbon species in the product gas varying by total flow rate, respectively. H<sub>2</sub>/CO ratio of all the tests was fixed at 1:1.

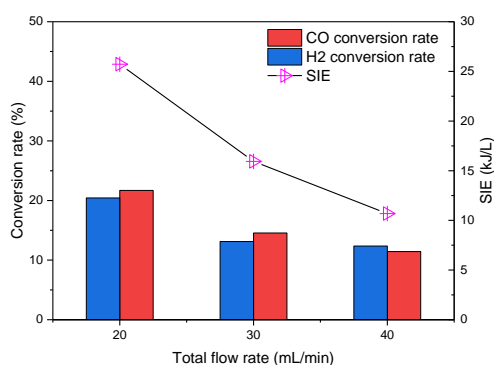


Figure 3-2. The SIE and conversion rate as a function of total flow rate ( $H_2/CO=1:1$ , frequency: 3000 Hz, peak-to-peak voltage: 6 kV)<sup>1</sup>.

Table 3-4. Gaseous products analysis of the experiments varying by total flow rate ( $H_2/CO=1:1$ , frequency: 3000 Hz, peak-to-peak voltage: 6 kV)<sup>1</sup>.

Total flow rate	Selectivity			Energy efficiency (%/W)		Carbon balance
	CO <sub>2</sub>	CH <sub>4</sub>	C2-C5	H <sub>2</sub>	CO	
40 ml/min	0.51	0.23	0.10	1.74	1.61	0.981
30 ml/min	0.57	0.31	0.11	1.65	1.83	0.985
20 ml/min	0.50	0.27	0.09	2.38	2.53	0.951

Table 3-5. Concentration distribution of C2-C5 hydrocarbons in the product gas varying by total flow rate<sup>1</sup>.

Total flow rate	C <sub>2</sub> H <sub>6</sub> (ppm)	C <sub>2</sub> H <sub>2</sub> +C <sub>2</sub> H <sub>4</sub> (ppm)	C <sub>3</sub> H <sub>8</sub> (ppm)	C <sub>3</sub> <sup>2</sup> (ppm)	C <sub>4</sub> H <sub>10</sub> (ppm)	C <sub>4</sub> <sup>2</sup> (ppm)	C <sub>5</sub> <sup>2</sup> (ppm)
40 ml/min	1921	67	520	401	74	67	37
30 ml/min	2583	64	550	420	68	175	49
20 ml/min	3278	71	634	515	79	215	56

<sup>1</sup> The overall error of the result is within  $\pm 10\%$

<sup>2</sup> Referring to C<sub>n</sub> species excluding n-paraffin

Logically, a lower flow rate induces a longer residence time, thus resulting in higher SIE as reactant molecules spend more time in the discharge, and vice versa. Consequently, the conversion rates and the concentrations of long-chain products were higher at a lower flow rate. According to the results, the conversion rates of reactants and the carbon balance were similar when varying the total flow rate from 40 ml/min to 30 ml/min, while significantly changed under a total flow rate of 20 ml/min under similar discharge power. The carbon balance under a total flow rate of 20 ml/min was notably lower than the other tests and the selectivity towards C2-5 was slightly lower, implying the more fraction of carbon from CO finally formed carbon deposits due to CO disproportioning reaction. While within a range of total flow rate higher than 20 ml/min, fewer carbon deposits were formed. Therefore, a low flow rate naturally led to higher SIE, thus increasing conversions of reactants, but the carbon deposition was also dramatic, leading to a lower total selectivity towards hydrocarbons.

### **3.2.3 Frequency**

The effects of different frequency from 2600 Hz to 3400 Hz with a gradient of 200 Hz of the applied signal were studied at a fixed total flow rate (30 ml/min) and fixed H<sub>2</sub>/CO ratio (2:1) in feeding gas. The SIE and conversion rates of reactants as a function of a different frequency is shown in Figure 3-3. Table 3-6 and Figure 3-7 represent the analysis of gaseous products analysis, the energy efficiency of the reactants, and carbon balance and the concentration of C2-C5 hydrocarbon species in the product gas varying by different frequency of power generator, respectively.

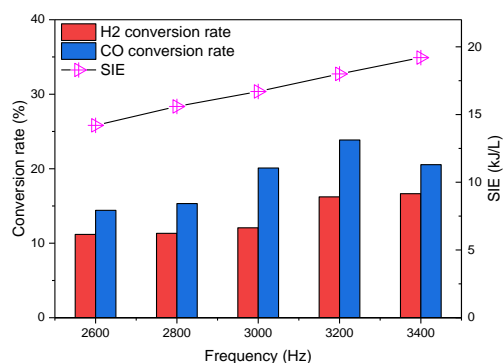


Figure 3-3. SIE and conversion rate of CO and H<sub>2</sub> as a function of the different frequency of power supply (total flow rate: 30 ml/min, H<sub>2</sub>/CO ratio = 2:1, peak-to-peak voltage: 6 kV)<sup>1</sup>.

Table 3-6. Product analysis of the experiments varying by the different frequency of power supply (total flow rate: 30 ml/min, H<sub>2</sub>/CO ratio = 2:1, peak-to-peak voltage: 6 kV)<sup>1</sup>.

Frequency	Selectivity			Energy efficiency(%/W)		Carbon balance
	CO <sub>2</sub>	CH <sub>4</sub>	C2-C5	H <sub>2</sub>	CO	
2600 Hz	0.58	0.33	0.10	1.57	2.04	0.974
2800 Hz	0.56	0.35	0.11	1.46	1.97	0.981
3000 Hz	0.48	0.36	0.13	1.45	2.41	0.989
3200 Hz	0.59	0.31	0.10	1.80	2.65	0.954
3400 Hz	0.60	0.30	0.09	1.70	2.10	0.957

Table 3-7. Concentration distribution of C2-C5 hydrocarbons in the product gas varying by the different frequency of power supply<sup>1</sup>.

Frequency	C <sub>2</sub> H <sub>6</sub> (ppm)	C <sub>2</sub> H <sub>2</sub> +C <sub>2</sub> H <sub>4</sub> (ppm)	C <sub>3</sub> H <sub>8</sub> (ppm)	C <sub>3</sub> <sup>2</sup> (ppm)	C <sub>4</sub> H <sub>10</sub> (ppm)	C <sub>4</sub> <sup>2</sup> (ppm)	C <sub>5</sub> <sup>2</sup> (ppm)
2600 Hz	2292	35	383	278	63	148	46
2800 Hz	2406	41	412	403	60	160	45
3000 Hz	2425	46	496	347	61	148	37
3200 Hz	2965	48	477	463	66	168	47
3400 Hz	2522	46	417	410	59	153	61

<sup>1</sup> The overall error of the result is within  $\pm 10\%$

<sup>2</sup> Referring to C<sub>n</sub> species excluding n-paraffin

As illustrated in the results, more power was absorbed into the DBD plasma with the frequency increasing. Therefore the conversion rate of the reactants and the energy efficiency of CO increased. While when the frequency was more than 3200 Hz, the conversion rate and energy efficiency of reactants started to decrease. One explanation for this phenomenon is that with the frequency increasing, the thermal instability issue also became more dramatic during experiments because the time between excitation cycles was shorter for the dissipation of heat and active species [231]. Thus, the discharge started the transition from the filament to glow discharge. As a result, the glass tube and electrode were partially heated on the interface with reactants. However, the overall flowing gas was not adequately heated because part of the heat dissipated into the air sufficiently by a depressed air gun, and the residence time of the gaseous reactants is as short as 20 seconds. The temperature difference between the inlet and outlet gas was less than 5 °C. Comparing the concentrations of the gaseous products, the concentrations of CO<sub>2</sub> and C2-C5 generally increased with the increase of frequency. However, considering the change of volume and the selectivity towards different products, the selectivity of C2-C5 hydrocarbons reached a peak at around a frequency of 3000 Hz, with the lowest selectivity towards CO<sub>2</sub>. It is reasonable that the selectivity of CO<sub>2</sub> increased as the frequency of signal increased within a specific range because the vibrational excitation of CO was effectively promoted, thus accelerating the CO disproportioning reaction. Meanwhile, more energy absorbed into DBD plasma, in turn, can promote the reaction of the activated C\* with H, as mentioned above. As a result, the selectivity towards CO<sub>2</sub> decreased at first then increased with the increase of frequency.

### **3.3. plasma tests with catalysts**

According to previous tests without plasma, the total flow rate of 30 ml/min, and

the frequency of 3000 Hz were chosen for the experiments with catalysts. The H<sub>2</sub>/CO ratio was fixed at 2 to evaluate the catalytical performance. The liquid products were condensed for 90 min for the offline analysis via GC-MS. These series of experiments were repeated three times. The experimental condition of tests with catalysts is listed in Table 3- 8.

Table 3-8. Experimental condition of plasma tests with catalysts.

Catalysts	H <sub>2</sub> /CO ratio	Frequency (Hz)	Total flow rate (ml/min)
blank	2	3000	30
aerogel	2	3000	30
10Cl-S	2	3000	30
20Cl-S	2	3000	30
20Cl-I	2	3000	30
20NO-I	2	3000	30

The catalysts samples were reduced in the H<sub>2</sub>/N<sub>2</sub> (5%:95%) flow at 600 °C for 10 h with a heating rate of 10 °C/min before placing into the reactor. The reduced catalysts were directly packed in the DBD reactor for the following plasma experiments.

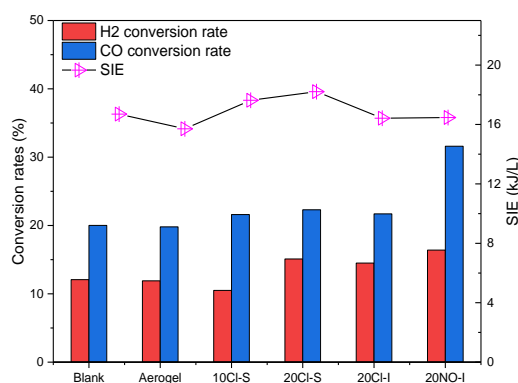


Figure 3-4. The SIE and conversion rate varying by the different catalysts (total flow rate: 30 ml/min, frequency: 3000 Hz, peak-to-peak voltage: 6 kV).

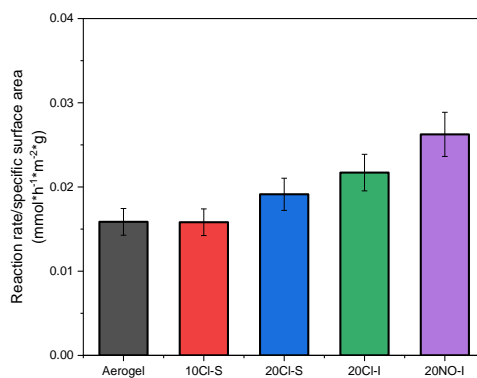


Figure 3-5. The reaction rates normalized to specific surface area varying by the different catalysts (total flow rate: 30 mL<sub>n</sub>/min, frequency: 3000 Hz, peak-to-peak voltage: 6 kV).

Figure 3-4 shows the SIE, conversion rate varying by the different catalysts. Figure 3-5 illustrates the reaction rates normalized to specific surface area varying by the different catalysts. Comparing the results of tests with and without SiO<sub>2</sub> aerogels, the SIE of the test with aerogels was lower, while the introduction of Co/SiO<sub>2</sub> increased the SIE compared with the blank test. The explanation could be that on the one hand, the introduction of aerogels reduced the discharge volume in the reactor, leading to lower absorbed power; on the other hand, the conductive property of the discharge space was modified and also the discharge behavior could be altered in turn, particularly with cobalt, leading to an increase of the discharge power. Meanwhile, as the dispersion of cobalt was not uniform via the impregnation method, the excessive cobalt caused more collapses and blocking of the pore structure as illustrated in the previous chapter, which caused the decrease of SIE. The conversion rate of the reactants, particularly CO, was remarkably high after placing the catalyst sample 20NO-I into the reactor. However, the other catalyst samples prepared by the chloride precursors did not obviously exhibit promoting the conversion rate even the Cl-S samples had a better dispersion of Co. One explanation could be that chloride ion was well-known harmful for FTS; the residual chloride ion in the catalysts could prohibit the conversion of reactants.

Table 3-9. Gaseous products analysis of the experiments varying by the different catalysts (total flow rate: 30 ml/min, H<sub>2</sub>/CO ratio = 2:1, peak-to-peak voltage: 6 kV, frequency: 3 kHz)<sup>1</sup>.

Catalysts	Selectivity				Energy efficiency (%/W)		Carbon balance
	CO <sub>2</sub>	CH <sub>4</sub>	C2-C5	Liquid products	H <sub>2</sub>	CO	
Blank	0.48	0.36	0.12	/	1.45	2.41	0.989
Aerogel	0.60	0.29	0.09	0.03	1.52	2.52	0.999
10Cl-S	0.53	0.28	0.12	0.07	1.45	2.41	1.06
20Cl-S	0.46	0.28	0.13	0.13	1.65	2.45	0.993
20Cl-I	0.53	0.28	0.10	0.09	1.76	2.64	0.982
20NO-I	0.44	0.27	0.12	0.17	1.98	3.83	0.946

Table 3-10. Concentration distribution of C2-C5 hydrocarbons in the product gas varying by the different catalysts<sup>1</sup>.

Catalysts	C <sub>2</sub> H <sub>6</sub> (ppm)	C <sub>2</sub> H <sub>2</sub> +C <sub>2</sub> H <sub>4</sub> (ppm)	C <sub>3</sub> H <sub>8</sub> (ppm)	C <sub>3</sub> <sup>2</sup> (ppm)	C <sub>4</sub> H <sub>10</sub> (ppm)	C <sub>4</sub> <sup>2</sup> (ppm)	C <sub>5</sub> <sup>2</sup> (ppm)
Aerogel	1916	45	524	277	73	111	31
10Cl-S	2303	46	594	346	126	141	59
20Cl-S	3232	59	865	296	208	148	92
20Cl-I	2600	49	562	372	90	106	37
20NO-I	4608	66	856	667	163	124	51

Table 3-11. Liquid product yield analysis of the experiments varying by the different catalysts by GC-MS (total flow rate: 30 ml/min, H<sub>2</sub>/CO ratio = 2:1, peak-to-peak voltage: 6 kV, frequency: 3 kHz)<sup>3</sup>.

Catalysts	H <sub>2</sub> O (%)	CH <sub>3</sub> OH (%)	CH <sub>3</sub> CHO (%)	CH <sub>3</sub> CH <sub>2</sub> OH (%)
10Cl-S	93.0	6.1	0.58	0.28
20Cl-S	92.6	6.2	0.74	0.26

20Cl-I	93.1	6.1	0.62	trace
20NO-I	85.0	13.4	1.3	0.32

<sup>1</sup> The overall error of the result is within  $\pm 10\%$

<sup>2</sup> Referring to C<sub>n</sub> species excluding n-paraffin

<sup>3</sup>The overall error of the result is within  $\pm 12\%$

The gaseous products analysis and the concentrations of C<sub>2</sub>-C<sub>5</sub> gaseous products formed after plasma treatments with different catalysts are presented in Table 3-9 and Table 3-10, respectively. Table 3-11 demonstrates the liquid product analysis of the experiments varying by the different catalysts. As the introduction of SiO<sub>2</sub> aerogel slightly decreased the SIE, only a negligible liquid was found, the selectivity to hydrocarbons also decreased. The aerogel support slightly decreased the SIE but promoting the formation of CO<sub>2</sub> due to plasma-surface interaction such as the change of residence time of active species on the surface, local hot spots, and enhancement of local electric field. Compared with aerogels, all the samples with cobalt remarkably promoted the formation of liquid products. Givotov et al. have also reported the direct synthesis of formaldehyde and then conversion into methanol via non-thermal plasma processing of syngas with sufficient high SIE [5]:



However, it has been proved that CH<sub>2</sub>O radicals are easily to decompose under plasma discharge [5], thus resulting in a low selectivity towards liquid chemicals without packing. While with packing, a part of methanol, ethanol, and acetaldehyde, which is attractive as these organic oxides are essential chemicals, was detected among the liquid products. Besides, the sample 20Cl-S and 20NO-I also promoted the formation of long-chain hydrocarbon products rather than CH<sub>4</sub> and slightly decreased the selectivity to CO<sub>2</sub>. The increase of Co loading amount from 10% to 20% significantly benefit the formation of liquid products and C<sub>2</sub>-C<sub>5</sub> hydrocarbons. Thus,

the cobalt catalysts were confirmed to promote the hydrocarbon synthesis and decrease the energy barrier of the formation of oxides such as alcohols and aldehydes with higher energy efficiency in our reactor. The explanations can be, on the one hand, the strong sorption behavior of the mesoporous structure in the support could inhibit the decomposition of  $\text{CH}_2\text{O}$  radicals as microdischarge is difficult to form in mesopores under typical DBD plasma (Debye sheath  $\gg$  mesopores). On the other hand, the introduction of Co catalysts promoted the conversions of reactants and the formation of  $\text{CH}_2\text{O}$  radicals. In the previous section, we found even the cobalt in the samples prepared by the sol-gel method was better dispersed, while a part of Co species could partially connect with  $\text{SiO}_2$  bone structure to form inactive Co species. This explained the higher activity of 20NO-I than 20Cl-S as shown in Figure 3-5. It should be noted that the reaction rates in Figure 3-5 were normalized to the specific surface area of the catalysts as the origin of active sites of catalysts was not well identified yet. Meanwhile, the plasma-catalytic surface reactions could be affected by packing any solid supports or catalysts. Therefore, the results indicated that the catalytic performance of the samples prepared by nitrate precursor was better than the others with a higher concentration of C2-C5 hydrocarbons, organic oxides, and notably higher energy efficiency. One point should be noticed that a part of water component could be produced via FTS reactions; however, the condensed vapor from the air could also be notable due to the temperature difference between the icy water trap and the atmosphere.

The catalysts after the experiments were also characterized by XPS. Except that a tiny peak of carbon was detected, no significant change was found in the surveys. No apparent phenomena of deactivation were found until 90 min among all the tests with the catalysts. The C1s peak region of some samples smoothed by Gaussian method is shown in Figure 3-6. The carbon species found in the blank sample was more like carbon black (C-C bonding at 284.5 eV). While among the Co loaded samples, less carbon and different carbon species were found. The XPS peaking of the

20Cl-S sample after the plasma experiments was illustrated in Figure 3-7. Not only carbon black (C-C bonding at 284.5 eV), but also organic carbon species (C-O bonding at 286 eV, O-C=O at 288 eV, unobtrusive satellite peak at 291 eV) were detected as the fitting peaks in Figure 3-7. Moreover, a notable  $\pi$ - $\pi^*$  satellite peak occurred at around 295.5 eV of binding energy without peaking. According to Gardella's and Beamson's study [232, 233], the extended delocalized electrons of the aromatic ring in ethylene terephthalate or pentaphenyl-trimethyl-siloxane structure results in the significantly high binding energy of  $\pi$ - $\pi^*$  satellite peak. Generally, it was not necessary to form a polymer, but the monomers could also lead to this phenomenon. Considering the obvious organic O-C=O and C-O peaks, the result implies the existence of C5+ organics on the catalysts.

Consequently, besides the organic oxides such as alcohols and aldehydes, a small part of esters and C5+ organics were synthesized on the catalysts. Due to their high boiling point and low production, these organics were beyond determination by GC-MS after condensation. The result confirms that the cobalt catalysts promoted the formation of organics and hydrocarbons via plasma catalytic approach. Therefore, less carbon deposition but more organic carbons were detected. The result supports that cobalt catalysts can promote the reactions of the excited C species with H, leading to the formation of hydrocarbons rather than CO<sub>2</sub>.

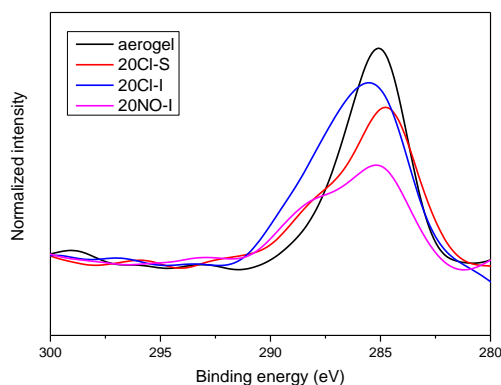


Figure 3-6. XPS peak region in C1s of the corresponding catalysts after the plasma experiments (smoothed by Gaussian method): Aerogel, 20Cl-S, 20Cl-I, 20NO-I.



conducted without placing catalysts at ambient conditions. Then the performance of the catalysts was evaluated by introducing silica aerogel support and different Co/SiO<sub>2</sub> aerogel catalysts described in the previous chapter.

C1 to C5 hydrocarbons were synthesized by this way at ambient conditions with a relatively low energy consumption compared to existing work in which the external pressure, heating, and high SIE were essential. The introduction of the cobalt catalysts significantly enhanced the synthesis of liquid organics and C2-C5 hydrocarbons rather than CO<sub>2</sub> and CH<sub>4</sub> from syngas by a plasma catalysis approach. Moreover, methanol, ethanol, and acetaldehyde were synthesized and detected among the liquid products via the catalysts; a small part of esters and C5+ organics were detected on the catalysts. Due to the different textural and structural properties, 20NO-I catalyst sample demonstrated a notable catalytic performance with remarkably high energy efficiency.

Then, a parametric experimental study revealed that a large portion of H<sub>2</sub> in the feeding gas favored the conversion of CO and the formation of hydrocarbons. A low flow rate naturally led to higher SIE, thus increasing conversions of reactants; however, the over selectivity towards hydrocarbons was lower due to the higher proportion of carbon deposits. It was also found that introducing aerogel support slightly decreased discharge power as expected. Nevertheless, the increase of Co loading amount significantly increases the yield of hydrocarbons and organic oxides but does not necessarily increase the discharge power probably due to the block and collapse of the porous structure.

Finally, based on the knowledge of the conventional FTS mechanism, some possible reaction pathways of non-thermal plasma promoted FTS associated with catalysis were proposed. In conclusion, the non-thermal plasma pathways provide a new perspective of FTS process at ambient conditions with relatively low energy consumption and broaden the field of further improvements.

# Chapter IV. Plasma-catalytic conversion of CO<sub>2</sub> and CH<sub>4</sub>

## Résumé du chapitre

Ce chapitre aborde l'étude de la conversion plasmocatalytique directe à pression et température ambiantes de CO<sub>2</sub> et CH<sub>4</sub> en produits liquides (hydrocarbures, alcools, cétones, etc.) et gaz de synthèse. Pour cela le même réacteur rempli a été utilisé, testé avec différents catalyseurs sur support d'aérogel de silice (Co et Fe) et pour différents rapports CO<sub>2</sub>/CH<sub>4</sub>. Là encore la même démarche que le chapitre précédent a été suivie, à savoir une série d'essais en plasma seul, puis une avec introduction du catalyseur sur son support d'aérogel. La performance des catalyseurs en couplage plasmocatalytique a ainsi été évaluée. Selon les conditions opératoires, la sélectivité globale en CO et H<sub>2</sub> peut atteindre respectivement 75% et 50%, les taux de conversion du CO<sub>2</sub> et du CH<sub>4</sub> environ 30% et 43%. Il est constaté que le rapport CO<sub>2</sub>/CH<sub>4</sub> affectait de manière significative les taux de conversion et la distribution des produits finis. Peu de liquides sont produits sans catalyseur, le catalyseur favorise clairement la synthèse de produits liquides. De plus, le support d'aérogel augmente les taux de conversion des réactifs et améliore légèrement la sélectivité vis-à-vis des produits liquides. La sélectivité en produits liquides peut atteindre jusqu'à 40% avec catalyseur sur support d'aérogel. Les principaux produits liquides étant le méthanol et l'acide acétique. En faisant varier les taux de CH<sub>4</sub> et de CO<sub>2</sub> en couplage plasmocatalytique nous produisons un petit nombre d'hydrocarbures à longue chaîne (hexane, heptane) mais aussi d'alcools (hexanol). La synergie positive de la catalyse et du plasma pour la conversion du CH<sub>4</sub> et CO<sub>2</sub> semble ainsi démontrée. Cela représente de façon évidente un potentiel pour la synthèse directe de produits chimiques liquides à valeur industrielle et de carburants à partir de CO<sub>2</sub> et de CH<sub>4</sub>.

## **Abstract**

This chapter is dedicated to the study of the direct plasma-catalytic conversion of CO<sub>2</sub> with CH<sub>4</sub> into liquid chemicals (methanol, ethanol, acetic acid and acetone, hexane, heptane, etc.) and syngas at atmospheric conditions. The same configuration of the reactor was used with packing different metallic catalysts (Co and Fe) loaded silica aerogel support. The catalyst samples were prepared by incipient wetness impregnation (IWI) method, then characterized and introduced into the DBD reactor to conduct plasma experiments. The first series of plasma tests were conducted without packing catalysts, then the performance of catalysts was evaluated by packing catalysts and comparing to packing silica aerogels alone. According to the results, the overall selectivity towards CO and H<sub>2</sub> was approximately 75% and 50%, respectively, where the conversion rates of CO<sub>2</sub> and CH<sub>4</sub> were approximately 30% and 43%, depending on the operating conditions. The ratio of CO<sub>2</sub>/CH<sub>4</sub> was found to significantly affected the conversions and the distribution of final products. Only negligible liquid products were produced without packing catalysts while packing aerogel promoted the conversion of reactants and slightly enhanced the overall selectivity towards liquid products. Most significantly, the total liquid selectivity can reach approximately 30%-40% after introducing the catalysts, where the main liquid products were methanol and acetic acid at a very considerable selectivity. By varying the ratio of CH<sub>4</sub> and CO<sub>2</sub>, a small number of long-chain hydrocarbons and alcohols (hexane, heptane, hexanol, etc.) were also detected with our catalysts. The positive synergy of plasma-catalysis in this process demonstrates great potential for the direct synthesis of value-added liquid chemicals and fuels from CO<sub>2</sub> and CH<sub>4</sub>.

## **4.1. Introduction**

As an efficient technique, CO<sub>2</sub> capturing is now progressively applied to chemical and energy industries. However, the storage and utilization of CO<sub>2</sub> still have

some significant issues regarding the high investment, transportation, and uncertainty of long-term storage[4]. Under this context, many efforts have dedicated into the chemical conversion of carbon dioxide with methane ( as two major greenhouse gases in the atmosphere) into value-added chemicals has attracted significant attention and interests to achieve a sustainable and low carbon emission [234, 235].

The CO<sub>2</sub> molecule is a well-known thermodynamically stable. The activation of CO<sub>2</sub> generally requires significant energy consumption, and hence, the efficient activation and conversion of CO<sub>2</sub> is a great challenge. Some researchers have made great efforts in the study of conventional thermochemical method, including dry reforming to syngas and direct conversion to liquid organics associated with various catalysts. However, the essential high temperature and the deactivation of catalysts are critical issues and drawbacks [236]. Non-thermal plasma (NTP) has been exploited and applied to various fields such as degradation of pollutants and synthesis of chemicals in recent decades, as it offers a unique pathway to induce thermodynamically unfavorable chemical reactions at a low temperature due to its high concentration of energetic and chemically active species [5]. The typical electron temperature (1-10 eV) of NTPs is sufficient to activate CO<sub>2</sub> (5.5 eV) and CH<sub>4</sub> (4.5 eV) molecules into reactive radicals, excited molecules, atoms, and ions, which are energetic enough to initiate chemical reactions between CO<sub>2</sub> and CH<sub>4</sub>. Although it has been regarded as a feasible approach with the advantage of non-essential heating, the low conversion rate of the feeding gases has a negative influence on the processes and the comprehension of the complex plasma-catalysts interaction should also be improved.

An enormous efforts have been dedicated to explore the plasma-catalytic conversion of CO<sub>2</sub> with CH<sub>4</sub>, including studies on the effects of different plasma types, different temperatures, experimental variables and reactors to improve the conversion and selectivity to syngas products [162, 166, 175, 178, 179, 183, 184, 186-190, 237]. Moreover, various catalysts have been investigated on plasma-catalytic

reforming of  $\text{CO}_2$  and  $\text{CH}_4$ , including zeolites and some metal catalysts with their supports[153, 238-242]. Tu et al. [163, 228] reported that the full packing of  $\text{Ni}/\text{Al}_2\text{O}_3$  catalysts in the discharge volume could modify the discharge behavior from a typical filamentary discharge to a combination of surface discharges and spatially limited microdischarges, leading to the decreasing of power in discharge and conversion of reactants. Zou et al. [181] have demonstrated the possibility of starch enhancing the oxygenate formation directly from methane and carbon dioxide. M. Scapinello and his co-workers[194] has explored the formation of carboxylic acids on the surface of copper and nickel electrodes. Some other researchers have also reported the formation of oxygenates as by-products in plasma promoted reforming, while the selectivity was still poor, and external heating was essential[162, 243, 244]. Li Wang et al.[245] demonstrated that a considerable production of liquid chemicals, including acetic acid, methanol, and acetone, were synthesized via a novel DBD reactor equipped with a ground water electrode. They reported that the combination of plasma process associated with Cu, Au, and Pt- $\text{Al}_2\text{O}_3$  shows potential for the direct production of oxygenates under ambient conditions. Until now, only limited efforts have been dedicated to the direct synthesis of liquid organics and hydrocarbons from  $\text{CO}_2$  and  $\text{CH}_4$  without external heating and pressure.

Herein, we used the coaxial DBD reactor described in the previous chapter and two metal catalysts (Co and Fe) with silica aerogel support for the direct plasma-catalytic synthesis of liquid organics and hydrocarbons synthesis at ambient conditions. The plasma experiments were firstly conducted in the tubular DBD reactor, and the influence of different variables was investigated. The highly porous and hydrophobic  $\text{SiO}_2$  aerogel support was prepared by the same method described in the previous chapter. The Co and Fe loaded  $\text{SiO}_2$  aerogel catalysts were obtained by incipient wetness impregnation method and then characterized. Finally, the catalysts were fully packed into the reactor, and the experimental study on catalytic performance was carried out and presented by comparing to no packing condition.

## 4.2. Experimental

### 4.2.1 Preparation of Fe/SiO<sub>2</sub> aerogel catalysts

Fe/SiO<sub>2</sub> aerogel catalysts with the targeted mass ratio of Fe loading (10% and 20% metal to silica) were prepared by the incipient wetness impregnation method. However, later plasma experiments indicated that 20% doping of Fe on SiO<sub>2</sub> aerogel led to the catalyst sample too conductive that the micro-discharge cannot generate in the discharge zone. Therefore, only 10% of Fe loading sample is discussed in the later sections.

The silica was synthesized by the method as described in the preceding chapter using polyethoxydisiloxane (P75W20, PCAS, <30%) as silica precursors via a sol-gel method. 10 g of P75W20 was added to 15 g of ethanol (Fisher Scientific, Absolute) in a polyethylene vial while stirring. The solution was kept for 5 min, after which 2625  $\mu$ L of distilled water was added to act as a hydrolysis agent, and 2955  $\mu$ l of (3-Aminopropyl) triethoxysilane (APTES, Thermo Fisher, 98%) solution (APTES: Ethanol = 1:50) was added to adjust the pH value for gelation. The final mixture solution was covered and allowed to gel and age at 60 °C for 48 h. Following the aging, 35 ml of Hexamethyldisilazane (HMDZ, Acros Organics, 98%) was added to the silica gels and left covered for 3 nights at ambient conditions to remove the hydroxyl groups. In the next step, the hydrophobic silica gels were washed in ethanol 5 times (over 2 days) to remove excessive HMDZ. The final gels were then transferred into an oven and dried for 2 h at 140 °C.

The targeted ethanolic solution of Fe(NO<sub>3</sub>)<sub>2</sub>·9H<sub>2</sub>O were mixed with the same volume of silica aerogels and kept impregnating for one night. After that, the samples were dried for 2 h at 140 °C and then calcined in air at 400 °C for 5 h with a heating rate of 10 °C/min to obtain Fe or Co silica aerogels. Before the experiments, the catalysts samples were reduced in H<sub>2</sub>/N<sub>2</sub> (5%/95%) flow at 600 °C for 10 h with a

heating rate of 10 °C/min.

The specific surface areas, pore volumes, and average pore sizes were obtained from the N<sub>2</sub> adsorption/desorption analyses conducted at 77 K (ASAP2020, Micromeritics Instrument Corporation). The BET specific surface areas were calculated from the adsorption isotherms at the relative pressure range of 0.1-1.0, and the BJH pore volumes were measured from the desorption isotherms. The micropore volume and micropore surface area were determined with the t-plot method.

The XRD patterns of the samples were recorded with an X-ray powder diffractometer (Cu K $\alpha$  = 1.5405 Å, X'Pert pro, Philips diffractometer PW1830). The diffractometer was operated at 45 kV and 30 mA. The samples were ground into fine powders for the measurements and recorded for 2 $\theta$  from 10° and 90° with a 0.08° step size for 14 min.

SEM observations were carried out on a 30 kV SUPRA 40 (Carl Zeiss AG) electronic microscope based on the 3rd generation GEMINI® column. Before observation, the samples were deposited on an adhesive conducting carbon tape and coated with a platinum layer with a thickness of 7 nm via Quorum (Q150 TES). The SEM images were acquired at 3 kV, and 6-10 mbar on a CCD camera with 7.5 $\mu$ m diaphragm and 4mm working distance, high-efficiency in-lens detector (in the chamber) or Everhart-Thornley secondary electron detector (in the column) was applied for high magnification.

TEM observations and analysis were carried out on a 200 kV FEI Tecnai F20-ST field emission gun microscope equipped with energy dispersive X-ray (EDX) device, scanning transmission electron microscopy (STEM) system, high angle annular dark-field (HAADF) detector and Gatan Imaging Filter (GIF). Powder samples were first crushed then dispersed in absolute Ethanol suspension, and a few drops were deposited on a copper grid covered with a holey carbon film. Conventional TEM images and diffraction patterns were acquired at 200 kV on a high-angle CCD camera using bright-field imaging mode. High-resolution TEM (HRTEM) images were

acquired using a CCD slow-scan camera. Local area fast Fourier transform (FFT) diffractograms, equivalent to electron diffraction patterns, were exploited to determine structural and crystallographic characteristics of observed samples. EDX microanalysis was combined with STEM-HAADF images (Z-contrast images) to perform chemical analyses on studied samples.

#### 4.2.2 Experimental analysis

The micro GC was calibrated for each gaseous component using standard gas cylinders with a wide range of concentrations. According to the measurements of the micro GC and the difference of the temperature, pressure and flow rate before and during each experiment, the conversion rate ( $x$ ) of CH<sub>4</sub> and CO<sub>2</sub> can be calculated according to:

$$x_{CH_4} = \frac{\text{moles of } CH_4 \text{ consumed}}{\text{moles of } CH_4 \text{ inlet}} \times 100 \% \quad (1)$$

$$x_{CO_2} = \frac{\text{moles of } CO_2 \text{ consumed}}{\text{moles of } CO_2 \text{ inlet}} \times 100 \% \quad (2)$$

The selectivity and yield of gaseous products can be calculated as:

$$S_{H_2} = \frac{\text{moles of } H_2 \text{ produced}}{2 \times \text{moles of } CH_4 \text{ consumed}} \times 100 \% \quad (3)$$

$$S_{CO} = \frac{\text{moles of } CO \text{ produced}}{\text{moles of } CO_2 \text{ consumed} + \text{moles of } CH_4 \text{ consumed}} \times 100 \% \quad (4)$$

$$Y_{H_2} = \frac{\text{moles of } H_2 \text{ produced}}{2 \times \text{moles of } CH_4 \text{ input}} \times 100 \% \quad (5)$$

$$Y_{CO} = \frac{\text{moles of } CO \text{ produced}}{\text{moles of } CO_2 \text{ input} + \text{moles of } CH_4 \text{ input}} \times 100 \% \quad (6)$$

$$S_{C_xH_y} = \frac{x \times \text{moles of } C_xH_y \text{ produced}}{\text{moles of } CO_2 \text{ consumed} + \text{moles of } CH_4 \text{ consumed}} \times 100 \% \quad (7)$$

The selectivity of CH<sub>4</sub> to CO is defined as:

$$S_{CH_4/CO} = \frac{\text{moles of } CO \text{ produced} - \text{moles of } CO_2 \text{ consumed}}{\text{moles of } CH_4 \text{ consumed}} \times 100 \% \quad (8)$$

The ratio of unsaturated hydrocarbons/saturated hydrocarbons can be calculated as:

$$R = \frac{\text{moles of unsaturated } C_{2-4}}{\text{moles of saturated } C_{2-4}} \times 100 \% \quad (9)$$

The carbon balance based on the inlet and outlet gas can be calculated as:

$$CB = \frac{\text{moles of C outlet}}{\text{moles of C inlet}} \times 100 \% \quad (10)$$

The GC-MS was calibrated using a standard liquid sample (20 vol% of methanol, ethanol, acetic acid, acetone, and water) to quantify the main products, and the results were normalized by abstracting water. As the selectivity to deposition was negligible as elaborated in the following section, then the selectivity towards liquid organics can be calculated due to:

$$S_{liquid} = 100\% - S_{CO} - S_{C_xH_y} \quad (11)$$

$$S_{C_xH_yO_z} = x * \text{mole\% of } C_xH_yO_z * S_{liquid} \quad (12)$$

The specific input energy (SIE) is defined as the formula following:

$$SIE = \frac{\text{Power of discharge}(kW)}{\text{Flow rate}(\frac{L}{min})} * 60(\frac{s}{min}) \quad (13)$$

The energy efficiency (EE) of the reactor based on the gas conversion is defined as the reactants converted per unit of applied power:

$$E_{CO_2} = \frac{\text{moles of } CO_2 \text{ consumed}}{\text{power}} \quad (14)$$

$$E_{CH_4} = \frac{\text{moles of } CH_4 \text{ consumed}}{\text{power}} \quad (15)$$

All the experiments were repeated three times for reproducibility.

## 4.3. Results and discussion

### 4.3.1 Characterization of catalysts

#### *N<sub>2</sub> adsorption/desorption*

The N<sub>2</sub> adsorption/desorption isotherms of the as-prepared Fe/SiO<sub>2</sub> aerogel sample and aerogel with their specific surface area, pore volume, and average pore size are illustrated in Figure 4-1 and Table 4-1. The isotherm of as-prepared Fe/SiO<sub>2</sub> aerogel sample is type IV curve (IUPAC classification), which is typical mesoporous materials with ink-bottle shaped and cylindrical-like pore structure. Thus, the mesoporous structure was well maintained after doping Fe on the SiO<sub>2</sub> aerogel. The same as Co/SiO<sub>2</sub> aerogel sample prepared by impregnation method and nitrate precursor, the Fe/SiO<sub>2</sub> aerogel sample exhibited a high surface area and strong adsorption capacity.

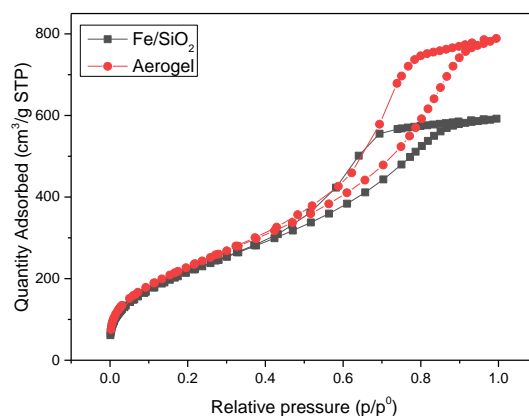


Figure 4-1. N<sub>2</sub> adsorption/desorption isotherms of the as-prepared Fe/SiO<sub>2</sub> aerogel catalyst sample and SiO<sub>2</sub> aerogel.

Table 4-1. Surface area, pore volume, and average pore size of the as-synthesized catalysts.

Catalysts	surface area <sup>a</sup> (m <sup>2</sup> /g)	average pore diameter (nm)	pore volume <sup>b</sup> (cm <sup>3</sup> /g)	t-plot micropore area <sup>c</sup> (m <sup>2</sup> /g)
Aerogel	736	8.2	1.72	20.79
Fe/SiO <sub>2</sub>	771	4.7	0.91	/

a Brunauer-Emmett-Teller method.

b Barrett-Joyner-Halenda method determination via N<sub>2</sub> adsorption data.

c t-plot method via Harkins-Jura equation.

### *X-ray diffraction*

The XRD spectra of the as-synthesized and spent catalysts with the characteristic peaks obtained from the standard database (PDF-2004) are in Figure 4-2. For the as-prepared samples, the clear Co peaks refer to Co<sub>3</sub>O<sub>4</sub>, while the Fe peaks were not as apparent as Co peaks. The positions of Fe peaks are similar to the characteristic peaks of Fe<sub>3</sub>O<sub>4</sub>. However, further characterization is essential to verify the species. The characteristic peaks of the spent Co samples are similar to the characteristic peaks of standard CoO, while the spent Fe samples seem to remain metallic forms. Considering the oxidation of metallic Co after tests, it is reasonable.

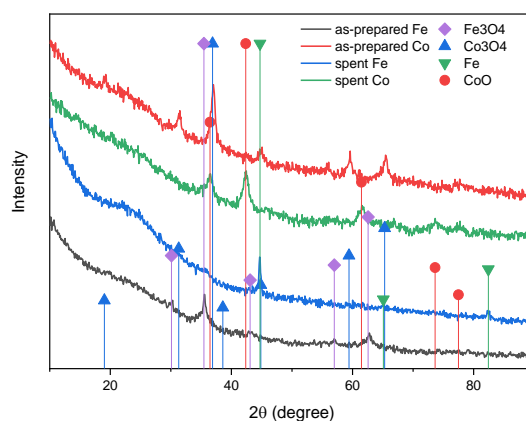


Figure 4-2. XRD spectra of the as-synthesized and spent catalysts sample.

### *X-ray photoelectron spectroscopy*

The XPS survey and selected Fe2p spectra of Fe/SiO<sub>2</sub> aerogel sample are illustrated in Figure 4-3 and Figure 4-4. Clearly shown in Figure 4-3, Si, O, Fe and a very tiny amount of C are detected as the main elements on Fe/SiO<sub>2</sub> aerogel sample indicating the iron nitrate in the catalyst samples has been successfully transformed to oxides. The characteristic peaks of Fe species are located at a binding energy of 723.5 eV and 711.4 eV respectively in the support as shown in Figure 4-4, and the

calculated atomic percent of iron is 9.1%. Moreover, the satellite features of Fe 2p peaks are absent in the XPS profile. According to the NIST database of Avantage and publications [246], the Fe species are confirmed to be Fe<sub>3</sub>O<sub>4</sub>. As the noise of background is too strong and the FWHM of Fe 2p 3/2 is more than 3 eV, the Fe species seem to contain a mixture of other oxides (Fe<sub>2</sub>O<sub>3</sub>) which can be easily reduced in H<sub>2</sub>/N<sub>2</sub> flow with heating.

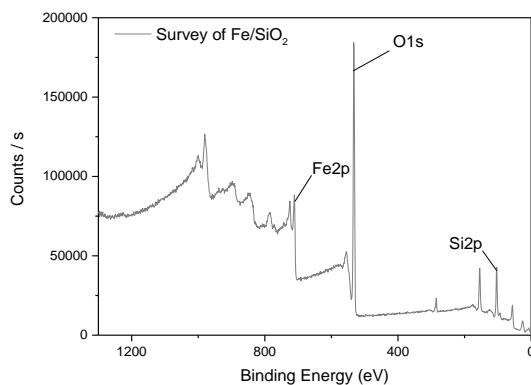


Figure 4-3. XPS survey of Fe/SiO<sub>2</sub> aerogel sample.

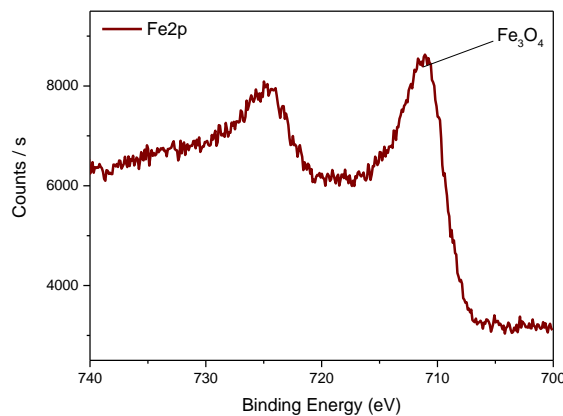


Figure 4-4. Fe 2p XPS spectra of the as-prepared Fe/SiO<sub>2</sub> aerogel sample.

### *SEM, TEM and HRTEM diffraction images*

The SEM micrographs of SiO<sub>2</sub> aerogel sample, Fe/SiO<sub>2</sub> aerogel sample, and SiO<sub>2</sub> aerogel are shown in Figure 4-5. The bone structure of SiO<sub>2</sub> aerogel, which is comprised of spherical clusters, is clearly shown in figure (c). Compared to the graph of SiO<sub>2</sub> aerogel, the matrix of SiO<sub>2</sub> bone is less apparent due to the well-dispersed Fe

species on SiO<sub>2</sub> aerogel support. However, the mesoporous structure is still well maintained. The same as Co/SiO<sub>2</sub> samples prepared by the impregnation method and nitrate precursor, the fibrous structure due to the strong interaction between the metal catalyst and support was not observed, indicating the inexistence of nonreducible iron species.

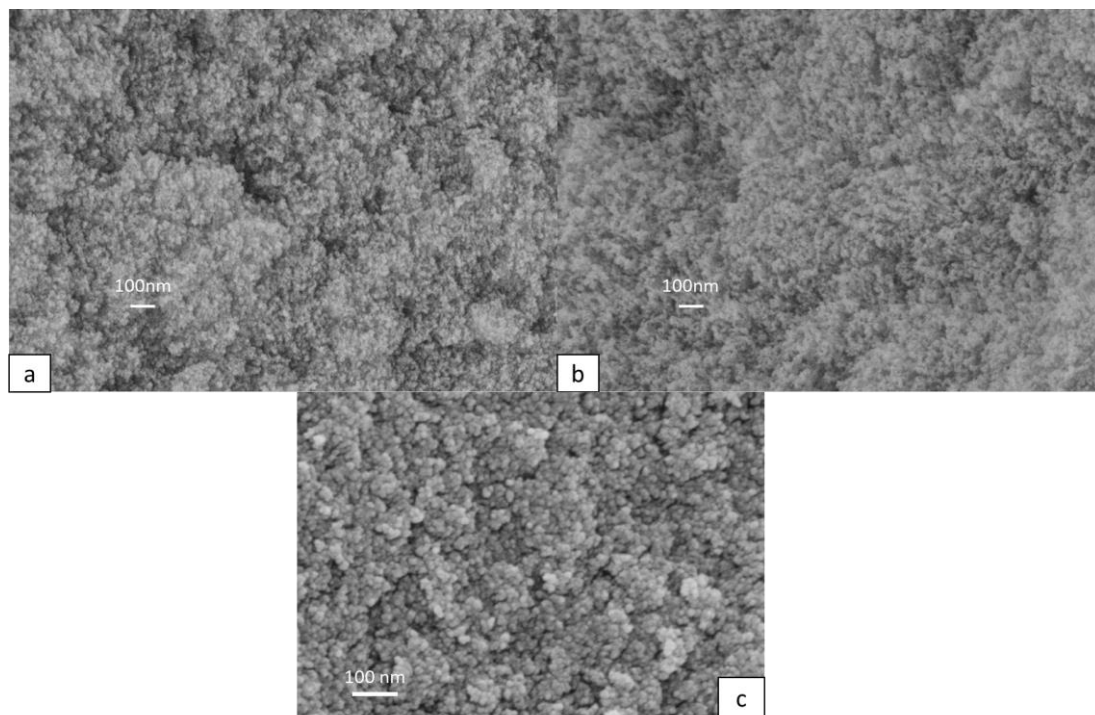


Figure 4-5. The SEM micrographs of a). SiO<sub>2</sub> aerogel, b). Fe/SiO<sub>2</sub> aerogel sample, c). SiO<sub>2</sub> aerogel.

The TEM and selected HRTEM diffraction images of the as-synthesized Fe/SiO<sub>2</sub> aerogel sample are shown in Figure 4-6. The TEM image indicates a uniform dispersion of Fe species on the SiO<sub>2</sub> aerogel support. Due to the diffraction image of the selected field of HRTEM image, the crystallite iron species is a cubic FCC (Fd-3m) structure with  $a=8.40 \text{ \AA}$  and  $Z=8$ , which refers to Fe<sub>3</sub>O<sub>4</sub>. The result is consistent with the result of XPS. Moreover, the other crystallite iron species are barely detected in the diffraction image, revealing that only a few amounts of iron oxides mixture (mainly Fe<sub>2</sub>O<sub>3</sub>) existed in the support considering the results of XPS. In any case, these iron oxides species have been proved to exhibit high reducibility in H<sub>2</sub>/N<sub>2</sub>

mixture flow according to some publications [247, 248].

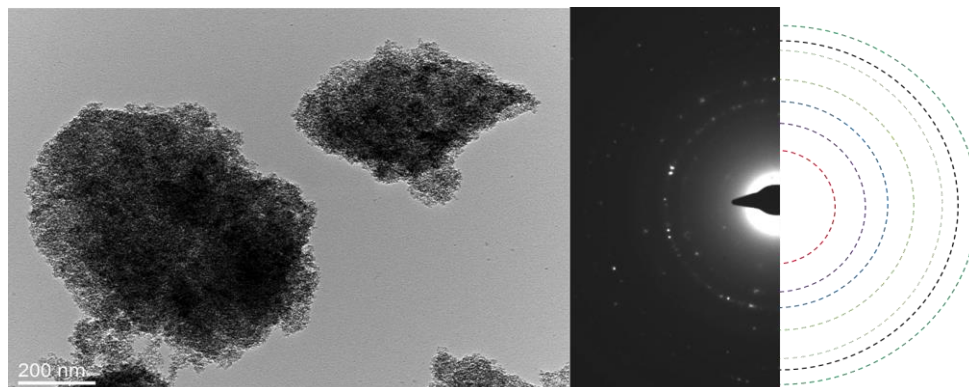


Figure 4-6. The TEM and the diffraction images of the as-synthesized Fe/SiO<sub>2</sub> catalyst.

### *TG analysis*

The DTG data curves of the spent aerogel samples of 6 hours' discharge under a flow of Argon and air are presented in Figure 4-7. The backgrounds were made by packing as-prepared aerogel samples. The photos of the samples after the TGA test under the flow of Argon and air are shown in Figure 4-8. After the TGA tests under the flow of Argon, the color of the samples changed from yellow into black, indicating the carbonization of the organics on the surface of the aerogel sample, which begins from 200 °C. The total mass loss was 0.95%. Meanwhile, after the TGA tests under airflow, the color of the samples was the same as as-prepared samples, indicating the carbon species has wholly oxidized. According to the DTG curve, two main mass loss peaks existed. The first one was similar to the work reported by Zhang [249], probably referring to the oxidation of carbon deposition. While the second one was more like the work published by Nousir [250], referring to the oxidation of polymeric species. The total mass loss of the sample under airflow was 2.6%. Thus, we can estimate that the carbon species deposition (including carbon deposition and carbon organics) of 1.65% (normalized to the weight of aerogel). Regarding the total selectivity, the selectivity to the deposition was less than 3%, which is too negligible. As a result, in the calculation of selectivity towards liquid products, we did not take the deposition into account.

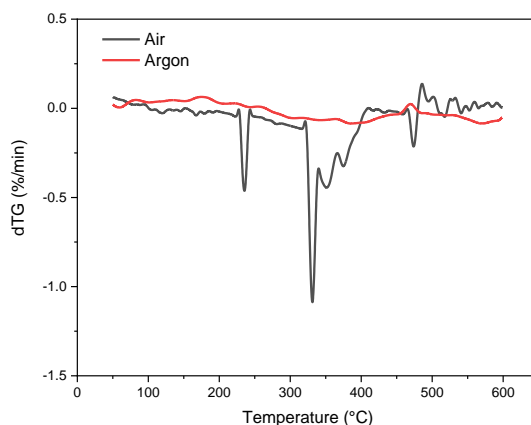


Figure 4-7. DTG data curves for the aerogel samples under a flow of 1). Argon, 2). Air ( $\text{CO}_2/\text{CH}_4=2:1$ ).



Figure 4-8. Aerogel samples after TGA test under a flow of 1). Argon, 2). Air ( $\text{CO}_2/\text{CH}_4=2:1$ ).

The C1s and O1s XPS spectra of spent  $\text{SiO}_2$  (smoothed by Gaussian method) are shown in Figure 4-9. Except that a tiny peak of carbon was detected, no significant change was found in the surveys. The peaking results are also shown in Figure 4-9. Three carbon bonds were detected by XPS: C-C bonding at 284.5 eV, C-O bonding at 286 eV, O-C=O at 288 eV, which is also coincided with the O1s peaking results. According to Gardella's and Beamson's study [232, 233], the existence of C-O and O-C=O bonding are referring to polymers (like ethylene terephthalate). However, the  $\pi$ - $\pi^*$  satellite feature was not visible. Considering the much more apparent C-C bonding, we deem that the depositions are carbon deposits and carbon contained polymers or monomers (containing aromatic ring structure and oxygen), which is in agreement with the results of TGA. The result implies the existence of C5+ organics on the

catalysts.

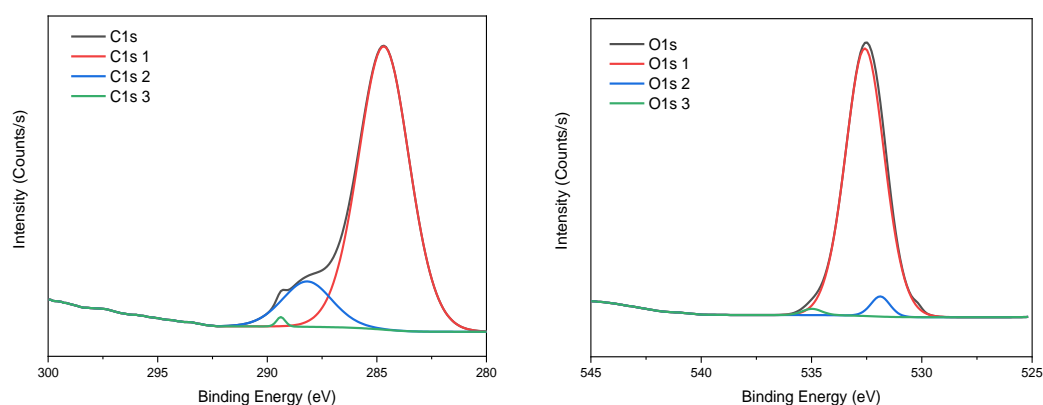


Figure 4-9. XPS spectra of C1s and O1s peaks with their peaking results of spent SiO<sub>2</sub> samples (CO<sub>2</sub>/CH<sub>4</sub>=2:1).

For further characterization of the deposition on spent Co and Fe catalysts, the comparison of C1s peaks of spent SiO<sub>2</sub>, Co/SiO<sub>2</sub>, and Fe/SiO<sub>2</sub> is shown in Figure 4-10. Clearly, the intensity of C1s peaks exhibited an order as spent Co/SiO<sub>2</sub> < spent Fe/SiO<sub>2</sub> << spent SiO<sub>2</sub>, which implies much less carbon deposition was formed on the Fe/SiO<sub>2</sub> and Co/SiO<sub>2</sub> samples. Moreover, the C1s peaks of the spent catalyst samples are broader than the spent SiO<sub>2</sub> sample.

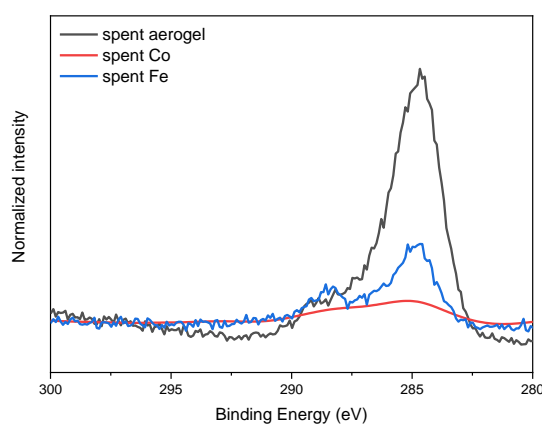


Figure 4-10. XPS spectra of C1s peak of 1). spent SiO<sub>2</sub> samples, 2). spent Co/SiO<sub>2</sub> and 3). spent Fe/SiO<sub>2</sub> (CO<sub>2</sub>/CH<sub>4</sub>=2:1).

The further peaking results of C1s peaks are shown in Figure 4-11. The  $\pi-\pi^*$

satellite feature, which exhibits the highest bonding energy, is clearly shown in the figure. Moreover, the peak of C-O or O-C=O is more prominent, implying more organic deposition (polymer or monomer) rather than carbon deposition were formed on these catalyst samples. The results indicate that the carbon-containing deposits on the catalyst samples are less than SiO<sub>2</sub> sample with more organic deposition. Considering that the selectivity to carbon deposition with packing SiO<sub>2</sub> sample was very low (less than 3%), the selectivity to carbon deposition when packing Co/SiO<sub>2</sub> or Fe/SiO<sub>2</sub> should be even less. Thus, it was not taken into account when calculating the selectivity to liquid products.

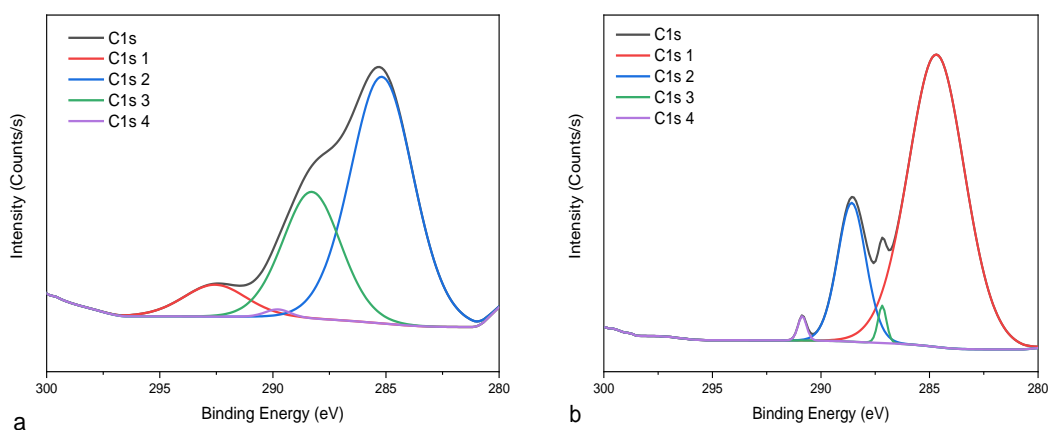


Figure 4-11. XPS peaking results of C1s peak of a). spent Co/SiO<sub>2</sub> and b). spent Fe/SiO<sub>2</sub>(CO<sub>2</sub>/CH<sub>4</sub>=2:1).

### 4.3.2 Thermodynamic equilibrium calculation

The thermodynamic equilibrium conversion rates of CO<sub>2</sub> and CH<sub>4</sub> as a function of temperature under different CO<sub>2</sub>/CH<sub>4</sub> ratio at 1 atm are illustrated in Figure 4-12, Figure 4-13, and Figure 4-14. The IR image of the reactor with the temperature distribution during discharge is shown in Figure 4-15. The thermodynamic equilibrium calculation is based on the minimized Gibbs free energy in a closed system. As the concentration of C<sub>3</sub><sup>+</sup> species in the gas phase is very poor in dry reforming process, the main gaseous components are assumed and set as CO<sub>2</sub>, CH<sub>4</sub>,

CO, H<sub>2</sub>, H<sub>2</sub>O, C<sub>2</sub>H<sub>6</sub>, CH<sub>3</sub>OH, CH<sub>3</sub>COOH; the solid phase is assumed to be carbon deposition. It is clearly shown that the reactions between CO<sub>2</sub> and CH<sub>4</sub> cannot initiate below 200 °C at any CH<sub>4</sub>/CO<sub>2</sub> ratio and at least 500 °C is essential to achieve a reasonable conversion rate of CH<sub>4</sub> and CO<sub>2</sub>. According to the image of IR camera during the plasma experiments, the highest wall temperature of our reactor during discharge is around 65 °C, while the average wall temperature of the reacting zone is approximately between 50 °C ~ 60 °C. The temperature difference of inlet and outlet gas measured by thermal probes at any case is almost negligible (less than 5 °C). Therefore, according to the thermodynamic equilibrium calculation, the heating due to electric discharge did not or negligibly contribute to the final conversion of CH<sub>4</sub> and CO<sub>2</sub>. The conversion of CH<sub>4</sub> and CO<sub>2</sub> is attributed to plasma discharge.

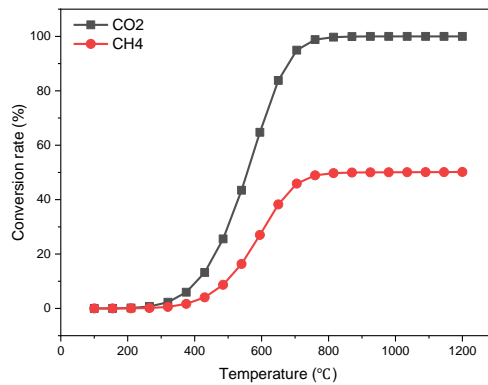


Figure 4-12. The thermodynamic equilibrium conversion rates of CO<sub>2</sub> and CH<sub>4</sub> as a function of temperature with CO<sub>2</sub>/CH<sub>4</sub> ratio = 1:2 at 1 atm (without plasma).

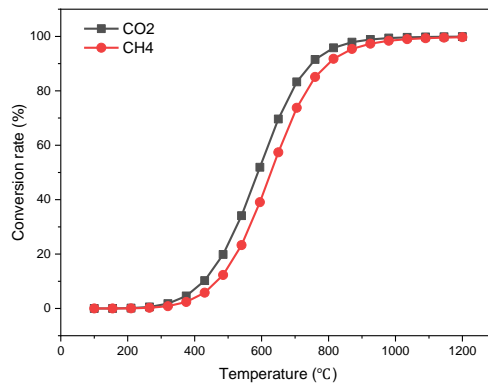


Figure 4-13. The thermodynamic equilibrium conversion rates of CO<sub>2</sub> and CH<sub>4</sub> as a function of

temperature with  $\text{CO}_2/\text{CH}_4$  ratio = 1:1 at 1 atm (without plasma).

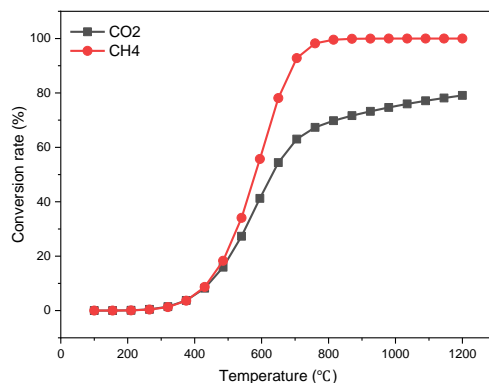


Figure 4-14. The thermodynamic equilibrium conversion rates of  $\text{CO}_2$  and  $\text{CH}_4$  as a function of temperature with  $\text{CO}_2/\text{CH}_4$  ratio = 2:1 at 1 atm (without plasma).

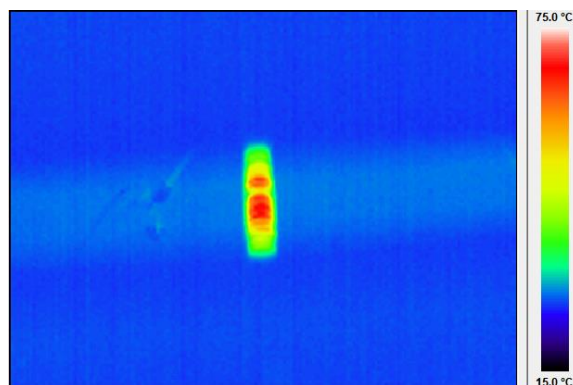


Figure 4-15. The IR image of the reactor during experiments.

### 4.3.3 Plasma experiments without catalysts

The plasma experiments without catalysts were conducted using a variable  $\text{CO}_2/\text{CH}_4$  ratio at a total flow rate of 30 ml/min and a variable total flow rate with a fixed  $\text{CO}_2/\text{CH}_4$  ratio of 2:1. The temperature of the reactor obtained from the IR camera in all of the tests was around 55 °C - 65 °C, which is far lower than the essential temperature to initiate the reaction of  $\text{CO}_2$  and  $\text{CH}_4$  according to the thermodynamic equilibrium calculation. Hence, we consider that conventional thermochemical reactions did not contribute to the conversion of  $\text{CO}_2$  and  $\text{CH}_4$ . The selectivity of gaseous products, conversion rate, and corresponding SIE are illustrated

in Figure 4-16. Table 4-2 shows discharge power, the selectivity of CH<sub>4</sub> to CO, the selectivity towards liquid chemicals, the energy efficiency of the plasma experiments, and the yield of syngas products of the corresponding experiments. CO, H<sub>2</sub>, and C<sub>2</sub>-5 hydrocarbons, mostly alkanes, were synthesized as the major products. Methanol, acetic acid, some other oxygenates and a significant peak of water were also detected in the liquid composition; however, the total selectivity towards liquid organics was only around 0.1 or even less (the detailed composition of selectivity towards liquid products is not listed). It should be noted that the water was one part generated through the reactions; the other part was condensed from the air when opening the condensing bottle due to the temperature difference, leading to a significant water peak in the spectra of GC-MS. Also, a very small amount of carbon black was found on the surface of the reactor and electrode in some of the plasma experiments without catalysts, while only negligible carbon black was found after placing the aerogel catalysts. The CO<sub>2</sub>/CH<sub>4</sub> ratio significantly affected the conversion rate of the reactants and the distribution of the products. The CO<sub>2</sub> and CH<sub>4</sub> conversion rates (from 19.2% and 37.8% to 29.6% and 43.2%) and the selectivity towards CO and H<sub>2</sub> (from 49% and 39.3% to 75.7% and 50.8%) increased with the CO<sub>2</sub>/CH<sub>4</sub> ratio with almost the same SIE, while the selectivity towards C<sub>2</sub>-C<sub>5</sub> hydrocarbons dramatically decreased (from 41.5% to 22.2%). The reactive species of CO<sub>2</sub> and CH<sub>4</sub> plasma, including CO, CO<sub>2</sub><sup>+</sup>, O, OH, and CH<sub>3</sub>, have been reported by some researchers [163, 245]. The initial steps for the electron-impact dissociation of CH<sub>4</sub> and CO<sub>2</sub> in a non-thermal plasma could be described as:



Simulation work on plasma methane conversion has revealed that reaction (17) is

responsible for 79% of CH<sub>4</sub> dissociation, while reactions (18) and (19) contribute 15% and 5% respectively [251]. This indicates that one part of the generated H finally formed H<sub>2</sub> due to the selectivity towards H<sub>2</sub> shown in Figure 16, while another part of H may combine with O, leading to the formation of H<sub>2</sub>O or OH species. The recombination reactions of CH<sub>x</sub> with the subsequent radicals resulted in the formation of higher hydrocarbons and oxygenates. Increasing the CH<sub>4</sub> ratio indeed increased the reactive CH<sub>3</sub> radicals. Therefore, the selectivity towards C2-C5 alkanes significantly increased. Notably, the ratio of unsaturated hydrocarbons to saturated hydrocarbons is negligible as shown in Table 4-2, indicating that the recombination reaction of H with unsaturated species was dominant in NTPs. Except for reaction (16), the vibrationally excited CO<sub>2</sub>(v) can also be generated in NTPs, and O radicals and H radicals can efficiently attack CO<sub>2</sub>(v) molecules to produce CO [5]:



However, recent simulation work [252] has demonstrated that the population of vibrational levels could be limited in DBD plasma, and the dominant CO<sub>2</sub>-splitting mechanisms were direct electron impact dissociation. Based on this understanding, instead of attacking CO<sub>2</sub>(v) molecules, the highly active O radicals could mainly combine with H to produce OH radicals and attack CH<sub>4</sub> molecules, along with producing OH and CH<sub>3</sub> radicals in the DBD reactor. Subsequently, the OH radicals could contribute to the formation of oxygenates (methanol, acetic acid, etc.) and water. Thus, O radicals could play a vital role in DBD plasma conversion of CO<sub>2</sub> and CH<sub>4</sub> and explain the increase in the conversion rate, energy efficiency of both reactants, yield of syngas products with the increase of CO<sub>2</sub> ratio, and the higher conversion rate of CH<sub>4</sub> compared to CO<sub>2</sub>. Another evidence was that no O<sub>2</sub> components were detected in the outlet gas, even with the highest CO<sub>2</sub> ratio, due to the limitation of reaction (20). We also noticed that the increase in CO<sub>2</sub> ratio increased the selectivity of CH<sub>4</sub> to CO. CH<sub>3</sub>OH, and CH<sub>2</sub>O radicals are known to be easily

decomposed when the translational temperature increases [5]. Therefore, the  $CH_xO$  radicals, which were generated via the recombination of O or OH with  $CH_x$  and contributed to the formation of oxygenates and chain growth, can also finally decompose into CO,  $H_2$ , and  $H_2O$ , resulting in the production of syngas instead of liquid organics. The increase in the  $CO_2$  ratio indeed increased the formation of  $CH_xO$  radicals in the gas atmosphere, leading to more dramatic decomposition into CO. Regarding the low selectivity towards liquid organics, the reaction route of decomposition could occur dominantly in the gas phase in DBD plasma:



The increase of total flow rate at a certain frequency and the peak-to-peak voltage between the reactor necessarily decreased the discharge power and energy efficiency, due to less residence time. Hence, the conversion rate of  $CO_2$  and  $CH_4$  decreased along with the increase of total flow rate, the same as the yield of products. However, the selectivity of  $CH_4$  to  $CO_2$  also decreased with a slight increase of selectivity towards liquid chemicals. The reasons can be the decrease in residence time and the lower translational temperature, which leads to less decomposition of oxygenated radicals and slightly higher total selectivity of liquid organics. Within a certain range, the high  $CO_2/CH_4$  ratio with a low total flow rate favors the formation of syngas products. In the case of  $CO_2/CH_4$  ratio of 2:1 with a 30 ml/min flow rate, the yield of CO and  $H_2$  in the outlet gas is 26.57% and 21.91%, respectively.

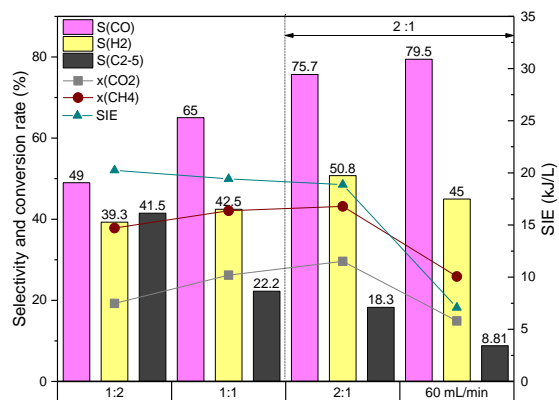


Figure 4-16. The selectivity of gaseous products, the conversion rates of reactants and the corresponding SIE varied by CO<sub>2</sub>/CH<sub>4</sub> ratio and total flow rate without catalysts (peak-to-peak voltage: 5.5 kV, frequency: 3 kHz).

Table 4-2. Discharge power, the selectivity of CH<sub>4</sub> to CO, the selectivity towards liquid chemicals, the energy efficiency of the plasma experiments and the yield of syngas products varied by CO<sub>2</sub>/CH<sub>4</sub> ratio and total flow rate without catalysts (peak-to-peak voltage: 5.5 kV, frequency: 3 kHz).

	S <sub>CH<sub>4</sub> to CO</sub>	R	Power (W)	EE (mmol/kJ)		Yield (%)		CB
				CO <sub>2</sub>	CH <sub>4</sub>	CO	H <sub>2</sub>	
1:2	0.357	0.051	10.1	0.129	0.508	15.44	14.85	0.983
1:1	0.414	0.037	9.71	0.276	0.442	22.00	17.87	0.966
2:1	0.513	0.033	9.45	0.427	0.311	26.57	21.91	0.984
60 ml/min	0.392	0.022	7.08	0.573	0.497	11.64	13.43	0.973

The plasma experiments with only CH<sub>4</sub> or CO<sub>2</sub> were also carried out without catalysts at the same peak-to-peak voltage, frequency, and total flow rate (30 ml/min). As shown in Figure 4-17, the conversion rates of CH<sub>4</sub> only (28.6%) and CO<sub>2</sub> only (15.2%) experiments are much lower than those of the gas mixture. Considering that the recombination of O<sub>2</sub> and CO occurred in NTP conditions, it is reasonable that the conversion is lower than the tests of the gas mixture, in which the O mainly reacted with CH<sub>x</sub> and H radicals as mentioned above. As a result, the conversion of CH<sub>4</sub> seemed to be significantly promoted by O, while the conversion of CO<sub>2</sub> was relatively less promoted by H according to reaction (21), and the recombination of O<sub>2</sub> and CO

was inhibited. The results confirmed that O was vital to the conversion of CH<sub>4</sub>. However, O<sub>2</sub>, as the main product of dissociation of CO<sub>2</sub>, was not found in the CO<sub>2</sub>/CH<sub>4</sub> plasma due to the activity of O<sub>2</sub> and the limitation of reaction (20). We also found that the carbon balance of the CO<sub>2</sub>-only test was almost 100%, while with CH<sub>4</sub> only the carbon balance was around 95%. In fact, the threshold energy for the electron impact dissociation of CH<sub>4</sub> into carbon black (~14 eV) is much higher than the average electron energy of DBD, thus inhibiting the formation of carbon deposition. This indicated that CH<sub>4</sub> mainly attributed to the tiny amount of carbon black. Based on this analysis, the possible reaction pathway under these conditions is proposed as shown in Scheme 4-1.

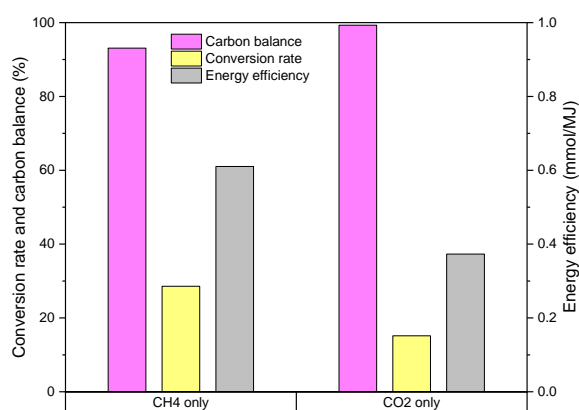
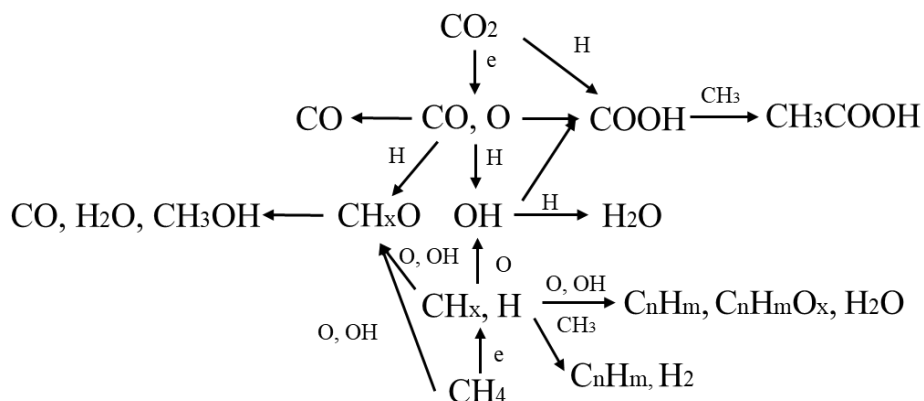


Figure 4-17. The carbon balance, conversion rates, and energy efficiency of CH<sub>4</sub>-only or CO<sub>2</sub>-only conditions without catalysts (peak-to-peak voltage: 5.5 kV, frequency: 3 kHz).



Scheme 4-1. Possible reaction pathways for the formation of gaseous and liquid products.

#### 4.3.4 Plasma experiments with catalysts

The plasma-catalytic experiments were carried out with reduced Co/SiO<sub>2</sub> aerogel and Fe/SiO<sub>2</sub> aerogel catalysts using a total flow rate of 30 ml/min, the same input electrical signal, and a variable CO<sub>2</sub>/CH<sub>4</sub> ratio. Figures 4-18 and 4-19 show the conversion rates, SIE, and energy efficiency without/with packing using a CO<sub>2</sub>/CH<sub>4</sub> ratio of 2:1, respectively; Figures 4-20 and 4-21 illustrate the corresponding selectivity of gaseous products and main liquid products respectively. As the selectivity towards liquid products is almost negligible compared to the experiments with packing, only the results with packing are listed. The total selectivity towards liquid without packing is shown in Table 4-3. Methanol, ethanol and acetic acid were detected as the main liquid products, while a small amount of acetone, 1-propanol, and methyl acetate was also found with the Co and Fe catalysts. The voltage data recording of the reactor and capacitor during a period's discharge without/with packing was shown in Figure 4-22.

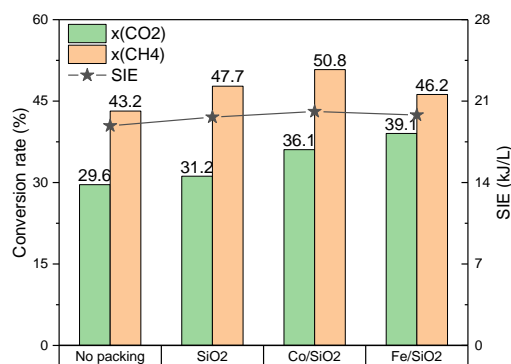


Figure 4-18. The conversion rates and SIE of the experiments without packing, with SiO<sub>2</sub> only, and with catalysts (peak-to-peak voltage: 5.5 kV, frequency: 3 kHz, total flow rate: 30 ml/min, CO<sub>2</sub>/CH<sub>4</sub> ratio = 2:1).

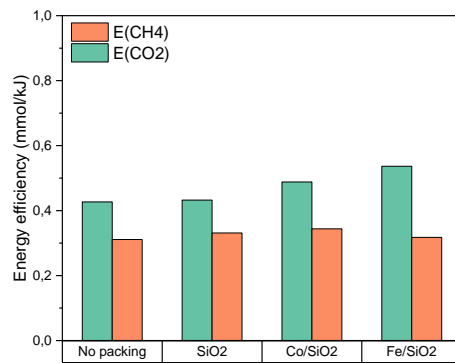


Figure 4-19. The energy efficiency of CO<sub>2</sub> and CH<sub>4</sub> without packing, with SiO<sub>2</sub> only, and with catalysts (peak-to-peak voltage: 5.5 kV, frequency: 3 kHz, total flow rate: 30 ml/min, CO<sub>2</sub>/CH<sub>4</sub> ratio = 2:1).

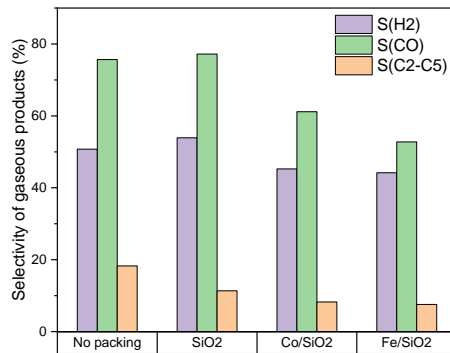


Figure 4-20. The selectivity of gaseous products without packing, with SiO<sub>2</sub> only, and with catalysts (peak-to-peak voltage: 5.5 kV, frequency: 3 kHz, total flow rate: 30 ml/min, CO<sub>2</sub>/CH<sub>4</sub> ratio = 2:1).

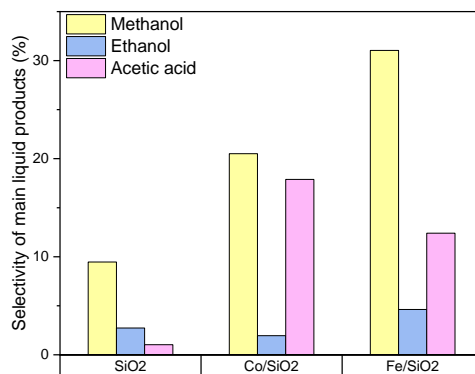


Figure 4-21. The selectivity of main liquid products without packing, with SiO<sub>2</sub> only, and with catalysts

(peak-to-peak voltage: 5.5 kV, frequency: 3 kHz, total flow rate: 30 ml/min, CO<sub>2</sub>/CH<sub>4</sub> ratio = 2:1).

Unlike Al<sub>2</sub>O<sub>3</sub> support [228], fully packing the SiO<sub>2</sub> aerogel support did not significantly alter the discharge behavior and decrease the conversions as shown in Figure 4-22 (a) and (b) as introducing SiO<sub>2</sub> aerogel avoided the extreme abatement of discharge volume and the alteration of conductivity. Compared to no-packing conditions, it is introducing the SiO<sub>2</sub> aerogel support negligibly altered the conversion rates and the energy efficiency of CO<sub>2</sub> and CH<sub>4</sub>, while the selectivity towards methanol increased. The reason can be the high sorption capacity of SiO<sub>2</sub> aerogel, which caused the sorption of reactive species, such as CH<sub>x</sub>O, into the mesoporous structure of silica aerogel, whereas previous simulation work [253] demonstrated that plasma was hardly formed as the mesopore size is much less than Debye sheath. As a result, the decomposition of CH<sub>x</sub>O into CO could be inhibited, and the residence time could also increase, thus decreasing the selectivity of CH<sub>4</sub> to CO (from 0.513 to 0.369) and promoting the formation of liquid organics. We can also observe a difference between the SiO<sub>2</sub> aerogel support before and after the experiments as shown in Figure 4-23. It was found carbon-containing deposits including carbon deposition and carbon-containing polymers or monomers were formed on the surface of spent SiO<sub>2</sub> sample rather than only carbon black according to results of TGA and XPS tests illustrated in section 4.3.1. Moreover, it was found that the overall selectivity towards carbon-containing deposits was less than 3% according to the TGA analysis. Therefore, it was not considered when calculating the selectivity to liquid products.

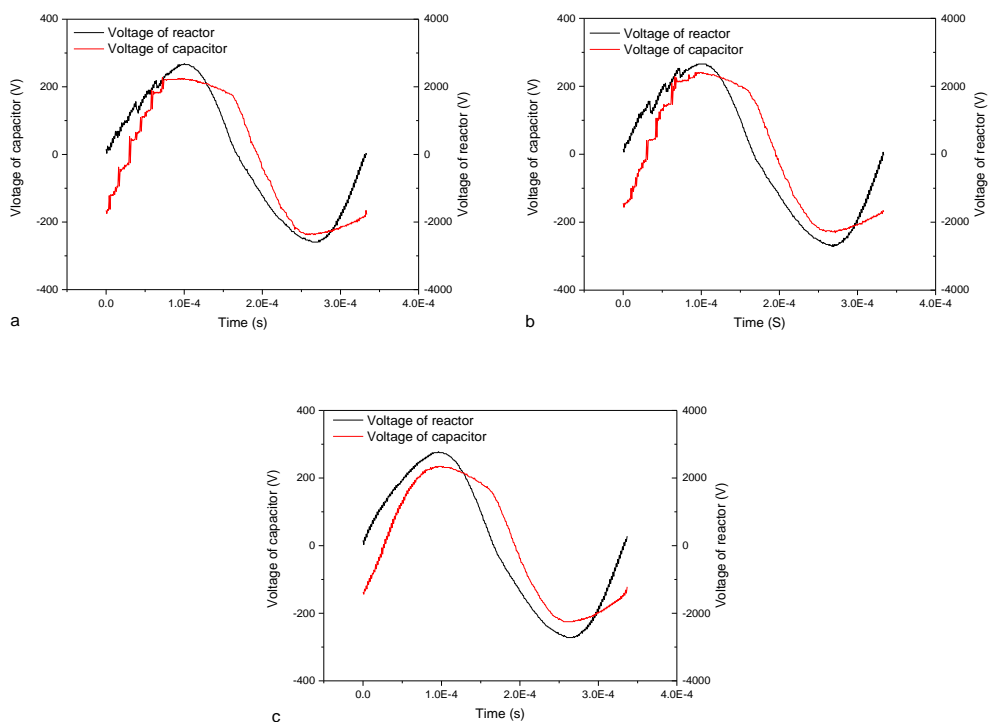


Figure 4-22. The voltage data recording of the reactor and capacitor during plasma experiments at a ratio of  $\text{CO}_2/\text{CH}_4 = 2:1$ : a). no packing; b). aerogel only; c). Co/SiO<sub>2</sub>.



Figure 4-23. The photo of silica aerogel support before and after plasma experiments.

Introducing the Co or Fe catalyst with its SiO<sub>2</sub> aerogel support greatly promoted the formation of liquid organics compared to SiO<sub>2</sub> aerogel only or no packing, as shown in Figure 4-21. Moreover, the conversion rates and energy efficiency of CO<sub>2</sub> and CH<sub>4</sub> increased, while the selectivity towards gaseous products significantly decreased. We also noted that the Co and Fe catalyst exhibited effects on discharge behavior (Figure 4-22 (c)) due to abatement of discharge volume and the modification of conductivity, resulting in a slight increase in discharge power. In addition to the

mesoporous structure of the SiO<sub>2</sub> aerogel, the well-dispersed Co and Fe in the supports significantly affected the selectivity of the products and shifted them towards liquid organics (methanol up to 20.5% and 31.0%, acetic acid up to 17.9% and 12.4%). The synergistic effects between catalysts and plasma are quite complicated and debated. Possible explanations are: 1) the introduction of the catalysts altered the discharge behavior and enhanced the local electric field near the metal catalysts, leading to more stable surface discharge. As a result, the initial dissociation steps were promoted; 2) the strong sorption behavior of the mesoporous structure in the support, as mentioned above, inhibited the decomposition of CH<sub>x</sub>O species; 3) the well-dispersed Co or Fe metal catalyst, as two conventional catalysts used for the direct synthesis of long-chain products in conventional FTS and reforming processes, is remarkably active to chemisorption of radicals, particularly oxygen contained groups or radicals in the discharge atmosphere of DBD plasma, the reaction of vicinal sorbed groups can finally form these liquid oxygenates. We also noted that Fe/SiO<sub>2</sub> was more favorable to alcoholic products with higher CO<sub>2</sub> conversion rates, while Co/SiO<sub>2</sub> favored the formation of acetic acid with a higher conversion rate of CH<sub>4</sub>. Furthermore, more long-chain chemicals (propanol, methyl acetate) were detected in the liquid products via GC-MS with Co/SiO<sub>2</sub>. One possible explanation is that Co, as a popular catalyst for chain growth in FTS, could be more capable of activating CH<sub>4</sub> into CH<sub>x</sub> and thus naturally more active in chain propagation. Besides, Gao et al. found surface cobalt atoms of the atomically thin layers have higher intrinsic activity and selectivity towards formate production during CO<sub>2</sub> electroreduction, at lower overpotentials, which was consistent with our results [254]. Meanwhile, Fe, which is well known to be capable of activating CO<sub>2</sub>, could lead to more enrichment of OH radicals, which ultimately contribute to the formation of short-chain alcohols at low temperatures. The C1s XPS spectra of catalyst samples and SiO<sub>2</sub> indicated that the carbon-containing deposits were even much less formed on the Co/SiO<sub>2</sub> and Fe/SiO<sub>2</sub> samples than on the SiO<sub>2</sub> sample. Moreover, the peaking results of the corresponding

C1s peaks revealed that more organic deposition (polymer or monomer) rather than carbon deposition were formed on these catalyst samples.

Plasma-catalytic experiments with various CO<sub>2</sub>/CH<sub>4</sub> ratios were also conducted under the same conditions. The selective tendency of gaseous products that vary by CO<sub>2</sub>/CH<sub>4</sub> ratio with packing catalysts is similar to the results without packing catalysts as shown in Figure 4-24 and Figure 4-25. Decreasing the CO<sub>2</sub>/CH<sub>4</sub> ratio logically leads to the generation of CH<sub>3</sub> radicals, therefore promoting the formation of long-chain products, such as ethanol, and decreasing the selectivity towards methanol. Indeed, more long-chain oxygenated species were detected, and hydrocarbons with particularly long chains (hexane, heptane) were found in the liquid products with the Co/SiO<sub>2</sub> catalyst as shown in Figure 4-26. Note that decreasing the CO<sub>2</sub>/CH<sub>4</sub> ratio significantly increased the selectivity towards acetic acid. As shown in Scheme 4-1, COOH radicals could be formed via the recombination of CO radicals with OH radicals and the combination of CO<sub>2</sub> and H radicals. Thus the selectivity towards acetic acid should logically decrease because fewer CO radicals and O radicals were generated in this condition. The results suggest that the catalysts could promote the conversion of CO<sub>2</sub> into COOH radicals instead of CH<sub>x</sub>O, and that production could depend more on H radicals than on CO<sub>2</sub>. It was clearly established once more that, whatever the ratio of CO<sub>2</sub>/CH<sub>4</sub>, the Co catalyst was more sensitive to acetic acid and long-chain products, while the Fe catalyst was more favorable to alcoholic products. Based on these results, we suggest that both Co and Fe are capable of activating the reactants and active to adsorb the radicals, especially O, OH, and CH<sub>x</sub> produced in NTP. Meanwhile, the adsorbed CH<sub>x</sub> can efficiently react with the adjacent OH to produce CH<sub>x</sub>O and alcoholic products, mainly methanol. The adsorbed CO<sub>2</sub> could react with the H radicals in the gas phase to produce COOH radicals, leading to the formation of organic acids, mainly acetic acid; the adsorbed CH<sub>x</sub> and CH<sub>x</sub>O would combine to form long-chain oxygenates (propanoic acid, butanol, etc.), or even react with H in the gas phase to produce long hydrocarbons and water, which in our study

was responsible for the chain growth. Following this assumption, a possible pathway is proposed in Scheme 4-2. Significant results detected a small amount of hexane, heptane and C6 ester (C<sub>6</sub>H<sub>12</sub>O<sub>2</sub>) in liquid products using a CO<sub>2</sub>/CH<sub>4</sub> ratio of 1:2 with Co catalysts, while a small amount of pentanol and heptanol were found in the liquid products with Fe catalysts under the same conditions. Consequently, the direct synthesis of value-added, liquid, oxygenated chemicals, and syngas was achieved with impressive selectivity and energy efficiency via this plasma-catalytic process.

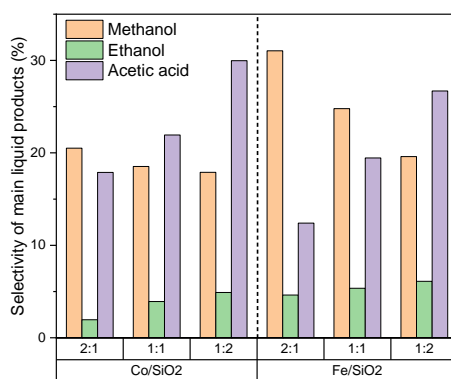


Figure 4-24. The selectivity of main liquid products as a function of catalysts and a CO<sub>2</sub>/CH<sub>4</sub> ratio from 2:1 to 1:2 (peak-to-peak voltage: 5.5 kV, frequency: 3 kHz, total flow rate: 30 ml/min).

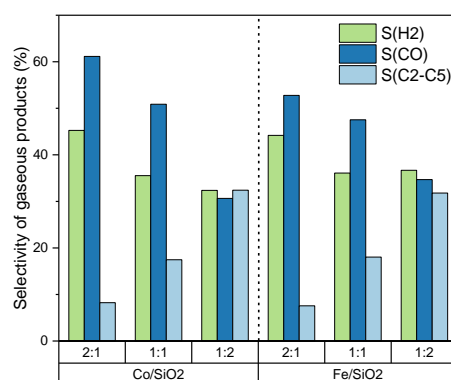


Figure 4-25. The selectivity of gaseous products as a function of catalysts and a CO<sub>2</sub>/CH<sub>4</sub> ratio from 2:1 to 1:2 (peak-to-peak voltage: 5.5 kV, frequency: 3 kHz, total flow rate: 30 ml/min).

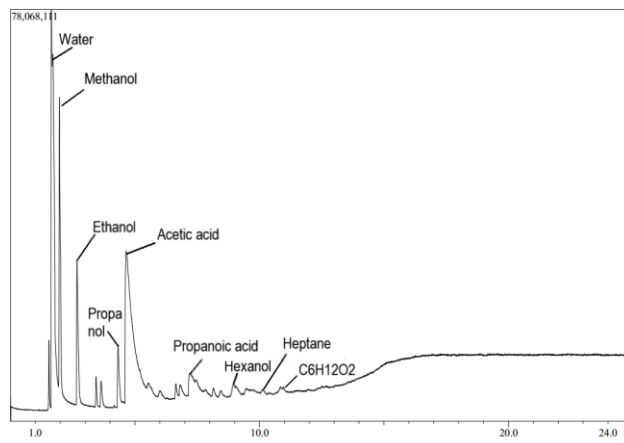
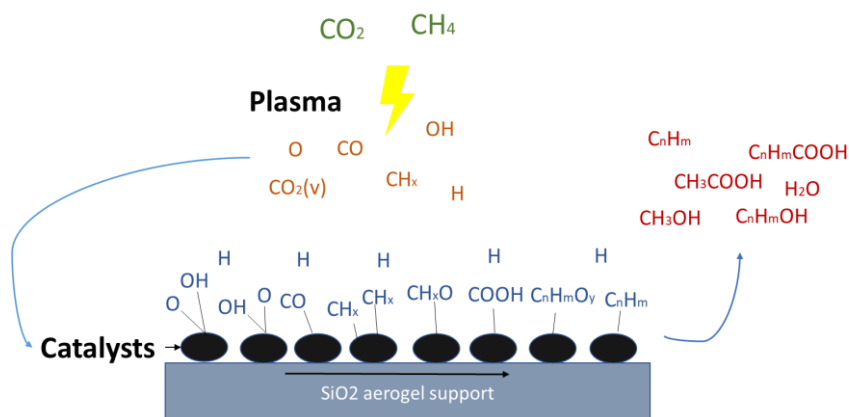


Figure 4-26. The GC-MS analysis of some important components in the condensed liquid products formed with Co/SiO<sub>2</sub> catalysts with a CO<sub>2</sub>/CH<sub>4</sub> ratio of 1:2.



Scheme 4-2. Possible reaction pathways for the formation of liquid products on the catalysts via plasma-catalytic approach.

## 4.4. Summary

In this chapter, the direct synthesis of value-added liquid chemicals from CO<sub>2</sub> and CH<sub>4</sub> by a plasma-catalytic process was achieved with considerable conversion rates at ambient conditions. The influence of different CO<sub>2</sub>/CH<sub>4</sub> ratios, SiO<sub>2</sub> aerogel packing, and supported catalysts packing was investigated. Except the cobalt catalyst described in the previous chapter, the Fe/SiO<sub>2</sub> aerogel catalysts were prepared and characterized, then introduced into the DBD reactor for the plasma reforming reactions of CO<sub>2</sub> with CH<sub>4</sub>.

Without packing, it was found that syngas and C<sub>2</sub> to C<sub>5</sub> gaseous hydrocarbons were the main products, while the total selectivity towards liquid products was

negligible, mainly due to the decomposition of  $\text{CH}_x\text{O}$  radicals. Increasing the  $\text{CO}_2/\text{CH}_4$  ratio increased the conversions of both reactants and the selectivity towards syngas, while selectivity towards  $\text{C}_2^+$  species decreased. In the case of  $\text{CO}_2/\text{CH}_4$  ratio of 2:1 with a 30 ml/min flow rate, the yield of CO and  $\text{H}_2$  in the outlet gas is 26.6% and 21.9%, respectively.

With packing, the results were very different. Firstly, the use of aerogel as a support for the catalyst made it possible to avoid: (i) a significant abatement in discharge volume, (ii) an alteration of the discharge behavior. Moreover, due to its high sorption capacity, the packing of  $\text{SiO}_2$  aerogel slightly favored the formation of liquid chemicals and the conversions of reactants. Secondly, the synergetic addition of an appropriate catalyst in the system significantly promoted the formation of the liquid chemicals up to a total liquid selectivity of 40%, where methanol and acetic acid were the main liquid products. The explanations are assumed to be: (i) enhancement of local electric field, (ii) more stable discharge behavior, (iii) the instinctive activity of Fe and Co to the chemisorption of reactive radicals. The results also revealed that an Fe catalyst preferentially led to the formation of alcoholic products, while a Co catalyst was more favorable to the formation of formate groups (mainly acids) and long-chain products (up to  $\text{C}_5$  oxygenates), which is in agreement with some published work on  $\text{CO}_2$  electroreduction. Moreover, with a high ratio of  $\text{CH}_4$ , a few  $\text{C}_5^+$  hydrocarbons (pentane and heptane) and a  $\text{C}_6$  ester were synthesized. To our knowledge, the plasma-catalytic performance for liquid production obtained here is outstanding compared to existing studies and broadens the way to the design of an efficient plasma-catalytic process for direct conversion of  $\text{CO}_2$  and  $\text{CH}_4$  into liquid chemicals.

# Chapter V. Direct synthesis of liquid chemicals and fuels for CO<sub>2</sub> and CH<sub>4</sub>

## Résumé du chapitre

Ce chapitre est dédié à l'étude de la synthèse directe de produits liquides à partir de CO<sub>2</sub> et CH<sub>4</sub> à l'aide du réacteur plasmocatalytique du chapitre précédent dans lequel il a été introduit non pas un catalyseur mais deux en même temps. Des combinaisons simples ou mixtes sont ainsi effectuées et testées parmi les matériaux suivants : Co, Fe, SiO<sub>2</sub> et HZSM-5. Les catalyseurs sont disposés dans le réacteur sous forme de granules mixtes (préparés par dopage/imprégnation) ou simples, mélangés ou séparés (configuration double lits). Les résultats semblent montrer que l'association sous forme de granules mixtes Co/HZSM-5 est particulièrement favorable à la conversion directe de CO<sub>2</sub> et CH<sub>4</sub> en produits liquides à longue chaîne. L'association sous forme de granules mixtes Fe/HZSM-5 permet de son côté d'obtenir lorsque la proportion de CO<sub>2</sub> est élevée une sélectivité importante vis-à-vis du méthanol. L'association en configuration double lits de granules Fe / aérogel de silice et de granules de HZSM-5 permet quant à elle, lorsque la proportion de CH<sub>4</sub> est élevée, d'atteindre une importante sélectivité vis-à-vis de l'acétique acétique. La synergie positive entre la combinaison de deux catalyseurs et du plasma pour la production de produits liquides à partir de CO<sub>2</sub> et CH<sub>4</sub> est ainsi démontrée.

## Abstract

This chapter is dedicated to studying the direct plasma-catalytic synthesis of liquid products from CO<sub>2</sub> and CH<sub>4</sub> using composite catalysts in the same reactor. The Co or Fe catalysts were prepared by doping Co or Fe on the SiO<sub>2</sub> or HZSM-5. The composite configuration was set up by different mixing method: metal doping (Co or Fe doping on HZSM-5 by impregnation), granule mixing (Co/SiO<sub>2</sub> or Fe/SiO<sub>2</sub> mixed with HZSM-5), and dual bed packing (one of Co/SiO<sub>2</sub> or Fe/SiO<sub>2</sub>, one layer of HZSM-5). HZSM-5 alone was also introduced in the experiment for comparison. The plasma-catalytic performance of the composite catalysts was investigated, and the formation of long-chain liquid chemicals and fuels was explored. According to the results, granule mixed Co/SiO<sub>2</sub> with HZSM-5 composite catalyst sample was particularly favorable for the direct conversion of CO<sub>2</sub> and CH<sub>4</sub> into long-chain liquid products. Meanwhile, packing Fe/HZSM-5 led to high selectivity to methanol without prominent side liquid products at a high CO<sub>2</sub> proportion in feeding gas. Packing granule mixed Fe/SiO<sub>2</sub> with HZSM-5 brought out high selectivity to acetic acid at a high CH<sub>4</sub> proportion. The synergy of composite catalysts with plasma in this process demonstrates great potential for directly synthesizing value-added long-chain liquid chemicals from CO<sub>2</sub> and CH<sub>4</sub> and manipulating the distribution of products.

## 5.1. Introduction

The previous chapter has clearly demonstrated the feasibility of direct synthesis of liquid chemicals with a considerable selectivity in the DBD reactor by introducing Co/SiO<sub>2</sub> or Fe/SiO<sub>2</sub> aerogel catalysts. Moreover, a few amounts of C<sub>5</sub>+ hydrocarbons and esters are also detected in the liquid products. As mentioned in the first chapter, direct plasma-catalytic synthesis of liquid hydrocarbons and fuels from CO<sub>2</sub> and CH<sub>4</sub> is more economical and environmentally benign than the indirect approach and regarded as the future technology of the energy recovery and CO<sub>2</sub> utilization. Meanwhile, plasma discharge can be simply generated by applying voltage, where the proportion of renewable energy such as solar, wind, and biomass is increasing. Therefore, plasma-catalytic synthesis of liquid hydrocarbons and fuels from CO<sub>2</sub> and CH<sub>4</sub> offers a promising solution to the storage of renewable energy. As discussed in Section 1.4.3 and 1.5.2, some researchers have explored the direct synthesis of liquid chemicals and fuels via conventional thermo-catalytical or plasma-catalytical pathway, and some results have been reported. However, most of the researches only studied the formation of liquid organic products such as methanol and acetic acid with unfavorable selectivity while the synthesis of long-chain hydrocarbons is barely reported. The exploration of the direct plasma-catalytic formation of liquid organics and hydrocarbon fuels still paused in the initial page. Great efforts are entailed not only on the catalyst development but also the mechanistic perspective. This chapter is dedicated to exploring the composite catalysts for the direct synthesis of liquid chemicals and fuels.

In recent decades, researchers have explored and studied diverse catalysts, bifunctional catalysts, supports, and promoters applied to the activation, dissociation, and conversion of CO<sub>2</sub>. Most of these efforts focused on CO<sub>2</sub> hydrogenation into methanol or C-C bonds. Studt et al. [255], Graciani et al. [256], Martin et al. [257] and Kattel et al. [258] have studied the direct CO<sub>2</sub> hydrogenation into methanol on

various oxide, bimetallic and bifunctional catalysts such as  $\text{In}_2\text{O}_3$ , Ni-Ga catalyst, Cu/ZnO and Cu/CeO<sub>2</sub>/TiO<sub>2</sub>. Significant results and conclusions have been obtained due to their work, particularly on the aspect of mechanism. Melaet et al. [259, 260] demonstrated the activation, dissociation, and the formation of methanol or C-C bond on the surface of Co catalysts. Wei et al. [261] has conducted the CO<sub>2</sub> hydrogenation experiments over a Na-Fe<sub>3</sub>O<sub>4</sub>/HZSM-5 zeolite bifunctional catalysts and explored directly converting CO<sub>2</sub> into a gasoline fuel by hydrogenation. By varying the packing method and the preparation method of catalysts, they successfully achieved a selectivity towards a gasoline fraction of 78% (mostly C5-C11 hydrocarbons) with a CO<sub>2</sub> conversion rate of 22%. The work also illustrated that the reduced Fe<sub>3</sub>O<sub>4</sub> catalyst is efficient on activating and dissociate CO<sub>2</sub> molecules and form (CH<sub>2</sub>)<sub>n</sub> groups, the introduction of HZSM-5 improved the selectivity towards C5-C11 hydrocarbons. Similar results have also been reported by Gao et al. with a higher selectivity towards C5+ [262]. They reported that oxygen vacancies on the In<sub>2</sub>O<sub>3</sub> surfaces activate CO<sub>2</sub> and hydrogen to form CH<sub>3</sub>OH, and then the transformation of CH<sub>3</sub>OH into C-C coupling subsequently occurs inside zeolite pores to produce gasoline-range hydrocarbons with a high octane number. However, the overall conversions of CO<sub>2</sub> are less than Wei's work. Apart from these researches, other studies also confirm the strong CO<sub>2</sub> adsorption behavior on the surface of reduced iron oxides or cobalt oxides, which are in agreement with our work presented in Chapter IV [263-266]. Moreover, these studies also reported zeolite catalysts such as HZSM-5 with a SiO<sub>2</sub>/Al<sub>2</sub>O<sub>3</sub> ratio between 120 to 200, which has been widely used in oil, bio-oil refinery, and methanol-to-hydrocarbon (MTHC) technology, exhibited high selectivity towards gasoline products due to its superior oligomerization. Thus, the combination of our Fe/SiO<sub>2</sub> or Co/SiO<sub>2</sub> aerogel catalysts with HZSM-5 could be feasible to improve the selectivity towards liquid hydrocarbons for the plasma-catalytic conversion of CH<sub>4</sub> and CO<sub>2</sub>.

Herein, this chapter is dedicated to combining the composite catalysts (Co/SiO<sub>2</sub>

or Fe/SiO<sub>2</sub> aerogel and HZSM-5) with plasma-catalysis to convert CO<sub>2</sub> and CH<sub>4</sub> into liquid chemicals and fuels. Co or Fe directly doped on HZSM-5 zeolite catalysts were also prepared, and different mixing methods of composite catalysts were also studied to make comparisons.

## 5.2. Experimental and materials

### 5.2.1 HZSM-5 and Co or Fe doped zeolite catalysts

The commercial HZSM-5 catalysts are purchased from Nankai University catalyst company, China, with a specific ratio of SiO<sub>2</sub> to Al<sub>2</sub>O<sub>3</sub> = 150. The size of the granule sample is similar to the aerogel samples (~1 mm). To activate HZSM-5 zeolite, the as-received samples were calcined in the air at 400 °C for 5 h.

The Co/SiO<sub>2</sub> and Fe/SiO<sub>2</sub> aerogel catalysts, which were prepared by the incipient wetness impregnation method with nitrate precursors, have been described in the preceding chapters. A series of Co or Fe doped HZSM-5 catalysts were prepared by incipient wetness impregnation method. The doped amount of Co or Fe is referred to the series of catalysts doped on SiO<sub>2</sub> aerogel. The targeted ethanolic solution of Co(NO<sub>3</sub>)<sub>2</sub>·6H<sub>2</sub>O or Fe(NO<sub>3</sub>)<sub>2</sub>·9H<sub>2</sub>O (Acros Organics, ≥ 99%) was introduced into the same volume of HZSM-5 zeolite and impregnated for one night. Following the impregnation procedure, the samples were dried at 140 °C for 2 h and calcined at 400 °C for 5 h in the air.

The specific surface areas, pore volumes, and average pore sizes of the as-calcined HZSM-5, as-synthesized Co/HZSM-5 and Fe/HZSM-5 catalysts were obtained from the N<sub>2</sub> adsorption/desorption analyses. The identification of species, surface, and structural properties was characterized and observed by XRD, XPS, SEM, and HRTEM as described in Chapter IV. The photo of as-calcined HZSM-5, as-synthesized Co/HZSM-5, and Fe/HZSM-5 catalysts are shown in Figure 5-1. Before the plasma experiments, all the samples were reduced at 600 °C for 10 h in a continuous gas flow of H<sub>2</sub>/N<sub>2</sub> mixture (5%/95%) under a flow rate of 40 ml/min with

a heating rate of 10 °C/min.

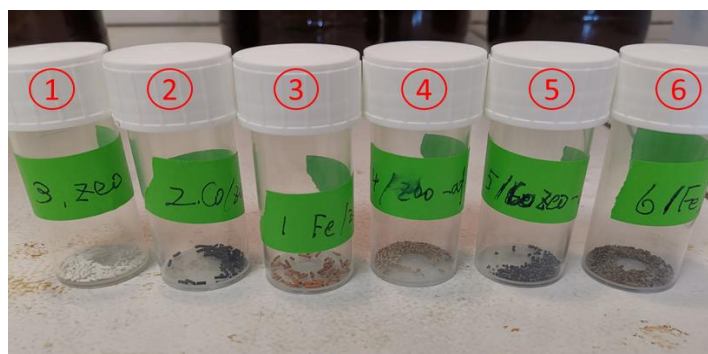
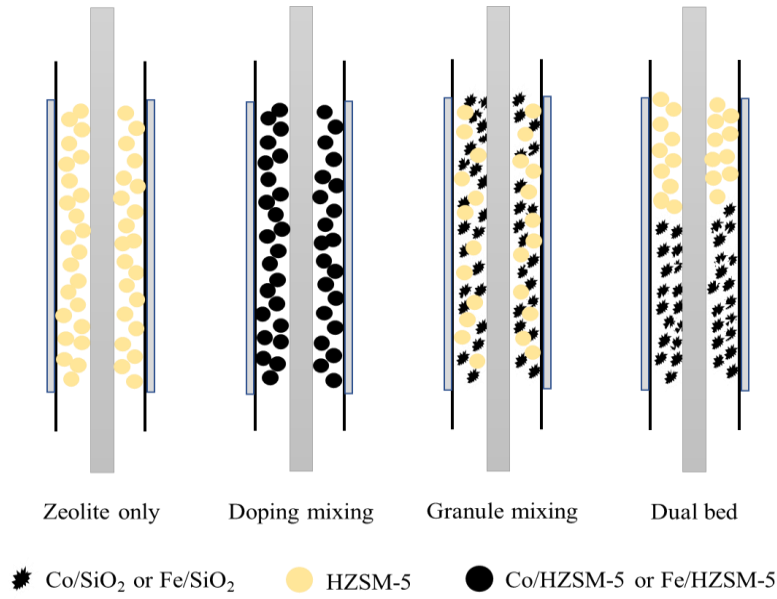


Figure 5-1. Photo of 1). as-received HZSM-5, 2). Co/HZSM-5, 3). Fe/HZSM-5, 4). spent HZSM-5(2 h), 5). spent Co/HZSM-5(2 h), 6). spent Fe/HZSM-5(2 h).

### 5.2.2 Experimental configuration

The mixing and packing method of these catalyst samples are illustrated in Scheme 5-1. The first plasma experiments of composite catalysts directly packed Co or Fe doped HZSM-5 (Co/HZSM-5 or Fe/HZSM-5) granules, which is named as doping mixing method. Another series of plasma experiments used the mixed the Co/SiO<sub>2</sub> or Fe/SiO<sub>2</sub> with HZSM-5. The granules of Co/SiO<sub>2</sub> sample or Fe/SiO<sub>2</sub> sample were mixed with the granules of HZSM-5 together at a mass ratio of two components of 1:1 by shaking in a vessel, respectively, which is named as granule-mixing packing. In the last series of plasma experiments, the granules of Co/SiO<sub>2</sub> or Fe/SiO<sub>2</sub> with the granules of HZSM-5 at a mass ratio of two components of 1:1 were packed in the reactor as a dual bed configuration, where the first layer was the granules of Co/SiO<sub>2</sub> sample or Fe/SiO<sub>2</sub> sample and the second layer was the granules of HZSM-5 sample. For comparisons, the granules of HZSM-5 were directly packed into the plasma reactor.



Scheme 5-1. Mixing and packing method of the catalyst samples.

The micro GC was calibrated for each gaseous component using standard gas cylinders with a wide range of concentrations. According to the measurements of the micro GC and the difference of the temperature, pressure and flow rate before and during each experiment, the conversion rate ( $x$ ) of CH<sub>4</sub> and CO<sub>2</sub> can be calculated according to:

$$x_{CH_4} = \frac{\text{moles of } CH_4 \text{ consumed}}{\text{moles of } CH_4 \text{ inlet}} \times 100 \% \quad (1)$$

$$x_{CO_2} = \frac{\text{moles of } CO_2 \text{ consumed}}{\text{moles of } CO_2 \text{ inlet}} \times 100 \% \quad (2)$$

The total conversion rates ( $x_{total}$ ) of CH<sub>4</sub> and CO<sub>2</sub> can be defined considering the dilution:

$$x_{total} = \frac{\text{moles of } CH_4 \text{ consumed} + \text{moles of } CO_2 \text{ consumed}}{\text{moles of } CH_4 \text{ inlet} + \text{moles of } CO_2 \text{ inlet}} \times 100 \% \quad (3)$$

The selectivity and yield of gaseous products can be calculated as:

$$S_{H_2} = \frac{\text{moles of } H_2 \text{ produced}}{2 \times \text{moles of } CH_4 \text{ consumed}} \times 100 \% \quad (4)$$

$$S_{CO} = \frac{\text{moles of } CO \text{ produced}}{\text{moles of } CO_2 \text{ consumed} + \text{moles of } CH_4 \text{ consumed}} \times 100 \% \quad (5)$$

$$Y_{H_2} = \frac{\text{moles of } H_2 \text{ produced}}{2 \times \text{moles of } CH_4 \text{ input}} \times 100 \% \quad (6)$$

$$Y_{CO} = \frac{\text{moles of } CO \text{ produced}}{\text{moles of } CO_2 \text{ input} + \text{moles of } CH_4 \text{ input}} \times 100 \% \quad (7)$$

$$S_{C_xH_y} = \frac{x \times \text{moles of } C_xH_y \text{ produced}}{\text{moles of } CO_2 \text{ consumed} + \text{moles of } CH_4 \text{ consumed}} \times 100 \% \quad (8)$$

The carbon balance based on the inlet and outlet gas can be calculated as:

$$CB = \frac{\text{moles of } C \text{ outlet}}{\text{moles of } C \text{ inlet}} \times 100 \% \quad (11)$$

The GC-MS was calibrated using a standard liquid sample (20 vol% of methanol, ethanol, acetic acid, acetone, and water) to quantify the main products, and the results were normalized by abstracting water. As a few carbon deposits can be found on the surface of zeolite after plasma experiments as shown in Figure 5-1, we estimated 12% of converted  $CH_4$  finally transformed into carbon deposits when packing HZSM-5 and 9% of converted  $CH_4$  finally transformed into carbon deposits when packing composite catalysts according to TGA analysis of spent catalysts (shown in the later section) and our previous work. Then the selectivity towards liquid organics can be calculated due to:

$$S_{liquid} = 100\% - S_{CO} - S_{C_xH_y} - \frac{0.12 \times \text{moles of } CH_4 \text{ consumed}}{\text{moles of consumed reactants}} \quad (12)$$

$$S_{C_xH_yO_z} = x * \text{mole}\% \text{ of } C_xH_yO_z * S_{liquid} \quad (13)$$

The specific input energy (SIE) is defined as the formula following:

$$SIE = \frac{\text{Power of discharge}(kW)}{\text{Flow rate}(\frac{L}{min})} * 60(\frac{s}{min}) \quad (14)$$

The energy cost (EC) is defined as the amount of energy consumed for the conversion of per molar reactants during the process:

$$EC (kJ/mol) = \frac{SIE(kJ/L) \times 24.5 (L/mol)}{x_{total}} \quad (15)$$

The energy efficiency of the reactor based on the gas conversion is defined as the reactants converted per mol of discharge power:

$$E_{CO_2} = \frac{\text{moles of } CO_2 \text{ consumed}}{\text{power of discharge}} \quad (16)$$

$$E_{CH_4} = \frac{\text{moles of } CH_4 \text{ consumed}}{\text{power of discharge}} \quad (17)$$

All the experiments were repeated three times for reproducibility.

### 5.3. Characterization of zeolite catalysts

#### 5.3.1 N<sub>2</sub> adsorption/desorption

The N<sub>2</sub> adsorption/desorption isotherms of as-received HZSM-5, as-prepared Fe/HZSM-5 and Co/HZSM-5 are shown in Figure 5-2. The surface area, pore volume, and average pore size of these corresponding samples are listed in Table 5-1. It is clearly shown in Figure 5-2 that the commercial HZSM-5 samples did not exhibit a flourishing porous structure or adsorption capacity compared with silica aerogel. Moreover, a large micropore area was detected in these samples. Obviously, doping Co or Fe on the HZSM-5 samples well maintained the porous structure of the zeolite and the specific surface area negligibly reduced after doping Co or Fe on the surface of zeolite samples due to the block of the porous structure.

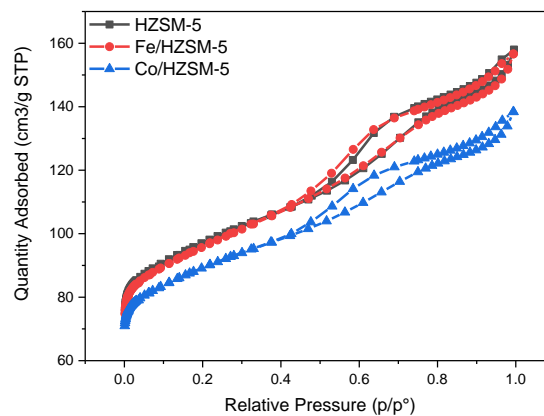


Figure 5-2. N<sub>2</sub> adsorption/desorption isotherms of 1). as-received HZSM-5, 2). as-prepared Fe/HZSM-5, 3). Co/HZSM-5.

Table 5-1. Surface area, pore volume, and average pore size of 1). as-received HZSM-5, 2). as-prepared Fe/HZSM-5, 3). Co/HZSM-5.

Catalysts	surface area <sup>a</sup> (m <sup>2</sup> /g)	average diameter (nm)	pore pore volume <sup>b</sup> (cm <sup>3</sup> /g)	t-plot area <sup>c</sup> (m <sup>2</sup> /g)	micropore
HZSM-5	326	2.9	0.15	191	
Fe/HZSM-5	308	2.8	0.14	185	
Co/HZSM-5	298	2.7	0.11	179	

a Brunauer-Emmett-Teller method.

b Barrett-Joyner-Halenda method determination via N<sub>2</sub> adsorption data.

c t-plot method via Harkins-Jura equation.

### 5.3.2 X-ray diffraction

The XRD spectra of as-received HZSM-5, as-synthesized Fe/HZSM-5, and as-synthesized Co/HZSM-5 are shown in Figure 5-3. The XRD patterns of HZSM-5 are well distinguished as branches of characteristic peaks, which has been described in many related publications. However, the characteristic peaks of the oxides of cobalt or iron evade the identification in the overall XRD patterns. It was found the XRD patterns of HZSM-5 were negligibly altered after doping Co or Fe expect slight differences in the intensity of the peaks. As well known, the characteristic peaks of the oxides of cobalt and iron are mainly located approximately at the 2θ of 35° and 37°, respectively. The XRD patterns of selected 2θ region of the corresponding samples from 31° to 43° is illustrated in Figure 2. The difference of XRD patterns of doping samples can be observed and marked at 2θ of 35° and 37° for Fe and Co, respectively, where the overlaps imply the existence of oxides species. Nevertheless, it is difficult to identify the exact species as the characteristic peaks are not well distinguished from the many peaks of HZSM-5 sample as well as the background noise. Moreover, comparing to doping on SiO<sub>2</sub> aerogel, the loading amount of Co or Fe on the mass base were the same as the aerogel samples, while the density of HZSM-5 is much higher than silica aerogel (0.63 g/ml for HZSM-5 and 0.15 g/ml for SiO<sub>2</sub> aerogel). As a result, the designed mass ratio of Fe or Co to HZSM-5 is only around 2.4%

(considering the mass loss while impregnating, drying and calcining, the final mass ratio of Fe and Co should be lower). As a result, the characteristic peaks of Co or Fe were rather unobvious comparing to the background noise and the characteristic peaks of HZSM-5.

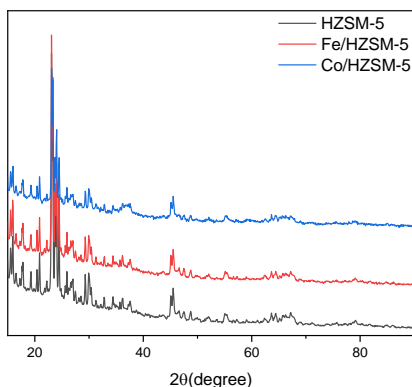
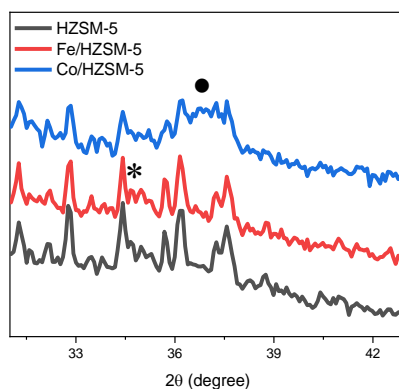


Figure 5-3. XRD patterns of 1). as-received HZSM-5, 2). Fe doped HZSM-5, and 3). Co doped HZSM-5.



\* refers to oxides of iron, • refers to oxides of cobalt

Figure 5-4. XRD patterns of the selected region of corresponding HZSM-5 samples from 31° to 43°.

The comparison of as-received or as-prepared catalyst samples with the spent catalyst samples are shown in Figure 5-5. It is found that the intensity of the characteristic peaks of spent samples is slightly lower than the as-received or as-prepared samples. The reason could be the formation of carbon deposit during

discharge and reduction of metallic oxides. However, it is difficult to verify the change of Co or Fe species before and after plasma experiments as the characteristic peaks of Co or Fe species appeared to overlap with the peak branches of HZSM-5 while the loading amount was few.

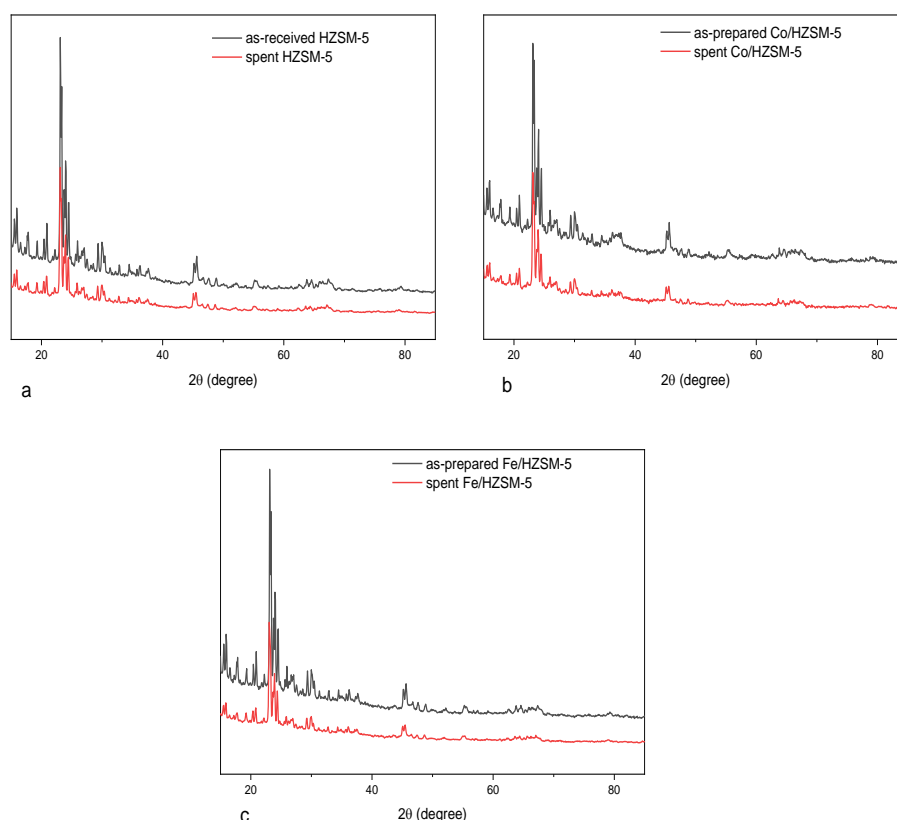


Figure 5-5. XRD patterns of a). as-received HZSM-5 and spent HZSM-5, b). as-prepared Co/HZSM-5 and spent Co/HZSM-5, and c). as-prepared Fe/HZSM-5 and spent Fe/HZSM-5.

### 5.3.3 X-ray photoelectron spectroscopy

XPS was applied to better identification of the surface metals on HZSM-5. The XPS survey profile of HZSM-5 is shown in Figure 5-6. Except for the peaks of Si, Al and O, a small peak of carbon was detected probably due to adventitious carbon contamination exposing to the atmosphere while delivering and the adhesive for compressing samples. The Fe 2p and Co 2p XPS profiles of Fe/HZSM-5 and Co/HZSM-5 are shown in Figure 5-7 and 5-8, respectively. The Fe 2p3 characteristic

peak is located at a binding energy of 710.8 eV with a typical Fe(III) satellite peak, which attributes to Fe<sub>2</sub>O<sub>3</sub> species according to NIST XPS database. However, the half-width of Fe 2p peaks is slightly more than 3 eV, indicating that a tiny amount of different iron oxides existed on the samples. On the other hand, the Co 2p<sub>3/2</sub> characteristic peak is located at a binding energy of 779.7 eV. The satellite feature of Co 2p<sub>3/2</sub> is apparently higher than 786 eV, which refers to the satellite feature of CoO. According to NIST XPS database, the existence of satellite feature is due to the 2+ and 3+ states of Co, indicating the Co species were mostly Co<sub>3</sub>O<sub>4</sub> (mixed oxidation of CoO and Co<sub>2</sub>O<sub>3</sub>). In any case, It has been reported by many publications that Fe<sub>2</sub>O<sub>3</sub> and Co<sub>3</sub>O<sub>4</sub> can be easily reduced in H<sub>2</sub>/N<sub>2</sub> gas flow at temperatures more than 400 °C.

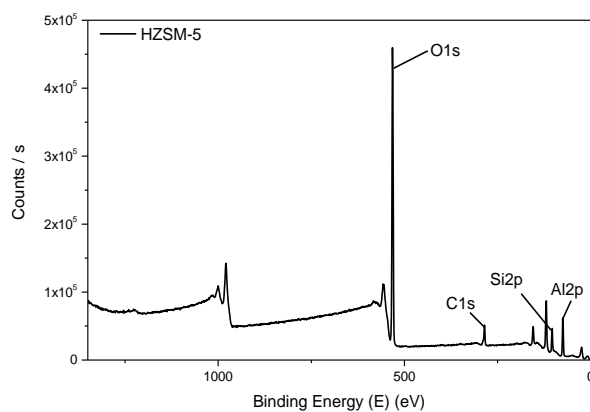


Figure 5-6. XPS survey profile of HZSM-5 sample.

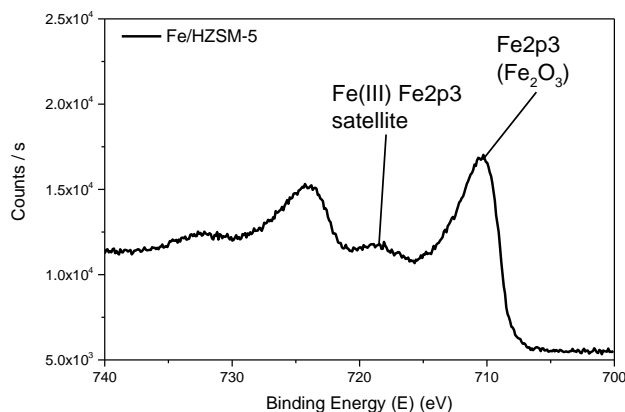


Figure 5-7. The Fe2p XPS profile of Fe/HZSM-5 sample.

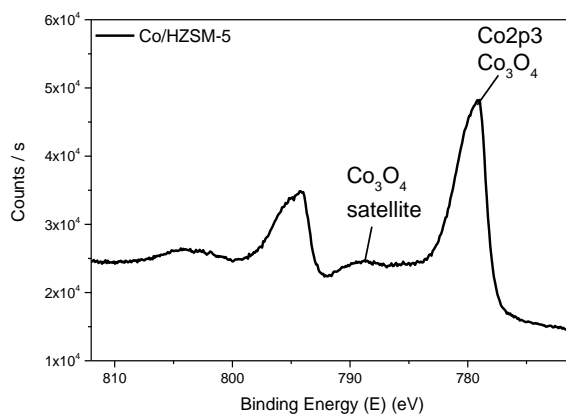


Figure 5-8. The Co2p XPS profile of Co/HZSM-5 sample.

To verify the carbon deposits on bifunctional zeolite samples, the C1s XPS profiles of as-received or as-prepared zeolite samples are compared with spent samples; the results are shown in Figure 5-9 and 5-10, respectively. The intensity of C-C bond peak (284.8 eV) and O-C=O (288.5 eV) of the spent HZSM-5 sample is apparently much higher than that of the as-received samples, indicating that the carbon containing depositions, including carbon deposit and carbon containing organics, were formed on the spent HZSM-5 sample. On the other hand, two different C1s peaks were detected on the spent Co/HZSM-5 and Fe/HZSM-5 samples: the more obvious one is similar to the C1s peaks of the spent HZSM-5 sample, while the intensity of other one is slightly higher than those of the as-prepared samples. The reason is due to the inhomogeneous dispersion of Co or Fe catalysts on the surface of HZSM-5, leading to an obvious C1s peak on the selected area of HZSM-5 and different C1s peaks on the selected area containing Co or Fe as shown in Figure 5-11. The results also revealed that the carbon depositions were less formed on the metallic catalysts than on the surface of HZSM-5, which resulted in 12% of converted CH<sub>4</sub> into carbon deposits on HZSM-5.

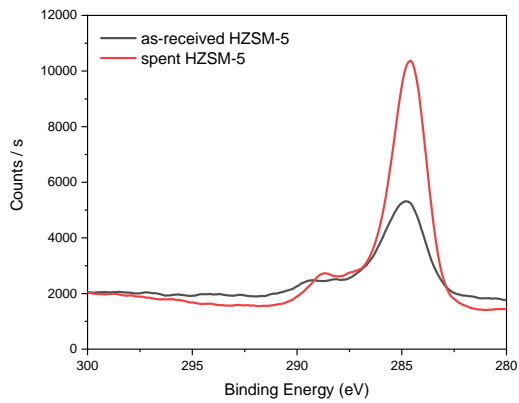


Figure 5-9. The C1s XPS profile of as-received and spent HZSM-5 samples.

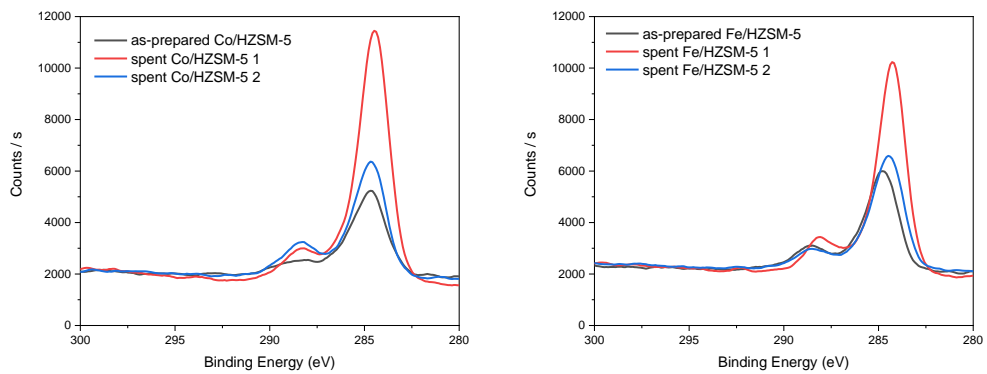


Figure 5-10. The C1s XPS profile of as-received and spent Co/HZSM-5 and Fe/HZSM-5 samples.

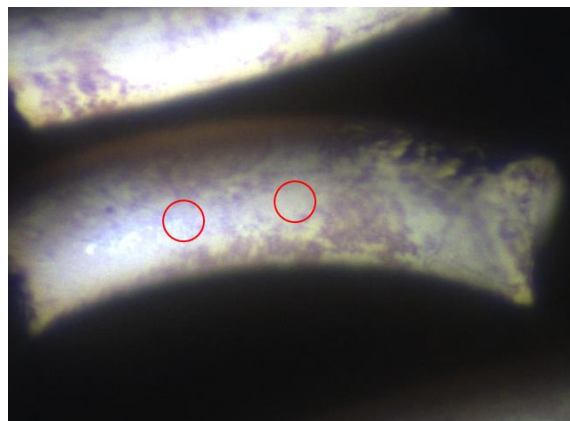


Figure 5-11. The C1s XPS scanning area of spent Fe/HZSM-5 samples.

### 5.3.4 SEM and TEM

The SEM images of Fe/HZSM-5 and Co/HZSM-5 samples with different

resolution are shown in Figure 5-12 and 5-13, respectively. The oxides of Co or Fe nanoparticles were dispersed on the surface of HZSM-5 structure. It can also be observed that a small amount of Co or Fe is aggregated on the surface of HZSM-5, leading to the decrease of specific surface area and pore volume. The nanoparticle size of the metallic catalysts is around 10~20 nm.

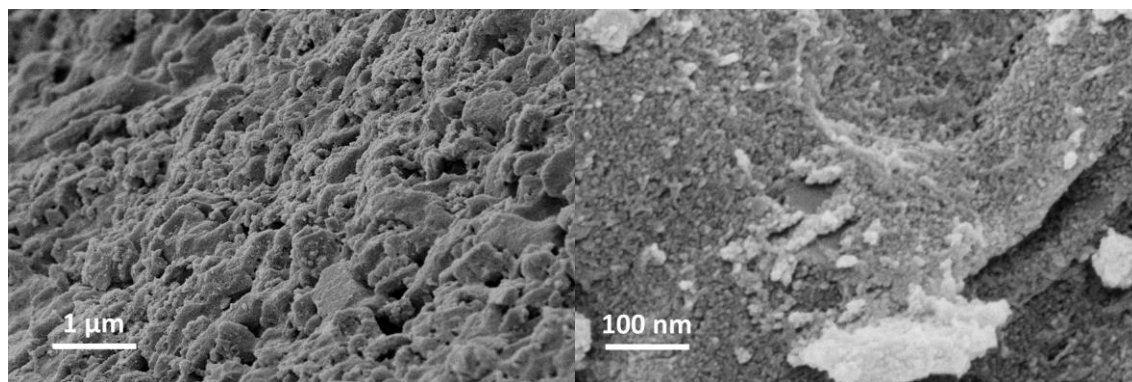


Figure 5-12. SEM observation of the Fe/HZSM-5 sample.

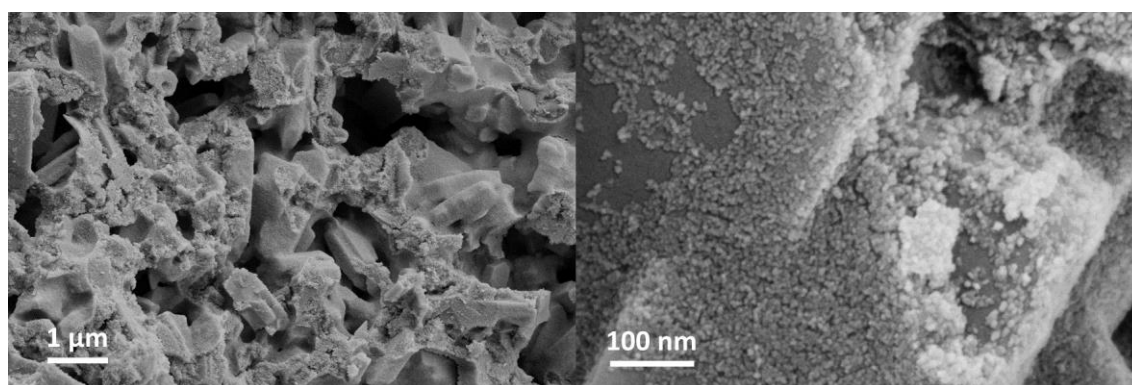


Figure 5-13. SEM observation of Co/HZSM-5 sample.

The TEM images and EDS images of Co/HZSM-5 sample are shown in Figure 5-14. The selective area diffraction pattern is shown in Figure 5-15. According to the diffraction pattern, the Co species are confirmed to be a cubic FCC (Fd-3m) structure with  $a=8.40 \text{ \AA}$ , referring to  $\text{Co}_3\text{O}_4$ , which is in a good coincidence with the results of XPS characterization. The TEM image also reveals the nanoparticle size of Co is around 10~20 nm. The EDS results clearly show that carbon element is nonexistent among the zeolite after sampling by ethanol, indicating that the carbonite peak

existing in XPS profile is due to the adventitious contamination rather than the carbonite species bonding with Si or Al.

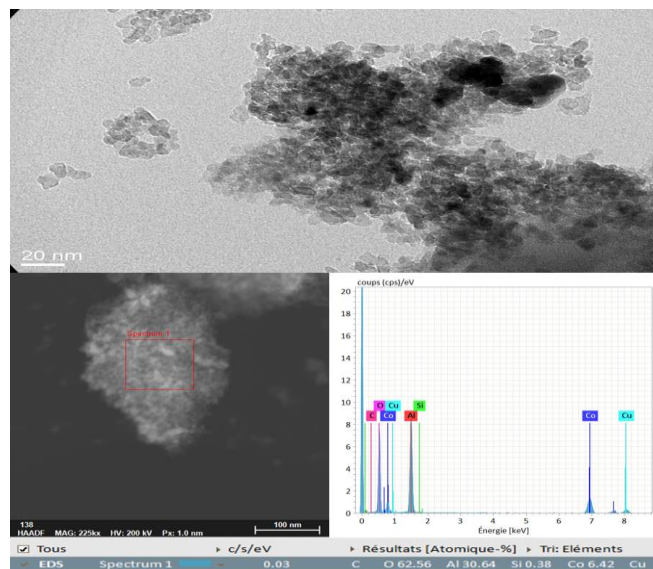


Figure 5-14. TEM images and EDS images of Co/HZSM-5 sample.

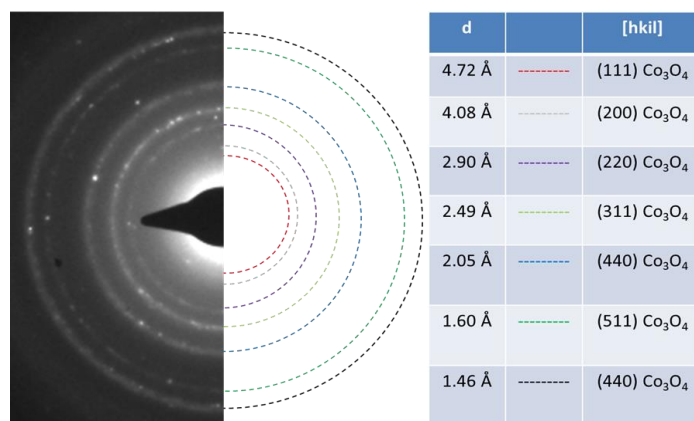


Figure 5-15. Selective area diffraction pattern of Co/HZSM-5 sample.

The TEM images and EDS images of Fe/HZSM-5 sample are shown in Figure 5-16. The selective area diffraction pattern is shown in Figure 5-17. Unlike the result of XPS profile, the result of EDS indicates a very low atomic component of Fe. The reason can be mass loss while sampling by ethanol. As a result, it is difficult to identify the Fe species according to selective area diffraction pattern as the crystallite structure of iron oxides is doped among the typical crystalline structure of zeolite

( $a=20 \text{ \AA}$ ) shown in Figure 5-17 and is difficult to distinguish. However, the results of XPS profiles have clearly confirmed the existence of  $\text{Fe}_2\text{O}_3$ .

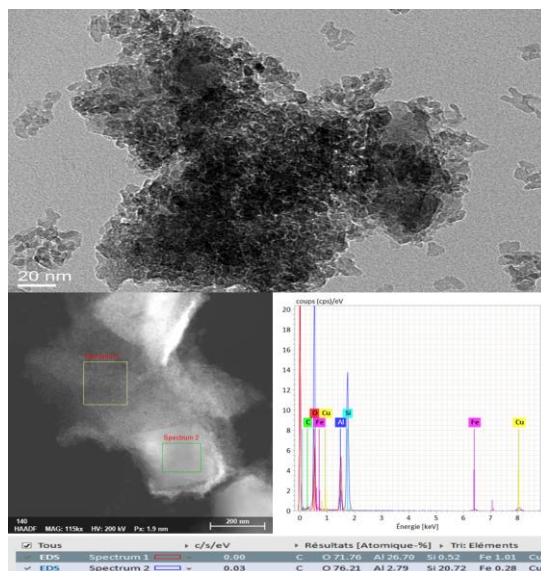


Figure 5-16. TEM images and EDS images of Fe/HZSM-5 sample.

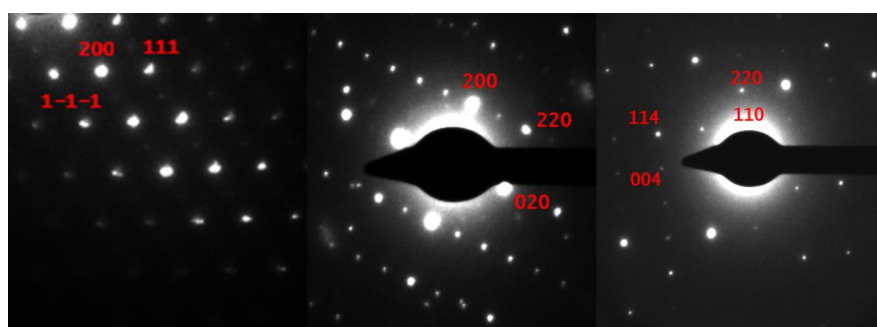


Figure 5-17. Selective area diffraction pattern of Fe/HZSM-5 sample.

### 5.3.4 TG analysis

The DTG curves of the spent HZSM-5 sample under the condition of air flow and argon flow are shown in Figure 5-18. The first weight loss peak of the sample under air flow is similar to the weight loss peak under argon flow at around  $100 \text{ }^\circ\text{C}$ ; this is due to the loss of water. However, the weight loss peaks of the samples under air flow and under argon flow are different after  $100 \text{ }^\circ\text{C}$ . The second weight loss peak of the sample under argon flow is probably due to carbonization of the carbon

containing organics. While for the sample under air flow, the two weight loss peaks are probably referring to the oxidation of carbon deposition reported by Zhang [249] and the oxidation of polymeric species reported by Nousir [250]. The photo of the corresponding samples after TG analysis is shown in Figure 5-19. According to the difference of the weight loss between the two conditions, we can estimate a net carbon deposition (including carbon deposition and carbon organics) of 0.7% normalized to the weight of HZSM-5.

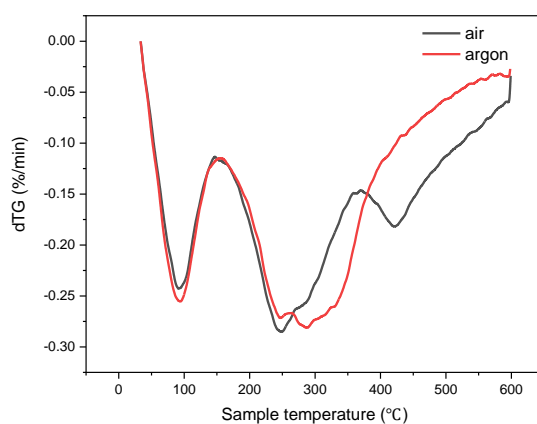


Figure 5-18. DTG curves of the spent HZSM-5 sample under the condition of 1) air flow and 2) argon flow.



Figure 5-19. Photo of 1). spent HZSM-5, 2). HZSM-5 after TG analysis under argon flow, 3). HZSM-5 after TG analysis under air flow.

## 5.4. Plasma experiments

All the plasma experiments were conducted at a total gas flow rate of 30 ml/min. The input signal was the same as the experiments described in the previous chapter (sinusoidal signal, frequency: 3000Hz, peak-to-peak voltage: 5.5 kV).

### 5.4.1 Effects of packing zeolite

Previously the effects of packing SiO<sub>2</sub> and Co or Fe doped catalysts have been studied. The first study was conducted to study the effects of packing HZSM-5 alone. The Lissajous figure for packing HZSM-5 and no packing is shown in Figure 5-20. It is clear that packing HZSM-5 altered the discharge behavior due to the modification of discharge volume and conductivity. As the Lissajous figure after packing was smoother than no packing, the discharge in the DBD reactor seemed to be more stable and began to transform from filamentary discharge towards surface discharge.

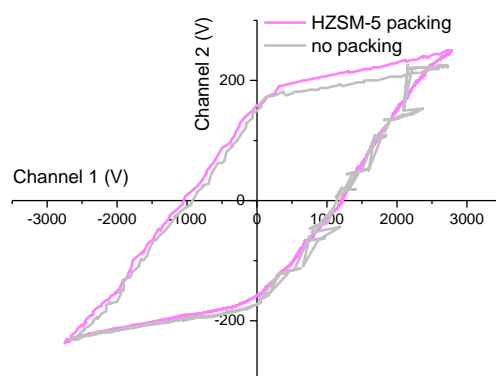


Figure 5-20. The Lissajous figure of packing HZSM-5 and no packing at same experimental condition ( $V_{pp}$ : 5.5 kV, frequency: 3 kHz, total flow rate: 30 ml/min, CO<sub>2</sub>/CH<sub>4</sub> ratio: 1:1).

The conversions of reactants, selectivity to different gaseous products and SIE as a function of different CO<sub>2</sub>/CH<sub>4</sub> ratio are shown in Figure 5-21. The energy cost, selectivity towards liquid chemicals, energy efficiencies of CO<sub>2</sub> and CH<sub>4</sub>, carbon balance of the process, and the yield of syngas products are listed in Table 5-2. The general tendency is similar to the tendency of these results without packing illustrated

in Figure 4-11 of Chapter IV. A high proportion of CO<sub>2</sub> component in the feeding gas led to the increase of conversions of reactants and the selectivity to syngas products while decreased the selectivity of C<sub>2</sub><sup>+</sup> species (mostly alkanes). Moreover, the energy efficiency of CO<sub>2</sub> significantly increased with the increase of CO<sub>2</sub> proportion from 0.094 mmol/kJ to 0.427 mmol/kJ; meanwhile, the energy cost remarkably reduced. The carbon balance of these experiments is around 0.95 while only a very little liquid was condensed in the trap, indicating the formation of carbon deposits on HZSM-5. It can be observed on the spent HZSM-5 sample shown in Figure 5-1. Unlike the SiO<sub>2</sub> aerogel, where the brown deposits can be mostly dissolved in acetone solution and seemed to be adsorbed liquid, the deposits on HZSM-5 sample are insoluble in acetone as shown in Figure 5-22, indicating most of the deposition is solid carbon black. Comparing to no packing condition or packing SiO<sub>2</sub> aerogel (Figure 4-11 and 4-13), packing HZSM-5 exhibited adverse effects on the process, resulting in a decrease of conversions and the formation of carbon deposition. The reason can be on the one hand, the introduction of HZSM-5 significantly enhanced the electric conductivity and decreased the discharge volume. As a result, the local electric field near the surface of HZSM-5 samples was enhanced and the discharge transformed to surface discharge, leading to a decrease of conversions. On the other hand, the enhanced local electric field can lead to higher average electron energy, thus promoting some elementary reactions in plasma. As discussed and illustrated in Chapter IV, a very small amount of CH<sub>4</sub> and CH<sub>2</sub>O in an NTP can be decomposed into solid carbon with sufficient electron energy shown as reaction (1) [5]. Packing HZSM-5 exhibited promotion on decomposition process on the surface thus enhancing the formation of deposition the surface even few publications have reported that the catalytic behaviors of HZSM-5 promoted the formation of coke in dry reforming, FTS, oil refinery or biomass pyrolysis processes. The decomposition of CH<sub>2</sub>O radicals led to the formation of syngas, water or coke instead of liquid chemicals. Unlike SiO<sub>2</sub>, the porous structure of HZSM-5 is ineffective to inhibit the

decomposition of CH<sub>2</sub>O radicals or even enhanced the process due to its low adsorption capacity and promotion on the local electron energy. Indeed, the calculated overall selectivity towards liquid products is as low as the experiments without packing. Thus, the selectivity towards different liquid components is not listed. However, it is quite interesting that a tiny number of higher hydrocarbons was detected in the liquid products as shown in Figure 5-23, which cannot find without packing or packing SiO<sub>2</sub> aerogel. Therefore, though the conversions were inhibited, packing HZSM-5 slightly promoted the formation of long-chain hydrocarbons due to its intrinsic nature of oligomerization.

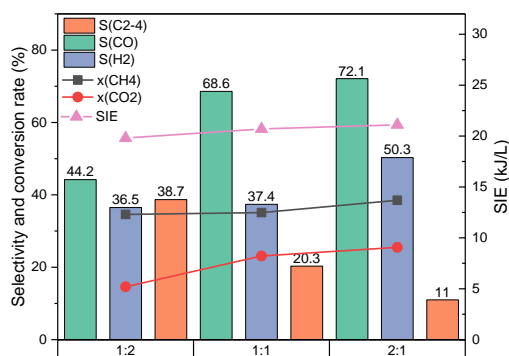


Figure 5-21. Conversions of reactants, selectivity to different gaseous products and SIE as a function of different CO<sub>2</sub>/CH<sub>4</sub> ratio (V<sub>pp</sub>: 5.5 kV, frequency: 3 kHz, total flow rate: 30 ml/min).

Table 5-2. Energy cost, the selectivity towards liquid chemicals, the energy efficiency of the plasma experiments, carbon balance and the yield of syngas products varied by CO<sub>2</sub>/CH<sub>4</sub> ratio (V<sub>pp</sub>: 5.5 kV, frequency: 3 kHz, total flow rate: 30 ml/min).

	S <sub>liquid</sub>	X <sub>total</sub> (%)	EC (kJ/mol)	Energy efficiency (mmol/kJ)		Yield (%)		CB
				CO <sub>2</sub>	CH <sub>4</sub>	CO	H <sub>2</sub>	
1:2	0.07	28.0	1856	0.094	0.445	13.8	14.2	0.940
1:1	0.02	34.1	1393	0.276	0.442	19.7	16.8	0.966
2:1	0.11	34.2	1355	0.427	0.311	20.8	19.4	0.958



Figure 5-22. Photo of spent samples (2 h) in pure acetone: 1). HZSM-5, 2). SiO<sub>2</sub> aerogel.

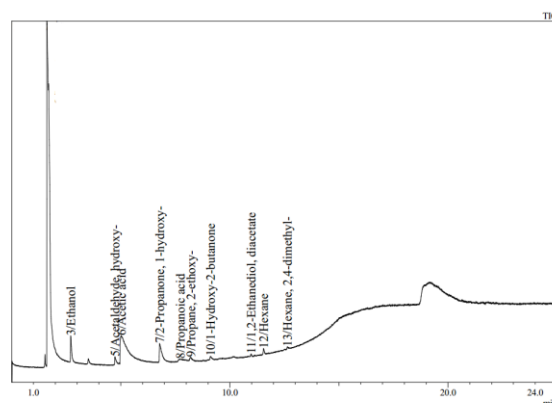


Figure 5-23. The GC-MS analysis of some components in the condensed liquid products formed with packing HZSM-5 at a CO<sub>2</sub>/CH<sub>4</sub> ratio of 1:2.

#### 5.4.2 Composite catalysts and packing method

The effects of composite catalysts with different packing methods were firstly conducted with different Co and HZSM-5 catalysts. For convenience, packing Co doped HZSM-5 catalyst is abbreviated as Co-doping; packing granule mixing of CoSiO<sub>2</sub> and HZSM-5 catalyst is abbreviated as Co-granule mixing; packing dual bed of CoSiO<sub>2</sub> and HZSM-5 catalyst is abbreviated as Co-dual bed. The CO<sub>2</sub>/CH<sub>4</sub> ratio was fixed at 2:1. Figure 5-24 presents the Lissajous figures of packing Co composite catalysts. Clearly, the discharge behaviors of these experiments with different packing methods were almost the same.

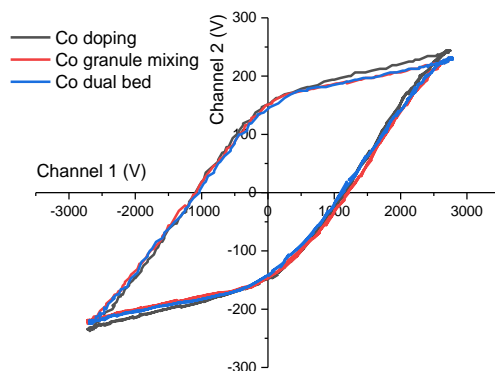


Figure 5-24. Lissajous figures of packing Co composite catalysts at same experimental condition ( $V_{pp}$ : 5.5 kV, frequency: 3 kHz, total flow rate: 30 ml/min,  $CO_2/CH_4$  ratio: 2:1).

The conversions of reactants, selectivity to different gaseous products, overall selectivity towards liquid chemicals and SIE as a function of different packing methods are shown in Figure 5-25. The total conversion rate of reactants and yield of syngas products are presented in Figure 5-26. Figure 5-27 illustrates the energy efficiency and energy cost of the process. The selectivity towards different main liquid products is shown in Figure 5-28. Similar to the results presented in the previous chapter, the introduction of Co catalysts sufficiently enhanced the formation of liquid products (selectivity up to 18.6%) comparing to packing HZSM-5 alone condition. Moreover, the conversions were significantly promoted than packing HZSM-5 alone, particularly the conversion rate of  $CO_2$ , which is even slightly higher than packing  $Co/SiO_2$  condition in the previous chapter at Co-granule mixing condition. The previous chapter also explained the association of  $SiO_2$  aerogel and Co has notable effects on the formation of  $CH_2O$  radicals and inhibits their decomposition. As discussed in the last section, packing HZSM-5 exhibited suppression on the formation of liquid chemicals, doping Co on the HZSM-5 seemed to improve the catalytic performance of HZSM-5 as the conversion of reactants was higher than no packing or packing HZSM-5. However, not only the conversion rates (48.6% of  $CH_4$  and 33% of  $CO_2$ ) but also the overall selectivity towards liquid chemicals (18.6%) and  $C_2+$  species are lower comparing to packing  $Co/SiO_2$  catalysts

(50.8% of CH<sub>4</sub>, 36.1% of CO<sub>2</sub> and 30.6% to liquid products) while the selectivity to syngas products is higher. More importantly, the same as packing Co/SiO<sub>2</sub>, negligible C<sub>2</sub>+ liquid chemicals were detected by GC-MS and the liquid products are almost only composed of methanol, acetic acid, and little ethanol. The reason could be that on the hand the local reactions in plasma discharge near Co particles were enhanced as discussed in the previous chapter; on the other hand, the oxygen-containing species were much more reactive to Co particles rather than HZSM-5. As a result, the reactive species were frequently chemisorbed and desorbed by Co particles rather than reacting on HZSM-5 due to its low adsorption capacity and possibly low activity at low temperature. Therefore, we deem that the catalytical improvement was mainly attributed to Co catalyst while the synergy of Co with HZSM-5 was less important at this condition.

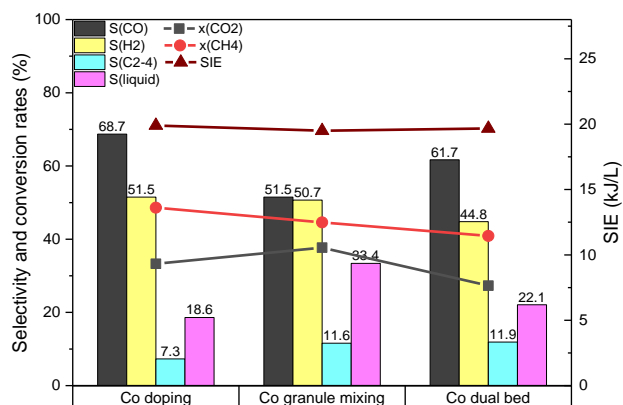


Figure 5-25. Conversions of reactants, selectivity to different gaseous products, overall selectivity towards liquid chemicals and SIE as a function of different packing methods ( $V_{pp}$ : 5.5 kV, frequency: 3 kHz, total flow rate: 30 ml/min, CO<sub>2</sub>/CH<sub>4</sub> ratio=2:1).

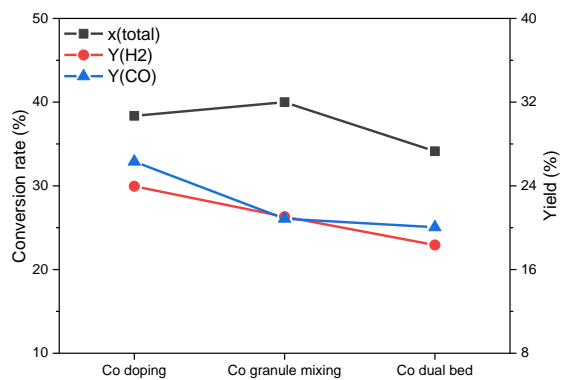


Figure 5-26. Total conversion of reactants and yield of H<sub>2</sub> and CO as a function of different packing methods (V<sub>pp</sub>: 5.5 kV, frequency: 3 kHz, total flow rate: 30 ml/min, CO<sub>2</sub>/CH<sub>4</sub> ratio=2:1).

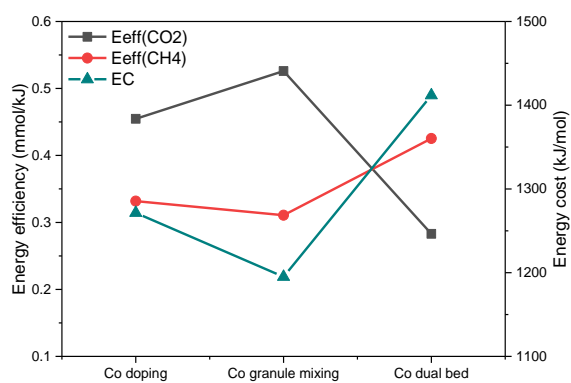


Figure 5-27. The energy efficiency of reactants and energy cost as a function of different packing methods (V<sub>pp</sub>: 5.5 kV, frequency: 3 kHz, total flow rate: 30 ml/min, CO<sub>2</sub>/CH<sub>4</sub> ratio=2:1).

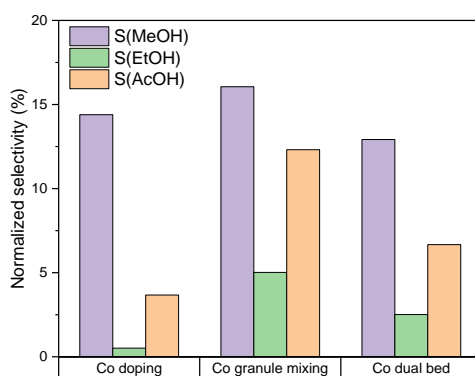


Figure 5-28. Normalized selectivity towards different liquid products as a function of different packing methods (V<sub>pp</sub>: 5.5 kV, frequency: 3 kHz, total flow rate: 30 ml/min, CO<sub>2</sub>/CH<sub>4</sub> ratio=2:1).

Comparing to Co-doping method, dual bed packing slightly promoted the

selectivity to C<sub>2</sub><sup>+</sup> species (to 11.9%) and liquid chemicals (22.1%) while the conversion rates decreased. It was found that the conversion rates of reactants or total conversion rate under dual bed packing condition were higher than those under packing HZSM-5 condition but lower than those under packing Co/SiO<sub>2</sub> aerogel or even without packing. Furthermore, the same as packing zeolite alone, a very small number of higher hydrocarbons can be detected in the liquid products. We suggested the two catalysts worked separately under dual bed packing condition. The layer of Co/SiO<sub>2</sub> significantly promoted the formation of methanol, ethanol, and acetic acid and improved the conversions to some extent. Meanwhile, the layer of HZSM-5 slightly promoted the formation of C<sub>2</sub><sup>+</sup> liquid chemicals; however, hindered the conversions of reactants during discharge as discussed previously. As a result, the conversions were limited to some extent, but the formation of liquid chemicals was promoted. The results indicate that the under dual bed packing condition the catalytic performance of the two catalysts appears to be mechanically separated with a negligible synergy between the two catalysts; however, the synergistic effects of plasma and each catalyst are obvious. It should also be noted that the energy cost of dual packing method is much higher than the other two packing methods.

Most significantly, Co granule mixing method exhibited the best catalytical performance comparing to the other packing methods and HZSM-5 or Co/SiO<sub>2</sub> alone, where the conversion of CO<sub>2</sub> (37.7%) and overall selectivity to liquid chemicals (33.4%) are even higher than packing Co/SiO<sub>2</sub> aerogel (36.0% and 30.6%, respectively). Meanwhile, the selectivity to syngas products, particularly CO, is lower. Furthermore, although the energy efficiency and energy cost are slightly higher than packing Co/SiO<sub>2</sub>, it is impressive that a branch of C<sub>2</sub><sup>+</sup> liquid chemicals and hydrocarbons were detected in liquid products (Figure 5-29) such as C<sub>7</sub>H<sub>16</sub>, butanol, propanoic acid, acetoin, pentanol, hexanol, C<sub>5</sub>H<sub>12</sub>O<sub>2</sub>, C<sub>7</sub>H<sub>14</sub>O, and their related isomers, at a CO<sub>2</sub>/CH<sub>4</sub> ratio of 2:1, where it is negligible under Co/SiO<sub>2</sub> packing condition. The reason can be firstly Co/SiO<sub>2</sub> significantly promoted the preliminary

reactions, particularly the activation of CH<sub>4</sub>, and inhibited the decomposition of oxygen-containing species due to higher local electron energy and strong adsorption behavior as discussed previously. The reactive radicals (CH<sub>x</sub>, CH<sub>2</sub>O, etc.) produced by plasma discharge were frequently chemisorbed by Co catalysts, reacted with vicinal groups then desorbed to form some liquid products such as methanol, ethanol and acetic acid. Meanwhile, as the granules of HZSM-5 were well mixed with Co/SiO<sub>2</sub>, some desorbed reactive species or some liquid products can be chemisorbed or passed via the pentasil chain channel of HZSM-5 and then oligomerized and isomerized to produce long-chain liquid chemicals and related isomers. The consumption of these species by HZSM-5 in the gaseous atmosphere could, in turn, affect the balance of the preliminary reactions to enhance the conversions of reactants. Consequently, long-chain liquid chemicals can be synthesized even at a high concentration of CO<sub>2</sub> in feeding gas, and more CO<sub>2</sub> were converted in this process. Notably, the previous chapter we reported that long-chain liquid chemicals could also be produced by Co/SiO<sub>2</sub> aerogel catalyst under a high concentration of CH<sub>4</sub> in feeding gas probably as more CH<sub>x</sub> radicals were chemisorbed thus promoting the chain propagation. However, the association of plasma with composite catalysts is more efficient for chain propagation and isomerization.

Therefore, based on the results, we confirm that the synergy of composite Co/SiO<sub>2</sub> and HZSM-5 was notable and remarkably improved the catalytic performance in this process. The synergistic effects between composite catalysts and plasma discharge effectively enhanced the conversion of reactants and promoted the formation of liquid chemicals, leading to synthesizing long-chain liquid products.

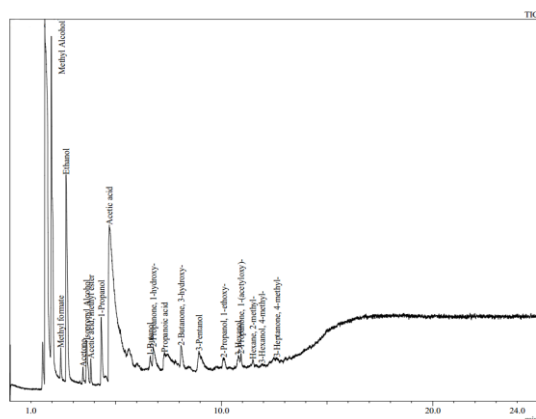


Figure 5-29. The GC-MS analysis of some components in the condensed liquid products formed under Co granule mixing at a CO<sub>2</sub>/CH<sub>4</sub> ratio of 2:1.

To evaluate and compare the catalytical performance of Fe composite catalysts, the plasma experiments were also conducted by Fe doping method and Fe granule mixing method at the same condition. As the composite catalysts seemed to work separately under dual bed packing condition, it was not considered in further experiments anymore. The conversions of reactants, selectivity to different gaseous products, overall selectivity towards liquid chemicals and SIE varying by different Fe packing methods are shown in Figure 5-30. The total conversion rate of reactants and yield of syngas products are illustrated in Figure 5-31. Figure 5-32 presents the energy efficiency and energy cost of the process. The selectivity towards different main liquid products is shown in Figure 5-33.

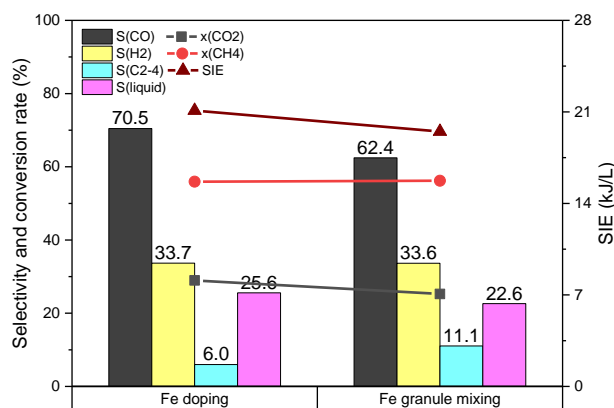


Figure 5-30. Conversions of reactants, selectivity to different gaseous products, overall selectivity

towards liquid chemicals and SIE as a function of different packing methods ( $V_{pp}$ : 5.5 kV, frequency: 3 kHz, total flow rate: 30 ml/min,  $CO_2/CH_4$  ratio=2:1).

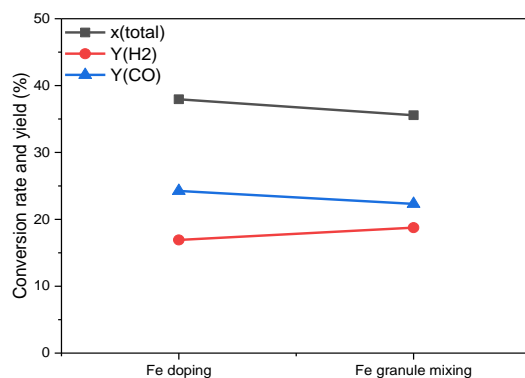


Figure 5-31. Total conversion of reactants and yield of  $H_2$  and  $CO$  as a function of different packing methods ( $V_{pp}$ : 5.5 kV, frequency: 3 kHz, total flow rate: 30 ml/min,  $CO_2/CH_4$  ratio=2:1).

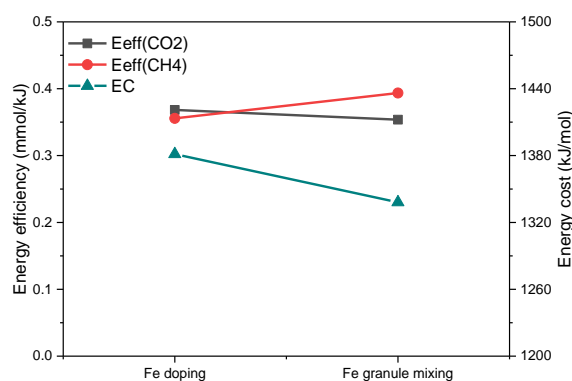


Figure 5-32. The energy efficiency of reactants and energy cost as a function of different packing methods ( $V_{pp}$ : 5.5 kV, frequency: 3 kHz, total flow rate: 30 ml/min,  $CO_2/CH_4$  ratio=2:1).

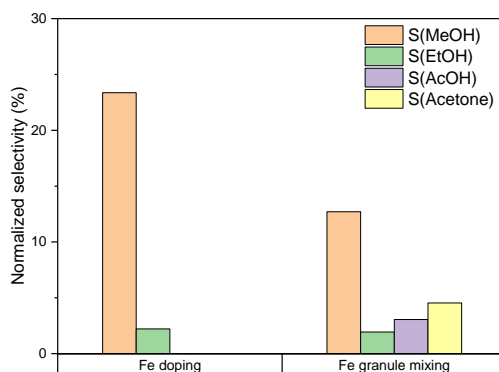


Figure 5-33. Normalized selectivity towards different liquid products as a function of different packing methods ( $V_{pp}$ : 5.5 kV, frequency: 3 kHz, total flow rate: 30 ml/min,  $CO_2/CH_4$  ratio=2:1).

Different from the catalytic performance of Co/HZSM-5, packing Fe/HZSM-5 catalyst remarkably promoted the conversion of CH<sub>4</sub> (up to ~ 58%) and the formation of liquid chemicals up to overall selectivity of 25.6%, where except water and a very small amount of ethanol, methanol was almost the only product. Moreover, the selectivity to C<sub>2</sub>+ gaseous products and H<sub>2</sub> was significantly lower than no packing, packing Fe/SiO<sub>2</sub>, HZSM-5 or Co doping condition. In Chapter IV, we have reported that the Fe/SiO<sub>2</sub> catalyst was highly selective towards alcoholic products (mainly methanol) at the CO<sub>2</sub>/CH<sub>4</sub> ratio of 2:1. Similarly, Fe/HZSM-5 bifunctional catalyst also exhibited highly selective performance for methanol formation at the same CO<sub>2</sub>/CH<sub>4</sub> condition. As the selectivity towards H<sub>2</sub> was remarkably lower while the conversion rate of CH<sub>4</sub> was relatively higher, we deemed that the synergy of Fe with HZSM-5 in plasma discharge enhanced the electronic dissociation of CH<sub>4</sub> into CH<sub>3</sub> radicals and H and then reacted with O on the surface of Fe/HZSM-5 to form OH radical as the local electric field was significantly promoted. Then probably due to the intrinsic nature Fe/HZSM-5, chemisorbed OH and radicals were more competitive to react with CH<sub>3</sub> radicals and desorbed to form methanol rather than chain growth in a plasma discharge. As a result, even though the conversion rate of CH<sub>4</sub> was higher, the selectivity towards C<sub>2</sub>+ species was notably low. Besides, Fe/HZSM-5 probably promoted reverse Water-gas shift reaction to produce CO and water, resulting in a high CO selectivity. The result is imposing as the conversion of CH<sub>4</sub> was remarkably enhanced, and the products were highly concentrated, particularly the liquid chemicals where the product was almost only methanol except water. Unlike Co/HZSM-5, the synergy between plasma, Fe, and HZSM-5 exhibited noticeable effects on this process.

Comparing to Fe doping condition, the overall selectivity towards liquid chemicals was slightly lower, while the selectivity towards gaseous C<sub>2</sub>+ hydrocarbons was much higher under granule mixing condition. Moreover, except methanol, a small

amount of ethanol, acetic acid and acetone were detected in the liquid chemicals. The conversion rates and selectivity to H<sub>2</sub> were similar, while the selectivity to CO decreased. Previously the results showed that both Fe/SiO<sub>2</sub> alone and bifunctional Fe/HZSM-5 promoted the combination of CH<sub>3</sub> radicals and OH radicals to form methanol on the surface of Fe site. However, the synergy of composite granule-mixed Fe/SiO<sub>2</sub> with HZSM-5 exhibited promotion on the formation of acetone comparing to packing Fe/HZSM-5, Fe/SiO<sub>2</sub> or Co composite catalysts, where acetone was negligible. As we found the combination of Co or Fe with HZSM-5 generally improved the conversion of CH<sub>4</sub>, granule-mixed Fe/SiO<sub>2</sub> and HZSM-5 not only enhanced the combination of OH with CH<sub>3</sub> radicals on the surface of Fe, but also the combination of desorbed CO and CH<sub>3</sub> radicals on the surface of HZSM-5 to form acetone as shown in reaction (2). As a result, the selectivity towards CO decreased due to this reaction and less decomposition of CH<sub>2</sub>O radicals after introducing SiO<sub>2</sub>. Noticed that the selectivity to H<sub>2</sub> was as low as Fe doping condition, indicating the reverse Water-gas shift reaction was also accelerated under Fe granule mixing condition.



#### 5.4.3 Effects of CO<sub>2</sub>/CH<sub>4</sub> ratio on the performance of composite catalysts

In Chapter IV, we have found that the CO<sub>2</sub>/CH<sub>4</sub> ratio affected the final liquid products strongly. Thus, the effects of CO<sub>2</sub>/CH<sub>4</sub> ratio on the catalytic performance of composite catalysts with metal doping or granule mixing packing were studied to explore the possibility of synthesizing long-chain liquid hydrocarbons and chemicals and improve the selectivity. Figure 5-34 illustrates the conversions of reactants, selectivity to different gaseous products, overall selectivity towards liquid chemicals and SIE varying by different Co packing methods and CO<sub>2</sub>/CH<sub>4</sub> ratio. The total conversion rate of reactants and yield of syngas products are shown in Figure 5-35.

Figure 5-36 presents the energy efficiency and energy cost of the process. The selectivity towards different main liquid products is illustrated in Figure 5-37.

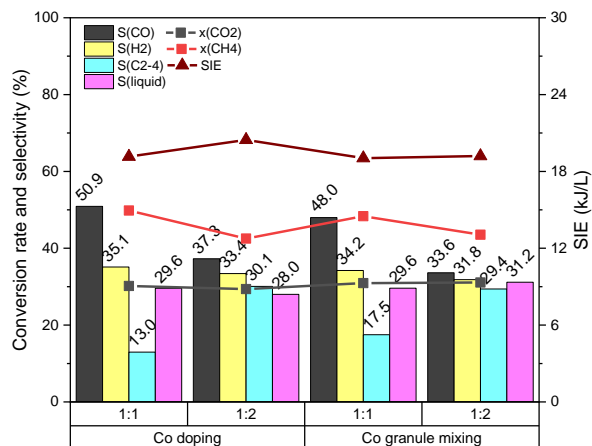


Figure 5-34. Conversions of reactants, selectivity to different gaseous products, overall selectivity towards liquid chemicals and SIE as a function of different Co packing methods and CO<sub>2</sub>/CH<sub>4</sub> ratio (V<sub>pp</sub>: 5.5 kV, frequency: 3 kHz, total flow rate: 30 ml/min).

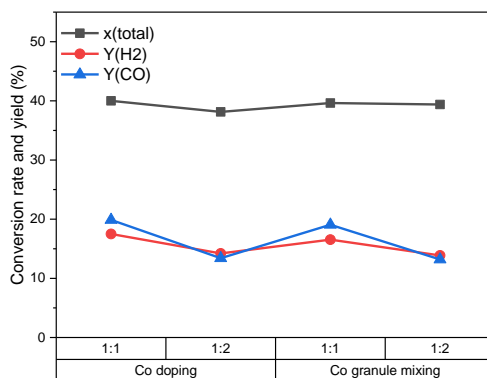


Figure 5-35. Total conversion of reactants and yield of H<sub>2</sub> and CO as a function of different Co packing methods and CO<sub>2</sub>/CH<sub>4</sub> ratio (V<sub>pp</sub>: 5.5 kV, frequency: 3 kHz, total flow rate: 30 ml/min).

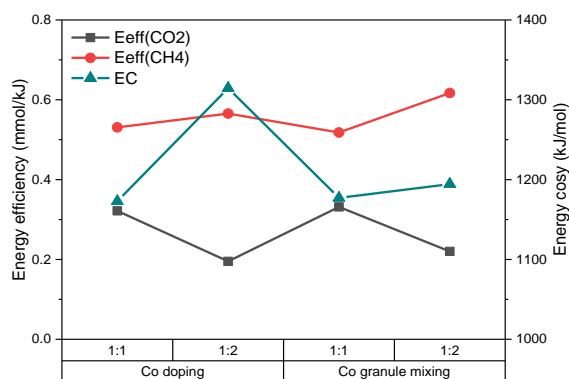


Figure 5-36. The energy efficiency of reactants and energy cost as a function of different Co packing methods and CO<sub>2</sub>/CH<sub>4</sub> ratio (V<sub>pp</sub>: 5.5 kV, frequency: 3 kHz, total flow rate: 30 ml/min).

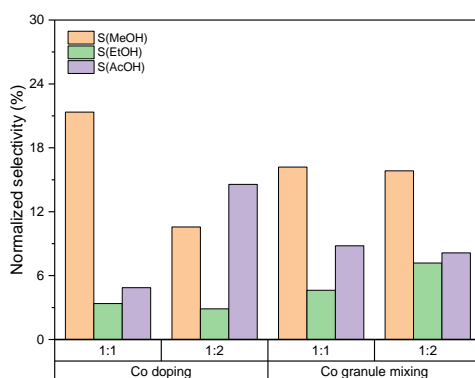


Figure 5-37. Normalized selectivity towards different liquid products as a function of different Co packing methods, and CO<sub>2</sub>/CH<sub>4</sub> ratio (V<sub>pp</sub>: 5.5 kV, frequency: 3 kHz, total flow rate: 30 ml/min).

Similarly, increasing the proportion of CH<sub>4</sub> component in the inlet gas marginally decreased the conversion rates or total conversion rate and significantly decreased the selectivity to syngas products, particularly CO, while significantly increased the selectivity to C<sub>2</sub>+ gaseous products. For Co doping condition, the overall selectivity to liquid chemicals greatly increased from 18.6% to 29.6% with CO<sub>2</sub>/CH<sub>4</sub> ratio from 2:1 to 1:1, then slightly changed to 28.0% with CO<sub>2</sub>/CH<sub>4</sub> ratio of 1:2. However, for Co granule mixing, the overall selectivity to liquid chemicals was similar (32.4%, 29.6%, and 31.4%, respectively). As discussed in the previous chapter, increasing CH<sub>4</sub> proportion in the feeding gas logically increased CH<sub>3</sub> radicals in the plasma atmosphere, leading to the formation of long-chain products such as

C2+ gaseous species, acetic acid, etc. Indeed, when packing Co/HZSM-5, the selectivity to acetic acid significantly increased with the increase of CH<sub>4</sub> proportion, which exhibited the same tendency as packing Co/SiO<sub>2</sub> aerogel catalyst. Meanwhile, the overall selectivity towards liquid chemicals were lower than pack Co/SiO<sub>2</sub> at the same condition as SiO<sub>2</sub> aerogel slightly promoted the formation of liquid chemicals due to inhibiting the decomposition of CH<sub>2</sub>O radicals. Nevertheless, packing granule mixed Co/SiO<sub>2</sub> with HZSM-5 exhibited a different tendency with packing Co/SiO<sub>2</sub> alone or Co doping. In the previous section, we have detected a certain amount of C2+ liquid chemicals. By increasing the proportion of CH<sub>4</sub>, we found the selectivity to methanol, and acetic acid decreased, while the selectivity to ethanol increased. Moreover, more long-chain species were detected in the liquid with more obvious peaks (such as C<sub>7</sub>H<sub>16</sub>, butanol, propanoic acid, acetoin, pentanol, hexanol, C5+ ester, C<sub>7</sub>H<sub>14</sub>O, C<sub>8</sub>H<sub>18</sub>O, etc.) as shown in Figure 5-38. The possible mechanism has been discussed in the previous section. Based on the results, we confirmed that the association of plasma and granule mixed Co/SiO<sub>2</sub> with HZSM-5 catalysts sufficiently altered the distribution of gaseous and liquid products and promoted chain propagation.

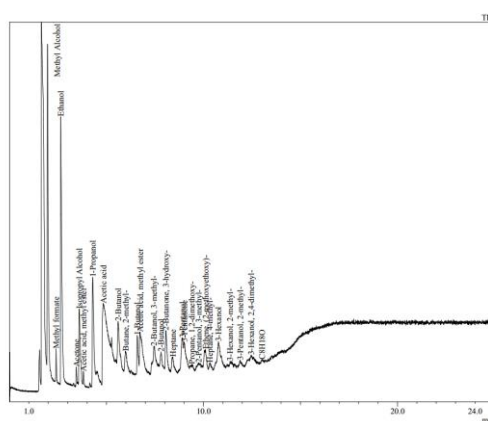


Figure 5-38. The GC-MS analysis of some components in the condensed liquid products formed under Co granule mixing at a CO<sub>2</sub>/CH<sub>4</sub> ratio of 1:2.

The Fe composite catalysts were also tested at the same conditions. Figure 5-39

shows the conversions of reactants, selectivity to different gaseous products, overall selectivity towards liquid chemicals and SIE varying by different Fe packing methods and CO<sub>2</sub>/CH<sub>4</sub> ratio. Figure 5-40 illustrates the total conversion rate of reactants and yield of syngas products. Figure 5-41 presents energy efficiency and energy cost. The selectivity towards different main liquid products is presented in Figure 5-42.

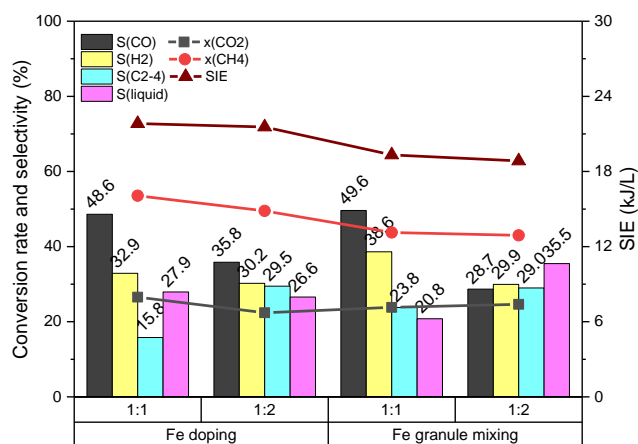


Figure 5-39. Conversions of reactants, selectivity to different gaseous products, overall selectivity towards liquid chemicals and SIE as a function of different Fe packing methods and CO<sub>2</sub>/CH<sub>4</sub> ratio (V<sub>pp</sub>: 5.5 kV, frequency: 3 kHz, total flow rate: 30 ml/min).

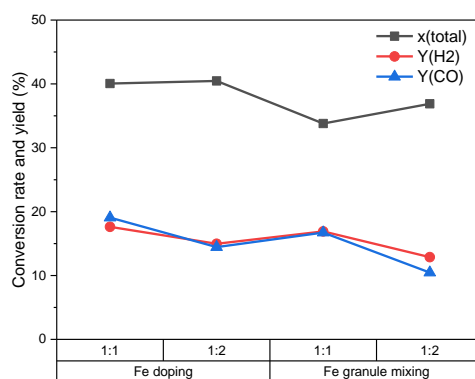


Figure 5-40. Total conversion of reactants and yield of H<sub>2</sub> and CO as a function of different Fe packing methods and CO<sub>2</sub>/CH<sub>4</sub> ratio (V<sub>pp</sub>: 5.5 kV, frequency: 3 kHz, total flow rate: 30 ml/min).

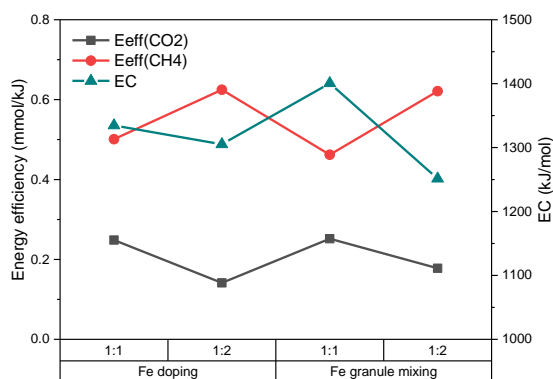


Figure 5-41. The energy efficiency of reactants and energy cost as a function of different Fe packing methods and CO<sub>2</sub>/CH<sub>4</sub> ratio (V<sub>pp</sub>: 5.5 kV, frequency: 3 kHz, total flow rate: 30 ml/min).

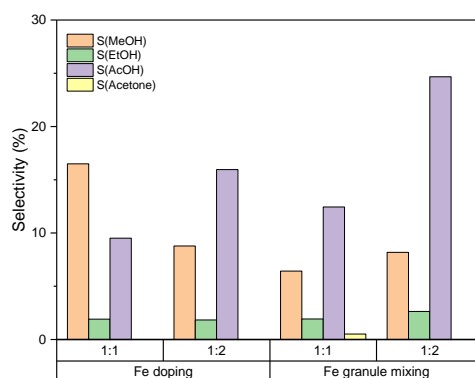


Figure 5-42. Normalized selectivity towards different liquid products as a function of different Fe packing methods, and CO<sub>2</sub>/CH<sub>4</sub> ratio (V<sub>pp</sub>: 5.5 kV, frequency: 3 kHz, total flow rate: 30 ml/min).

A similar tendency of the selectivity to gaseous products, overall selectivity to liquid chemicals and conversions was found comparing to packing Co series composite catalysts. Clearly, the highest selectivity to liquid chemicals under metal doping condition was achieved at a CO<sub>2</sub>/CH<sub>4</sub> ratio of 1:1, while for granule mixing condition the highest selectivity to liquid chemicals was at a CO<sub>2</sub>/CH<sub>4</sub> ratio of 1:2, which is the same as packing Co/SiO<sub>2</sub> or Fe/SiO<sub>2</sub> catalysts. The reason could be that when packing metal doped HZSM-5, the catalytic performance was mainly depended on the metal catalyst under plasma discharge, while packing granule mixed Co/SiO<sub>2</sub> or Fe/SiO<sub>2</sub> with HZSM-5, a strong synergy between the composite catalysts occurred with plasma discharge, the synergistic effects between metal silica aerogel, HZSM-5

and plasma significantly altered the distribution of gaseous and liquid products and improved the selectivity to long-chain products. It was found the selectivity to acetic acid increased with the increase of CH<sub>4</sub> proportion when packing Fe composite catalysts as same as packing Fe/SiO<sub>2</sub>. Particularly, packing granule mixed Fe/SiO<sub>2</sub> with HZSM-5 greatly promoted the formation of acetic acid at high ratio of CH<sub>4</sub> (~26%). Unlike packing Co series composite catalysts, where the chain propagation was improved, although a small amount of long-chain liquid chemicals were found when packing Fe series composite catalysts, the liquid products were highly concentrated on methanol and acetic acid as shown in Figure 5-41 and 5-42. Packing Fe/HZSM-5 at a high CO<sub>2</sub> proportion led to high selectivity to methanol while packing granule mixed Fe/SiO<sub>2</sub> with HZSM-5 brought out high selectivity to acetic acid. Comparing to Co series composite catalysts, Fe composite catalysts appeared to be more selective towards specific products such as methanol and acetic acid.

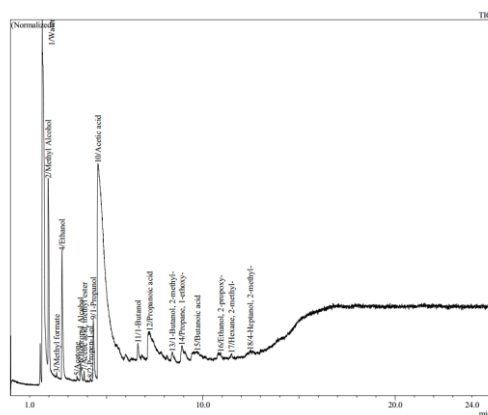


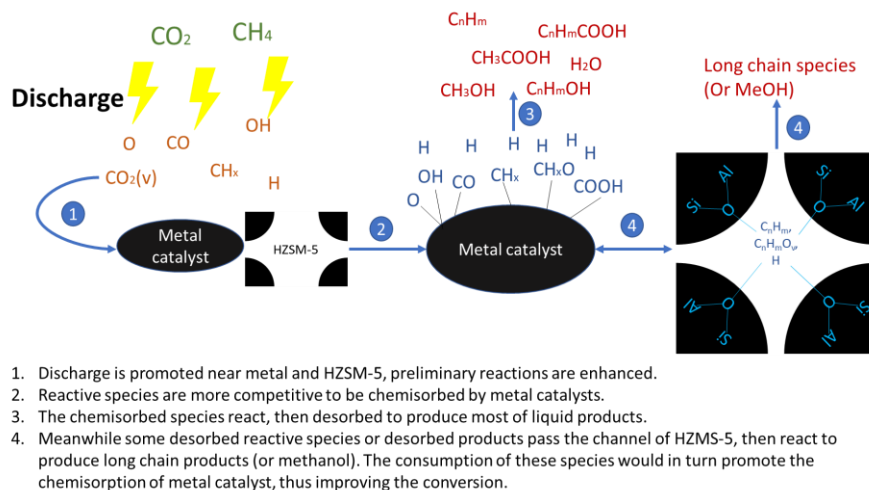
Figure 5-43. The GC-MS analysis of some components in the condensed liquid products formed under Fe granule mixing at a CO<sub>2</sub>/CH<sub>4</sub> ratio of 1:2.

Based on the results, we concluded the effects of packing different materials on non-thermal plasma conversion of CO<sub>2</sub> with CH<sub>4</sub> as presented in Table 5-3. Generally, the synergistic effects of composite catalysts and plasma significantly affected the distribution of products. By packing granule mixed Co/SiO<sub>2</sub> with HZSM-5, more long-chain liquid products were detected. While by packing Fe/HZSM-5 at a high

CO<sub>2</sub> proportion led to high selectivity to methanol, by packing granule mixed Fe/SiO<sub>2</sub> with HZSM-5 brought out high selectivity to acetic acid. Based on the results, we also proposed the possible synergistic reactions between composite catalysts with plasma for the formation of liquid products on the surface of catalysts as shown in Scheme 5-2.

Table 5-3. The effects of packing different materials on non-thermal plasma conversion of CO<sub>2</sub> with CH<sub>4</sub>

Material	Effects
HZSM-5 alone	– on conversions, + on coke formation, slight + on the formation of long-chain products
Co doping	+ on conversions (particularly CH <sub>4</sub> ), + on coke formation, + on the formation of liquid chemicals, + on the formation of long-chain products
Co granule mixing	+ on conversions, ++ on the formation of liquid chemicals, ++ on the formation of long-chain products
Fe doping	++ on conversions (particularly CH <sub>4</sub> ), + on coke formation, ++ on formation of liquid chemicals (mainly MeOH depending on CO <sub>2</sub> /CH <sub>4</sub> ratio), + on reverse Water gas shift reaction
Fe granule mixing	++ on the formation of liquid chemicals (mainly on AcOH depending on CO <sub>2</sub> /CH <sub>4</sub> ratio), + on reverse Water-gas shift reaction
Dual bed	Catalytic performance was mechanically separate, null or negligible synergistic effects were found.



Scheme 5-2. Possible synergistic reactions between composite catalysts with plasma for the formation of liquid products on the surface of catalysts

## 5.5. Summary

In this chapter, we prepared three series of composite catalysts with different mixing method: metal doping on HZSM-5 by impregnation, granule mixing, and dual bed packing. Then the commercially purchased HZSM-5 and the composite doping catalysts were characterized. The catalytic performance of different composite catalysts with different mixing method was evaluated, and the effects of  $\text{CO}_2/\text{CH}_4$  ratio on the catalytic performance were studied. Moreover, HZSM-5 was also introduced in the reactor at the same experimental condition for comparison.

Generally, packing metal granule mixing composite catalysts promoted the formation of long-chain liquid chemicals and conversion rates due to (i). enhancement of local electronic energy; (ii). the instinctive activity of Co or Fe to the chemisorption of reactive radicals. (iii). the instinctive nature of HZSM-5 for isomerization and oligomerization and synergistic effects between Co or Fe with HZSM-5. Moreover, probably due the own nature of Co and Fe, it is found that by packing granule mixed Co/SiO<sub>2</sub> with HZSM-5, more long-chain liquid products were detected, particularly at a  $\text{CO}_2/\text{CH}_4$  ratio of 1:2, where more long-chain liquid chemicals with higher concentration were found (such as C<sub>7</sub>H<sub>16</sub>, butanol, propanoic

acid, acetoin, pentanol, hexanol, C<sub>5</sub>+ ester, C<sub>7</sub>H<sub>14</sub>O, C<sub>8</sub>H<sub>18</sub>O, etc.). While packing Fe/HZSM-5 at a high CO<sub>2</sub> proportion led to high selectivity to methanol, packing granule mixed Fe/SiO<sub>2</sub> with HZSM-5 at the high proportion of CH<sub>4</sub> brought out high selectivity to acetic acid.

Unlike granule mixing packing, the catalytic improvement when packing metal doping composite catalysts is mainly attributed to the metal catalysts instead of the synergistic effects due to low adsorption capacity and possibly low activity of HZSM-5 at low temperature. However, it is found the Co or Fe doping composite catalysts improved the conversion of CH<sub>4</sub>. Interestingly, with packing Fe/HZSM-5 at a high CO<sub>2</sub> proportion, the liquid products were only enrichment of methanol with considerable selectivity. For the dual packing, the catalytic performance of the two catalysts appears to be mechanically separated with a negligible synergy between the two catalysts. As packing HZSM-5 only led to decrease of conversions and formation of coke due to the enhancement of electric conductivity and decrease of the discharge volume, dual bed packing finally resulted in lower conversions and energy efficiency than the other mixing methods. To our knowledge, the work has demonstrated a new way to directly synthesizing long-chain liquid chemicals via composite catalysts and providing a new perspective for manipulating the distribution of liquid chemicals direct from the plasma-catalytic conversion of CO<sub>2</sub> with CH<sub>4</sub>.

# Chapter VI. Conclusion and future perspectives

## Conclusions et perspectives d'avenir

Pour résumer, cette thèse a initié une première étude complète sur : (i) d'une part, la synthèse Fischer-Tropsch et (ii) d'autre part, la conversion directe du  $\text{CO}_2/\text{CH}_4$ , par la voie plasmocatalytique en conditions de pression et température ambiantes. Tandis que la synthèse Fischer-Tropsch plasmocatalytique ne permet pour l'heure de produire de chaînes carbonées supérieures à C4, la conversion plasmocatalytique du  $\text{CO}_2/\text{CH}_4$  montre elle un remarquable potentiel pour la production de composés liquides : alcools, acides carboxyliques et hydrocarbures à longue chaîne C5+. Dans ce dernier cas, le passage à l'emploi simultané de deux catalyseurs à la place d'un seul permet de manipuler la distribution des produits liquides tout en améliorant la sélectivité vis-à-vis des hydrocarbures à longue chaîne et le taux de conversion global du  $\text{CO}_2/\text{CH}_4$ . Les travaux de cette thèse démontrent ainsi la faisabilité d'une conversion plasmocatalytique efficace d'un mélange  $\text{CO}_2/\text{CH}_4$  en carburants de synthèse ou molécules nobles. Sur la base de nos travaux et en perspective des travaux futurs, quelques recommandations peuvent être finalement émises dont la nécessité de :

1. Optimiser la source de plasma afin de mieux contrôler l'énergie spécifique injectée et l'élévation de la température électronique. Cela passe en grande partie par l'évolution de l'alimentation électrique et davantage d'accord avec la décharge.

2. Améliorer les catalyseurs : lien plus fort entre le catalyseur et son support, meilleurs aérogels et meilleurs couches catalytiques en termes de porosité et structuration, nouvelles combinaisons catalytiques, étendre la gamme métallique des catalyseurs, l'emploi simultanée de plusieurs catalyseurs, introduction de promoteurs tels que des métaux alcalins...

3. Compléter l'étude de l'influence de la stœchiométrie du gaz réactif sur la conversion et les produits.

4. Etudier l'effet d'une dilution du gaz réactif dans un gaz plasmagène inerte.

5. Enfin, tenter de modéliser la chimie en phase plasma puis la conversion plasmocatalytique dans son ensemble en cherchant à savoir s'il y a une interaction directe entre le plasma et le catalyseur.

## 6.1. Comparison with literature

This section is dedicated to comparing this work with the results of existing works derived from literature, which study plasma-catalytic FTS and plasma-catalytic conversion of CO<sub>2</sub> and CH<sub>4</sub>, in same aspects including the conversion rates, energy efficiency, experimental conditions, and production.

As the FTS process has been successfully industrialized, it could be interesting also to compare the plasma-catalytic process to an industrial process. However, the term “energy efficiency” of conventional FTS in publications is based on estimated or software simulated HHV or LHV of aiming products to feedstocks (Syngas or biomass). Meanwhile, many publications also used thermal efficiency, carbon conversion efficiency, or efficiency of overall processes as FTS is usually combined with biomass gasification. On the other hand, the term “energy efficiency” used in a plasma process is generally based on the conversion of reactants to specific input energy rather than evaluating the real energy efficiency of the two processes, where all the gaseous and liquid products would be considered to determine the reaction enthalpy. As the products are quite different, the term “energy efficiency” based on HHV or LHV of aiming products to feedstocks is not incomparable and inappropriate. We consider the term “energy efficiency” based on the conversion of reactants to specific input energy could be more appropriate to discuss.

Different from plasma-catalytic FTS, which was scarcely reported, many works of literature are on the field of plasma-catalytic reforming CO<sub>2</sub> with CH<sub>4</sub>. Herein, we mainly consider those based on DBD plasma. Similarly, as various gaseous and liquid products are synthesized in the process plasma-catalytic conversion of CO<sub>2</sub> and CH<sub>4</sub>, where a considerable amount of liquid chemicals is formed, it is not appropriate to take the products into account when comparing energy efficiency. Thus, we determine the energy efficiency as the reactants converted to the input energy:

$$E_{\text{reactant } i} = \frac{\text{moles of reactant } i \text{ converted}}{\text{power of discharge}} \quad (1)$$

$$E_{total} = \frac{\text{moles of reactants converted}}{\text{power of discharge}} = \sum_i E_{reactant i} \quad (2)$$

The terms of energy cost and conversions have been presented in the previous chapter.

### 6.1.1 Plasma-catalytic conversion of CO with H<sub>2</sub>

Rohani et al. have studied the hydrocarbon synthesis from syngas under a high-pressure arc discharge [148, 149]. As the volume of the reactor chamber is 2.56 cm<sup>3</sup>, which is much larger than the interelectrode gap (1mm), the discharge volume was much less than the volume of the reactor, resulting in dilution of the product gases. Therefore, the conversion rates of CO and H<sub>2</sub> were rather low (less than 2%). It is unfair to compare energy efficiency as the experimental condition of that work was totally different. However, we can still have an overall idea of how efficient the two processes are by comparing the SIE, conversions, and products.

Figure 6-1 shows the total energy efficiency as a function of conversion of reactants by comparing this work with the plasma FTS of Rohani and Samuel's works and conventional FTS of Im-orb's work [267]. Noted that as the total conversion of Rohani and Samuel's works was overall less than 1%, we overestimated the value of 1%. Moreover, since the size of the reactor in this work was nearly four times than the reactor of their works, the nominal total conversion was estimated at 4% for the comparison. Obviously, much higher conversions can be achieved with relatively higher energy efficiency in our work comparing to Rohani and Samuel's works, where a very high SIE was applied in the reactor even ignoring the energy used for compressing inlet gas. More importantly, only CH<sub>4</sub>, C<sub>2</sub>, and C<sub>3</sub> species with very low concentrations were detected in their works. While not only CH<sub>4</sub> and C<sub>2</sub>-C<sub>5</sub> hydrocarbons, but also some useful liquid chemicals such as methanol in liquid products and aromatics in aerogels were detected with much higher concentration. Comparing to a typical industrial FTS process, as the industrial FTS process includes recycling, gas turbine power generating and heat recovery, leading to very high

conversion and low energy consumption, the overall energy efficiency of plasma process was much lower than a typical industrial FTS process as expected. However, the research of plasma FTS process is on the very beginning stage and has great potential for improvement for the further studies.

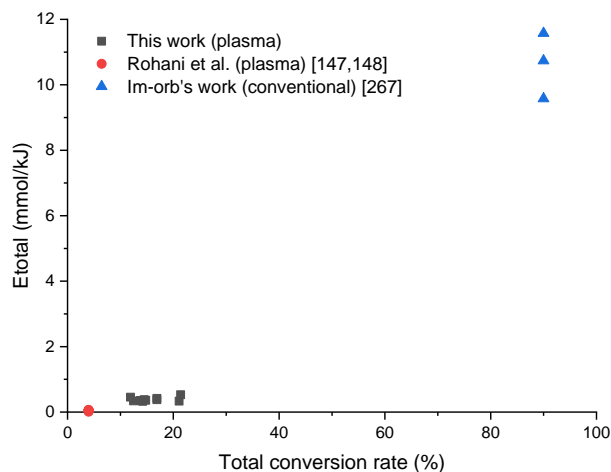


Figure 6-1. Experimental data collected from the literature for plasma and conventional FTS process, showing total energy efficiency as a function of conversion of reactants.

### 6.1.2 Plasma-catalytic conversion of CO<sub>2</sub> with CH<sub>4</sub>

Figure 6-2 and Figure 6-3 show the experimental data collected and recalculated to represent total conversion, SIE, and energy efficiency of plasma converting CO<sub>2</sub> with CH<sub>4</sub>. It is important to note that the experimental conditions of these works are different, while the type of plasma is DBD. For some of these plasma experiments, whose conditions were far away from ambient condition, the energy consumed for heating or compressing is not taken into account. While the dilution of feeding gas (if used) is considered when calculating conversion, SIE, and energy efficiency. In Zhang's work [241], a very high conversion (around 74%) was achieved with packing 12% Cu-12% Ni/ $\gamma$ -Al<sub>2</sub>O<sub>3</sub> and Ar dilution at 450 °C, and the selectivity was very considerable (75% to CO and 56% to H<sub>2</sub>, respectively). However, the energy efficiency as calculated was as low as 0.12 mmol/kJ. Some of these works have

reported that the conversion would slightly increase with the temperature, while a few publications reported the reversal tendency probably due to the intrinsic nature of catalysts. According to the thermodynamic equilibrium calculation shown in Chapter IV, it was found that thermodynamic equilibrium can contribute to the conversions of reactants from 200 °C. In our process, a considerable conversion (around 40%) and remarkably high energy efficiency (around 0.8 mmol/kJ) can be achieved with a relatively low SIE (around 500 kJ/mol) comparing to the others while no external heating or compressing was applied. Thus, comparing to these literature, our plasma-catalytic process using SiO<sub>2</sub> series catalysts or composite SiO<sub>2</sub> series catalysts with HZSM-5 is definitely more competitive concerning energy efficiency and conversions.

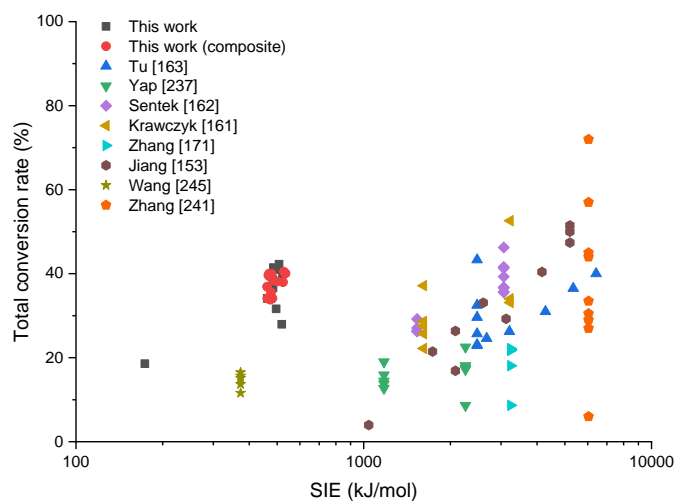


Figure 6-2. Experimental data collected from the literature for DBD plasma conversion of CO<sub>2</sub> with CH<sub>4</sub>, showing the total conversion as a function of SIE.

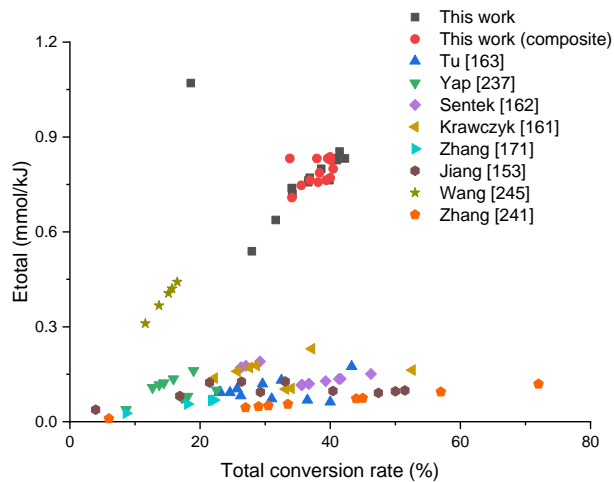


Figure 6-3. Experimental data collected from the literature for DBD plasma conversion of CO<sub>2</sub> with CH<sub>4</sub>, showing the total energy efficiency as a function of total conversion rate.

Table 6-1 illustrates the comparison of experimental conditions and products for this work with some related literature. Most importantly, except the syngas products, a very considerable number of value-added liquid products, including methanol and acetic acid as main products and long-chain hydrocarbons as byproducts can be produced through our process over the SiO<sub>2</sub> series catalysts under the ambient condition without dilution. Particularly when packing granule mixed Co/SiO<sub>2</sub> with HZSM-5, more long-chain liquid chemicals with higher concentration were detected (such as C<sub>7</sub>H<sub>16</sub>, butanol, propanoic acid, acetoin, pentanol, hexanol, C<sub>5</sub>+ ester, C<sub>7</sub>H<sub>14</sub>O, C<sub>8</sub>H<sub>18</sub>O, etc.). While among these publications, where syngas is the main products with a few C<sub>2</sub>-4 gaseous byproducts, the formation of high-value liquid products was scarcely reported. Therefore, the process using a metal loaded SiO<sub>2</sub> catalysts or composite catalysts described in this work exhibits a high potential for manipulating the long-chain products with high energy efficiency and conversions. Comparing to some published works, our catalysts have demonstrated excellent performance, and the process has made significant improvements in energy efficiency and direct synthesis of liquid products.

Table 6-1. The comparison of this work with the results of related literature.

Literatures	Temperature (°C)	Dilution	Main products				
			Syngas	C2-4	MeOH	AcOH	Long chain
<b>This work</b>	<b>Ambient</b>	<b>No</b>	<b>main</b>	<b>10% to 40%</b>	<b>Up to 25%</b>	<b>Up to 30%</b>	<b>Up to C8</b>
[171]	110	No	main	~40%	/	/	/
[163]	270	No	main	/	/	/	/
[237]	Ambient and 300	He	major	Up to 20%	/	/	/
[241]	110	No	main	Up to 50%	/	/	/
[161]	130 to 340	Ar	main	Up to 18%	< 3%	< 2%	Detected
[162]	120 to 290	Ar	main	Up to 30%	< 3%	< 2%	/
[153]	50-100-150	No	main	main	/	/	Detected/carbon deposit
[245]	Ambient	No	main	Up to 25%	Up to 15%	Up to 35%	Detected

## 6.2. Conclusions

The indirect or direct approach of plasma converting CO<sub>2</sub> and CH<sub>4</sub> into liquid chemicals has shown great potential for anthropogenic CO<sub>2</sub> recycling, the feasibility to achieve a low carbon emission in industrial processes and the alternative for the storage of renewable energy. However, more efforts are essential to improve the conversion, selectivity, and efficiency to accomplish the approaches. This work has studied the plasma-catalytical FTS of the indirect approach and converting CO<sub>2</sub> with CH<sub>4</sub> of the direct approach mainly by employing the SiO<sub>2</sub> aerogel series catalysts or composite catalysts. The results described in the previous chapters elaborated that the SiO<sub>2</sub> series catalysts have demonstrated excellent performance for the direct synthesis of value-added liquid products, while the composite SiO<sub>2</sub> series catalysts with HZSM-5 exhibited significant enhancement on the long-chain products. In this section, the major conclusions are presented below.

### 6.2.1 Plasma-catalytic FTS

Chapter II established a DBD reactor with its analytical apparatuses for the

plasma-catalysis associated FTS and CO<sub>2</sub> reforming with CH<sub>4</sub> directly into value-added liquid products. The hydrophobic SiO<sub>2</sub> aerogel support with the high specific area was prepared via ambient drying method after surface modification. Different Co catalysts were synthesized by impregnation method and sol-gel method with a different precursor for plasma-catalytic FTS. The power consumed by the DBD reactor was calculated via the Lissajous method by connecting a capacitance in series with the DBD reactor. The gas products and liquid products are separated by an icy water trap, then the gas products were analyzed by an on-line Micro GC, while the liquid products were analyzed offline through a GC-MS. To obtain a more precise result, two temperature probes, an IR camera, and a pressure probe right in the inlet and outlet of the reactor to record the temperature difference of the gas flow and the pressure before and during discharge for data calibration. According to temperature monitoring, a strong non-equilibrium condition was well maintained, and the experimental atmosphere was very close to ambient condition.

Chapter III aimed to explore the possibility of the non-thermal plasma promoted FTS at ambient conditions, which has been barely studied before. Different experimental variables were evaluated without packing catalysts, and then the different Co/SiO<sub>2</sub> catalysts were introduced into the reactor to evaluate the plasma-catalytic synergistic effects. The results showed C1 to C5 hydrocarbons were synthesized at ambient conditions with relatively low energy consumption (~18 kJ/L of SIE) compared to conventional FTS process or the previous related study of our group, where the external pressure, heating and high SIE were essential. Interestingly, the Co/SiO<sub>2</sub> aerogel catalysts were confirmed to enhance the synthesis of liquid organics and C2-C5 hydrocarbons rather than the formation of CO<sub>2</sub> and CH<sub>4</sub> from syngas by a plasma catalysis approach. Moreover, methanol, ethanol, and acetaldehyde were synthesized and detected among the liquid products via the catalysts; a small part of esters and C5+ organics were detected on the catalysts. Probably due to the different textural and structural properties, 20NO-I catalyst

sample demonstrated high catalytic activity and notable performance with remarkably high energy efficiency.

The parametric experimental study revealed that a large portion of H<sub>2</sub> in the feeding gas favored the conversion of CO and the formation of hydrocarbons. A low flow rate naturally led to higher SIE, thus increasing conversions of reactants. However, the over selectivity towards hydrocarbons was lower, probably due to the formation of carbon deposits. Introducing aerogel support slightly decreased the discharge power as we expected. Nevertheless, the increase of Co loading amount significantly increases the yield of hydrocarbons and organic oxides but does not necessarily increase the discharge power probably due to the block and collapse of the porous structure.

However, unlike a conventional FTS process, C<sub>5</sub>-C<sub>11</sub> liquid olefins and paraffin were barely synthesized via this process. The main reason could be the different mechanism and reactions occurred between thermochemical approach and plasma approach. The difference of operating condition could also be one of the reasons; however, gasoline species were not detected either in the previous study using a high-pressure arc discharge. This work has demonstrated the feasibility of plasma-catalytic FTS, while more efforts are essential to carry out further study on this topic.

### **6.2.2 Plasma-catalytic conversion of CO<sub>2</sub> with CH<sub>4</sub>**

Chapter IV has carried out the direct synthesis of value-added liquid chemicals from CO<sub>2</sub> and CH<sub>4</sub> through a plasma-catalytic process in the same reactor. Except Co/SiO<sub>2</sub> prepared by the impregnation method and nitrite precursor, Fe, as a well-known catalyst used in CO<sub>2</sub> hydrogenation, was also employed and prepared by the same method. By introducing the catalysts, considerable conversions can be attained at ambient conditions. The influence of different CO<sub>2</sub>/CH<sub>4</sub> ratios, SiO<sub>2</sub> aerogel packing, and supported catalysts packing were also investigated. It was found that syngas and C<sub>2</sub> to C<sub>5</sub> gaseous hydrocarbons were the main products, while the total selectivity towards liquid products was negligible, mainly due to the decomposition of

$\text{CH}_x\text{O}$  radicals without packing catalysts. Besides, a very small amount of carbon black was synthesized. Increasing the  $\text{CO}_2/\text{CH}_4$  ratio led to enhancing the conversions of both reactants and the selectivity towards syngas, while selectivity towards  $\text{C}_2+$  species decreased. In the case of  $\text{CO}_2/\text{CH}_4$  ratio of 2:1 with a 30 ml/min flow rate, the yield of CO and  $\text{H}_2$  in the outlet gas is 26.57% and 21.91%, respectively.

With packing catalysts, the results were very different. The introduction of  $\text{SiO}_2$  aerogel did not alter the discharge behavior as the discharge volume, and electric conductivity were not significantly changed. Moreover, due to its high adsorption capacity, the packing of  $\text{SiO}_2$  aerogel slightly favored the formation of liquid chemicals and the conversions of reactants. Only negligible carbon containing deposits, including carbon deposition and carbon containing polymer or monomer, was detected on the  $\text{SiO}_2$  aerogel. More importantly, the synergetic addition of an appropriate catalyst in the system significantly promoted the formation of the liquid chemicals up to a total liquid selectivity of 40%, where methanol and acetic acid were the main liquid products. The explanations are assumed to be: (i) enhancement of local electric field, (ii) more stable discharge behavior, (iii) the instinctive activity of Fe and Co to the chemisorption of reactive radicals. Besides, less carbon containing deposits were found comparing to  $\text{SiO}_2$  aerogel support. The results also revealed that a Fe catalyst preferentially led to the formation of alcoholic products, while a Co catalyst was more favorable to the formation of formate groups (mainly acids) and long-chain products (up to  $\text{C}_5$  oxygenates). Moreover, with a high ratio of  $\text{CH}_4$ , a few  $\text{C}_5+$  hydrocarbons (pentane and heptane) and a  $\text{C}_6$  ester were synthesized. As far as know, the plasma-catalytic performance for liquid production obtained here is outstanding compared to existing studies and broadens the way to the design of an efficient plasma-catalytic process for direct conversion of  $\text{CO}_2$  and  $\text{CH}_4$  into liquid chemicals.

For further improvement of manipulating liquid products, Chapter V studied the possibility for synthesizing long-chain products by employing composite catalysts

with different packing method: metal doping on HZSM-5 by impregnation, granule mixing, and dual bed packing. For comparison, HZSM-5 was also introduced in the reactor at the same experimental condition. It was found packing metal granule mixing composite catalysts promoted the formation of long-chain liquid chemicals and conversion rates due to (i). enhancement of local electronic energy; (ii). the instinctive activity of Co or Fe to the chemisorption of reactive radicals. (iii). the instinctive nature of HZSM-5 for isomerization and oligomerization and synergistic effects between Co or Fe with HZSM-5. Meanwhile, obvious difference in catalytic performance can be observed between the granule mixed Fe and Co catalysts probably due to the own nature of Co and Fe. It is found that by packing granule mixed Co/SiO<sub>2</sub> with HZSM-5, more long-chain liquid products were detected, particularly at a CO<sub>2</sub>/CH<sub>4</sub> ratio of 1:2, where more long-chain liquid chemicals with higher concentration were found (such as C<sub>7</sub>H<sub>16</sub>, butanol, propanoic acid, acetoin, pentanol, hexanol, C<sub>5</sub>+ ester, C<sub>7</sub>H<sub>14</sub>O, C<sub>8</sub>H<sub>18</sub>O, etc.). While packing Fe/HZSM-5 at a high CO<sub>2</sub> proportion led to high selectivity to methanol, packing granule mixed Fe/SiO<sub>2</sub> with HZSM-5 at the high proportion of CH<sub>4</sub> brought out high selectivity to acetic acid.

Unlike granule mixing packing, the catalytic improvement when packing metal doping composite catalysts is mainly attributed to the metal catalysts instead of the synergistic effects. Interestingly, with packing Fe/HZSM-5 at a high CO<sub>2</sub> proportion, the liquid products were highly concentrated on methanol with a considerable selectivity (excluding water). For the dual packing, the catalysts seemed to work mechanically separated with negligible synergistic effects. As packing HZSM-5 decreased the conversions of reactants and promoted the formation of coke due to the enhancement of electric conductivity and decrease of the discharge volume, dual bed packing finally resulted in lower conversions and energy efficiency than the other mixing methods. This work has demonstrated a new way to directly synthesizing long-chain liquid chemicals via composite catalysts and providing a new perspective

for manipulating the distribution of liquid chemicals direct from the plasma-catalytic conversion of CO<sub>2</sub> with CH<sub>4</sub>.

### 6.3. Future perspectives and recommendation

In this work, an early study on plasma-catalytic FTS was carried out by employing different Co/SiO<sub>2</sub> aerogel catalysts. However, C<sub>5</sub>-C<sub>11</sub> gasoline species were barely found in the products due to different condition and reaction mechanism. The plasma-catalytic FTS was feasible, while great efforts on this topic are essential. On the basis of this work, we propose some recommendation and future perspectives on this topic:

1. Optimization of the reactor and power supply to achieve higher mean electron energy (higher voltage, higher frequency, different signal, etc).
2. Catalyst development: both on the SiO<sub>2</sub> aerogel development (preparation method) and doped metal catalysts (different metal catalysts, preparation, and treatment method, promoters, etc.).
3. Effects of dilution with inert gas.
4. Plasma-catalytic modeling to obtain a better insight into plasma-catalytic FTS.

Later the work on the plasma-catalytic conversion of CH<sub>4</sub> with CO<sub>2</sub> has obtained fascinating results. A remarkable selectivity to liquid products, including methanol, acetic acid, and long-chain hydrocarbons was achieved. By introducing composite catalysts, it is feasible to manipulate the distribution of liquid products and improve the selectivity to long-chain hydrocarbons. Furthermore, the energy efficiency and conversions benefited from introducing these catalysts and exhibited very strong competitiveness comparing with published works. This work has demonstrated the feasibility for direct synthesis of fuel species from CO<sub>2</sub> and CH<sub>4</sub>. Based on the work, some recommendations for future work are proposed:

1. Support side: SiO<sub>2</sub> aerogel prepared by different precursor and methods;

different aerogels such as  $\text{TiO}_2$  aerogel or carbon aerogel; variety ordered porous structure from macropores to mesopores.

2. Catalyst side: different loading metals including noble and transition metals; treatment method including plasma reduction, different calcining temperature; introduction of promoters such as alkaline metals; different composite catalysts.

3. Bench optimization: different operating temperatures; optimization of the reactor for applying OES fiber; power supply optimization for various electric signals and applying energy; the constant temperature of pipelines and a down-stream outlet for products collecting;

4. Plasma modeling to obtain a better insight into the mechanisms of synergistic effects on liquid formation.

# References

- [1] I. Statistics, CO<sub>2</sub> Emissions From Fuel Combustion Highlights 2016, Paris. International Energy Agency, (2016).
- [2] I. Statistics, Key World Energy Statistics, Paris. International Energy Agency, (2016).
- [3] I. Statistics, Tracking Clean Energy Progress 2015, Paris. International Energy Agency, (2016).
- [4] J. Koornneef, A. Ramírez, W. Turkenburg, A. Faaij, The environmental impact and risk assessment of CO<sub>2</sub> capture, transport and storage—An evaluation of the knowledge base, *Progress in Energy and Combustion Science*, 38 (2012) 62-86.
- [5] A. Fridman, *Plasma chemistry*, Cambridge university press 2008.
- [6] I. Statistics, Key Renewables Trends, Paris. International Energy Agency, (2016).
- [7] R.J. Goldston, P.H. Rutherford, *Introduction to plasma physics*, CRC Press 1995.
- [8] B. Graham, Technological plasmas, *Physics World*, 14 (2001) 31.
- [9] A. Fridman, L.A. Kennedy, *Plasma physics and engineering*, CRC press 2004.
- [10] P.J. Dickerman, Determination of the Equilibrium Temperature of a Plasma, *Journal of Applied Physics (US)*, 29 (1958).
- [11] J.R. Hollahan, A.T. Bell, *Techniques and applications of plasma chemistry*, (1974).
- [12] F. Fischer, H. Tropsch, The direct synthesis of petroleum hydrocarbons with standard pressure. (Second report.), *Berichte Der Deutschen Chemischen Gesellschaft*, 59 (1926) 832-836.
- [13] C.H. Bartholomew, History of cobalt catalyst design for FTS, *Proceedings of the National Spring Meeting of the American Institute of Chemical Engineers (AIChE'03)*, 2003.
- [14] P. Sabatier, J.B. Senderens, New methane synthesis, *C. R. Hebd. Seances Acad. Sci.*, 134 (1902) 514-516.
- [15] F. Fischer, H. Tropsch, Concerning the synthesis of upper links in the aliphatic sequence from carbon oxide, *Berichte Der Deutschen Chemischen Gesellschaft*, 56 (1923) 2428-2443.
- [16] D. Leckel, Diesel production from Fischer–Tropsch: the past, the present, and new concepts, *Energy & Fuels*, 23 (2009) 2342-2358.
- [17] J. Van Dyk, M. Keyser, M. Coertzen, Syngas production from South African coal sources using Sasol–Lurgi gasifiers, *International Journal of Coal Geology*, 65 (2006) 243-253.
- [18] M. Dry, A. Steynberg, Commercial FT process applications, *Studies in Surface Science and Catalysis*, 152 (2004) 406-481.
- [19] M. Dry, J. Hoogendoorn, Technology of the Fischer-Tropsch process, *Catalysis Reviews—Science and Engineering*, 23 (1981) 265-278.
- [20] H. Kölbl, M. Ralek, The Fischer-Tropsch synthesis in the liquid phase, *Catalysis Reviews Science and Engineering*, 21 (1980) 225-274.
- [21] V. Rao, G. Stiegel, G. Cinquegrane, R. Srivastava, Iron-based catalysts for slurry-phase Fischer-Tropsch process: Technology review, *Fuel processing technology*, 30 (1992) 83-107.
- [22] R. Srivastava, V. Rao, G. Cinquegrane, G. Stiegel, *Catalysts for Fischer-Tropsch, Hydrocarbon Processing (USA)*, 69 (1990).
- [23] M.E. Dry, The Fischer–Tropsch process: 1950–2000, *Catalysis today*, 71 (2002) 227-241.
- [24] T. Kaneko, F. Derbyshire, E. Makino, D. Gray, M. Tamura, K. Li, Coal liquefaction,

Ullmann's Encyclopedia of Industrial Chemistry, (2005).

[25] C.A. Mims, L.E. McCandlish, Evidence of rapid chain growth in the Fischer-Tropsch synthesis over iron and cobalt catalysts, *J. Phys. Chem.:(United States)*, 91 (1987).

[26] V. Frøseth, S. Storsæter, Ø. Borg, E.A. Blekkan, M. Rønning, A. Holmen, Steady state isotopic transient kinetic analysis (SSITKA) of CO hydrogenation on different Co catalysts, *Applied Catalysis A: General*, 289 (2005) 10-15.

[27] J. Yang, Y. Qi, J. Zhu, Y.-A. Zhu, D. Chen, A. Holmen, Reaction mechanism of CO activation and methane formation on Co Fischer-Tropsch catalyst: A combined DFT, transient, and steady-state kinetic modeling, *Journal of catalysis*, 308 (2013) 37-49.

[28] D. Hibbitts, E. Dybeck, T. Lawlor, M. Neurock, E. Iglesia, Preferential activation of CO near hydrocarbon chains during Fischer-Tropsch synthesis on Ru, *Journal of Catalysis*, 337 (2016) 91-101.

[29] M. Ojeda, R. Nabar, A.U. Nilekar, A. Ishikawa, M. Mavrikakis, E. Iglesia, CO activation pathways and the mechanism of Fischer-Tropsch synthesis, *Journal of Catalysis*, 272 (2010) 287-297.

[30] X.-Q. Gong, R. Raval, P. Hu, CO dissociation and O removal on Co (0001): a density functional theory study, *Surface science*, 562 (2004) 247-256.

[31] Q. Ge, M. Neurock, Adsorption and activation of CO over flat and stepped Co surfaces: A first principles analysis, *The Journal of Physical Chemistry B*, 110 (2006) 15368-15380.

[32] M. Zhuo, K.F. Tan, A. Borgna, M. Saeys, Density functional theory study of the CO insertion mechanism for Fischer-Tropsch synthesis over Co catalysts, *The Journal of Physical Chemistry C*, 113 (2009) 8357-8365.

[33] M. Vannice, The catalytic synthesis of hydrocarbons from H<sub>2</sub>CO mixtures over the group VIII metals: I. The specific activities and product distributions of supported metals, *Journal of Catalysis*, 37 (1975) 449-461.

[34] C.H. Bartholomew, R.J. Farrauto, Hydrogen production and synthesis gas reactions, *Fundamentals of Industrial Catalytic Processes*, Second Edition, (2006) 339-486.

[35] G.P. Van der Laan, A.A. Beenackers, Intrinsic kinetics of the gas-solid Fischer-Tropsch and water gas shift reactions over a precipitated iron catalyst, *Applied Catalysis A: General*, 193 (2000) 39-53.

[36] V.R.R. Pendyala, G. Jacobs, J.C. Mohandas, M. Luo, W. Ma, M.K. Gnanamani, B.H. Davis, Fischer-Tropsch synthesis: Attempt to tune FTS and WGS by alkali promoting of iron catalysts, *Applied Catalysis A: General*, 389 (2010) 131-139.

[37] B.H. Davis, Fischer-Tropsch Synthesis: Comparison of Performances of Iron and Cobalt Catalysts, *Industrial & Engineering Chemistry Research*, 46 (2007) 8938-8945.

[38] S. Krishnamoorthy, M. Tu, M.P. Ojeda, D. Pinna, E. Iglesia, An investigation of the effects of water on rate and selectivity for the Fischer-Tropsch synthesis on cobalt-based catalysts, *Journal of Catalysis*, 211 (2002) 422-433.

[39] A.Y. Khodakov, W. Chu, P. Fongarland, Advances in the development of novel cobalt Fischer-Tropsch catalysts for synthesis of long-chain hydrocarbons and clean fuels, *Chemical reviews*, 107 (2007) 1692-1744.

[40] A. Barbier, A. Tuel, I. Arcon, A. Kodre, G.A. Martin, Characterization and catalytic behavior of Co/SiO<sub>2</sub> catalysts: influence of dispersion in the Fischer-Tropsch reaction, *Journal of catalysis*, 200 (2001) 106-116.

[41] A. Lapidus, A. Krylova, V. Kazanskii, V. Borovkov, A. Zaitsev, J. Rathousky, A. Zupal, M. Jancalkova, Hydrocarbon synthesis from carbon monoxide and hydrogen on impregnated cobalt catalysts Part I. Physico-chemical properties of 10% cobalt/alumina and 10% cobalt/silica, *Applied catalysis*, 73 (1991) 65-81.

[42] A. Lapidus, A. Krylova, J. Rathousky, A. Zupal, M. Janc'ka, Hydrocarbon synthesis from carbon monoxide and hydrogen on impregnated cobalt catalysts II: Activity of 10% Co/Al<sub>2</sub>O<sub>3</sub> and 10% Co/SiO<sub>2</sub> catalysts in Fischer-Tropsch synthesis, *Applied Catalysis A: General*, 80 (1992) 1-11.

[43] G.W. Huber, C.G. Guymon, T.L. Conrad, B.C. Stephenson, C.H. Bartholomew, Hydrothermal stability of Co/SiO<sub>2</sub> Fischer-Tropsch synthesis catalysts, (2001).

[44] H. Li, J. Li, H. Ni, D. Song, Studies on cobalt catalyst supported on silica with different pore size for Fischer-Tropsch synthesis, *Catalysis letters*, 110 (2006) 71-76.

[45] J. Li, Y. Xu, D. Wu, Y. Sun, Hollow mesoporous silica sphere supported cobalt catalysts for F-T synthesis, *Catalysis Today*, 148 (2009) 148-152.

[46] A. Saib, M. Claeys, E. Van Steen, Silica supported cobalt Fischer-Tropsch catalysts: effect of pore diameter of support, *Catalysis Today*, 71 (2002) 395-402.

[47] E. Iglesia, Design, synthesis, and use of cobalt-based Fischer-Tropsch synthesis catalysts, *Applied Catalysis A: General*, 161 (1997) 59-78.

[48] J. Li, G. Jacobs, T. Das, Y. Zhang, B. Davis, Fischer-Tropsch synthesis: effect of water on the catalytic properties of a Co/SiO<sub>2</sub> catalyst, *Applied Catalysis A: General*, 236 (2002) 67-76.

[49] T.K. Das, W.A. Conner, J. Li, G. Jacobs, M.E. Dry, B.H. Davis, Fischer-Tropsch synthesis: Kinetics and effect of water for a Co/SiO<sub>2</sub> catalyst, *Energy & fuels*, 19 (2005) 1430-1439.

[50] G.K.K. Gunasooriya, A.P. van Bavel, H.P. Kuipers, M. Saeys, Key Role of Surface Hydroxyl Groups in C-O Activation during Fischer-Tropsch Synthesis, *ACS Catalysis*, 6 (2016) 3660-3664.

[51] P. Dutta, B. Dunn, E. Eyring, N. Shah, G. Huffman, A. Manivannan, M. Seehra, Characteristics of Cobalt Nanoneedles in 10% Co/Aerogel Fischer-Tropsch Catalyst, *Chemistry of materials*, 17 (2005) 5183-5186.

[52] B.C. Dunn, D.J. Covington, P. Cole, R.J. Pugmire, H.L. Meuzelaar, R.D. Ernst, E.C. Heider, E.M. Eyring, N. Shah, G.P. Huffman, Silica Xerogel Supported Cobalt Metal Fischer-Tropsch Catalysts for Syngas to Diesel Range Fuel Conversion, *Energy & fuels*, 18 (2004) 1519-1521.

[53] D. Carta, M.F. Casula, A. Corrias, A. Falqui, D. Loche, G. Mountjoy, P. Wang, Structural and magnetic characterization of Co and Ni silicate hydroxides in bulk and in nanostructures within silica aerogels, *Chemistry of Materials*, 21 (2009) 945-953.

[54] Z. Ma, B.C. Dunn, G.C. Turpin, E.M. Eyring, R.D. Ernst, R.J. Pugmire, Solid state NMR investigation of silica aerogel supported Fischer-Tropsch catalysts, *Fuel processing technology*, 88 (2007) 29-33.

[55] B.C. Dunn, P. Cole, D. Covington, M.C. Webster, R.J. Pugmire, R.D. Ernst, E.M. Eyring, N. Shah, G.P. Huffman, Silica aerogel supported catalysts for Fischer-Tropsch synthesis, *Applied Catalysis A: General*, 278 (2005) 233-238.

[56] D. Loche, M.F. Casula, A. Corrias, S. Marras, P. Moggi, Bimetallic FeCo nanocrystals supported on highly porous silica aerogels as Fischer-Tropsch catalysts, *Catalysis letters*, 142 (2012) 1061-1066.

[57] A. Martínez, G. Prieto, Breaking the dispersion-reducibility dependence in oxide-supported

cobalt nanoparticles, *Journal of Catalysis*, 245 (2007) 470-476.

[58] B. Sexton, A. Hughes, T. Turney, An XPS and TPR study of the reduction of promoted cobalt-kieselguhr Fischer-Tropsch catalysts, *Journal of Catalysis*, 97 (1986) 390-406.

[59] B. Ernst, S. Libs, P. Chaumette, A. Kiennemann, Preparation and characterization of Fischer-Tropsch active Co/SiO<sub>2</sub> catalysts, *Applied Catalysis A: General*, 186 (1999) 145-168.

[60] P. Arnoldy, J.A. Moulijn, Temperature-programmed reduction of CoOAl<sub>2</sub>O<sub>3</sub> catalysts, *Journal of Catalysis*, 93 (1985) 38-54.

[61] R. Xie, D. Li, B. Hou, J. Wang, L. Jia, Y. Sun, Silylated Co<sub>3</sub>O<sub>4</sub>-m-SiO<sub>2</sub> catalysts for Fischer-Tropsch synthesis, *Catalysis Communications*, 12 (2011) 589-592.

[62] L. Shi, J. Chen, K. Fang, Y. Sun, CH<sub>3</sub>-modified Co/Ru/SiO<sub>2</sub> catalysts and the performances for Fischer-Tropsch synthesis, *Fuel*, 87 (2008) 521-526.

[63] E. Rytter, A. Holmen, On the support in cobalt Fischer-Tropsch synthesis—Emphasis on alumina and aluminates, *Catalysis Today*, 275 (2016) 11-19.

[64] G. Jacobs, J.A. Chaney, P.M. Patterson, T.K. Das, B.H. Davis, Fischer-Tropsch synthesis: study of the promotion of Re on the reduction property of Co/Al<sub>2</sub>O<sub>3</sub> catalysts by in situ EXAFS/XANES of Co K and Re L III edges and XPS, *Applied Catalysis A: General*, 264 (2004) 203-212.

[65] J. Li, X. Zhan, Y. Zhang, G. Jacobs, T. Das, B.H. Davis, Fischer-Tropsch synthesis: effect of water on the deactivation of Pt promoted Co/Al<sub>2</sub>O<sub>3</sub> catalysts, *Applied Catalysis A: General*, 228 (2002) 203-212.

[66] C.J. Bertole, C.A. Mims, G. Kiss, The effect of water on the cobalt-catalyzed Fischer-Tropsch synthesis, *Journal of Catalysis*, 210 (2002) 84-96.

[67] P.M. Maitlis, A. de Klerk, *Greener Fischer-Tropsch Processes: For Fuels and Feedstocks*, John Wiley & Sons 2013.

[68] F. Fisher, H. Tropsch, Conversion of methane into hydrogen and carbon monoxide, *Brennst.-Chem.*, 9 (1928).

[69] W. Lewis, E. Gilliland, W.A. Reed, Reaction of methane with copper oxide in a fluidized bed, *Industrial & Engineering Chemistry*, 41 (1949) 1227-1237.

[70] R. Reitmeier, K. Atwood, H. Bennett, H. Baugh, Production of Synthetic Gas-Reaction of Light Hydrocarbons with Steam and Carbon Dioxide, *Industrial & Engineering Chemistry*, 40 (1948) 620-626.

[71] N.J. Rostrup, Process for the production of a reforming catalyst, Google Patents, 1974.

[72] J.R. Rostrup-Nielsen, Process for the catalytic steam reforming of hydrocarbons, Google Patents, 1975.

[73] T. Sodesawa, A. Dobashi, F. Nozaki, Catalytic reaction of methane with carbon dioxide, *Reaction Kinetics and Catalysis Letters*, 12 (1979) 107-111.

[74] A. Ashcroft, A.K. Cheetham, M. Green, P. Vernon, Partial oxidation of methane to synthesis gas using carbon dioxide, *Nature*, 352 (1991) 225.

[75] J.T. Richardson, M. Garrat, J.K. Hung, Carbon dioxide reforming with Rh and Pt-Re catalysts dispersed on ceramic foam supports, *Applied Catalysis A: General*, 255 (2003) 69-82.

[76] E. Ruckenstein, Y. Hang Hu, The effect of precursor and preparation conditions of MgO on the CO<sub>2</sub> reforming of CH<sub>4</sub> over NiO/MgO catalysts, *Applied Catalysis A: General*, 154 (1997) 185-

205.

[77] C. Batiot-Dupeyrat, F. Martinez-Ortega, M. Ganne, J.M. Tatibouet, Methane catalytic combustion on La-based perovskite type catalysts in high temperature isothermal conditions, *Applied Catalysis a-General*, 206 (2001) 205-215.

[78] C. Batiot-Dupeyrat, G. Valderrama, A. Meneses, F. Martinez, J. Barrault, J.M. Tatibouet, Pulse study of CO<sub>2</sub> reforming of methane over LaNiO<sub>3</sub>, *Applied Catalysis a-General*, 248 (2003) 143-151.

[79] Z.Y. Hou, T. Yashima, Small amounts of Rh-promoted Ni catalysts for methane reforming with CO<sub>2</sub>, *Catalysis Letters*, 89 (2003) 193-197.

[80] M. Garcia-Dieguez, I.S. Pieta, M.C. Herrera, M.A. Larrubia, L.J. Alemany, RhNi nanocatalysts for the CO<sub>2</sub> and CO<sub>2</sub> + H<sub>2</sub>O reforming of methane, *Catalysis Today*, 172 (2011) 136-142.

[81] B. Pawelec, S. Damyanova, K. Arishtirova, J.L.G. Fierro, L. Petrov, Structural and surface features of PtNi catalysts for reforming of methane with CO<sub>2</sub>, *Applied Catalysis a-General*, 323 (2007) 188-201.

[82] B. Steinhauer, M.R. Kasireddy, J. Radnik, A. Martin, Development of Ni-Pd bimetallic catalysts for the utilization of carbon dioxide and methane by dry reforming, *Applied Catalysis a-General*, 366 (2009) 333-341.

[83] K. Nagaoka, K. Takanabe, K. Aika, Modification of Co/TiO<sub>2</sub> for dry reforming of methane at 2 MPa by Pt, Ru or Ni, *Applied Catalysis a-General*, 268 (2004) 151-158.

[84] G. Valderrama, C.U. de Navarro, M.R. Goldwasser, CO<sub>2</sub> reforming of CH<sub>4</sub> over Co-La-based perovskite-type catalyst precursors, *Journal of Power Sources*, 234 (2013) 31-37.

[85] G. Moradi, F. Khezeli, H. Hemmati, Syngas production with dry reforming of methane over Ni/ZSM-5 catalysts, *Journal of Natural Gas Science and Engineering*, 33 (2016) 657-665.

[86] L.L. Xu, H.L. Song, L.J. Chou, One-Pot Synthesis of Ordered Mesoporous NiO-CaO-Al<sub>2</sub>O<sub>3</sub> Composite Oxides for Catalyzing CO<sub>2</sub> Reforming of CH<sub>4</sub>, *Acs Catalysis*, 2 (2012) 1331-1342.

[87] J. Deng, W. Chu, B. Wang, W. Yang, X.S. Zhao, Mesoporous Ni/Ce<sub>1-x</sub>Ni<sub>x</sub>O<sub>2-y</sub> heterostructure as an efficient catalyst for converting greenhouse gas to H<sub>2</sub> and syngas, *Catalysis Science & Technology*, 6 (2016) 851-862.

[88] J. Deng, W. Chu, B. Wang, W. Yang, X.S. Zhao, Mesoporous Ni/Ce<sub>1-x</sub>Ni<sub>x</sub>O<sub>2-y</sub> heterostructure as an efficient catalyst for converting greenhouse gas to H<sub>2</sub> and syngas, *Catalysis Science & Technology*, 6 (2016) 851-862.

[89] M. Garcia-Dieguez, I.S. Pieta, M.C. Herrera, M.A. Larrubia, I. Malpartida, L.J. Alemany, Transient study of the dry reforming of methane over Pt supported on different gamma-Al<sub>2</sub>O<sub>3</sub>, *Catalysis Today*, 149 (2010) 380-387.

[90] H. Arbag, S. Yasyerli, N. Yasyerli, G. Dogu, Activity and stability enhancement of Ni-MCM-41 catalysts by Rh incorporation for hydrogen from dry reforming of methane, *International Journal of Hydrogen Energy*, 35 (2010) 2296-2304.

[91] A.N. Pinheiro, A. Valentini, J.M. Sasaki, A.C. Oliveira, Highly stable dealuminated zeolite support for the production of hydrogen by dry reforming of methane, *Applied Catalysis a-General*, 355 (2009) 156-168.

[92] Y.H. Hu, E. Ruckenstein, An optimum NiO content in the CO<sub>2</sub> reforming of CH<sub>4</sub> with

NiO/MgO solid solution catalysts, *Catalysis Letters*, 36 (1996) 145-149.

[93] Y.H. Cui, H.D. Zhang, H.Y. Xu, W.Z. Li, Kinetic study of the catalytic reforming of CH<sub>4</sub> with CO<sub>2</sub> to syngas over Ni/α-Al<sub>2</sub>O<sub>3</sub> catalyst: The effect of temperature on the reforming mechanism, *Applied Catalysis a-General*, 318 (2007) 79-88.

[94] S. Therdthianwong, A. Therdthianwong, C. SiangChin, S. Yonprapat, Synthesis gas production from dry reforming of methane over Ni/Al<sub>2</sub>O<sub>3</sub> stabilized by ZrO<sub>2</sub>, *International Journal of Hydrogen Energy*, 33 (2008) 991-999.

[95] W.-J. Jang, D.-W. Jeong, J.-O. Shim, H.-M. Kim, H.-S. Roh, I.H. Son, S.J. Lee, Combined steam and carbon dioxide reforming of methane and side reactions: Thermodynamic equilibrium analysis and experimental application, *Applied energy*, 173 (2016) 80-91.

[96] S. Wang, G. Lu, G.J. Millar, Carbon dioxide reforming of methane to produce synthesis gas over metal-supported catalysts: state of the art, *Energy & fuels*, 10 (1996) 896-904.

[97] M.K. Nikoo, N. Amin, Thermodynamic analysis of carbon dioxide reforming of methane in view of solid carbon formation, *Fuel Processing Technology*, 92 (2011) 678-691.

[98] C. Papadopoulou, H. Matralis, X. Verykios, Utilization of biogas as a renewable carbon source: dry reforming of methane, *Catalysis for alternative energy generation*, Springer 2012, pp. 57-127.

[99] M.C. Bradford, M.A. Vannice, The role of metal-support interactions in CO<sub>2</sub> reforming of CH<sub>4</sub>, *Catalysis today*, 50 (1999) 87-96.

[100] T. Osaki, T. Mori, Role of potassium in carbon-free CO<sub>2</sub> reforming of methane on K-promoted Ni/Al<sub>2</sub>O<sub>3</sub> catalysts, *Journal of Catalysis*, 204 (2001) 89-97.

[101] Z. Cheng, X. Zhao, J. Li, Q. Zhu, Role of support in CO<sub>2</sub> reforming of CH<sub>4</sub> over a Ni/γ-Al<sub>2</sub>O<sub>3</sub> catalyst, *Applied Catalysis A: General*, 205 (2001) 31-36.

[102] U. Portugal, A. Santos, S. Damyanova, C. Marques, J. Bueno, CO<sub>2</sub> reforming of CH<sub>4</sub> over Rh-containing catalysts, *Journal of Molecular Catalysis A: Chemical*, 184 (2002) 311-322.

[103] B. Fidalgo, A. Arenillas, J. Menéndez, Mixtures of carbon and Ni/Al<sub>2</sub>O<sub>3</sub> as catalysts for the microwave-assisted CO<sub>2</sub> reforming of CH<sub>4</sub>, *Fuel processing technology*, 92 (2011) 1531-1536.

[104] A.E.C. Luna, M.E. Iriarte, Carbon dioxide reforming of methane over a metal modified Ni-Al<sub>2</sub>O<sub>3</sub> catalyst, *Applied Catalysis A: General*, 343 (2008) 10-15.

[105] S. Zeng, L. Zhang, X. Zhang, Y. Wang, H. Pan, H. Su, Modification effect of natural mixed rare earths on Co/γ-Al<sub>2</sub>O<sub>3</sub> catalysts for CH<sub>4</sub>/CO<sub>2</sub> reforming to synthesis gas, *international journal of hydrogen energy*, 37 (2012) 9994-10001.

[106] G. Zhang, A. Su, Y. Du, J. Qu, Y. Xu, Catalytic performance of activated carbon supported cobalt catalyst for CO<sub>2</sub> reforming of CH<sub>4</sub>, *Journal of colloid and interface science*, 433 (2014) 149-155.

[107] M. Vasiliades, M. Makri, P. Djinić, B. Erjavec, A. Pintar, A. Efstathiou, Dry reforming of methane over 5 wt% Ni/Ce<sub>1-x</sub>Pr<sub>x</sub>O<sub>2-δ</sub> catalysts: performance and characterisation of active and inactive carbon by transient isotopic techniques, *Applied Catalysis B: Environmental*, 197 (2016) 168-183.

[108] Z. Hou, P. Chen, H. Fang, X. Zheng, T. Yashima, Production of synthesis gas via methane reforming with CO<sub>2</sub> on noble metals and small amount of noble-(Rh-) promoted Ni catalysts, *International journal of hydrogen energy*, 31 (2006) 555-561.

[109] P. Djinović, I.G.O. Črnivec, J. Batista, J. Levec, A. Pintar, Catalytic syngas production from greenhouse gases: Performance comparison of Ru-Al<sub>2</sub>O<sub>3</sub> and Rh-CeO<sub>2</sub> catalysts, *Chemical Engineering and Processing: Process Intensification*, 50 (2011) 1054-1062.

[110] C. Shi, P. Zhang, Effect of a second metal (Y, K, Ca, Mn or Cu) addition on the carbon dioxide reforming of methane over nanostructured palladium catalysts, *Applied Catalysis B: Environmental*, 115 (2012) 190-200.

[111] I. Sarusi, K. Fodor, K. Baán, A. Oszkó, G. Pótári, A. Erdőhelyi, CO<sub>2</sub> reforming of CH<sub>4</sub> on doped Rh/Al<sub>2</sub>O<sub>3</sub> catalysts, *Catalysis Today*, 171 (2011) 132-139.

[112] C. Crisafulli, S. Scirè, S. Minicò, L. Solarino, Ni-Ru bimetallic catalysts for the CO<sub>2</sub> reforming of methane, *Applied Catalysis A: General*, 225 (2002) 1-9.

[113] J. Zhang, H. Wang, A.K. Dalai, Development of stable bimetallic catalysts for carbon dioxide reforming of methane, *Journal of Catalysis*, 249 (2007) 300-310.

[114] A. Horváth, G. Stefler, O. Geszti, A. Kienneman, A. Pietraszek, L. Gucci, Methane dry reforming with CO<sub>2</sub> on CeZr-oxide supported Ni, NiRh and NiCo catalysts prepared by sol-gel technique: relationship between activity and coke formation, *Catalysis today*, 169 (2011) 102-111.

[115] M. Ocsachoque, F. Pompeo, G. Gonzalez, Rh-Ni/CeO<sub>2</sub>-Al<sub>2</sub>O<sub>3</sub> catalysts for methane dry reforming, *Catalysis Today*, 172 (2011) 226-231.

[116] F. Menegazzo, M. Signoretto, F. Pinna, P. Canton, N. Pernicone, Optimization of bimetallic dry reforming catalysts by temperature programmed reaction, *Applied Catalysis A: General*, 439 (2012) 80-87.

[117] K. Nagaoka, K. Takanabe, K.-i. Aika, Modification of Co/TiO<sub>2</sub> for dry reforming of methane at 2 MPa by Pt, Ru or Ni, *Applied Catalysis A: General*, 268 (2004) 151-158.

[118] K. Takanabe, K. Nagaoka, K. Nariai, K.-i. Aika, Titania-supported cobalt and nickel bimetallic catalysts for carbon dioxide reforming of methane, *Journal of Catalysis*, 232 (2005) 268-275.

[119] A.F. Lucrédio, J.M. Assaf, E.M. Assaf, Methane conversion reactions on Ni catalysts promoted with Rh: Influence of support, *Applied Catalysis A: General*, 400 (2011) 156-165.

[120] B. Faroldi, E.A. Lombardo, L.M. Cornaglia, Surface properties and catalytic behavior of Ru supported on composite La<sub>2</sub>O<sub>3</sub>-SiO<sub>2</sub> oxides, *Applied Catalysis A: General*, 369 (2009) 15-26.

[121] M. Ghelamallah, P. Granger, Impact of barium and lanthanum incorporation to supported Pt and Rh on  $\alpha$ -Al<sub>2</sub>O<sub>3</sub> in the dry reforming of methane, *Fuel*, 97 (2012) 269-276.

[122] H. Arandiyani, Y. Peng, C. Liu, H. Chang, J. Li, Effects of noble metals doped on mesoporous LaAlNi mixed oxide catalyst and identification of carbon deposit for reforming CH<sub>4</sub> with CO<sub>2</sub>, *Journal of Chemical Technology & Biotechnology*, 89 (2014) 372-381.

[123] N. El Hassan, M. Kaydouh, H. Geagea, H. El Zein, K. Jabbour, S. Casale, H. El Zakhem, P. Massiani, Low temperature dry reforming of methane on rhodium and cobalt based catalysts: active phase stabilization by confinement in mesoporous SBA-15, *Applied Catalysis A: General*, 520 (2016) 114-121.

[124] P. Frontera, A. Macario, A. Aloise, P. Antonucci, G. Giordano, J. Nagy, Effect of support surface on methane dry-reforming catalyst preparation, *Catalysis today*, 218 (2013) 18-29.

[125] H. Wang, E. Ruckenstein, Carbon dioxide reforming of methane to synthesis gas over supported rhodium catalysts: the effect of support, *Applied Catalysis A: General*, 204 (2000) 143-152.

[126] J.C. Wu, H.-C. Chou, Bimetallic Rh-Ni/BN catalyst for methane reforming with CO<sub>2</sub>,

Chemical Engineering Journal, 148 (2009) 539-545.

[127] R.-j. ZHANG, G.-f. XIA, M.-f. LI, W. Yu, N. Hong, D.-d. LI, Effect of support on the performance of Ni-based catalyst in methane dry reforming, *Journal of Fuel Chemistry and Technology*, 43 (2015) 1359-1365.

[128] B. Steinhauer, M.R. Kasireddy, J. Radnik, A. Martin, Development of Ni-Pd bimetallic catalysts for the utilization of carbon dioxide and methane by dry reforming, *Applied Catalysis A: General*, 366 (2009) 333-341.

[129] J. Raskó, F. Solymosi, Reactions of adsorbed CH<sub>3</sub> species with CO<sub>2</sub> on Rh/SiO<sub>2</sub> catalyst, *Catalysis letters*, 46 (1997) 153-157.

[130] J. Raskó, F. Solymosi, Adsorption of CH<sub>3</sub> and Its Reactions with CO<sub>2</sub> over TiO<sub>2</sub>, *Catalysis letters*, 54 (1998) 49-54.

[131] Y. Fujiwara, Y. Taniguchi, K. Takaki, M. Kurioka, T. Jintoku, T. Kitamura, Palladium-catalyzed acetic acid synthesis from methane and carbon dioxide, in: M. de Pontes, R.L. Espinoza, C.P. Nicolaidis, J.H. Scholtz, M.S. Scurrill (Eds.) *Studies in Surface Science and Catalysis*, Elsevier 1997, pp. 275-278.

[132] W. Huang, K.C. Xie, J.P. Wang, Z.H. Gao, L.H. Yin, Q.M. Zhu, Possibility of Direct Conversion of CH<sub>4</sub> and CO<sub>2</sub> to High-Value Products, *Journal of Catalysis*, 201 (2001) 100-104.

[133] E.M. Wilcox, G.W. Roberts, J.J. Spivey, Direct catalytic formation of acetic acid from CO<sub>2</sub> and methane, *Catalysis Today*, 88 (2003) 83-90.

[134] M. Zerella, S. Mukhopadhyay, A.T. Bell, Synthesis of Mixed Acid Anhydrides from Methane and Carbon Dioxide in Acid Solvents, *Organic Letters*, 5 (2003) 3193-3196.

[135] Y.-H. Ding, W. Huang, Y.-G. Wang, Direct synthesis of acetic acid from CH<sub>4</sub> and CO<sub>2</sub> by a step-wise route over Pd/SiO<sub>2</sub> and Rh/SiO<sub>2</sub> catalysts, *Fuel Processing Technology*, 88 (2007) 319-324.

[136] W. Huang, W.Z. Sun, F. Li, Efficient synthesis of ethanol and acetic acid from methane and carbon dioxide with a continuous, stepwise reactor, *AIChE Journal*, 56 (2010) 1279-1284.

[137] A.M. Rabie, M.A. Betiha, S.-E. Park, Direct synthesis of acetic acid by simultaneous co-activation of methane and CO<sub>2</sub> over Cu-exchanged ZSM-5 catalysts, *Applied Catalysis B: Environmental*, 215 (2017) 50-59.

[138] T. Nishiyama, K.-I. Aika, Mechanism of the oxidative coupling of methane using CO<sub>2</sub> as an oxidant over PbO/MgO, *Journal of Catalysis*, 122 (1990) 346-351.

[139] K. Asami, T. Fujita, K.-i. Kusakabe, Y. Nishiyama, Y. Ohtsuka, Conversion of methane with carbon dioxide into C<sub>2</sub> hydrocarbons over metal oxides, *Applied Catalysis A: General*, 126 (1995) 245-255.

[140] J.A. Labinger, J.E. Bercaw, Understanding and exploiting C-H bond activation, *Nature*, 417 (2002) 507-514.

[141] I.H. Hristov, T. Ziegler, Density Functional Theory Study of the Direct Conversion of Methane to Acetic Acid by RhCl<sub>3</sub>, *Organometallics*, 22 (2003) 3513-3525.

[142] S. Chempath, A.T. Bell, Density Functional Theory Analysis of the Reaction Pathway for Methane Oxidation to Acetic Acid Catalyzed by Pd<sup>2+</sup> in Sulfuric Acid, *Journal of the American Chemical Society*, 128 (2006) 4650-4657.

[143] S. Wannakao, C. Warakulwit, K. Kongpatpanich, M. Probst, J. Limtrakul, Methane Activation in Gold Cation-Exchanged Zeolites: A DFT Study, *ACS Catalysis*, 2 (2012) 986-992.

[144] W. Panjan, J. Sirijaraensre, C. Warakulwit, P. Pantu, J. Limtrakul, The conversion of CO<sub>2</sub> and CH<sub>4</sub> to acetic acid over the Au-exchanged ZSM-5 catalyst: a density functional theory study, *Physical Chemistry Chemical Physics*, 14 (2012) 16588-16594.

[145] J.-F. Wu, S.-M. Yu, W.D. Wang, Y.-X. Fan, S. Bai, C.-W. Zhang, Q. Gao, J. Huang, W. Wang, Mechanistic Insight into the Formation of Acetic Acid from the Direct Conversion of Methane and Carbon Dioxide on Zinc-Modified H-ZSM-5 Zeolite, *Journal of the American Chemical Society*, 135 (2013) 13567-13573.

[146] R. Zhang, L. Song, H. Liu, B. Wang, The interaction mechanism of CO<sub>2</sub> with CH<sub>3</sub> and H on Cu (111) surface in synthesis of acetic acid from CH<sub>4</sub>/CO<sub>2</sub>: A DFT study, *Applied Catalysis A: General*, 443-444 (2012) 50-58.

[147] R. Shavi, J. Ko, A. Cho, J.W. Han, J.G. Seo, Mechanistic insight into the quantitative synthesis of acetic acid by direct conversion of CH<sub>4</sub> and CO<sub>2</sub>: An experimental and theoretical approach, *Applied Catalysis B: Environmental*, 229 (2018) 237-248.

[148] V. Rohani, S. Iwarere, F. Fabry, D. Mourard, E. Izquierdo, D. Ramjugernath, L. Fulcheri, Experimental study of hydrocarbons synthesis from syngas by a tip-tip electrical discharge at very high pressure, *Plasma Chemistry and Plasma Processing*, 31 (2011) 663.

[149] S. Iwarere, V. Rohani, D. Ramjugernath, F. Fabry, L. Fulcheri, Hydrocarbons synthesis from syngas by very high pressure plasma, *Chemical Engineering Journal*, 241 (2014) 1-8.

[150] W.S. Al-Harrasi, K. Zhang, G. Akay, Process intensification in gas-to-liquid reactions: plasma promoted Fischer-Tropsch synthesis for hydrocarbons at low temperatures and ambient pressure, *Green Processing and Synthesis*, 2 (2013) 479-490.

[151] H. Gesser, N. Hunter, D. Probawono, The CO<sub>2</sub> reforming of natural gas in a silent discharge reactor, *Plasma chemistry and plasma processing*, 18 (1998) 241-245.

[152] L. Zhou, B. Xue, U. Kogelschatz, B. Eliasson, Nonequilibrium plasma reforming of greenhouse gases to synthesis gas, *Energy & Fuels*, 12 (1998) 1191-1199.

[153] T. Jiang, Y. Li, C.-j. Liu, G.-h. Xu, B. Eliasson, B. Xue, Plasma methane conversion using dielectric-barrier discharges with zeolite A, *Catalysis Today*, 72 (2002) 229-235.

[154] Y. Li, G.-h. Xu, C.-j. Liu, B. Eliasson, B.-z. Xue, Co-generation of syngas and higher hydrocarbons from CO<sub>2</sub> and CH<sub>4</sub> using dielectric-barrier discharge: effect of electrode materials, *Energy & fuels*, 15 (2001) 299-302.

[155] Y.-p. Zhang, Y. Li, Y. Wang, C.-j. Liu, B. Eliasson, Plasma methane conversion in the presence of carbon dioxide using dielectric-barrier discharges, *Fuel Processing Technology*, 83 (2003) 101-109.

[156] D. Bin, Z. Xiu-ling, G. Wei-min, H. Ren, Study on the methane coupling under pulse corona plasma by using CO<sub>2</sub> as oxidant, *Plasma Science and Technology*, 2 (2000) 577.

[157] S. Yao, F. Ouyang, A. Nakayama, E. Suzuki, M. Okumoto, A. Mizuno, Oxidative coupling and reforming of methane with carbon dioxide using a high-frequency pulsed plasma, *Energy & Fuels*, 14 (2000) 910-914.

[158] A. Huang, G. Xia, J. Wang, S.L. Suib, Y. Hayashi, H. Matsumoto, CO<sub>2</sub> reforming of CH<sub>4</sub> by atmospheric pressure ac discharge plasmas, *Journal of catalysis*, 189 (2000) 349-359.

[159] C. Qi, D. Wei, T. Xumei, Y. Hui, D. Xiaoyan, Y. Yongxiang, CO<sub>2</sub> reforming of CH<sub>4</sub> by atmospheric pressure abnormal glow plasma, *Plasma Science and Technology*, 8 (2006) 181.

- [160] D. Li, X. Li, M. Bai, X. Tao, S. Shang, X. Dai, Y. Yin, CO<sub>2</sub> reforming of CH<sub>4</sub> by atmospheric pressure glow discharge plasma: a high conversion ability, *International Journal of Hydrogen Energy*, 34 (2009) 308-313.
- [161] K. Krawczyk, M. Młotek, B. Ulejczyk, K. Schmidt-Szałowski, Methane conversion with carbon dioxide in plasma-catalytic system, *Fuel*, 117 (2014) 608-617.
- [162] J. Sentek, K. Krawczyk, M. Młotek, M. Kalczewska, T. Kroker, T. Kolb, A. Schenk, K.-H. Gericke, K. Schmidt-Szałowski, Plasma-catalytic methane conversion with carbon dioxide in dielectric barrier discharges, *Applied Catalysis B: Environmental*, 94 (2010) 19-26.
- [163] X. Tu, J. Whitehead, Plasma-catalytic dry reforming of methane in an atmospheric dielectric barrier discharge: Understanding the synergistic effect at low temperature, *Applied Catalysis B: Environmental*, 125 (2012) 439-448.
- [164] D. Mei, X. Zhu, Y.-L. He, J.D. Yan, X. Tu, Plasma-assisted conversion of CO<sub>2</sub> in a dielectric barrier discharge reactor: understanding the effect of packing materials, *Plasma Sources Science and Technology*, 24 (2014) 015011.
- [165] Y. Zeng, X. Zhu, D. Mei, B. Ashford, X. Tu, Plasma-catalytic dry reforming of methane over  $\gamma$ -Al<sub>2</sub>O<sub>3</sub> supported metal catalysts, *Catalysis Today*, 256 (2015) 80-87.
- [166] X. Tu, J.C. Whitehead, Plasma dry reforming of methane in an atmospheric pressure AC gliding arc discharge: Co-generation of syngas and carbon nanomaterials, *International Journal of Hydrogen Energy*, 39 (2014) 9658-9669.
- [167] H.J. Gallon, X. Tu, J.C. Whitehead, Effects of Reactor Packing Materials on H<sub>2</sub> Production by CO<sub>2</sub> Reforming of CH<sub>4</sub> in a Dielectric Barrier Discharge, *Plasma Processes and Polymers*, 9 (2012) 90-97.
- [168] R. Snoeckx, R. Aerts, X. Tu, A. Bogaerts, Plasma-Based Dry Reforming: A Computational Study Ranging from the Nanoseconds to Seconds Time Scale, *The Journal of Physical Chemistry C*, 117 (2013) 4957-4970.
- [169] R. Snoeckx, Y.X. Zeng, X. Tu, A. Bogaerts, Plasma-based dry reforming: improving the conversion and energy efficiency in a dielectric barrier discharge, *RSC Advances*, 5 (2015) 29799-29808.
- [170] A. Bogaerts, C. De Bie, R. Snoeckx, T. Kozák, Plasma based CO<sub>2</sub> and CH<sub>4</sub> conversion: A modeling perspective, *Plasma Processes and Polymers*, 14 (2017) 1600070.
- [171] K. Zhang, T. Mukhriza, X. Liu, P.P. Greco, E. Chiremba, A study on CO<sub>2</sub> and CH<sub>4</sub> conversion to synthesis gas and higher hydrocarbons by the combination of catalysts and dielectric-barrier discharges, *Applied Catalysis A: General*, 502 (2015) 138-149.
- [172] S.-G. Wang, D.-B. Cao, Y.-W. Li, J. Wang, H. Jiao, CO<sub>2</sub> reforming of CH<sub>4</sub> on Ni (111): a density functional theory calculation, *The Journal of Physical Chemistry B*, 110 (2006) 9976-9983.
- [173] S.-G. Wang, X.-Y. Liao, J. Hu, D.-B. Cao, Y.-W. Li, J. Wang, H. Jiao, Kinetic aspect of CO<sub>2</sub> reforming of CH<sub>4</sub> on Ni (111): a density functional theory calculation, *Surface science*, 601 (2007) 1271-1284.
- [174] C. Pistonesi, A. Juan, B. Irigoyen, N. Amadeo, Theoretical and experimental study of methane steam reforming reactions over nickel catalyst, *Applied surface science*, 253 (2007) 4427-4437.
- [175] Y. Yang, Methane conversion and reforming by nonthermal plasma on pins, *Industrial &*

engineering chemistry research, 41 (2002) 5918-5926.

[176] M.-w. Li, G.-h. Xu, Y.-l. Tian, L. Chen, H.-f. Fu, Carbon dioxide reforming of methane using DC corona discharge plasma reaction, *The Journal of Physical Chemistry A*, 108 (2004) 1687-1693.

[177] M.-W. Li, Y.-L. Tian, G.-H. Xu, Characteristics of carbon dioxide reforming of methane via alternating current (AC) corona plasma reactions, *Energy & fuels*, 21 (2007) 2335-2339.

[178] N. Seyed-Matin, A.H. Jalili, M.H. Jenab, S.M. Zekordi, A. Afzali, C. Rasouli, A. Zamaniyan, DC-pulsed plasma for dry reforming of methane to synthesis gas, *Plasma Chemistry and Plasma Processing*, 30 (2010) 333-347.

[179] A. Aziznia, H.R. Bozorgzadeh, N. Seyed-Matin, M. Baghalha, A. Mohamadizadeh, Comparison of dry reforming of methane in low temperature hybrid plasma-catalytic corona with thermal catalytic reactor over Ni/ $\gamma$ -Al<sub>2</sub>O<sub>3</sub>, *Journal of Natural Gas Chemistry*, 21 (2012) 466-475.

[180] H. Gesser, N. Hunter, D. Probawono, The CO<sub>2</sub> reforming of natural gas in a silent discharge reactor, *Plasma chemistry and plasma processing*, 18 (1998) 241-245.

[181] J.-J. Zou, Y.-p. Zhang, C.-J. Liu, Y. Li, B. Eliasson, Starch-enhanced synthesis of oxygenates from methane and carbon dioxide using dielectric-barrier discharges, *Plasma Chemistry and Plasma Processing*, 23 (2003) 69-82.

[182] Q. Wang, B.-H. Yan, Y. Jin, Y. Cheng, Dry reforming of methane in a dielectric barrier discharge reactor with Ni/Al<sub>2</sub>O<sub>3</sub> catalyst: interaction of catalyst and plasma, *Energy & Fuels*, 23 (2009) 4196-4201.

[183] K.L. Pan, W.C. Chung, M.B. Chang, Dry reforming of CH<sub>4</sub> with CO<sub>2</sub> to generate syngas by combined plasma catalysis, *IEEE Transactions on Plasma Science*, 42 (2014) 3809-3818.

[184] W.-C. Chung, K.-L. Pan, H.-M. Lee, M.-B. Chang, Dry reforming of methane with dielectric barrier discharge and ferroelectric packed-bed reactors, *Energy & Fuels*, 28 (2014) 7621-7631.

[185] A. Ghorbanzadeh, R. Lotfalipour, S. Rezaei, Carbon dioxide reforming of methane at near room temperature in low energy pulsed plasma, *international journal of hydrogen energy*, 34 (2009) 293-298.

[186] D. Li, X. Li, M. Bai, X. Tao, S. Shang, X. Dai, Y. Yin, CO<sub>2</sub> reforming of CH<sub>4</sub> by atmospheric pressure glow discharge plasma: a high conversion ability, *International Journal of Hydrogen Energy*, 34 (2009) 308-313.

[187] H. Long, S. Shang, X. Tao, Y. Yin, X. Dai, CO<sub>2</sub> reforming of CH<sub>4</sub> by combination of cold plasma jet and Ni/ $\gamma$ -Al<sub>2</sub>O<sub>3</sub> catalyst, *international journal of hydrogen energy*, 33 (2008) 5510-5515.

[188] L. Xiang, M.-g. BAI, X.-m. TAO, S.-y. SHANG, Y.-x. YIN, X.-y. DAI, Carbon dioxide reforming of methane to synthesis gas by an atmospheric pressure plasma jet, *Journal of Fuel Chemistry and Technology*, 38 (2010) 195-200.

[189] A. Indarto, J.-W. Choi, H. Lee, H.K. Song, Effect of additive gases on methane conversion using gliding arc discharge, *Energy*, 31 (2006) 2986-2995.

[190] Z. Bo, J. Yan, X. Li, Y. Chi, K. Cen, Plasma assisted dry methane reforming using gliding arc gas discharge: effect of feed gases proportion, *International Journal of Hydrogen Energy*, 33 (2008) 5545-5553.

[191] B. Eliasson, C.-j. Liu, U. Kogelschatz, Direct conversion of methane and carbon dioxide to

higher hydrocarbons using catalytic dielectric-barrier discharges with zeolites, *Industrial & engineering chemistry research*, 39 (2000) 1221-1227.

[192] Y. Li, C.-J. Liu, B. Eliasson, Y. Wang, Synthesis of oxygenates and higher hydrocarbons directly from methane and carbon dioxide using dielectric-barrier discharges: product distribution, *Energy & fuels*, 16 (2002) 864-870.

[193] J.-g. Wang, C.-j. Liu, Y.-p. Zhang, B. Eliasson, A DFT study of synthesis of acetic acid from methane and carbon dioxide, *Chemical Physics Letters*, 368 (2003) 313-318.

[194] M. Scapinello, L.M. Martini, P. Tosi, CO<sub>2</sub> hydrogenation by CH<sub>4</sub> in a dielectric barrier discharge: catalytic effects of nickel and copper, *Plasma Processes and Polymers*, 11 (2014) 624-628.

[195] L.M. Martini, G. Dilecce, G. Guella, A. Maranzana, G. Tonachini, P. Tosi, Oxidation of CH<sub>4</sub> by CO<sub>2</sub> in a dielectric barrier discharge, *Chemical Physics Letters*, 593 (2014) 55-60.

[196] G. Scarduelli, G. Guella, D. Ascenzi, P. Tosi, Synthesis of Liquid Organic Compounds from CH<sub>4</sub> and CO<sub>2</sub> in a Dielectric Barrier Discharge Operating at Atmospheric Pressure, *Plasma Processes and Polymers*, 8 (2011) 25-31.

[197] T. Manley, The electric characteristics of the ozonator discharge, *Transactions of the electrochemical society*, 84 (1943) 83-96.

[198] S. Dai, Y. Ju, H. Gao, J. Lin, S. Pennycook, C. Barnes, Preparation of silica aerogel using ionic liquids as solvents, *Chemical Communications*, (2000) 243-244.

[199] B. Dou, J. Li, Y. Wang, H. Wang, C. Ma, Z. Hao, Adsorption and desorption performance of benzene over hierarchically structured carbon-silica aerogel composites, *Journal of hazardous materials*, 196 (2011) 194-200.

[200] M. Casula, A. Corrias, G. Paschina, Iron-cobalt-silica aerogel nanocomposite materials, *Journal of sol-gel science and technology*, 26 (2003) 667-670.

[201] T.Y. Amiri, J. Moghaddas, Cogeled copper-silica aerogel as a catalyst in hydrogen production from methanol steam reforming, *International Journal of Hydrogen Energy*, 40 (2015) 1472-1480.

[202] N. Seaton, Determination of the connectivity of porous solids from nitrogen sorption measurements, *Chemical Engineering Science*, 46 (1991) 1895-1909.

[203] J.C. Groen, L.A. Peffer, J. Pérez-Ramírez, Pore size determination in modified micro-and mesoporous materials. Pitfalls and limitations in gas adsorption data analysis, *Microporous and Mesoporous Materials*, 60 (2003) 1-17.

[204] G. Ertl, H. Knä, J. Weitkamp, *Preparation of solid catalysts*, John Wiley & Sons 2008.

[205] A.n. Martínez, C. López, F. Márquez, I. Díaz, Fischer-Tropsch synthesis of hydrocarbons over mesoporous Co/SBA-15 catalysts: the influence of metal loading, cobalt precursor, and promoters, *Journal of Catalysis*, 220 (2003) 486-499.

[206] Y. Wang, M. Noguchi, Y. Takahashi, Y. Ohtsuka, Synthesis of SBA-15 with different pore sizes and the utilization as supports of high loading of cobalt catalysts, *Catalysis Today*, 68 (2001) 3-9.

[207] S. Sun, N. Tsubaki, K. Fujimoto, The reaction performances and characterization of Fischer-Tropsch synthesis Co/SiO<sub>2</sub> catalysts prepared from mixed cobalt salts, *Applied Catalysis A: General*, 202 (2000) 121-131.

[208] D.G. Castner, P.R. Watson, I.Y. Chan, X-ray absorption spectroscopy, X-ray photoelectron spectroscopy, and analytical electron microscopy studies of cobalt catalysts. 1. Characterization of

calcined catalysts, *The Journal of Physical Chemistry*, 93 (1989) 3188-3194.

[209] D. Yin, W. Li, W. Yang, H. Xiang, Y. Sun, B. Zhong, S. Peng, Mesoporous HMS molecular sieves supported cobalt catalysts for Fischer–Tropsch synthesis, *Microporous and mesoporous materials*, 47 (2001) 15-24.

[210] I. Puskas, T. Fleisch, P. Full, J. Kaduk, C. Marshall, B. Meyers, Novel aspects of the physical chemistry of Co/SiO<sub>2</sub> Fischer–Tropsch catalyst preparations: the chemistry of cobalt silicate formation during catalyst preparation or hydrogenation, *Applied Catalysis A: General*, 311 (2006) 146-154.

[211] P.-J. Yu, C.-C. Hsieh, P.-Y. Chen, B.-J. Weng, Y.W. Chen-Yang, Highly active and reusable silica-aerogel-supported platinum–cobalt bimetallic catalysts for the dehydrogenation of ammonia borane, *RSC Advances*, 6 (2016) 112109-112116.

[212] M. Salim, E. Khawaja, X-ray photoelectron spectroscopy study of sodium germanate glass containing cobalt oxide, *Journal of non-crystalline solids*, 151 (1992) 71-80.

[213] J. Van Elp, J. Wieland, H. Eskes, P. Kuiper, G. Sawatzky, F. De Groot, T. Turner, Electronic structure of coo, li-doped coo, and licoo<sub>2</sub>, *Physical Review B*, 44 (1991) 6090.

[214] V. Jiménez, J. Espinós, A. González-Elipe, Control of the stoichiometry in the deposition of cobalt oxides on SiO<sub>2</sub>, *Surface and interface analysis*, 26 (1998) 62-71.

[215] H. Ming, B.G. Baker, Characterization of cobalt Fischer-Tropsch catalysts I. Unpromoted cobalt-silica gel catalysts, *Applied Catalysis A: General*, 123 (1995) 23-36.

[216] J. Chai, J. Pan, S. Wang, C. Huan, G. Lau, Y. Zheng, S. Xu, Thermal behaviour of ultra-thin Co overlayers on rutile TiO<sub>2</sub> (100) surface, *Surface science*, 589 (2005) 32-41.

[217] T. Matsuzaki, K. Takeuchi, T. Hanaoka, H. Arakawa, Y. Sugi, Hydrogenation of carbon monoxide over highly dispersed cobalt catalysts derived from cobalt (II) acetate, *Catalysis today*, 28 (1996) 251-259.

[218] I. Puskas, T.H. Fleisch, J.B. Hall, B.L. Meyers, R.T. Roginski, Metal-support interactions in precipitated, magnesium-promoted cobaltsilica catalysts, *Journal of Catalysis*, 134 (1992) 615-628.

[219] T. Motohashi, Y. Katsumata, T. Ono, R. Kanno, M. Karppinen, H. Yamauchi, Synthesis and Properties of CoO<sub>2</sub>, the x= 0 End Member of the Li<sub>x</sub> CoO<sub>2</sub> and Na<sub>x</sub> CoO<sub>2</sub> Systems, *Chemistry of Materials*, 19 (2007) 5063-5066.

[220] K. Inagaki, M. Higaki, Y. Matsui, K. Kurita, M. Suzuki, K. Yoshida, T. Maeda, Digital protection method for power transformers based on an equivalent circuit composed of inverse inductance, *IEEE Transactions on Power Delivery*, 3 (1988) 1501-1510.

[221] G. Baoming, A.T. de Almeida, Z. Qionglin, W. Xiangheng, An equivalent instantaneous inductance-based technique for discrimination between inrush current and internal faults in power transformers, *IEEE Transactions on Power Delivery*, 20 (2005) 2473-2482.

[222] U. Kogelschatz, Dielectric-barrier discharges: their history, discharge physics, and industrial applications, *Plasma chemistry and plasma processing*, 23 (2003) 1-46.

[223] H.L. Chen, H.M. Lee, S.H. Chen, Y. Chao, M.B. Chang, Review of plasma catalysis on hydrocarbon reforming for hydrogen production—Interaction, integration, and prospects, *Applied Catalysis B: Environmental*, 85 (2008) 1-9.

[224] J. Van Durme, J. Dewulf, C. Leys, H. Van Langenhove, Combining non-thermal plasma with heterogeneous catalysis in waste gas treatment: A review, *Applied Catalysis B: Environmental*, 78

(2008) 324-333.

[225] T. Nozaki, K. Okazaki, Non-thermal plasma catalysis of methane: principles, energy efficiency, and applications, *Catalysis today*, 211 (2013) 29-38.

[226] E.C. Neyts, K. Ostrikov, M.K. Sunkara, A. Bogaerts, Plasma catalysis: synergistic effects at the nanoscale, *Chemical reviews*, 115 (2015) 13408-13446.

[227] E.C. Neyts, Plasma-surface interactions in plasma catalysis, *Plasma Chemistry and Plasma Processing*, 36 (2016) 185-212.

[228] X. Tu, H.J. Gallon, M.V. Twigg, P.A. Gorry, J.C. Whitehead, Dry reforming of methane over a Ni/Al<sub>2</sub>O<sub>3</sub> catalyst in a coaxial dielectric barrier discharge reactor, *Journal of Physics D: Applied Physics*, 44 (2011) 274007.

[229] V. Volchenok, N. Egorov, V. Komarov, S. Kupriyanov, V. Ochkin, N. Sobolev, E. Truvacheev, Chemical composition of the plasma in a CO laser at room temperature, *Sov. Phys.-Tech. Phys.(Engl. Transl.);(United States)*, 21 (1976).

[230] V.D. Rusanov, A.A. Fridman, *The physics of a chemically active plasma*, Moscow Izdatel Nauka, (1984).

[231] F. Massines, G. Gouda, N. Gherardi, E. Croquesel, Study of glow dielectric barrier discharge in various atmospheres, *Proc. HAKONE VII Conference*, Greifswald, 2000.

[232] J.A. Gardella Jr, S.A. Ferguson, R.L. Chin,  $\pi^* \leftarrow \pi$  shakeup satellites for the analysis of structure and bonding in aromatic polymers by X-ray photoelectron spectroscopy, *Applied spectroscopy*, 40 (1986) 224-232.

[233] G. Beamson, D. Clark, N. Hayes, D.S. Law, Effect of crystallinity on the XPS spectrum of poly (ethylene terephthalate), *Surface Science Spectra*, 3 (1994) 357-365.

[234] M. Aresta, A. Dibenedetto, A. Angelini, Catalysis for the valorization of exhaust carbon: from CO<sub>2</sub> to chemicals, materials, and fuels. Technological use of CO<sub>2</sub>, *Chemical reviews*, 114 (2013) 1709-1742.

[235] C.W. Li, J. Ciston, M.W. Kanan, Electroreduction of carbon monoxide to liquid fuel on oxide-derived nanocrystalline copper, *Nature*, 508 (2014) 504.

[236] Y.H. Hu, E. Ruckenstein, Catalytic conversion of methane to synthesis gas by partial oxidation and CO<sub>2</sub> reforming, *ChemInform*, 35 (2004) no-no.

[237] D. Yap, J.-M. Tatibouët, C. Batiot-Dupeyrat, Catalyst assisted by non-thermal plasma in dry reforming of methane at low temperature, *Catalysis Today*, 299 (2018) 263-271.

[238] K. Zhang, B. Eliasson, U. Kogelschatz, Direct Conversion of Greenhouse Gases to Synthesis Gas and C<sub>4</sub> Hydrocarbons over Zeolite HY Promoted by a Dielectric-Barrier Discharge, *Industrial & Engineering Chemistry Research*, 41 (2002) 1462-1468.

[239] K. Zhang, U. Kogelschatz, B. Eliasson, Conversion of greenhouse gases to synthesis gas and higher hydrocarbons, *Energy & fuels*, 15 (2001) 395-402.

[240] K. Zhang, T. Mukhriza, X. Liu, P.P. Greco, E. Chiremba, A study on CO<sub>2</sub> and CH<sub>4</sub> conversion to synthesis gas and higher hydrocarbons by the combination of catalysts and dielectric-barrier discharges, *Applied Catalysis A: General*, 502 (2015) 138-149.

[241] A.-J. Zhang, A.-M. Zhu, J. Guo, Y. Xu, C. Shi, Conversion of greenhouse gases into syngas via combined effects of discharge activation and catalysis, *Chemical Engineering Journal*, 156 (2010) 601-606.

[242] F. Zhu, H. Zhang, X. Yan, J. Yan, M. Ni, X. Li, X. Tu, Plasma-catalytic reforming of CO<sub>2</sub>-rich biogas over Ni/ $\gamma$ -Al<sub>2</sub>O<sub>3</sub> catalysts in a rotating gliding arc reactor, *Fuel*, 199 (2017) 430-437.

[243] V. Goujard, J.-M. Tatibouët, C. Batiot-Dupeyrat, Use of a non-thermal plasma for the production of synthesis gas from biogas, *Applied Catalysis A: General*, 353 (2009) 228-235.

[244] K. Kozlov, P. Michel, H.-E. Wagner, Synthesis of organic compounds from mixtures of methane with carbon dioxide in dielectric-barrier discharges at atmospheric pressure, *Plasmas and Polymers*, 5 (2000) 129-150.

[245] L. Wang, Y. Yi, C. Wu, H. Guo, X. Tu, One-step reforming of CO<sub>2</sub> and CH<sub>4</sub> into high-value liquid chemicals and fuels at room temperature by plasma-driven catalysis, *Angewandte Chemie International Edition*, 56 (2017) 13679-13683.

[246] A. Grosvenor, B. Kobe, M. Biesinger, N. McIntyre, Investigation of multiplet splitting of Fe 2p XPS spectra and bonding in iron compounds, *Surface and Interface Analysis: An International Journal devoted to the development and application of techniques for the analysis of surfaces, interfaces and thin films*, 36 (2004) 1564-1574.

[247] H.-Y. Lin, Y.-W. Chen, C. Li, The mechanism of reduction of iron oxide by hydrogen, *Thermochimica Acta*, 400 (2003) 61-67.

[248] A. Pineau, N. Kanari, I. Gaballah, Kinetics of reduction of iron oxides by H<sub>2</sub>: Part I: Low temperature reduction of hematite, *Thermochimica Acta*, 447 (2006) 89-100.

[249] Z.L. Zhang, X.E. Verykios, Carbon dioxide reforming of methane to synthesis gas over supported Ni catalysts, *Catalysis Today*, 21 (1994) 589-595.

[250] S. Nouisir, S. Keav, J. Barbier, M. Bensitel, R. Brahmi, D. Duprez, Deactivation phenomena during catalytic wet air oxidation (CWAO) of phenol over platinum catalysts supported on ceria and ceria-zirconia mixed oxides, *Applied Catalysis B: Environmental*, 84 (2008) 723-731.

[251] C. De Bie, B. Verheyde, T. Martens, J. van Dijk, S. Paulussen, A. Bogaerts, Fluid modeling of the conversion of methane into higher hydrocarbons in an atmospheric pressure dielectric barrier discharge, *Plasma Processes and Polymers*, 8 (2011) 1033-1058.

[252] T. Kozák, A. Bogaerts, Splitting of CO<sub>2</sub> by vibrational excitation in non-equilibrium plasmas: a reaction kinetics model, *Plasma Sources Science and Technology*, 23 (2014) 045004.

[253] Y.R. Zhang, K. Van Laer, E.C. Neyts, A. Bogaerts, Can plasma be formed in catalyst pores? A modeling investigation, *Appl. Catal. B-Environ.*, 185 (2016) 56-67.

[254] S. Gao, Y. Lin, X. Jiao, Y. Sun, Q. Luo, W. Zhang, D. Li, J. Yang, Y. Xie, Partially oxidized atomic cobalt layers for carbon dioxide electroreduction to liquid fuel, *Nature*, 529 (2016) 68.

[255] F. Studt, I. Sharafutdinov, F. Abild-Pedersen, C.F. Elkjær, J.S. Hummelshøj, S. Dahl, I. Chorkendorff, J.K. Nørskov, Discovery of a Ni-Ga catalyst for carbon dioxide reduction to methanol, *Nature chemistry*, 6 (2014) 320.

[256] J. Graciani, K. Mudiyansele, F. Xu, A.E. Baber, J. Evans, S.D. Senanayake, D.J. Stacchiola, P. Liu, J. Hrbek, J.F. Sanz, Highly active copper-ceria and copper-ceria-titania catalysts for methanol synthesis from CO<sub>2</sub>, *Science*, 345 (2014) 546-550.

[257] O. Martin, A.J. Martín, C. Mondelli, S. Mitchell, T.F. Segawa, R. Hauert, C. Drouilly, D. Curulla-Ferré, J. Pérez-Ramírez, Indium oxide as a superior catalyst for methanol synthesis by CO<sub>2</sub> hydrogenation, *Angewandte Chemie International Edition*, 55 (2016) 6261-6265.

[258] S. Kattel, P.J. Ramirez, J.G. Chen, J.A. Rodriguez, P. Liu, Active sites for CO<sub>2</sub>

- hydrogenation to methanol on Cu/ZnO catalysts, *Science*, 355 (2017) 1296-1299.
- [259] C.-S. Li, G. Melaet, W.T. Ralston, K. An, C. Brooks, Y. Ye, Y.-S. Liu, J. Zhu, J. Guo, S. Alayoglu, High-performance hybrid oxide catalyst of manganese and cobalt for low-pressure methanol synthesis, *Nature communications*, 6 (2015) 6538.
- [260] G. Melaet, W.T. Ralston, C.-S. Li, S. Alayoglu, K. An, N. Musselwhite, B. Kalkan, G.A. Somorjai, Evidence of Highly Active Cobalt Oxide Catalyst for the Fischer–Tropsch Synthesis and CO<sub>2</sub> Hydrogenation, *Journal of the American Chemical Society*, 136 (2014) 2260-2263.
- [261] J. Wei, Q. Ge, R. Yao, Z. Wen, C. Fang, L. Guo, H. Xu, J. Sun, Directly converting CO<sub>2</sub> into a gasoline fuel, *Nature communications*, 8 (2017) 15174.
- [262] P. Gao, S. Li, X. Bu, S. Dang, Z. Liu, H. Wang, L. Zhong, M. Qiu, C. Yang, J. Cai, Direct conversion of CO<sub>2</sub> into liquid fuels with high selectivity over a bifunctional catalyst, *Nature chemistry*, 9 (2017) 1019.
- [263] R.W. Dorner, D.R. Hardy, F.W. Williams, H.D. Willauer, Heterogeneous catalytic CO<sub>2</sub> conversion to value-added hydrocarbons, *Energy & Environmental Science*, 3 (2010) 884-890.
- [264] Y. Zhu, S. Zhang, Y. Ye, X. Zhang, L. Wang, W. Zhu, F. Cheng, F. Tao, Catalytic conversion of carbon dioxide to methane on ruthenium–cobalt bimetallic nanocatalysts and correlation between surface chemistry of catalysts under reaction conditions and catalytic performances, *Acs Catalysis*, 2 (2012) 2403-2408.
- [265] S. Abelló, D. Montané, Exploring Iron-based Multifunctional Catalysts for Fischer–Tropsch Synthesis: A Review, *ChemSusChem*, 4 (2011) 1538-1556.
- [266] A. Hakim, T.S. Marliza, N.M. Abu Tahari, R.W. Wan Isahak, R.M. Yusop, W.M. Mohamed Hisham, A.M. Yarmo, Studies on CO<sub>2</sub> adsorption and desorption properties from various types of iron oxides (FeO, Fe<sub>2</sub>O<sub>3</sub>, and Fe<sub>3</sub>O<sub>4</sub>), *Industrial & Engineering Chemistry Research*, 55 (2016) 7888-7897.
- [267] K. Im-orb, A. Arpornwichanop, Techno-environmental analysis of the biomass gasification and Fischer-Tropsch integrated process for the co-production of bio-fuel and power, *Energy*, 112 (2016) 121-132.
- [268] D. Li, V. Rohani, F. Fabry, A. Parakkulam Ramaswamy, M. Sennour, L. Fulcheri, Experimental study on plasma-catalytic synthesis of hydrocarbons from syngas, *Applied Catalysis A: General*, (2019) 117269.
- [269] D. Li, V. Rohani, F. Fabry, A.P. Ramaswamy, M. Sennour, L. Fulcheri, Direct conversion of CO<sub>2</sub> and CH<sub>4</sub> into liquid chemicals by plasma-catalysis, *Applied Catalysis B: Environmental*, (2019) 118228.

## **Related publications:**

Chapter II and III have been adapted from [268]:

**D. Li**, V. Rohani, F. Fabry, A. Parakkulam Ramaswamy, M. Sennour, L. Fulcheri, Experimental study on plasma-catalytic synthesis of hydrocarbons from syngas, *Applied Catalysis A: General*, (2019) 117269.

Chapter IV have been adapted from [269]:

**D. Li**, V. Rohani, F. Fabry, A.P. Ramaswamy, M. Sennour, L. Fulcheri, Direct conversion of CO<sub>2</sub> and CH<sub>4</sub> into liquid chemicals by plasma-catalysis, *Applied Catalysis B: Environmental*, (2019) 118228.

## **Conferences:**

D. Li et al., (2019) Experimental study on plasma promoted catalytic synthesis of hydrocarbons from syngas. June 9-14, *ISPC-24*, Naples, Italy.

D. Li et al., (2019) High yield direct synthesis of liquid organics from CO<sub>2</sub> and CH<sub>4</sub> in a plasma-catalysis packed bed reactor. June 9-14, *ISPC-24*, Naples, Italy.

# Acknowledgment

First and foremost, I would like to thank my primary supervisor Laurent Fulcheri, who provided me constant support and constructive guidance not only on academics but also on life. Laurent has taught me many things, but nothing is more precious than the enthusiasm and the motivation for pursuing goals, which has made me always positive and motivated in my life. Similar gratitude to my co-supervisor, Vandad Rohani, who has supervised me not only on academics but also on a Ph.D. career. My supervisors nurtured my passion for plasma and provided me degrees of freedom to be academically excited in some topics. If not for their dedication, this study would undoubtedly never have achieved fruition.

I would also like to thank particularly those, to whom I always asked for help and assistance in the past three years: Fredric Fabry, the research engineer of plasma lab, who has unreservedly helped me so much on plasma experiments part; Pierre Ilbizian, the Laboratory engineer of chemical lab, who kindly directed me in chemical experiments. Cedric Sernissi and Patrick Leroux, who have contributed so much on the building of the bench.

Also, special thanks to all the colleagues who have guided and helped me with the preparation and characterization of materials. I will always remember and appreciate their kindness and patience. Luckily, they are now free from my bothering. And all to the administrative members of the PERSEE group for their kind help to solve all administrative issues and IT issues.

I also want to thank my dear Ph.D. colleagues that I have had the pleasure of working with, those who have finished and left, and those who are going to finish. Too many my dear colleagues, too few the margins to list them. We have always shared our thoughts on academics, movies, foods, cultures, and funny jokes and memes. I shall never forget our group trips, beers, coffees, parties, and, most importantly, football. It is always nice days with them around.

Of course, I must say thank you to my parents. My parents have no idea of what plasma chemistry is, but they are experts on what love and dedication are, and always encourage me to do what I want. I also must thank my lovely brother and sister, a pair of twins. Their births have mellowed me. I also want to thank my Chinese friends. For the past three years, we have always kept in touch, but what a pity I missed the important days of some friends.

Finally, I would like to thank the Chinese Scholarship Council and my dear motherland for providing me the opportunity.

These were happiest and most challenging three years I have ever had. I could image soon later, as I faced the new colleagues, I was to remember that distant morning when Laurent took me to Mines-Paristech in Sophia.



## RÉSUMÉ

---

Cette thèse porte sur l'étude de la synthèse Fischer-Tropsch (FTS) et de la conversion directe de CO<sub>2</sub> et de CH<sub>4</sub> en produits liquides à valeur ajoutée par un procédé couplant plasma non-thermique et catalyse hétérogène. Un réacteur plasmocatalytique de type DBD coaxial rempli a été conçu et testé dans cette thèse avec ses appareils d'analyse et de diagnostics. Le réacteur fonctionne dans des conditions ambiantes, le catalyseur et son support se présentent sous la forme de granules empaquetées dans le réacteur. Le support est en aérogel de silice et a été synthétisé par traitement de surface puis séchage ambiant. Le chapitre 3 est dédié à l'étude expérimentale de la synthèse Fischer-Tropsch plasmocatalytique. Dans ce chapitre, les expériences ont d'abord été conduites en plasma seul sans catalyseur en portant une attention particulière à l'influence du débit de gaz, du ratio H<sub>2</sub>/CO et de la fréquence d'excitation électrique sur la conversion du gaz de synthèse. Puis, dans un deuxième temps, le couple catalyseur/support (Co/SiO<sub>2</sub>) a été introduit dans le réacteur afin d'étudier les résultats de la conversion en association plasmocatalytique. Les chapitres 4 et 5 portent eux sur la conversion plasmocatalytique directe du CO<sub>2</sub> et du CH<sub>4</sub> en produits liquides et gaz de synthèse. Dans le chapitre 4, la même démarche que celle du chapitre 3 a été employée, à savoir la conduite comparative d'expériences avec et sans catalyseur. Les couples deux catalyseur/support utilisés successivement dans ce chapitre sont Co/SiO<sub>2</sub> et Fe/SiO<sub>2</sub>. Le chapitre 5 étend l'étude en proposant une association plasmocatalytique à deux catalyseurs. Ainsi des combinaisons binaires parmi les couples suivants Co/SiO<sub>2</sub>, Fe/SiO<sub>2</sub>, HZSM-5/HZSM-5, Co/HZSM-5 et Fe/HZSM-5 ont été étudiées. Ce couplage a permis d'augmenter la sélectivité vis-à-vis des produits liquides produits en chapitre 4 et d'en produire de nouveaux. Ainsi des alcools, acides carboxyliques et des hydrocarbures C<sub>5</sub><sup>+</sup> ont été synthétisés. La thèse finit par une comparaison des résultats avec ceux de la littérature provenant de procédés proches ; l'efficacité énergétique et la productivité brute ont notamment été comparées. Quelques voies de réaction possibles ont également été proposées pour initier une réflexion plus théorique. Enfin, des recommandations en vue d'une optimisation/amélioration de la FTS et de la conversion directe CO<sub>2</sub>/CH<sub>4</sub> par voie plasmocatalytique sont fournies et discutées.

## MOTS CLÉS

---

Plasma-catalyse; Synthèse d'hydrocarbure; CO<sub>2</sub>; Fischer Tropsch; Aérogel de silice; Produit liquide;

## ABSTRACT

---

This thesis deals with the study of Fischer-Tropsch synthesis (FTS) and the direct conversion of CO<sub>2</sub> and CH<sub>4</sub> into value-added liquid products by a process coupling non-thermal plasma and heterogeneous catalysis. A coaxial dielectric barrier discharge (DBD) plasma-catalytic reactor was designed and tested in this thesis with its analysis and diagnostic devices. The reactor operates under ambient conditions, the catalyst and its support are under the form of granules packaged in the reactor. The support is in silica aerogel and was synthesized by surface treatment and ambient drying. Chapter 3 is dedicated to the experimental study of plasma-catalytic Fischer-Tropsch synthesis. In this chapter, the experiments were first conducted in plasma alone without catalyst, paying particular attention to the influence of the gas flow rate, the H<sub>2</sub>/CO ratio and the electrical excitation frequency on the syngas conversion. Then, in a second step, the catalyst/support couple (Co/SiO<sub>2</sub>) was introduced into the reactor in order to study the results of the conversion under plasma-catalytic combination. Chapters 4 and 5 deal with the direct plasma-catalytic conversion of CO<sub>2</sub> and CH<sub>4</sub> into liquid products and syngas. In Chapter 4, the same approach as in Chapter 3 was used, a comparative study of experiments with and without catalyst was done. The two catalyst/support couples used successively in this chapter are Co/SiO<sub>2</sub> and Fe/SiO<sub>2</sub>. Chapter 5 extends the study by proposing a plasma-catalytic combination with two catalysts at the same time. The effects of packing composite catalysts (Co/SiO<sub>2</sub> or Fe/SiO<sub>2</sub> with HZSM-5, Co/HZSM-5 and Fe/HZSM-5) were studied. The combination of catalysts has made it possible to increase the liquid products selectivity and to produce new liquid products compared to Chapter 4. Thus alcohols, carboxylic acids and C<sub>5</sub><sup>+</sup> hydrocarbons were synthesized. The thesis ends with a comparison of the results with those of the literature from close processes; energy efficiency and gross productivity were compared. Some possible ways of reaction have also been proposed to initiate a more theoretical reflection. Finally, recommendations for optimization/improvement of FTS and direct conversion of CO<sub>2</sub>/CH by plasma-catalytic route are provided and discussed.

## KEYWORDS

---

Plasma-catalysis; Hydrocarbons synthesis; CO<sub>2</sub>; Silica aerogel; Fischer Tropsch; Liquid products;